

**Interaction Range, Universality
and the
Upper Critical Dimension**

Interaction Range, Universality and the Upper Critical Dimension

PROEFSCHRIFT

ter verkrijging van de graad van doctor
aan de Technische Universiteit Delft,
op gezag van de Rector Magnificus Prof. dr. ir. J. Blaauwendraad,
in het openbaar te verdedigen ten overstaan van een commissie,
door het College van Dekanen aangewezen,
op dinsdag 9 december 1997 te 13.30 uur
door

Erik LUIJTEN

doctorandus in de natuurkunde
geboren te Nijmegen

Dit proefschrift is goedgekeurd door de promotoren:

Prof. dr. H. W. J. Blöte
Prof. dr. ir. J. J. J. Kokkedee

Samenstelling promotiecommissie:

Rector Magnificus,	voorzitter
Prof. dr. H. W. J. Blöte,	Rijksuniversiteit Leiden, promotor
Prof. dr. ir. J. J. J. Kokkedee,	Technische Universiteit Delft, promotor
Prof. dr. H. van Beijeren,	Universiteit Utrecht
Prof. dr. K. Binder,	Johannes Gutenberg-Universität Mainz
Prof. dr. S. W. de Leeuw,	Technische Universiteit Delft
Prof. dr. J. M. J. van Leeuwen,	Rijksuniversiteit Leiden

Published and distributed by:

Delft University Press
Mekelweg 4
2628 CD Delft
The Netherlands
Telephone: +31 15 2783254
Fax: +31 15 2781661
E-mail: dup@dup.tudelft.nl

ISBN 90-407-1552-1 / CIP

Copyright © 1997 by E. Luijten

All rights reserved. No part of the material protected by this copyright notice may be reproduced or utilized in any form or by any means, electronic or mechanical, including photocopying, recording or by any information storage and retrieval system, without permission from the publisher: Delft University Press.

Printed in the Netherlands

Contents

1	Introduction and outline	1
2	Monte Carlo algorithm for spin models with long-range interactions	7
2.1	Introduction	7
2.2	Cluster methods	8
2.3	Building clusters in systems with long-range interactions	10
2.3.1	Long-range Hamiltonian	10
2.3.2	Look-up table	12
2.3.3	Continuous bond probability	12
2.3.4	Comparison to conventional cluster algorithms	15
2.4	A “trivial” example: the mean-field model	16
2.5	Generalizations	19
	References	20
3	The Ising model in three dimensions	23
3.1	Introduction	23
3.2	Models and algorithms	25
3.3	Random numbers	28
3.4	A test of universality	28
3.5	Determination of the renormalization exponents	33
3.5.1	The energy	34
3.5.2	The specific heat	35
3.5.3	The spin–spin correlation function	36
3.5.4	The magnetic susceptiblity	38
3.5.5	The temperature derivative of χ	40
3.5.6	The temperature derivative of Q	41
3.6	Simultaneous fits for the three models	42
3.7	Discussion and conclusion	44
	References	46

4	Critical behaviour of spin models with algebraically decaying interactions I	49
	<i>At and above the upper critical dimension</i>	
4.1	Introduction	49
4.2	Rigorous results for the one-dimensional case	51
4.3	Renormalization-group study of the critical behaviour	52
4.4	Numerical results and comparison with earlier results	60
4.4.1	Simulations	60
4.4.2	Determination of the critical temperatures, the amplitude ratio Q and the thermal exponent	61
4.4.3	Determination of critical exponents	70
4.5	Conclusions	76
	References	77
5	Critical behaviour of spin models with algebraically decaying interactions II	79
	<i>Below the upper critical dimension</i>	
5.1	Introduction	79
5.2	Renormalization-group study of the nonclassical regime	80
5.3	The 1D Ising model with long-range interactions	90
5.4	The 2D Ising model with long-range interactions	96
5.4.1	Introduction	96
5.4.2	Regime A: $1 < \sigma < 7/4$	96
5.4.3	Regime B: $7/4 \leq \sigma \leq 2$	96
5.4.4	Regime C: $\sigma > 2$	99
5.4.5	Discussion and conclusion	100
5.5	The 3D Ising model with long-range interactions	102
5.5.1	Introduction	102
5.5.2	Systems with a decay parameter $\sigma = 1.6, 1.8, 2.0$	102
5.5.3	Systems with a decay parameter $\sigma = 2.2, 2.5, 3.0$	103
5.5.4	Discussion and conclusions	104
5.6	Conclusion	104
	References	105
6	The Ising model in four and five dimensions	107
6.1	Introduction	107
6.2	Theory	110
6.3	The specific heat of the mean-field model	115
6.4	Numerical results for the case $d = 5$	117
6.4.1	General considerations	117
6.4.2	The amplitude ratio Q	117
6.4.3	The magnetic susceptibility	120
6.4.4	The spin–spin correlation function	120

6.4.5	The fourth power of the magnetization density	121
6.4.6	The energy	122
6.4.7	The specific heat	123
6.4.8	The first temperature derivative of the specific heat	124
6.4.9	The second temperature derivative of the specific heat	124
6.4.10	The temperature derivative of the magnetic susceptibility	126
6.4.11	The temperature derivative of Q	127
6.5	Numerical results for the case $d = 4$	127
6.5.1	General considerations	127
6.5.2	The amplitude ratio Q	128
6.5.3	The magnetic susceptibility	130
6.5.4	The spin–spin correlation function	131
6.5.5	The fourth power of the magnetization density	132
6.5.6	The energy	133
6.5.7	The specific heat	134
6.5.8	The first temperature derivative of the specific heat	135
6.5.9	The second temperature derivative of the specific heat	136
6.5.10	The temperature derivative of the magnetic susceptibility	137
6.5.11	The temperature derivative of Q	137
6.6	Discussion and conclusions	138
6.6.1	The five-dimensional Ising model	138
6.6.2	The four-dimensional Ising model	142
	References	144
7	Crossover from Ising to classical critical behaviour in two-dimensional systems	147
7.1	Introduction	147
7.2	Range dependence of critical amplitudes	149
7.3	Monte Carlo results	156
7.3.1	Definition of the model	156
7.3.2	Determination of the critical temperature	157
7.3.3	Range dependence of the magnetization density	161
7.3.4	Range dependence of the susceptibility	162
7.3.5	Spin–spin correlation function	163
7.4	Crossover scaling	166
7.5	Finite-size crossover scaling	167
7.5.1	General considerations	167
7.5.2	Absolute magnetization density	168
7.5.3	Magnetic susceptibility	171
7.5.4	Spin–spin correlation function	172
7.5.5	Universal amplitude ratio	172

7.6	Thermal crossover scaling	176
7.6.1	General considerations	176
7.6.2	Absolute magnetization density	177
7.6.3	Magnetic susceptibility	182
7.7	Effective exponents	188
7.8	Conclusions	192
	References	193
A	Some exact calculations for the mean-field model	195
B	Fourier transform of a spherically shaped interaction profile	199
	Summary	201
	Samenvatting	205
	Acknowledgements	209
	Curriculum Vitae	211
	List of publications	213

Chapter 1

Introduction and outline

Among the most challenging problems in theoretical physics are those which involve a large number of coupled degrees of freedom. In such problems, the macroscopic properties of a system are determined by microscopic behaviour on many different length scales, all of which must be taken into account for the solution of the problem. Examples are quantum electrodynamics, turbulence and critical phenomena. The latter subject deals with the behaviour of systems near a critical point. From every-day experience, we know that substances can appear in different phases; e.g., water can be a solid, a liquid or a gas. Transitions between these phases can be induced by changing the temperature of the substance or the pressure under which it is placed. Starting in the gas phase and increasing the pressure while keeping the temperature fixed at some (sufficiently low) value, the substance will at a certain pressure go over to the solid or to the liquid phase. This transition is marked by a sudden change (a discontinuity) in the density of the substance. However, if we repeat the same experiment at a higher temperature, the jump in the density will be smaller, and at some temperature it will even vanish. At this *critical* point (i.e., at this particular temperature and pressure) the distinction between the gas and liquid phase has completely disappeared. Here, some remarkable aspects arise: despite the fact that the fundamental interactions are short-ranged, they cooperate in such a way that density fluctuations occur *at all length scales*. The correlation length, which measures the size of the largest fluctuations in the system, diverges. This divergence, in turn, is responsible for the fact that several macroscopic properties are independent of the microscopic details—they are *universal*. Indeed, these properties solely depend on a small number of global features of the system under consideration: its dimensionality, the number of components of the order parameter, the symmetry of the interaction and of the order parameter and the range of the interactions. Hence, at their critical point greatly different physical systems exhibit a close resemblance. In order to calculate the macroscopic properties, the fluctuations at smaller length

scales can by no means be neglected. What is the proper way to deal with this phenomenon? How can one explain the universality of critical properties and the way in which they depend on global parameters? In which way can the universal parameters be calculated? These questions have plagued theorists for a long time. The relevance of this problem can hardly be overestimated: gas–liquid critical points, the onset of superconductivity and superfluidity, magnetic ordering and Bose–Einstein condensation all constitute examples of critical phenomena, whereas also the Higgs mechanism for the generation of quark masses is based on a spontaneous symmetry breaking. To handle such problems, Kenneth G. Wilson introduced in 1971 the idea of the renormalization group.¹ He showed that the problem could be tackled by treating one length scale at a time, i.e., by integrating out the short-distance fluctuations and subsequently rescaling the remaining part of the Hamiltonian. Upon iteration, this Hamiltonian then approaches a fixed point and universality emerges from the existence of such fixed points in the space of Hamiltonians. Furthermore, he demonstrated that the universal properties can be calculated with the help of methods from quantum field theory. For these insights, he was awarded the Nobel Prize in Physics in 1982. References [1, 2] provide a simplified account of the ideas underlying the renormalization-group theory.

Naturally, the invention of the renormalization-group (RG) theory did not imply the immediate solution of all outstanding problems in the field of critical phenomena. In the first place does this theory rely on several nontrivial assumptions and hence it is important to justify these assumptions by independent confirmations of the RG predictions. Secondly, there are problems in which no agreement exists on the proper application of the RG theory. Furthermore, in general the RG theory cannot provide us with information on nonuniversal aspects of critical-point phenomena. An alternative tool is provided by computer simulations, the application of which has greatly been stimulated by the increase of computer power over the last decades. Among these methods, Monte Carlo simulations enjoy a particular popularity. Because near the critical point the microscopic details of the system are irrelevant, it is most convenient to consider *spin models*, which consist of a lattice structure with a (classical) spin placed on each lattice site. An additional advantage of these models is that extremely efficient simulation algorithms have been developed for them in recent years. The investigation of critical phenomena by means of such numerical calculations requires some particular considerations. Namely, one can only investigate systems of finite extent, in which the diverging correlation length will be truncated, such that critical singularities are rounded. However, this hindrance can be turned into an advantage by invoking the results of RG theory. Indeed, due to the scale invariance at the critical point, thermodynamic properties scale with the

¹Although the concept of renormalization predates the ideas of Wilson, he was the first to apply them successfully to the field of critical phenomena. See Ref. [1] for a historical review.

correlation length in a precisely predicted way, from which one can derive the finite-size dependence of these properties and extrapolate the numerical data accordingly. This is called *finite-size scaling*. Thus, considerable effort has been spent in the past on the verification of renormalization predictions. In particular, attention has been paid to the dependence of critical properties on the number of spatial dimensions and on the number of components of the order parameter. However, much more scarce are studies of their dependence on the range of the interactions. Actually, the vast majority of the pertinent results are RG calculations and approximate numerical treatments of one-dimensional systems. The reason for this is evident: the required computational efforts rapidly grow with increasing interaction range, which until now has prevented accurate investigation of these systems. It is the main purpose of this thesis to change this situation.

In Chapter 2 we introduce a new Monte Carlo algorithm for spin models with (isotropic) long-range interactions. This algorithm forms one of the cornerstones for the research presented in the remaining part of this thesis. It is an algorithm of the Wolff-cluster type; as a consequence critical slowing down is virtually eliminated. The novelty of this algorithm, however, lies in the fact that its speed is *independent* of the number of spin–spin interactions per spin. This may be called a remarkable property, since in Monte Carlo simulations the evolution of a system is determined by taking into account all interactions that are present. Thus, the interaction range no longer poses a limit on simulations of spin models, which clearly opens the way to many new applications. We will use this algorithm to study the critical behaviour of one-component spin models with a variety of spin–spin interactions. The combined effects of the reduction of critical slowing down and the independence of the number of interactions lead to an increase of the computational efficiency that, for the largest systems studied, amounts to a factor of the order of 10^8 with respect to Metropolis-type simulations.

However, before actually applying this algorithm we will first study (Chapter 3) one of the most well-known spin models: the three-dimensional Ising model. The important rôle of this model in the field of phase transitions and critical phenomena justifies a high-precision determination of its universal critical properties. In addition, this chapter provides a nice illustration of the concept of universality: we investigate three different models which all are believed to belong to the same universality class and we show that they indeed exhibit (within the statistical uncertainties) the same critical exponents. As a side-effect, this allows us to introduce many concepts that will prove to be useful in the subsequent study of spin models with long-range interactions.

The following two chapters are then devoted to spin models with interactions that decay as a power of the distance between the spins. This type of interactions provides an interesting extension of short-range interactions. On the one hand, these interactions are essentially identical to short-range forces if their decay is very rapid.

On the other hand, one recovers classical or mean-field-like behaviour (i.e., the behaviour found in systems in which all interactions are identical) if the decay is sufficiently slow. Since the decay parameter can be varied continuously, a smooth interpolation between these two extremes is possible. Indeed, by increasing the power with which the interactions decay, critical fluctuations are less suppressed, which is similar to the effect caused by decreasing the spatial dimensionality in systems with only short-range interactions. In Chapter 4 we treat the regime where the critical behaviour is essentially classical, for spin models in one, two and three dimensions. Between this classical regime and the short-range regime, an intermediate region is expected, which remains hitherto largely unexplored. Even the very boundaries of this region in terms of the decay rate of the spin–spin interactions are subject to debate. It is the objective of Chapter 5 to clarify many of the open questions in this regime.

As will be shown, the regimes in Chapters 4 and 5 are separated by the *upper critical dimension*. In a parameter space that incorporates both the interaction range and the dimensionality, short-range models constitute just a special case, where the pivotal rôle is played by the four-dimensional model. Thus it is natural to study some high-dimensional models with short-range interactions as well, which is done in Chapter 6. In this counterpart of Chapter 3 we present an extensive study of the critical properties of the Ising model in four and five dimensions. We pay considerable attention to the peculiar effects at the upper critical dimension. The close connections between quantum field theory (QFT) and critical phenomena, as revealed by RG theory, and the fact that QFT operates in four dimensions make this case particularly interesting. Indeed, it is believed that the universal properties of the Ising model are described by a scalar ϕ^4 field theory, which is renormalizable in four dimensions. Furthermore, we verify various renormalization predictions for the five-dimensional Ising model. These numerical investigations require highly accurate numerical data, which also yield, as a spin-off, very precise estimates for the critical couplings.

In Chapter 7 we take a different approach to the crossover from Ising-like to classical critical behaviour. It is expected that a system exhibits such crossover behaviour if the difference between the temperature and the critical temperature is increased. However, the precise nature of this behaviour has remained unclarified until now, because it extends over a large temperature range and hence most systems have left the critical region before completing the crossover. We cope with this situation by studying systems with a variable interaction range, such that each spin interacts equally with all its neighbours within a distance R . Also these systems can be dealt with by the algorithm presented in Chapter 2. In this way we can tune the parameter that determines the crossover behaviour without making the temperature distance to the critical point too large. This not only allows us to observe the entire crossover region, but also provides strong evidence for the universal nature of the

crossover.

This thesis is the result of my research over the last three and a half years. Naturally, my insight in the renormalization-group theory and in critical phenomena has evolved over time. The extremely lucid lecture notes of the late Shang-keng Ma [3] have set me on the right track on many occasions. Next, I turned to Daniel Amit's book [4], which has become such a dear travel companion to me that it has acquired the honorary title of "The Green Book". Indeed, although I started out as a statistical physicist, this book has convinced me of the power of the field-theoretic formulation of renormalization theory (also called renormalized perturbation theory), which will continue to captivate me for a long time to come. It is well possible that this thesis reflects this change of perspective at a few instances, but it has been my concern that clarity be maintained. Finally, it is my hope to have demonstrated that numerical calculations can provide a very useful extension of theoretical concepts. However, I also want to state that the converse—numerical work without theoretical knowledge—is an inefficient approach to physical problems and should be left to computer enthusiasts alone.

References

- [1] K. G. Wilson, *Sci. Am.* **241**, 140 (1979) [August 1979].
- [2] K. G. Wilson, *Rev. Mod. Phys.* **55**, 583 (1983) [Nobel Prize lecture].
- [3] S.-k. Ma, *Modern Theory of Critical Phenomena* (Addison–Wesley, Redwood, California, 1976).
- [4] D. J. Amit, *Field Theory, the Renormalization Group, and Critical Phenomena*, second edition (World Scientific, Singapore, 1984).

Chapter 2

Monte Carlo algorithm for spin models with long-range interactions

2.1 Introduction

The study of systems with long-range interactions is notoriously difficult, due to the large number of interactions that has to be taken into account. This has discouraged the application of Monte Carlo methods, whereas at the same time only very few exact solutions are available for these models. Furthermore, other numerical analyses of these systems suffer from serious difficulties. They often truncate the interaction beyond a certain distance, thus introducing errors in the calculation, or are restricted to small system sizes, which limits the accuracy that can be obtained in a finite-size analysis. In this chapter, we present a Monte Carlo method for the simulation of spin models with long-range interactions which is capable of simulating large systems within a reasonable amount of computing time. The algorithm, which is based on the well-known Wolff cluster method [1], does not make any approximation except for the inherent statistical errors. In the process of cluster formation the amount of time per spin visit is *independent of the system size*, despite the fact that each spin interacts with *all* other spins in the system. This fact, together with the reduction of critical slowing down in cluster algorithms, makes this algorithm very suitable for the study of critical phenomena in models with long-range interactions. Therefore it will allow an accurate numerical analysis of a variety of ferromagnetic long-range models, some of which are considered in this thesis.

The outline of this chapter is as follows. In Sec. 2.2 we start with a brief review of the Wolff cluster algorithm. Then, two efficient cluster-building algorithms for long-

range interactions are discussed in Sec. 2.3. We illustrate this Monte Carlo method in Sec. 2.4 with some simulations of the mean-field Ising model. Section 2.5 contains generalizations of the algorithm to other systems, such as general $O(n)$ models with long-range interactions.

2.2 Cluster methods

Cluster algorithms for spin models [2] are based on the Fortuin–Kasteleyn mapping of the Potts model on a random-cluster model [3, 4]. The Potts Hamiltonian \mathcal{H}_P is given by

$$\beta\mathcal{H}_P = -K \sum_{\langle ij \rangle} \delta_{s_i s_j} \quad (s = 1, \dots, q), \quad (2.1)$$

where $\beta = 1/k_B T$, $\sum_{\langle ij \rangle}$ denotes a summation over all nearest-neighbour pairs and q is the possible number of states for each spin. The partition function is thus given by

$$Z_{\text{Potts}} = \sum_{\{s_i\}} \exp(-\beta\mathcal{H}_P). \quad (2.2)$$

It can be shown that this is equivalent to the Whitney polynomial [5], which gives the partition function of the random-cluster model,

$$Z_{\text{RC}} = \sum_G q^C \nu^l, \quad (2.3)$$

where \sum_G denotes a sum over all graphs on the lattice, l denotes the number of bonds in the graph, $\nu = e^K - 1$ and C is the number of connected components in the graph. A connected component consists of sites connected directly or indirectly by bonds (a single, isolated site is regarded as a cluster as well). Now, the random-cluster distribution of graphs is reproduced by the Potts model by *activating* bonds between parallel spins with a probability $\nu/(1+\nu)$, where G is the set of active bonds. Spins connected by active bonds are said to form a *cluster*.

All spins belonging to one cluster are in the same state and uncorrelated with all other spins in the system. Swendsen and Wang [6] were the first to realize that this can be used to construct an efficient Monte Carlo algorithm, which was subsequently improved by Wolff [1]. Let us briefly review the Wolff cluster method for the Ising model. First, a random site is chosen, which contains the first spin of the cluster. Then bonds are activated between this spin and its neighbours, with probability

$$p(s_i, s_j) = \delta_{s_i s_j} \frac{\nu}{1+\nu} = \delta_{s_i s_j} (1 - e^{-K}), \quad (2.4)$$

where K is the Potts coupling between neighbouring spins. This process is repeated iteratively by activating bonds between each newly added spin and its neighbours, thus creating a *cluster* of spins connected by active bonds. Then all the spins in this cluster are reversed and a new cluster is formed. The great advantage of the Wolff cluster algorithm for this system compared to the Metropolis algorithm is the drastic change in critical slowing down. For example, for the two-dimensional Ising model the dynamical critical exponent z is reduced from $z = 2.1665 \pm 0.0012$ [7] to $z \approx 0.25$ [8] and for the three-dimensional Ising model from $z \approx 2.05$ [9] to $z \approx 0.4$ [10]. So, roughly speaking, for a system consisting of L^d spins, the amount of time to reach equilibrium is decreased by a factor $\mathcal{O}(L^2)$. The dynamical critical exponent for the mean-field Ising model, is reduced from $z = 2$ [11] to $z = 0$ [10, 12]. However, in this case the correlation length ξ does not scale with the linear system size, but with $L^{d/4}$, so the correlation time τ scales as $\tau \sim \xi^2 \sim L^{d/2}$ and critical slowing down is hence reduced by a factor $\mathcal{O}(L^{d/2})$. This result is in agreement with the requirement that in the mean-field model only the total number of particles L^d should appear in the scaling relations.

The Fortuin–Kasteleyn mapping can also be applied to systems with different interaction strengths by associating a certain type of bond with each type of interaction. The corresponding generalization of Eq. (2.3) is then [5]

$$Z = \sum_G q^C v_1^{l_1} v_2^{l_2} v_3^{l_3} \dots, \quad (2.5)$$

where now l_i denotes the number of bonds of class i in the graph and $v_i = e^{K_i} - 1$ (K_i is the strength of the coupling between two spins connected by a bond of class i).

This allows the application of the Wolff cluster method to spin models with an arbitrary number of different interactions, in particular long-range interactions. With each value of the interaction strength, i.e., with each spin distance, we associate a different bond class. Then, we activate bonds between each spin in the cluster and *all* other spins in the system with a bond-activation probability p that depends on the interaction strength between the two spins. Once a complete cluster has been formed, its spins are reversed and the formation of a new cluster is started. Clearly, this process becomes very time consuming if the range of the spin–spin interactions becomes large, just as in the case of Metropolis-type simulations. Here, we present a method in which the number of operations required to activate a bond is independent of the number of spins in the system. The efficiency of this method can be illustrated by the following simple example. If p were equal for each spin pair, one out of p^{-1} spins would be added to the cluster, and it would take $\mathcal{O}(p^{-1}) \sim \mathcal{O}(L^0)$ operations per spin to update a configuration, compared to $\mathcal{O}(L^d)$ operations *per spin* for a Metropolis algorithm. Taking into account the decrease in critical slowing down, we see that the efficiency of this method is typically a factor $\mathcal{O}(L^{d+z})$ larger than the

conventional Monte Carlo algorithm. Since our method only concerns the cluster-formation process, it may also be applied to the Swendsen–Wang method [6].

2.3 Building clusters in systems with long-range interactions

2.3.1 Long-range Hamiltonian

In systems with long-range interactions, the Hamiltonian (2.1) is generalized to

$$\beta \mathcal{H}_{\text{LR}} = - \sum_{\langle ij \rangle} K_{ij} \delta_{s_i s_j}, \quad (2.6)$$

where the sum runs over all spin pairs. As an example, we will take $K_{ij} = f r_{ij}^{-(d+\sigma)}$ ($f > 0$), which is one of the most commonly studied long-range interactions and to which also a large part of this thesis will be devoted. Here r_{ij} denotes the distance between spins s_i and s_j , d is the dimensionality of the system and $\sigma > 0$ is a parameter which determines the power-law decay of the interaction. We have written the exponent as the sum of d and σ to emphasize the fact that the integrated interaction does not converge for $\sigma \leq 0$.

We now have to devise an algorithm to build a cluster of spins, activating bonds between each pair of spins with a probability given by Eq. (2.4) in which K is replaced by K_{ij} . For simplicity we discuss here a one-dimensional system, but below the method will be generalized to arbitrary dimensionalities. We start with a spin on a randomly chosen site i and activate bonds between this spin and all other spins s_j in the system with a probability $p(s_i, s_j) = \delta_{s_i s_j} p_{ij}$, where p_{ij} denotes the probability of activating a bond between two spins in the same state at distance $|i - j|$ (in units of lattice spacing). Generalizing Eq. (2.4), we find $p_{ij} = 1 - \exp[-f|i - j|^{-(d+\sigma)}] = 1 - \exp(-K_{ij})$. Each time we activate a bond, the corresponding spin is added to the cluster. Furthermore, the spin address is placed on the *stack*. This is a list of spin addresses from which an address is removed once it has been read. When all neighbours of the first spin have been considered, we read a new spin from the stack and repeat the process. This cycle ends when the stack is empty, i.e., if all neighbours of all spins in the cluster have been considered. The spin from which we are currently activating bonds will be called the *current spin*. Now, the essential point of our algorithm is the avoidance of considering each single bond. The key element in achieving this lies in splitting up the bond-activation probability $p(s_i, s_j)$ into two parts, namely the Kronecker delta testing whether the spins s_i and s_j are identical¹ and the “provisional” bond-activation probability p_{ij} . This enables us to define the

¹For convenience, the term “identical” will be used to refer to spins in the same state.

concept of the *cumulative bond probability* $C(k)$, from which we can read off which bond is the next one to be provisionally activated,

$$C(j) \equiv \sum_{n=1}^j P(n) \quad (2.7)$$

with

$$P(n) = \left[\prod_{m=1}^{n-1} (1 - p_m) \right] p_n . \quad (2.8)$$

$p_j \equiv 1 - \exp(-K_j)$ is an abbreviation for p_{0j} (and $K_j \equiv K_{0j}$), i.e., we define the origin at the position of the current spin. $P(n)$ is the probability that in the first step $n - 1$ bonds are skipped and the n th bond is provisionally activated. Now the next bond j that is provisionally activated is determined by a (pseudo)random number $g \in [0, 1)$: $j - 1$ bonds are skipped if $C(j - 1) \leq g < C(j)$. If the j th bond is placed to a spin s_j that is indeed identical to the current spin s_i then s_j is added to the cluster (i.e., the j th bond is activated). Subsequently we skip again a number of bonds before another bond at a distance $k > j$ is provisionally activated. Due to the requirement $k > j$ we must shift the function P ,

$$P_j(k) = \left[\prod_{m=j+1}^{k-1} (1 - p_m) \right] p_k , \quad (2.9)$$

and Eq. (2.8) is simply a special case of Eq. (2.9). The appropriate cumulative probability is now given by a generalization of Eq. (2.7),

$$C_j(k) = \sum_{n=j+1}^k P_j(n) . \quad (2.10)$$

By using the specific form of the bond-activation probability one finds that this reduces to

$$C_j(k) = 1 - \exp \left(- \sum_{n=j+1}^k K_n \right) , \quad (2.11)$$

i.e., the probability that the next bond will be activated to a spin at a distance in the range $[j+1, k]$ is given by an expression that has the same form as the original bond-activation probability, in which the coupling constant is replaced by the sum of all the couplings with the spins in this range. In the following subsections we consider two possibilities of calculating the bond distance k from a given $C_j(k)$.

2.3.2 Look-up table

The first possibility is the construction of a look-up table. This means that we carry out the sum in (2.11) explicitly for a large number of distances k , up to a certain cutoff, and store the results in a table. Then, after drawing a random number, we can derive the corresponding bond distance from this table. In principle we need for each value of j another look-up table containing the $C_j(k)$. This is hardly feasible and fortunately not necessary, as follows from a comparison of Eqs. (2.7) and (2.10). Namely (assume $k > j$),

$$\begin{aligned} C(k) = C_0(k) &= C(j) + \left[\prod_{i=1}^j (1 - p_i) \right] C_j(k) \\ &= C(j) + [1 - C(j)] C_j(k) \end{aligned} \quad (2.12)$$

or $C_j(k) = [C(k) - C(j)]/[1 - C(j)]$. So we can calculate $C_j(k)$ directly from $C(k)$. In practice one realizes this by using the bond distance j of the previous bond that was provisionally activated to rescale the (new) random number g to $g' \in [C(j), 1]$; $g' = C(j) + [1 - C(j)]g$. Since we only consider ferromagnetic interactions, $\lim_{j \rightarrow \infty} C(j)$ exists and is smaller than 1, cf. Eq. (2.11).

This method is very fast, since we have to calculate all cumulative probabilities only once, but it has two major drawbacks. First, we can accommodate only a limited number of bond distances in our look-up table and must therefore devise some approximation scheme to handle the tail of the long-range interaction, which is essential for the critical behaviour in the case of slowly decaying interactions (small σ). This issue is addressed in the next subsection. Secondly, this method is impractical in more than one dimension, as the number of distances for which the cumulative bond probability has to be calculated increases quickly with the dimensionality of the system (for a fixed cutoff).

Finally, let us mention here one detail that has been omitted in the above discussion. In Eqs. (2.8) and (2.9), p_m denotes the probability of activating a bond to a spin at distance m . This means that this is the probability of a bond to the right *or* to the left. This can be taken into account by doubling the interaction strength K_m . Once a bond distance m has been obtained, its direction can be determined by an additional random number. Some care has to be exercised to ensure that a bond at the same distance but in the opposite direction is still allowed.

2.3.3 Continuous bond probability

An alternative for the look-up table exists for interactions which can be explicitly summed. In those cases, Eq. (2.11) can be solved for k , yielding an expression for the bond distance in terms of $C_j(k)$, i.e., in terms of the random number g . For the

interaction $K_{ij} = f|i - j|^{-(d+\sigma)}$ the sum appearing in the right-hand side of (2.11) is (for $j = 0$) the truncated Riemann zeta function, which cannot be expressed in closed form. However, we may approximate this sum by an integral,

$$\sum_{n=j}^k K_n = \sum_{n=j}^k \frac{f}{n^{d+\sigma}} \approx f \int_{j-\frac{1}{2}}^{k+\frac{1}{2}} dx x^{-(d+\sigma)}. \quad (2.13)$$

By replacing the sum by this integral we still have an exact Monte Carlo scheme, but the interaction has been altered from K_{ij} to

$$K(|i - j|) = f \int_{|i-j|-\frac{1}{2}}^{|i-j|+\frac{1}{2}} dx x^{-(d+\sigma)}. \quad (2.14)$$

Since both interactions exhibit the same long-range behaviour, we expect the same universal properties, e.g., the same critical exponents. However, their short-range behaviour differs, so all nonuniversal quantities, such as the critical temperature, will have different values. We can estimate the difference between the discrete and the continuous interaction by expanding the integrand in Eq. (2.14) in a Taylor series,

$$\begin{aligned} K(m) &= \int_{m-\frac{1}{2}}^{m+\frac{1}{2}} dx \frac{f}{x^{d+\sigma}} = K_m + K_m^{(2)} \int_{m-\frac{1}{2}}^{m+\frac{1}{2}} dx \frac{1}{2}(x - m)^2 + \mathcal{O}(K_m^{(4)}) \\ &\approx K_m + \frac{1}{24} K_m^{(2)}. \end{aligned} \quad (2.15)$$

So up to leading order in $1/m$ the relative difference between K_m and $K(m)$ is given by

$$\frac{1}{24} \frac{K_m^{(2)}}{K_m} = \frac{(d + \sigma)(d + \sigma + 1)}{24m^2}. \quad (2.16)$$

This approach is easily generalized to any number of dimensions. The interaction with a spin at lattice site \mathbf{n} is then given by the integral of K over the elementary d -dimensional (hyper)cube centered around \mathbf{n} and the cumulative bond probability yields the (not necessarily integer-valued) distance k at which the first provisional bond is placed. To this end, the sum in (2.11) is replaced by a d -dimensional integral of the coupling K . As K is isotropic, only an integral over the radius remains, which runs from the minimal bond distance (j) up to k . Thus for $d = 2$ Eq. (2.11) reduces to

$$C_j(k) = 1 - \exp \left[-\frac{2\pi f}{\sigma} \left(\frac{1}{j^\sigma} - \frac{1}{k^\sigma} \right) \right] \quad (2.17)$$

and in $d = 3$ the factor 2π is simply replaced by 4π . Equating $C_j(k)$ to the random number g we find

$$k = \left[j^{-\sigma} + \frac{\sigma}{2\pi f} \ln(1 - g) \right]^{-1/\sigma}. \quad (2.18)$$

Rescaling of the random number is no longer required: the lowest value, $g = 0$, leads to a provisional bond at the same distance as the previous one, $k = j$. If $g = C_j(\infty) = 1 - \exp[-(2\pi f/\sigma) j^{-\sigma}]$ the next provisional bond lies at infinity and thus $g \in [C_j(\infty), 1)$ yields no bond at all. Once the distance k has been obtained, $d - 1$ further random numbers g_1, g_2, \dots are required to determine the *direction* of the bond. In $d = 2$, we set $\phi = g_1/(2\pi)$. The coordinates of the next provisional bond (relative to the current spin) are then $(r_x, r_y) = (k \cos \phi, k \sin \phi)$, which are rounded to the nearest integer coordinates. Finally, the periodic boundary conditions are applied to map these coordinates onto a lattice site. For the next provisional bond, j is set equal to k (*not* to the rounded distance!) and a new k is determined. If no bond has been placed yet, j is set to $1/2$, the lowest possible bond distance. Hence it is possible to find a $1/2 \leq k < \sqrt{2}/2$ and an angle ϕ such that the corresponding lattice site is the origin. This does not affect the bond probabilities, but it is of course a “wasted” Monte Carlo step. For $d = 3$ the process is similar, except that we need another random number g_2 to determine a second angle $-\pi/2 < \psi \leq \pi/2$, such that $\sin \psi$ is distributed uniformly; $\sin \psi = 1 - 2g_2$. The bond coordinates are given by $(k \cos \psi \cos \phi, k \cos \psi \sin \phi, k \sin \psi)$.

This approach can also be applied in the one-dimensional case, where the geometrical factor 2π in (2.17) must be replaced by 2, which reflects the fact that bonds can be put to the left and to the right of the origin. The direction of the bond is then simply determined by another random number. This approach can be used to cope with the first problem mentioned at the end of Sec. 2.3.2, namely the limited size M of the look-up table: beyond the bond distance M the sum in (2.11) is approximated by an integral. Thus, if the random number g lies in the interval $[C(M), C(\infty))$, the bond distance k is determined from the one-dimensional version of (2.18), where the lower part of the integral is replaced by an explicit sum

$$k = \left[\left(M + \frac{1}{2} \right)^{-\sigma} + \sigma \left(\frac{1}{K} \ln(1 - g) + \sum_{n=1}^M \frac{1}{n^{1+\sigma}} \right) \right]^{-1/\sigma}. \quad (2.19)$$

Here, the geometrical factor is absent, since the expressions in Sec. 2.3.2 are concerned with one direction only. The use of an additional random number may be avoided by treating “left” and “right” separately in the simulations. The approximation (2.19) effectively introduces a modification of the spin–spin interaction, which however can be made arbitrarily small by increasing M . Note that the offset $1/2$ in

the first term ensures a precise matching of the discrete sum and the integral approximation: the random number $g = C(M) = 1 - \exp[-K \sum_{n=1}^M n^{-(1+\sigma)}]$ yields $k = M + 1/2$ which is precisely the lowest k that is rounded to the integer bond distance $M + 1$.

The accuracy of this procedure is further limited by the finite resolution of random numbers. Suppose, e.g., that the original random numbers are integers in the range $[0, 2^{32} - 1]$. Then the discreteness of the random numbers is no longer negligible for bond distances l such that $C(l) - C(l - 1)$ is of the order 2^{-32} . For higher dimensionalities, the discreteness of the angles also limits the lattice sites that can be selected for a provisional bond, but this generally occurs at distances larger than l . Once the value of l has been determined, with a safe margin, there are various approaches to this limitation. One may, e.g., draw another random number to determine the precise bond distance. A simpler approach is to distribute all bonds beyond l uniformly over the lattice, in order to prevent that certain lattice sites are never selected. However, one should take care that such simple approaches do not modify the critical behaviour in an essential way. If l is relatively small, the error introduced by a random distribution of the bond distances might be larger than the effect of an interaction which decreases slightly nonmonotonically at large distances. Furthermore, in order to preserve the symmetry of the lattice, such a uniform distribution of the bonds should occur outside a square (cube) with sides that are a multiple of the linear system size instead of outside a circle (sphere) with radius l .

2.3.4 Comparison to conventional cluster algorithms

We may check independently that the probability of activating the first bond at a distance k , as calculated from the cumulative probability, is equal to that in the conventional approach. We first treat the situation in which all bond-activation probabilities p are equal.

Consider a cluster spin, say s_0 , with a chain of neighbours denoted s_1, \dots, s_k , of which m spins are antiparallel to s_0 and $l = k - m$ spins are parallel to s_0 , among which s_k . In the conventional Wolff cluster algorithm, the probability that s_k is the *first* spin to be added to the cluster is given by

$$1^m (1 - p)^{l-1} p = (1 - p)^{l-1} p. \quad (2.20)$$

On the other hand, if we use the cumulative bond probability (2.10), this probability is calculated as follows. Either the k th spin is selected directly [if the first random number lies between $C(k - 1)$ and $C(k)$] or one of the m antiparallel spins is selected, say s_a , which is of course not added to the cluster. In the latter case, another random number is drawn and a new spin is selected. Again, this may be the k th spin, or one of the remaining antiparallel spins between s_a and s_k . Now, let us show that the sum of these probabilities of adding s_k as the first spin to the cluster

is equal to (2.20). Denote the number of selected, “intermediate”, antiparallel spins by i . There are $\binom{m}{i}$ possibilities of selecting i intermediate spins. The probability of selecting s_k after each of these sequences of spins is $p^i(1-p)^{m-i}(1-p)^{l-1}p$. The total probability is the sum over all numbers of intermediate spins

$$\sum_{i=0}^m \binom{m}{i} p^i(1-p)^{m-i}(1-p)^{l-1}p = (1-p)^{l-1}p, \quad (2.21)$$

which is indeed equal to (2.20).

Now, we can extend this reasoning to the situation in which not all p are equal. We assume again that there are m sequentially numbered antiparallel spins and introduce a mapping $A[n]$, such that $A[1], \dots, A[i]$ are the i selected intermediate spins and $A[i+1], \dots, A[m]$ the remaining antiparallel spins. The factor $p^i(1-p)^{m-i}$ in Eq. (2.21) is now replaced by $\prod_{j=1}^i p_{A[j]} \prod_{j=i+1}^m (1-p_{A[j]})$ and the problem is reduced to proving that the sum over all permutations A and all numbers $i \in [0, m]$ yields unity. Although we cannot use the binomial theorem in this case, it is easily seen that this statement holds. Namely, for *any* sequence characterized by the product $p_{A[1]} \dots p_{A[i]}(1-p_{A[i+1]}) \dots (1-p_{A[j]}) \dots (1-p_{A[m]})$ ($i < j \leq m$) there exists an identical sequence except that the intermediate spin $A[j]$ is selected as well. In the corresponding product, the factor $(1-p_{A[j]})$ is replaced by $p_{A[j]}$ and the two products add up to a new product in which the factor for the spin in case is equal to unity. This procedure can be repeated until all permutations have been added. In words, this simply comes down to the statement that any intermediate spin is selected or not, and the total probability for this is of course unity.

2.4 A “trivial” example: the mean-field model

As an illustration of the method described in this chapter, we have carried out a Monte Carlo simulation of the mean-field model, described by the Hamiltonian

$$\beta \mathcal{H}_{\text{MF}} = -\frac{K}{2N} \sum_i \sum_{j \neq i} s_i s_j \quad (s = \pm 1), \quad (2.22)$$

in which N is the number of spins in the system. This model can be regarded as an extremely long-range system, since each spin interacts equally with every other spin. It is equivalent to the system described by Eq. (2.6) with $K_{ij} = fr_{ij}^{-(d+\sigma)}$ in the limit $\sigma \downarrow 0$, where periodic boundary conditions are employed and the coupling K_{ij} must be suitably normalized.² It has been solved exactly and exhibits a phase transition

²For the one-dimensional case with interactions decaying as $n^{-(d+\sigma)}$, this can be easily shown by calculating the effective coupling between two spins. This yields a sum over all periodic images, which can be expressed in terms of the generalized Riemann zeta function $\zeta(s, q) \equiv \sum_{i=0}^{\infty} (i+q)^{-s}$ ($q > 0$). Since $\lim_{\sigma \downarrow 0} \sigma \zeta(1+\sigma, q) = 1$, we find that all spin-spin interactions are equally strong.

at $K = K_c = 1$ (see, e.g., Chapter 3 of Ref. [13]; note the difference in the coupling constant in Eq. (3.1.3) of this reference compared to Eq. (2.22) above). Furthermore, it has classical values for the critical exponents α , β , γ and δ . It should be noted that for this particular model a relatively efficient Monte Carlo simulation can be carried out even with the Metropolis algorithm, since the total interaction energy between one spin s_i and all the other spins is simply given by

$$-\frac{K}{2N}s_i \sum_{j \neq i} s_j = -\frac{K}{2N}s_i(M - s_i). \quad (2.23)$$

Here $M = Nm = \sum_j s_j$ is the total magnetization. Of course, this is only possible because the coupling between all spin pairs is equal in this model. In our simulations, which purely serve as a test for the algorithm described above, we have *not* used the total magnetization. For other cluster simulations of this model, see Refs. [12, 14].

We have carried out Monte Carlo simulations for systems with sizes in the range 2 to 64 000, constructing 10^6 Wolff clusters per simulation. This took less than 30 hours of CPU time on a modest workstation, of which approximately 20 hours were spent on the two largest systems, consisting of 32 000 and 64 000 spins, respectively.

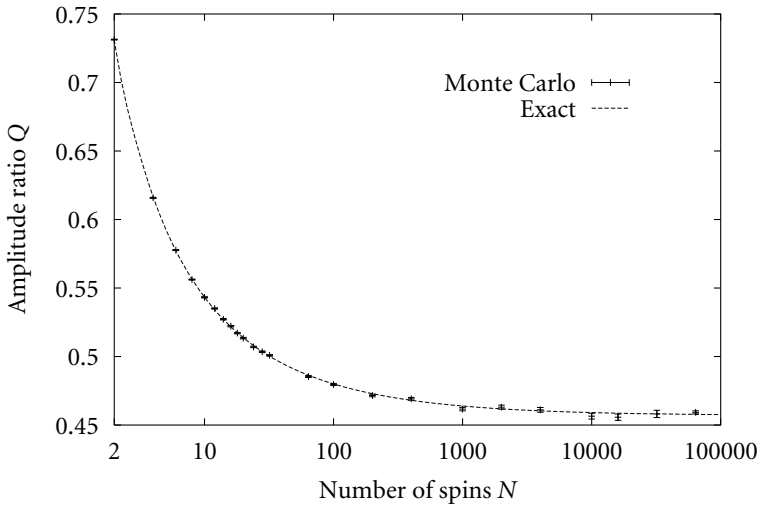


Figure 2.1: Comparison between exact (dashed line) and Monte Carlo data for the dimensionless amplitude ratio Q at the critical temperature for system sizes in the range 2 to 64 000. For most systems, the size of the error bars does not exceed the symbol size. The exact data for system sizes smaller than 10 000 were obtained by explicit summation over all values of the magnetization, whereas the data for larger systems were calculated from the finite-size expansion (A.14).

Of the various quantities that were sampled we consider here only the dimensionless amplitude ratio

$$Q \equiv \frac{\langle m^2 \rangle^2}{\langle m^4 \rangle}, \quad (2.24)$$

which is directly related to the fourth-order cumulant introduced by Binder [15]. Figure 2.1 shows the Monte Carlo data for $Q(K_c)$ as a function of the system size together with exactly calculated values. One observes that the Monte Carlo data conform quite well to the exact curve. In the thermodynamic limit, this amplitude ratio takes at the critical temperature the value $4\Gamma^2(\frac{3}{4})/\Gamma^2(\frac{1}{4}) \approx 0.45694658\dots$. In Appendix A (page 195), we derive an expression for $Q(K_c)$ for finite systems to order $1/N$ by expansion of the partition function. The form of this expansion agrees with the expression for Q_N obtained from finite-size scaling [16],

$$Q_N = Q_\infty + a_1 N^{y'} + a_2 N^{2y'} + a_3 N^{3y'} + \dots \\ + b_1 t N^{y_t} + b_2 (t N^{y_t})^2 + \dots \quad (2.25)$$

Here y' is the exponent of the leading correction to scaling (which is derived in Appendix A as well), y_t is the temperature exponent and t represents the temperature field, in which we have also included a correction to scaling,

$$t = (K - K_c)[1 + b_3 N^{y'}], \quad (2.26)$$

where K_c denotes the critical coupling. Note that we have expressed the scaling function in terms of N . The usual values for the exponents are recovered by replacing N by L^d .

In Fig. 2.2, Q is plotted versus the spin–spin coupling for a range of system sizes. Fitting our data for $N \geq 4$ to Eq. (2.25), we have obtained the results listed in Table 2.1. The estimates for Q , K_c , y_t and a_1 were obtained while keeping y' fixed at its theoretical value. *Vice versa*, the result for y' was obtained in a similar analysis, in

Table 2.1: Results of a least-squares analysis of the Monte Carlo data for the mean-field model. The numbers in parentheses represent the errors in the last decimal places.

	Theory	MC
Q_∞	0.45694658...	0.4565 (5)
K_c	1	0.99998 (3)
y_t	$\frac{1}{2}$	0.498 (4)
y'	$-\frac{1}{2}$	-0.52 (4)
a_1	0.214002...	0.219 (6)

which the thermal exponent γ_t was kept fixed. Given the amount of computer time invested, the accuracy of the Monte Carlo data is very good and the agreement between the theoretical values and the results of the Monte Carlo simulations is quite satisfactory.

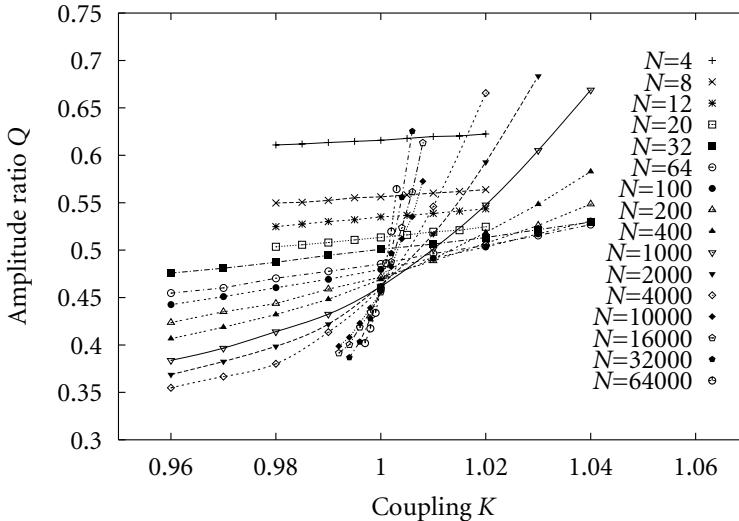


Figure 2.2: The dimensionless amplitude ratio Q as a function of the spin–spin coupling for several system sizes. For clarity the following system sizes that were used in the finite-size analysis have been omitted from the figure: $N = 6, 10, 14, 16, 18, 24, 28$. The size of the error bars does not exceed the symbol size. Note the large corrections to scaling for small systems.

2.5 Generalizations

The algorithm described in Sec. 2.3 can be generalized in several ways. First, the form of the interaction may be modified. As long as the interaction is an integrable function of the distance, this generalization is completely straightforward. If the interaction is not integrable, one can use a look-up table in the one-dimensional case, whereas an approximation scheme may be devised for a system of higher dimensionality. Secondly, the algorithm may also be applied to long-range XY and Heisenberg models. The generalization to these systems is as follows. First, for each new cluster a spin-flip direction i is chosen at random. Then each spin which may be added to the cluster is selected just as in the case of the Potts model, i.e., with a probability $1 - \exp(-K)$, where K is the Potts coupling with this spin. So, the concept of the *cumulative probability* can be applied in precisely the same way. However, the condi-

tion in the Potts model that only bonds between identical spins are activated, which is expressed by the Kronecker delta in Eq. (2.4), must be replaced by the condition that the bond between \mathbf{s}_1 and \mathbf{s}_2 is activated with probability

$$\frac{1 - \exp(\min\{0, Ks_{1,i}s_{2,i}\})}{1 - \exp(-K)} . \quad (2.27)$$

The numerator in this expression is equal to that derived by Wolff [1, Eq. (5)], where $s_{k,i}$ refers to the projection in direction i of spin \mathbf{s}_k . It should be noted that the spin from which we are currently activating bonds, \mathbf{s}_1 , has already been flipped, which explains the absence of a minus sign in front of K . The denominator comes from the fact that we have selected spin \mathbf{s}_2 with a probability $1 - \exp(-K)$. So once a spin has been selected, its component in direction i is reversed with a probability given by Eq. (2.27). In this way, the algorithm described above can be extended to general $O(n)$ models, just as the original Wolff algorithm.

Furthermore, an extension of this algorithm to the case in which additional antiferromagnetic interactions are present may be envisaged (cf. Refs. [17, 18]). Although competing interactions will move the system away from the percolation threshold and thus annul the advantage of the suppression of critical slowing down, the gain due to the fact that not every bond has to be considered remains in existence.

References

- [1] U. Wolff, *Phys. Rev. Lett.* **62**, 361 (1989).
- [2] R. H. Swendsen, J.-S. Wang and A. M. Ferrenberg, *New Monte Carlo Methods for Improved Efficiency of Computer Simulations in Statistical Mechanics*, in *The Monte Carlo Method in Condensed Matter Physics*, edited by K. Binder (Springer, Berlin, 1992).
- [3] P. W. Kasteleyn and C. M. Fortuin, *J. Phys. Soc. Jpn. Suppl.* **26s**, 11 (1969).
- [4] C. M. Fortuin and P. W. Kasteleyn, *Physica* **57**, 536 (1972).
- [5] R. J. Baxter, S. B. Kelland and F. Y. Wu, *J. Phys. A* **9**, 397 (1976).
- [6] R. H. Swendsen and J.-S. Wang, *Phys. Rev. Lett.* **58**, 86 (1987).
- [7] M. P. Nightingale and H. W. J. Blöte, *Phys. Rev. Lett.* **76**, 4548 (1996).
- [8] C. F. Baillie and P. D. Coddington, *Phys. Rev. B* **43**, 10617 (1991).
- [9] D. Stauffer and R. Knecht, *Int. J. Mod. Phys. C* **7**, 893 (1996).
- [10] P. Tamayo, R. C. Brower and W. Klein, *J. Stat. Phys.* **58**, 1083 (1990).
- [11] S.-k. Ma, *Modern Theory of Critical Phenomena* (Addison-Wesley, Redwood, California, 1976).
- [12] N. Persky, R. Ben-Av, I. Kanter and E. Domany, *Phys. Rev. E* **54**, 2351 (1996).
- [13] R. J. Baxter, *Exactly Solved Models in Statistical Mechanics* (Academic, London, 1982).

- [14] T. S. Ray, P. Tamayo and W. Klein, *Phys. Rev. A* **39**, 5949 (1989).
- [15] K. Binder, *Z. Phys. B* **43**, 119 (1981).
- [16] M. N. Barber, *Finite-size Scaling*, in *Phase Transitions and Critical Phenomena*, Vol. 8, edited by C. Domb and J. L. Lebowitz (Academic, London, 1983).
- [17] J.-S. Wang, R. H. Swendsen and R. Kotecký, *Phys. Rev. Lett.* **63**, 109 (1989).
- [18] J.-S. Wang, R. H. Swendsen and R. Kotecký, *Phys. Rev. B* **42**, 2465 (1990).

Chapter 3

Critical properties of the three-dimensional Ising model

3.1 Introduction

The objective of this chapter is twofold. In the first place we present the results of an accurate study of three models which are expected to belong to the universality class of the three-dimensional Ising model. Very precise results for the critical properties of these models are obtained. Secondly, in the course of this chapter we introduce the concepts that will return in many of the investigations presented in later chapters, such as the derivation of scaling functions and the determination of the critical point with the help of a universal amplitude ratio. The relative simplicity of the models treated in the current chapter allows for a particular clear illustration of these concepts.

As mentioned in Chapter 1, the universality hypothesis states that the nature of a phase transition is solely determined by global properties of the system, such as its dimensionality and the symmetry of the order parameter. Thus, it is believed that most three-dimensional systems with *short-range* interactions and a scalar order parameter (such as density or unidirectional magnetization) belong to the 3D Ising universality class. This implies that the critical exponents, as well as other universal quantities, are identical for all these models. This universality class comprises, in addition to anisotropic magnetic systems, also models for binary alloys, gas-liquid systems and liquid mixtures.

In the case of two-dimensional Ising-like models, the evidence that universality holds is very strong. However, in three dimensions, where exact results are scarce and numerical techniques tend to be less accurate than in two dimensions, the situation is less satisfactory. Numerical uncertainties in the renormalization exponents amount to the order of several times 10^{-3} . Since many years the most accu-

rate results are those obtained by ε -, coupling-constant and series expansions [1–11], whereas in recent times quite accurate estimates have also been obtained by the coherent-anomaly method [12] and the Monte Carlo renormalization-group method [13, 14]. However, the increasing power of computers as well as the advent of new algorithms has opened the way to very precise numerical studies of Ising-like models. As far as the universal properties are concerned, the simulation of spin models offers a clear advantage because of the availability of highly efficient cluster algorithms that are easily implemented. This has led to increasingly accurate results from Monte Carlo-based methods [15–26].

However, slight differences occur between recent results for the scaling dimensions (exponents). One possible explanation is that universality is not satisfied. In order to solve the issue whether these deviations are real, it is desirable to obtain more accurate Monte Carlo data for the supposed universal quantities. An important obstacle for higher accuracies of these analyses is the presence of corrections to scaling. The dominant correction is attributed to an irrelevant renormalization exponent with an approximate value $y_1 \approx -0.83$ [8]. This means that the corrections decay rather slowly (albeit we will encounter much worse cases in later chapters) and thus jeopardize the accuracy of the analysis. For this reason, we explore what modifications of the simple cubic Ising model with nearest-neighbour interactions can influence the amplitude of these corrections to scaling. If we can thus suppress the leading irrelevant field, we may expect a decrease of the ill effects due to the corrections to scaling. One can, for instance, choose a different lattice structure. Series expansions using the body-centered cubic lattice [8] have indicated that corrections to scaling are relatively small in this model. However, here we prefer to introduce continuously variable parameters to adjust the irrelevant scaling field.

It is known [27] that the introduction of positive couplings with a range beyond the nearest neighbours in the simple cubic Ising model leads to a decrease of the correction-to-scaling amplitudes. We quote some results for the Hamiltonian

$$\mathcal{H}/k_B T = -K_{\text{nn}} \sum_{\langle \text{nn} \rangle} s_i s_j - K_{2\text{n}} \sum_{(2\text{n})} s_i s_j - K_{3\text{n}} \sum_{[3\text{n}]} s_i s_j - K_{\square} \sum_{\square} s_i s_j s_k s_l, \quad (3.1)$$

where the subscripts $\langle \text{nn} \rangle$, (2n) and $[3\text{n}]$ indicate a sum over nearest-neighbour, second-neighbour (diagonals of the elementary faces) and third-neighbour pairs (body diagonals in the elementary cubes), respectively, and \square indicates a sum over four-spin products in all elementary faces of the cubic lattice. The associated couplings are denoted by K_{nn} , $K_{2\text{n}}$, $K_{3\text{n}}$ and K_{\square} , respectively. The spins s_i can assume the values $+1$ and -1 . These results were obtained by Monte Carlo simulation on the Delft Ising System Processor (DISP) [28, 29]; they indicated that the introduction of positive $K_{2\text{n}}$, $K_{3\text{n}}$ or K_{\square} reduces the correction-to-scaling amplitude. Third-neighbour couplings $K_{3\text{n}}$ appear to be quite effective; for a ratio $K_{3\text{n}}/K_{\text{nn}} \approx 0.4$ the

corrections were found to be small. Considerably stronger second-neighbour couplings are required to obtain a similar effect [27].

Another approach is to introduce a third spin state $s_i = 0$: this yields the spin-1 Ising model. The weight of the $s_i = 0$ state can be varied by means of a term $D \sum_i s_i^2$ in the Hamiltonian. Preliminary calculations showed that the corrections become small for $D \approx 0.7$. In our actual simulations we have used $D = \ln 2$, for reasons that will be explained in Sec. 3.2.

Thus, we have selected the following three Ising models: (1) the spin- $\frac{1}{2}$ Ising model with $K_{3n}/K_{nn} = 0$ (the nearest-neighbour model), (2) the spin- $\frac{1}{2}$ Ising model with $K_{3n}/K_{nn} = 0.4$ and (3) the spin-1 model with $D = \ln 2$ and nearest-neighbour interactions. The algorithms used to simulate these models are described in Sec. 3.2. In addition to corrections to scaling, another obstacle to higher accuracies is the requirement of sufficiently accurate random numbers, in order to avoid biased results. In Sec. 3.3 we briefly comment on the random-number generator that has been used. An analysis of the results for the dimensionless ratio $Q = \langle m^2 \rangle^2 / \langle m^4 \rangle$ is given in Sec. 3.4, followed by an analysis of the magnetic and temperature renormalization exponents in Sec. 3.5. The results for the three models turn out to satisfy universality: they are equal within the statistical inaccuracies. Assuming universality, Q as well as the critical points of the three models can be obtained with a better precision, as is demonstrated in Sec. 3.6. Finally, a discussion of these results in relation with the existing literature and with fundamental questions concerning universality is presented in Sec. 3.7.

3.2 Models and algorithms

The present Monte Carlo analysis concerns three different Ising models. These can be represented in terms of a spin-1 Hamiltonian on the simple cubic lattice,

$$\mathcal{H}/k_B T = -K_{nn} \sum_{\langle ij \rangle} s_i s_j - K_{3n} \sum_{[kl]} s_k s_l + D \sum_m s_m^2, \quad (3.2)$$

where the subscripts “nn” and $\langle ij \rangle$ refer to nearest neighbours and “3n” and $[kl]$ to third-nearest neighbours (along body diagonals of the elementary cubes), respectively. The spins can assume three discrete values $s_i = 0, \pm 1$. The three models are specified in Table 3.1.

For $D = -\infty$ the $s_i = 0$ states are excluded and thus models 1 and 2 can be simulated by the Swendsen–Wang (SW) [30], the largest-cluster (LC) [31] or the Wolff [32] method. In cluster algorithms, one has to “activate” a bond between two spins s_i and s_j , coupled with strength K_{ij} , with a probability $p(K_{ij}) \delta_{s_i s_j}$, where $p(K_{ij}) \equiv [1 - \exp(-2K_{ij})]$. The presence of different types of bonds in model 2 thus leads to different bond probabilities but poses no further problems. If the bond

Table 3.1: The ratio K_{3n}/K_{nn} and the value for D [see Eq. (3.2)] for the three models.

Model #	K_{3n}/K_{nn}	D	Description of model
1	0	$-\infty$	spin- $\frac{1}{2}$ model with nn couplings
2	0.4	$-\infty$	spin- $\frac{1}{2}$ model with nn and 3n couplings
3	0	$\ln 2$	spin-1 model with nn couplings

is active, sites i and j belong to the same cluster. The simplest way to simulate this is to draw a random number for each bond and check whether it is smaller than $p(K_{ij})\delta_{s_i,s_j}$. Following this procedure, the speed of the algorithm decreases as the number of interacting neighbours increases. When the couplings (and hence the bond probabilities) are small, a more efficient procedure is possible, which in essence is a simplified version of the algorithm described in Chapter 2. As a first step in the SW or LC cluster formation process one obtains, for each type of bond K_{ij} , a list of bonds that should be activated if they connect equal spins. To this purpose, one introduces bond variables $b_{ij} = 0$ or 1 ; the probability that $b_{ij} = 1$ is equal to $p(K_{ij})$. The distribution $P(k) \equiv p(1-p)^{k-1}$, where we write p as an abbreviation for $p(K_{ij})$, expresses the probability that $(k-1)$ subsequent bond variables equal zero, while the k th bond variable is one. Thus one random number r can be transformed into an integer k ,

$$k = 1 + [\ln(r)/\ln(1-p)] , \quad (3.3)$$

where the square brackets denote the integer part. After evaluation of k , the next $(k-1)$ entries in the list of bond variables are set to zero and the k th variable is set to one. By repetition of these steps a complete list of bond variables (for all bonds with strength K_{ij} in the lattice) is obtained. Such lists are generated for each different type of bond. After completion of these lists, the cluster formation is trivial. This procedure was found to improve the speed of the simulation of model 2 considerably. One may still choose between the Swendsen–Wang or largest-cluster method. The latter method was observed to lead to shorter relaxation times and is therefore more efficient. The same principle was applied to Wolff-type simulations of model 2. Random numbers are, as above, transformed into integers k . During the cluster formation, $(k-1)$ bonds of the pertinent type are skipped and the spin connected to the k th bond is added to the Wolff cluster provided that it has the right sign. This leads to a considerably faster Wolff algorithm, in particular because the generation of high-quality random numbers is relatively time consuming.

In the spin-1 case, transitions between zero and nonzero spin values require special attention. It is not immediately obvious how cluster algorithms could produce these transitions. We follow two different methods for the simulation of the spin-1

model. The first one uses a hybrid algorithm in which Metropolis sweeps alternate with cluster steps. The cluster algorithm acts on the nonzero spins only. Since we do not come close to the tricritical point where the ordered Ising phases meet the spin-zero phase, the regions of zero spins remain limited in size and we do not expect serious critical slowing down due to the equilibration between zero and nonzero spin values.

The second method uses a mapping on a spin- $\frac{1}{2}$ model. We consider a Hamiltonian with two spins $t_i = \pm 1$ and $u_i = \pm 1$ on site i (for all i) of the simple cubic lattice,

$$\mathcal{H}_h/k_B T = -M_1 \sum_{\langle ij \rangle} (t_i + u_i)(t_j + u_j) - M_2 \sum_m t_m u_m . \quad (3.4)$$

Using the transformation $s_i = (t_i + u_i)/2$ and $v_i = (1 + t_i)(1 - u_i)/4$, the partition function of this model is, up to a constant factor,

$$Z_h = \sum_{\{s_k\}} \left(\prod_{\langle ij \rangle} \exp [4M_1 s_i s_j] \prod_m \sum_{v_m=0}^{1-|s_m|} \exp [2M_2 s_m^2] \right) , \quad (3.5)$$

with $s_i = 0, \pm 1$. Summation over the allowed values of v_m yields a factor 2 if $s_m = 0$. Thus

$$Z_h = 2^N \sum_{\{s_k\}} \exp \left[4M_1 \sum_{\langle ij \rangle} s_i s_j + (2M_2 - \ln 2) \sum_m s_m^2 \right] , \quad (3.6)$$

where N denotes the number of spins in the system. This is, apart from the prefactor 2^N , precisely the partition sum for Eq. (3.2) for $K_{nn} = 4M_1$, $K_{3n} = 0$ and $D = \ln 2 - 2M_2$. Equation (3.4) may thus serve for the application of cluster algorithms to the spin-1 Ising model. The special choice $D = \ln 2$ leads to $M_2 = 0$ so that the spin- $\frac{1}{2}$ Hamiltonian simplifies. We have used three different methods to simulate the spin-1 model: the Metropolis–cluster (MLC) method, the full-cluster (FC) method and the Metropolis–Wolff (MW) method. In the Metropolis-type simulations the transition probabilities were chosen such that after each step the probability of a state is described by the Boltzmann distribution (so-called heat-bath probabilities). The MLC method alternates one Metropolis sweep with one largest-cluster inversion and the MW method alternates one Metropolis sweep with 5 or 10 (depending on the system size) Wolff steps. The FC method applies largest-cluster flips to the spin- $\frac{1}{2}$ representation of the model: no Metropolis sweeps are included here.

3.3 Random numbers

Significant systematic errors may be introduced in Monte Carlo simulations by using inadequate random-number generators. It is well known that linear congruential methods based on the truncation of 32-bit integers are unsuitable for long simulations. Even their period of about 10^9 would be too restrictive. On the other hand, also random-number generators based on binary feedback shift registers may introduce serious errors (see, e.g., Refs. [28, 33–36]). In most cases, the production rule selects two bits from the register and assigns their modulo-2 sum to the new bit. Thus the deviations from randomness are dominated by three-bit correlations. A number of algorithms of this type, using 127-bit shift registers with a period in the order of 10^{38} , have been rejected on the basis of long tests [29] using Metropolis simulations of the critical Ising model. Recent tests by Ferrenberg *et al.* [37] have shown that such deviations also occur when cluster algorithms are used together with random generators based on a generalized feedback shift register [38].

It is clear that, for the long simulations implied by the present analysis of the 3D Ising model, the random-number generators should be selected with great care. All our simulations, both those in this chapter and those in later chapters, employed random-number generators that are based on extensive research [39, 40]. In the majority of the simulations we used a generator based on a feedback shift register with a large length, which was then combined via an exclusive-or operation with another shift-register-based generator of a different length, in order to suppress the dominant (three-bit) correlations. These generators used the production rules $a_i = a_{i-9218} \oplus a_{i-9689}$ and $b_i = b_{i-97} \oplus b_{i-127}$, respectively, where a_i and b_i are 32-bit integers and \oplus stands for bitwise modulo-2 addition.

The data in Ref. [23] were obtained using a generator that combined the sequence a_i with random numbers generated by a multiplicative rule. No obvious discrepancies between those data and our results were observed, nor were there any systematic differences between the Swendsen–Wang, largest-cluster and Wolff-type simulations. Also in the case of models 2 and 3 we checked for the presence of significant differences between the result of the different types of spin-updating algorithms (see Table 3.2) but none were found. This may be viewed as a confirmation of the high quality of the random-number generator used.

3.4 A test of universality

We have performed extensive simulations of models 1, 2 and 3, using the cluster methods described in Sec. 3.2. The total simulation time amounts to approximately two years on three average workstations. We chose systems with size $L \times L \times L$ and periodic boundaries. The lengths of the runs for the various models and methods

are given in Table 3.2 for each system size.

We have sampled and analyzed the dimensionless amplitude ratio

$$Q_L(K_{\text{nn}}) = \frac{\langle m^2 \rangle_L^2}{\langle m^4 \rangle_L}, \quad (3.7)$$

where m is the magnetization density. This quantity, which will play an important rôle throughout this thesis, is directly related to the Binder cumulant $B \equiv -3 + 1/Q$ (see Ref. [41]; several equivalent definitions have been introduced by subsequent authors), which in turns differs by a (nontrivial) factor $(L/\xi)^d$ from the renormalized coupling constant. The finite-size scaling behaviour of Q_L can be derived within the framework provided by the renormalization-group theory. By $f(t, h, u, L^{-1}) = L^{-d}F$ we denote the free-energy density as a function of the temperature and magnetic scaling fields, an irrelevant field u and the finite-size field [42, 43]. Here, we define the free energy as $F = \ln Z$, so without the normal factor $-k_B T$. Its behaviour under renormalization with a scale factor b is

$$f(t, h, u, L^{-1}) = b^{-d} f(b^{y_t} t, b^{y_h} h, b^{y_u} u, b/L) + g(t, h), \quad (3.8)$$

where y_t , y_h and y_u are the pertinent renormalization exponents, $d = 3$ is the dimensionality and g is the analytic part of the transformation. In a ϕ^4 theory this analytic term does not depend on the magnetic scaling field, as this field only couples to the uniform magnetization (the $\mathbf{k} = \mathbf{0}$ mode in momentum space). However, in a lattice model this dependence cannot *a priori* be omitted. By differentiating k times with respect to h , and setting $b = L$ and $h = 0$, one obtains

$$f^{(k)}(t, u, L^{-1}) = L^{ky_h - d} f^{(k)}(L^{y_t} t, L^{y_u} u, 1) + g^{(k)}(t), \quad (3.9)$$

where the dependence on h is no longer needed and therefore suppressed. The expectation values of the second and fourth magnetization moments require differentiations of the free energy with respect to the physical magnetic field H ,

$$\langle m^2 \rangle = L^{-d} \left(\frac{\partial^2 f}{\partial H^2} \right)_{H=0} \quad (3.10)$$

and

$$\langle m^4 \rangle = L^{-3d} \left(\frac{\partial^4 f}{\partial H^4} \right)_{H=0} + 3L^{-2d} \left(\frac{\partial^2 f}{\partial H^2} \right)_{H=0}^2. \quad (3.11)$$

The Ising up-down symmetry implies that h is an odd function of H . Thus the correspondence between the derivatives with respect to h and H is

$$\frac{\partial^2 f}{\partial H^2} = f^{(2)} \left(\frac{\partial h}{\partial H} \right)^2 \quad (3.12)$$

Table 3.2: Length of Monte Carlo runs in millions of sampled configurations. SW stands for Swendsen–Wang, LC for largest cluster and W for Wolff. For SW and LC, each new configuration corresponds with one cluster decomposition of the lattice. In the Wolff case, 5 (5W) or 10 (10W) Wolff clusters were flipped before a new configuration was used for data taking. For the spin-1 model (model 3) LC, 5W and 10W are preceded by M in order to indicate a Metropolis sweep through the lattice. FC indicates the full-cluster algorithm for the spin-1 model; it flips the largest cluster of a spin- $\frac{1}{2}$ version of the model.

L	Model 1				Model 2				Model 3			
	SW	LC	5W	10W	SW	LC	5W	10W	FC	MLC	M5W	M10W
3	48	52	200			100	200		100	100	300	
4	160	40	200			150	100		100	100	300	
5	48	52	200			150	100		100	100	400	
6	48	52	200			150	100		100	100	400	
7	48	52	200			150	100		100	100	400	
8	48	52	200		10	140	100		100	100	400	
9	48	52	200		10	140	100		100	100	300	
10	48	52	200		10	140	100		100	100	300	
11	48	52	200			150	100		100	100	300	
12	28	72	200			150	100		100	100	200	
13	28	72	200			100	100				250	
14	28	72	200			100	100				200	
15	20	30		200		50		100			200	
16	20	30		150		50		100			200	
18	12	38		150		50		50			120	
20	20	10		70		50		50			120	
22	18	12		70		20		80			120	
24	8	12		80		20		80			150	
28	10	10		100		20		80			50	50
32	2	18		180		25		75				100
40		10		90		20		80				100

and

$$\frac{\partial^4 f}{\partial H^4} = f^{(4)} \left(\frac{\partial h}{\partial H} \right)^4 + 4f^{(2)} \frac{\partial h}{\partial H} \frac{\partial^3 h}{\partial H^3}, \quad (3.13)$$

where, as before, $f^{(k)}$ stands for $\partial^k f / \partial h^k$ and all derivatives with respect to H are evaluated at $H = 0$. In the vicinity of the finite-size limit (t small and L finite), we may Taylor-expand the right-hand side of Eq. (3.9) in t and u . After the appropriate substitutions, the finite-size expansion of $Q_L(K_{\text{nn}})$ follows as

$$Q_L(K_{\text{nn}}) = Q + a_1(K_{\text{nn}} - K_c)L^{\gamma_t} + a_2(K_{\text{nn}} - K_c)^2L^{2\gamma_t} + a_3(K_{\text{nn}} - K_c)^3L^{3\gamma_t} + \dots + b_1L^{\gamma_i} + b_2L^{\gamma_2} + \dots, \quad (3.14)$$

where the a_i and b_i are nonuniversal coefficients and $\gamma_2 = d - 2\gamma_h$. The last term is due to the above-mentioned possible field dependence of the analytic part g in Eq. (3.9). The nonlinear dependence of h on H leads to even more rapidly decaying contributions, which are omitted. Terms of the same form, but with different exponents, may be due to other (subdominant) irrelevant fields. Because powers of the geometric factor $\partial h / \partial H$ cancel in the first term, Q is a *universal* constant.

The bulk of the numerical data were taken at couplings $K_{\text{nn}} = 0.221653$, 0.128006 and 0.393410 for models 1, 2 and 3 respectively, close to the critical points. The results in terms of Q_L are collected in Table 3.3. A few points at somewhat different couplings were included in order to estimate the (thermal) coefficients a_i in Eq. (3.14). The procedure of the analysis is as follows. We computed $Q_L(K_{\text{nn}})$ for several values of L and K_{nn} (near the critical points K_c) for the three models and fitted Eq. (3.14) to the data. The following parameters were used as input: $\gamma_t = 1.584$ (4) (from ε -expansion [6]; because the data were taken at couplings so close to the critical points, the results of the fits are practically independent of the precise value); $\gamma_i = -0.83$ (5) (from series expansions [8]; the fit for model 1 is rather sensitive to the precise value) and $\gamma_2 = -1.963$ (3) (from renormalization arguments given above and the ε -expansion result [6] for the magnetic exponent; the fit is insensitive to the precise value because this is a subdominant correction to scaling). The results are summarized in Table 3.4. It is stressed that the error margins quoted here include the uncertainty due to the possible variations in γ_i , γ_t and γ_2 (γ_h). The fits for model 1 indicated that system sizes $L < 7$ should be discarded; they reveal finite-size effects not included in Eq. (3.14), exceeding the statistical error margins. The fits for models 2 and 3, which exhibit much smaller finite-size effects, include system sizes $L \geq 6$. The fit for model 2 clearly reveals a correction with exponent $\gamma_2 \approx -1.96$. In fact, the large residuals in the absence of such a correction demonstrated its presence. As indicated above, this correction may arise from the analytic part of the transformation, although we cannot exclude contributions due to a second irrelevant exponent. Since there is no obvious reason why this term should be

Table 3.3: Numerical results for the dimensionless ratio $Q_L = \langle m^2 \rangle_L^2 / \langle m^4 \rangle_L$ for the three Ising models defined in Sec. 3.2. These data were taken at couplings $K_{nn} = 0.221653, 0.128006$ and 0.393410 for models 1, 2 and 3, respectively.

L	Model 1	Model 2	Model 3
3	0.66839 (2)	0.64244 (3)	0.61894 (2)
4	0.65976 (2)	0.63164 (3)	0.62134 (2)
5	0.65373 (2)	0.62642 (3)	0.62242 (2)
6	0.64919 (2)	0.62370 (3)	0.62273 (2)
7	0.64579 (3)	0.62217 (3)	0.62277 (2)
8	0.64318 (3)	0.62126 (3)	0.62288 (2)
9	0.64107 (3)	0.62087 (3)	0.62280 (3)
10	0.63943 (3)	0.62051 (4)	0.62280 (3)
11	0.63803 (3)	0.62045 (4)	0.62275 (3)
12	0.63688 (3)	0.62026 (4)	0.62272 (3)
13	0.63591 (4)	0.62030 (4)	0.62267 (5)
14	0.63514 (4)	0.62034 (5)	0.62262 (5)
15	0.63441 (3)	0.62041 (4)	0.62266 (5)
16	0.63376 (4)	0.62050 (5)	0.62247 (5)
18	0.63270 (4)	0.62057 (6)	0.62248 (7)
20	0.63187 (6)	0.62081 (6)	0.62230 (8)
22	0.63117 (6)	0.62101 (6)	0.62211 (8)
24	0.63052 (6)	0.62098 (7)	0.62201 (7)
28	0.62958 (6)	0.62142 (7)	0.62177 (9)
32	0.62879 (5)	0.62174 (8)	0.62129 (8)
40	0.62761 (8)	0.62250 (9)	0.62050 (9)

absent in general, we have included it in the fitting procedures for models 1 and 3 as well. Furthermore, we observe that the amplitude b_1 of the leading correction to scaling can be suppressed. This amplitude has become small in the spin-1 model (model 3) and has even changed sign in model 2. In model 1, the amplitude b_1 is relatively large and we have attempted to determine the irrelevant exponent by including it as a parameter in the fit. However, for an acceptable fit it was necessary to include the correction term $b_2 L^{\gamma_2}$. Unfortunately, this frustrated the determination of γ_1 for model 1: if we fixed $\gamma_2 = -1.963$ the exponent γ_1 shifted toward γ_2 and if we included both γ_1 and γ_2 as free parameters, they approached the same value.

In order to take into account the finite-size effects revealed by the system sizes omitted in the previous fits, we have repeated our data analysis with an additional correction to scaling $b_3 L^{\gamma_3}$ in Eq. (3.14), where $\gamma_3 = -2\gamma_h$. This term, which is due

Table 3.4: Results of a data analysis of the three models, including system sizes $L \geq 7$ for model 1 and $L \geq 6$ for models 2 and 3. Besides the amplitude ratio Q , the critical couplings K_c and the nonuniversal coefficients a_1 , a_2 , b_1 and b_2 are listed.

	Model 1	Model 2	Model 3
Q	0.6232 (8)	0.6229 (3)	0.6231 (2)
K_c	0.2216542 (8)	0.1280034 (4)	0.3934214 (8)
a_1	0.862 (10)	1.43 (4)	0.659 (6)
a_2	0.54 (6)	1.5 (2)	0.352 (15)
b_1	0.102 (10)	-0.043 (4)	0.001 (2)
b_2	0.11 (3)	0.351 (13)	-0.018 (9)

to the nonlinear dependence of the magnetic scaling field on the physical magnetic field, enabled us to include all system sizes $L \geq 5$ for models 1, 2 and 3 in the analysis. The results, which are presented in Table 3.5, are consistent with those obtained previously. Again, the error margins quoted include the uncertainty due to the errors in y_i , y_t and y_h . The results for Q satisfy universality within a margin of less than 10^{-3} . To our knowledge, this is the most precise verification so far for 3D Ising-like models.

Table 3.5: Results of a data analysis of the three models, where all system sizes $L \geq 5$ were used and a third correction term was included. Besides the ratio Q , the nonuniversal coefficients a_1 , a_2 , b_1 , b_2 and b_3 and the critical couplings K_c are listed.

	Model 1	Model 2	Model 3
Q	0.6235 (7)	0.6231 (4)	0.6235 (3)
K_c	0.2216547 (8)	0.1280036 (5)	0.3934224 (10)
a_1	0.862 (9)	1.43 (4)	0.659 (6)
a_2	0.54 (6)	1.5 (2)	0.352 (15)
b_1	0.098 (9)	-0.045 (6)	-0.004 (3)
b_2	0.15 (4)	0.37 (2)	0.02 (2)
b_3	-4.9 (8)	-1.4 (8)	-2.0 (7)

3.5 Determination of the renormalization exponents

This section presents finite-size analyses of the energy, specific heat, spin-spin correlations over half the system size, susceptibility, the temperature derivative of the sus-

ceptibility and the temperature derivative of the ratio Q_L . Taking $h = 0$ and $b = L$ in Eq. (3.8) leads to

$$f(t, u, L^{-1}) = L^{-d} f(L^{\gamma_t} t, L^{\gamma_i} u, 1) + g(t). \quad (3.15)$$

Expansion in t and u yields

$$\begin{aligned} f(t, u, L^{-1}) = L^{-d} & \left(f^{(0,0)} + f^{(1,0)} L^{\gamma_t} t + \frac{1}{2} f^{(2,0)} L^{2\gamma_t} t^2 + \dots \right. \\ & \left. + f^{(0,1)} L^{\gamma_i} u + f^{(1,1)} L^{\gamma_t + \gamma_i} t u + \dots \right) \\ & + g^{(0)} + g^{(1)} t + \frac{1}{2} g^{(2)} t^2 + \dots, \end{aligned} \quad (3.16)$$

where $f^{(k,l)}$ stands for $\partial^{k+l} f / \partial t^k \partial u^l$. The finite-size scaling behaviour of the energy and that of the specific heat follow by differentiation.

3.5.1 The energy

In the simulations the nearest-neighbour sum $S_{\text{nn}} = \sum_{\langle \text{nn} \rangle} s_i s_j$ was sampled. For model 1, this sum is proportional to the energy; for models 2 and 3 its scaling behaviour is similar. Its expectation value is equal to

$$\langle S_{\text{nn}} \rangle = \frac{\partial f}{\partial K_{\text{nn}}} = \frac{\partial f}{\partial t} \frac{\partial t}{\partial K_{\text{nn}}} + \frac{\partial f}{\partial u} \frac{\partial u}{\partial K_{\text{nn}}}. \quad (3.17)$$

The finite-size scaling behaviour of this quantity thus follows by differentiating Eq. (3.16) and substitution in Eq. (3.17),

$$\begin{aligned} \langle S_{\text{nn}} \rangle = c_0 + c_1 (K_{\text{nn}} - K_c) + \dots \\ + L^{\gamma_t - d} [a_0 + a_1 (K_{\text{nn}} - K_c) L^{\gamma_t} + a_2 (K_{\text{nn}} - K_c)^2 L^{2\gamma_t} + \dots \\ + b_1 L^{\gamma_i} + b_2 L^{\gamma_i - \gamma_t} + \dots], \end{aligned} \quad (3.18)$$

where the a_i , b_i and c_i are unknown coefficients. Analysis of the numerical results for $\langle S_{\text{nn}} \rangle$ enables a determination of these coefficients and of γ_t . The dominant singular term in Eq. (3.18) is the one with amplitude a_0 . The $(K_{\text{nn}} - K_c)$ -dependent term with amplitude c_1 is dominated by the term with coefficient a_1 and has therefore been omitted from the scaling formula. Since the bulk of the data were taken very close to the critical points, only linear and quadratic terms in $(K_{\text{nn}} - K_c)$ have been included. Without the correction term with coefficient b_2 , we had to exclude system sizes $L < 8$ in the analysis of model 1 in order to obtain an acceptable residual. The resulting estimate for γ_t is: 1.586 (6). Inclusion of the second irrelevant term enabled us to include all system sizes $L \geq 5$. For consistency, we have included

this term in the data analyses for models 2 and 3 as well. Table 3.6 summarizes the results obtained from least-squares fits according to Eq. (3.18), at the critical points listed in Table 3.5, for system sizes $L \geq 5$. Since the singular behaviour of $\langle S_{\text{nn}} \rangle$ is rather weak, the results $\gamma_t \approx 1.59$ for each of the three models are relatively inaccurate but consistent with the existing literature. The uncertainty due to the errors in K_c and γ_i has been included in the error margins.

Table 3.6: Results of a data analysis of the nearest-neighbour sum $\langle S_{\text{nn}} \rangle$ for the three models.

	Model 1	Model 2	Model 3
γ_t	1.599 (8)	1.589 (9)	1.591 (7)
c_0	0.99051 (8)	0.66298 (9)	0.59451 (6)
a_0	2.14 (6)	2.20 (7)	1.73 (4)
b_1	0.14 (15)	0.16 (17)	0.04 (12)
b_2	-2.0 (4)	-0.6 (4)	-0.9 (3)

3.5.2 The specific heat

The fluctuations in S_{nn} are related to the specific-heat-like quantity

$$c_{\text{nn}} = K_{\text{nn}}^2 \frac{\partial^2 f}{\partial K_{\text{nn}}^2} = K_{\text{nn}}^2 [\langle S_{\text{nn}}^2 \rangle - \langle S_{\text{nn}} \rangle^2]. \quad (3.19)$$

We consider f as a function of the scaling fields t and u ,

$$c_{\text{nn}} = K_{\text{nn}}^2 \left[\frac{\partial f}{\partial t} \frac{\partial^2 t}{\partial K_{\text{nn}}^2} + \frac{\partial f}{\partial u} \frac{\partial^2 u}{\partial K_{\text{nn}}^2} + \frac{\partial^2 f}{\partial t^2} \left(\frac{\partial t}{\partial K_{\text{nn}}} \right)^2 + 2 \frac{\partial^2 f}{\partial t \partial u} \frac{\partial t}{\partial K_{\text{nn}}} \frac{\partial u}{\partial K_{\text{nn}}} + \frac{\partial^2 f}{\partial u^2} \left(\frac{\partial u}{\partial K_{\text{nn}}} \right)^2 \right]. \quad (3.20)$$

Taking the appropriate derivatives in Eq. (3.16) and collecting the leading analytic and singular terms leads to

$$c_{\text{nn}} = p_0 + p_1(K_{\text{nn}} - K_c) + \dots + L^{2\gamma_t-d} [q_0 + q_1(K_{\text{nn}} - K_c)L^{\gamma_t} + q_2(K_{\text{nn}} - K_c)^2 L^{2\gamma_t} + \dots + r_1 L^{\gamma_i} + \dots] + L^{\gamma_t-d} [s_0 + s_1(K_{\text{nn}} - K_c)L^{\gamma_t} + \dots]. \quad (3.21)$$

The numerical results for c_{nn} of models 1–3 were subjected to a fit of this form with $y_i = -0.83$ and the K_c values in Table 3.5 as input parameters. The terms with amplitudes p_1 and s_1 are dominated by that with amplitude q_1 and were omitted from the fit formula, as well as quadratic terms in $(K_{\text{nn}} - K_c)$. System sizes $L < 6$ display finite-size corrections not included in Eq. (3.21) and were discarded. The main results of these fits are shown in Table 3.7, where the error margins include the uncertainties in K_c and y_i . Also in the present case we find consistent, but inaccurate values of y_i . This may be related to the fact that the leading power of L in Eq. (3.21) is close to zero, so that this term, which has the coefficient q_0 , interferes with the term with coefficient p_0 .

Table 3.7: Results of a data analysis of the specific-heat-like quantity c_{nn} obtained from the fluctuations of the nearest-neighbour sum S_{nn} for each of the three models.

	Model 1	Model 2	Model 3
y_t	1.60 (2)	1.579 (15)	1.59 (2)
p_0	-0.8 (7)	-0.6 (3)	-3 (2)
q_0	1.5 (5)	0.8 (3)	3.5 (14)
q_1	2.2 (2)	1.39 (12)	3.7 (4)
r_1	-0.4 (4)	0.11 (14)	0.0 (9)
s_0	-0.4 (3)	-0.24 (13)	-1.0 (7)

3.5.3 The spin–spin correlation function

In our simulations we have also sampled the spin–spin correlation function $g(\mathbf{r})$,

$$g(\mathbf{r}) = \langle s(\mathbf{0})s(\mathbf{r}) \rangle, \quad (3.22)$$

over half the system size ($r = L/2$), for even system sizes. This quantity can be derived from the free energy F by differentiating with respect to two physical magnetic fields H_0 and H_r , which couple to the spins at positions $\mathbf{0}$ and \mathbf{r} , respectively. We consider the two fields as independent and find

$$g(\mathbf{r}) = \left(\frac{\partial^2 F}{\partial H_0 \partial H_r} \right)_{H_0=H_r=0} = \left(\frac{\partial^2 F}{\partial h_0 \partial h_r} \frac{\partial h_0}{\partial H_0} \frac{\partial h_r}{\partial H_r} \right)_{H_0=H_r=0}, \quad (3.23)$$

where h denotes the leading magnetic scaling field and the derivatives with respect to this field are evaluated at $h_0 = h_r = 0$. Using Eq. (3.9) one obtains upon expansion in t and u the scaling behaviour of the correlation function,

$$g = L^{2y_h - 2d} \left[a_0 + a_1 (K_{\text{nn}} - K_c) L^{y_t} + a_2 (K_{\text{nn}} - K_c)^2 L^{2y_t} + \dots \right. \\ \left. + b_1 L^{y_i} + \dots \right], \quad (3.24)$$

where the coefficients a_i and b_i are different from those in Eq. (3.18). The volume factor L^{-2d} results from the fact that both H_0 and H_r only couple to a local spin.

We have fitted the terms shown in (3.24) to our data. The large residuals for all three models strongly suggested the presence of an additional correction to scaling $b_2 L^{y'}$. A problem for the determination of y' is the presence of the leading correction term $b_1 L^{y_i}$. Only in the spin-1 model (model 3), where the amplitude b_1 is small and the term thus may be omitted, a reasonable determination was possible, yielding $y' = -2.1$ (1). This could be a second irrelevant exponent, although we have not observed it in the analysis of the ratio Q or the energy-like quantity S_{nn} . In Q , it may have been masked by the term $b_2 L^{y'}$, but this is less likely for S_{nn} , where the exponent of the second correction term is approximately equal to -2.4 . A more convincing explanation can be given by considering correlation functions between local “blocks” of spins, centered around the positions $\mathbf{0}$ and \mathbf{r} , respectively. In terms of a real-space renormalization transformation one can easily envisage that such block correlations arise in the renormalization process. These functions will contain, in addition to the leading contribution decaying as $r^{-\eta-1}$ (where we have introduced the critical exponent $\eta = 5 - 2y_h$), contributions coming from spins originally separated by, e.g., a distance $r \pm 1$, which hence decay as $(r \pm 1)^{-\eta-1}$. Thus, the total correlation function can be written schematically as

$$r^{-\eta-1} \left[1 + \left(\frac{r+1}{r} \right)^{-\eta-1} + \left(\frac{r-1}{r} \right)^{-\eta-1} \right], \quad (3.25)$$

which can be expanded around r , yielding a function of the form $r^{-\eta-1} [1 + zr^{-2} + \mathcal{O}(r^{-4})]$. Although this is not unlike the expansion postulated by Kadanoff [44] and Wilson [45], the so-called Operator Product Expansion or Short Distance Expansion (SDE), it should be kept in mind that these expansions were concerned with two-point correlation functions at short distances, cf. also Refs. [46, Sec. II-2-6] and [47, Ch. 12]. Whereas the SDE yields higher-order contributions that differ from the leading contribution to the correlation function by *even* negative powers of the wave vector (for large momenta), the expansion mentioned here yields higher-order contributions differing from the leading singular behaviour by even negative powers of the spin-spin distance r . The reason for this is that the present expansion relies on the fact that the distance r between correlated blocks is large with respect to the difference between $r+1$ and r (or the block size). Setting $r = L/2$ we find additional corrections in Eq. (3.24) decaying as powers of L^{-2} . This is in good agreement with the above-mentioned value for y' and hence we have included this correction in the scaling formula. Table 3.8 shows the main results of an analysis for system sizes $L \geq 8$, where we have included three correction terms, $b_1 L^{y_i}$, $b_2 L^{y'}$ and $b_3 L^{2y'}$, with the exponents y_i and y' fixed at -0.83 and -2 , respectively. We have not included the term proportional to L^{2y_i} because b_1 is already quite small. The errors quoted in

the table include the uncertainties in K_c , y_t and y_i . The estimates of y_h for each of the three models are consistent and in agreement with the existing literature.

Table 3.8: Results of a data analysis of the spin–spin correlation function g for the three models.

	Model 1	Model 2	Model 3
y_h	2.480 (2)	2.482 (3)	2.482 (3)
a_0	1.54 (3)	1.09 (3)	0.91 (3)
a_1	4.91 (6)	6.14 (10)	2.36 (4)
a_2	6.9 (3)	14.4 (7)	2.60 (6)
b_1	-0.44 (17)	0.19 (16)	0.02 (15)

3.5.4 The magnetic susceptibility

The magnetic susceptibility χ can be calculated from the average square magnetization, which is sampled in the Monte Carlo simulations,

$$\chi = L^d \langle m^2 \rangle. \quad (3.26)$$

Using Eqs. (3.9), (3.10) and (3.12), we find for the finite-size scaling behaviour:

$$\chi = g^{(2)}(t) + L^{2y_h-d} f^{(2)}(L^{y_t} t, L^{y_i} u, 1), \quad (3.27)$$

which yields, upon expansion in t and u ,

$$\begin{aligned} \chi = & c_0 + c_1(K_{nn} - K_c) + \dots \\ & + L^{2y_h-d} [a_0 + a_1(K_{nn} - K_c)L^{y_t} + a_2(K_{nn} - K_c)^2 L^{2y_t} + \dots \\ & + b_1 L^{y_i} + \dots], \end{aligned} \quad (3.28)$$

where the a_i , b_i and c_i are nonuniversal coefficients. In Table 3.9, we present the results of fits of the susceptibility for the models 1–3 at the critical points listed in Table 3.5. For model 1, system sizes $L \geq 8$ were included in the analysis and for models 2 and 3, which exhibit smaller corrections to scaling, all system sizes $L \geq 6$ were used. The coefficient c_1 in Eq. (3.28) was set to zero in all analyses, because the term containing it is much smaller than the $(K_{nn} - K_c)$ -dependent term with amplitude a_1 . The errors include the margins due to the uncertainties in K_c , y_i and y_t . For each of the three models the coefficients a_0 , a_1 , a_2 and b_1 are in good agreement with the corresponding coefficients in Table 3.8.

Table 3.9: Results of a data analysis of the susceptibility χ for the three models.

	Model 1	Model 2	Model 3
y_h	2.4812 (11)	2.4817 (10)	2.4826 (9)
c_0	-0.6 (2)	-0.20 (7)	-0.50 (6)
a_0	1.559 (16)	1.126 (9)	0.926 (7)
a_1	4.88 (6)	6.16 (8)	2.36 (3)
a_2	6.9 (4)	14.4 (7)	2.62 (7)
b_1	-0.37 (5)	0.14 (3)	-0.05 (2)

On the other hand, one might derive the scaling formula for χ from that of the spin-spin correlation function g , because χ is equal to the spatial integral of g ,

$$\chi = \int g(r) r^{d-1} dr . \quad (3.29)$$

Assuming that the integral in Eq. (3.29) preserves the form of the corrections to scaling in g (for η nonzero), we expect the same type of corrections in the correlation function and the susceptibility. Only the terms proportional to c_0, c_1, \dots in (3.28), which arise from the analytical part of the free energy, are absent in Eq. (3.24). These contributions come from the small- r cutoff in Eq. (3.29). Thus, we have included in the scaling formula the additional corrections that we observed in the analysis of the correlation function. As the term proportional to $L^{y'}$ interferes with the constant contribution c_0 , we have only included the correction $b_2 L^{2y'}$. This allowed us to include system sizes $L \geq 5$ for all three models. The results, which are presented in Table 3.10, are consistent with those obtained in the previous analysis. Just as in

Table 3.10: Results of a data analysis of the susceptibility χ for the three models, where all system sizes $L \geq 5$ were employed and an additional correction to scaling was included in the scaling formula.

	Model 1	Model 2	Model 3
y_h	2.4812 (11)	2.4810 (14)	2.4817 (13)
c_0	-0.4 (2)	0.0 (2)	-0.33 (13)
a_0	1.560 (15)	1.134 (13)	0.934 (10)
a_1	4.88 (6)	6.18 (8)	2.37 (3)
a_2	6.9 (3)	14.5 (7)	2.64 (7)
b_1	-0.37 (4)	0.10 (6)	0.01 (13)
b_2	-4.5 (12)	-2.9 (16)	-2.6 (13)

the analysis of the correlation function, we find consistent results for y_h , which are in agreement with the literature. However, the values for y_h are more accurate than those obtained in the previous subsection and our resulting estimate for the magnetic renormalization exponent is $y_h = 2.4815$ (15). The error margin amounts to two standard deviations, in order to take into account a possible arbitrariness in the fit formula.

3.5.5 The temperature derivative of χ

In the simulations we have also sampled the correlation between m^2 and S_{nn} . This allows us to calculate the temperature derivative of the susceptibility,¹

$$\frac{\partial \chi}{\partial K_{nn}} = L^d (\langle m^2 S_{nn} \rangle - \langle m^2 \rangle \langle S_{nn} \rangle) . \quad (3.30)$$

The scaling behaviour of this quantity can be derived directly from that of the susceptibility, Eq. (3.28),

$$\begin{aligned} \frac{\partial \chi}{\partial K_{nn}} = & c_1 + \dots \\ & + L^{2y_h + y_t - d} \left[a_1 + 2a_2(K_{nn} - K_c)L^{y_t} + 3a_3(K_{nn} - K_c)^2L^{2y_t} + \dots \right. \\ & \left. + \tilde{b}_1L^{y_i} + \dots \right] . \end{aligned} \quad (3.31)$$

The term with amplitude \tilde{b}_1 comes from a term proportional to $(K_{nn} - K_c)L^{y_t + y_i}$, included in the ellipsis in Eq. (3.28). Just as in the analysis of the spin–spin correlation function, the residuals for all three models indicated the presence of an additional correction to scaling $\tilde{b}_2L^{y'}$, which indeed follows from the discussion in the previous subsection. Table 3.11 shows the results of an analysis at the critical points listed in Table 3.5, where this additional correction was included. All system sizes $L \geq 6$ were used. The exponents y_i and y' were kept fixed at -0.83 and -2 , respectively. The error margins include the uncertainties in K_c and y_i . The fit yields values for $(2y_h + y_t)$ and the results for y_t have been obtained by fixing y_h at the best estimate from the previous subsection. This implies an additional error margin of 0.003 for y_t . For models 1 and 3, there is a reasonable agreement between the amplitudes a_1 and a_2 as shown in Table 3.10 and those in Table 3.11. The differences are explained from the approximations in the scaling formulae. For model 2, no such agreement is expected, because an additional term arises in the temperature derivative of the susceptibility due to the temperature dependence of K_{3n} (the ratio between K_{nn} and K_{3n} is fixed).

¹This refers to the derivative of the *scaled* susceptibility defined in Eq. (3.26). The actual magnetic susceptibility carries an additional temperature dependence, since it is defined as $\chi/k_B T$.

Table 3.11: Results of a data analysis of the temperature derivative of the susceptibility $\partial\chi/\partial K_{\text{nn}}$ for the three models, where all system sizes $L \geq 6$ were employed and an additional correction to scaling was included in the scaling formula.

	Model 1	Model 2	Model 3
γ_t	1.585 (3)	1.584 (4)	1.587 (4)
c_1	31 (11)	1 (9)	12 (7)
a_1	5.11 (9)	3.73 (6)	2.39 (5)
a_2	6.46 (10)	8.04 (9)	2.53 (3)
a_3	-2.4 (4)	-4.4 (5)	-0.53 (5)
\tilde{b}_1	-2.6 (3)	0.1 (3)	-0.1 (2)
\tilde{b}_2	-13 (3)	-6 (2)	-5.5 (16)

3.5.6 The temperature derivative of Q

Another quantity of interest arises from the correlation between the magnetization distribution and the nearest-neighbour sum S_{nn} ,

$$\frac{\partial Q}{\partial K_{\text{nn}}} = Q \left(2 \frac{\langle m^2 S_{\text{nn}} \rangle - \langle m^2 \rangle \langle S_{\text{nn}} \rangle}{\langle m^2 \rangle} - \frac{\langle m^4 S_{\text{nn}} \rangle - \langle m^4 \rangle \langle S_{\text{nn}} \rangle}{\langle m^4 \rangle} \right). \quad (3.32)$$

The determination of m and S_{nn} in the simulations enables the sampling of this quantity with very little additional effort. Returning to Eq. (3.14) and noting that the ellipses include terms proportional to $(K_{\text{nn}} - K_c)L^{\gamma_t + \gamma_i}$ and to $(K_{\text{nn}} - K_c)L^{\gamma_2}$, we obtain the finite-size scaling behaviour

$$\begin{aligned} \frac{1}{Q} \frac{\partial Q}{\partial K_{\text{nn}}} &= L^{\gamma_t} \left[u_0 + u_1 (K_{\text{nn}} - K_c)L^{\gamma_t} + u_2 (K_{\text{nn}} - K_c)^2 L^{2\gamma_t} + \dots \right. \\ &\quad \left. + \nu L^{\gamma_i} + w L^{\gamma_2 - \gamma_t} + \dots \right]. \end{aligned} \quad (3.33)$$

The numerical data for the three models were subjected to a fit on the basis of Eq. (3.33), where we have included system sizes $L \geq 7$ for model 1 and $L \geq 5$ for models 2 and 3. In this case the leading power of L stands well apart from the less singular terms and the results for γ_t (Table 3.12; uncertainties in K_c , γ_i and γ_h are included in all error margins) appear to be more accurate than those in the preceding subsections. The results suggest that the correction due to the leading irrelevant field is very small. Therefore we have repeated our analysis with the coefficient ν fixed to zero. We expect this to work especially well for models 2 and 3, where the irrelevant field is notably smaller than in the first model. Indeed, we have obtained accurate and consistent results for the models 2 and 3, as shown in Table 3.13. These results, together with those presented in Table 3.12, lead us to our final result, $\gamma_t = 1.587(2)$.

Just as in the final result for γ_h in Sec. 3.5.4, we quote here an error margin of two standard deviations. Both for model 1 and for model 3 there is a reasonable agreement between the quantity u_0 (Table 3.12) and a_1/Q (Table 3.4).

Table 3.12: Results of a data analysis of the derivative of the quantity Q with respect to the nearest-neighbour coupling K_{nn} .

	Model 1	Model 2	Model 3
γ_t	1.589 (2)	1.587 (2)	1.5878 (14)
u_0	1.341 (14)	1.351 (9)	1.057 (6)
u_1	-0.21 (3)	0.00 (5)	-0.012 (9)
u_2	-10.7 (6)	-28.3 (11)	-4.80 (12)
ν	-0.01 (6)	0.00 (3)	0.02 (2)
w	-0.5 (2)	0.46 (8)	-0.13 (5)

Table 3.13: Results of a data analysis of the derivative of the quantity Q with respect to the nearest-neighbour coupling K_{nn} for models 2 and 3, where the leading correction to scaling has been omitted.

	Model 2	Model 3
γ_t	1.5868 (3)	1.5867 (2)
u_0	1.3512 (11)	1.0623 (7)
u_1	0.00 (5)	-0.013 (9)
u_2	-28.3 (11)	-4.81 (12)
w	0.457 (15)	-0.091 (9)

3.6 Simultaneous fits for the three models

Considering the results in the preceding sections, it is reasonable to assume now that universality is *exactly* satisfied for the three models under investigation. Thus we have made a fit of the combined data for the ratio Q , allowing only single values of Q and γ_i for the three models. The other parameters a_1 , a_2 , K_c , b_1 and b_2 [see Eq. (3.14)] are nonuniversal and occur in triplicate. Now, system sizes $L < 8$ had to be discarded, except when an additional correction to scaling proportional to $L^{-2\gamma_h}$ was added to the scaling formula. In the latter case, all system sizes $L \geq 5$ could be included. Some of the results are summarized in Tables 3.14 and 3.15, respectively, where the error margins include the uncertainty introduced by the error in γ_t and γ_h .

Table 3.14: Results of a data analysis assuming universality of $Q_L = \langle m^2 \rangle_L^2 / \langle m^4 \rangle_L$ for the three investigated Ising models. System sizes $L \geq 8$ were included in the fit. The table lists nonuniversal parameters: the critical points and the amplitudes of the *two* correction terms. Furthermore, this analysis yielded the universal parameters $Q = 0.6232$ (2) and $y_1 = -0.78$ (3).

	Model 1	Model 2	Model 3
K_c	0.2216550 (6)	0.1280037 (4)	0.3934217 (8)
b_1	0.086 (8)	-0.040 (5)	-0.001 (2)
b_2	0.18 (3)	0.34 (2)	0.000 (14)

Table 3.15: Results of a data analysis assuming universality of $Q_L = \langle m^2 \rangle_L^2 / \langle m^4 \rangle_L$ for the three investigated Ising models. System sizes $L \geq 5$ were included in the fit. The table lists nonuniversal parameters: the critical points and the amplitudes of the *three* correction terms. Furthermore, this analysis yielded the universal parameters $Q = 0.6233$ (2) and $y_1 = -0.82$ (3).

	Model 1	Model 2	Model 3
K_c	0.2216546 (5)	0.1280039 (4)	0.3934220 (7)
b_1	0.096 (7)	-0.046 (5)	-0.002 (2)
b_2	0.15 (3)	0.38 (2)	0.007 (12)
b_3	-4.9 (8)	-1.7 (7)	-1.7 (5)

Let us now compare the results of the various fits. In the first place, we see that the results in Tables 3.14 and 3.15 are consistent, just as was the case for Tables 3.4 and 3.5 in Sec. 3.4. Also the values for the universal quantity Q , 0.6232 (2) and 0.6233 (2), respectively, agree. Secondly, the simultaneous fit with only the first two corrections to scaling (Table 3.14) yields results that are consistent with those presented in Table 3.4. Only the amplitude b_2 and the critical coupling K_c for model 1 appear to be somewhat too low in Table 3.4, as we already had seen from the second fit in Sec. 3.4. Finally, when we compare the results in Tables 3.5 and 3.15, i.e., including a third correction to scaling, as well as the corresponding Q values, we see a very good agreement. These comparisons, in addition to the fact that the term $b_3 L^3$ allowed us to include all system sizes $L \geq 5$, lead us to the conclusion that the fits presented in Table 3.15 can be considered as the most accurate results. In addition to the nonuniversal constants given in the table and the universal amplitude ratio Q , this analysis yielded the (universal) irrelevant exponent $y_1 = -0.82$ (3). This value is in very good agreement with that obtained by Nickel and Rehr [8]. Although there is

one more unknown (y_i), the results for Q and K_c obtained in this section are more accurate than those of the three separate fits. One of the reasons is that the fit for model 3 is insensitive to the value of y_i , so that, e.g., Q is determined accurately.

3.7 Discussion and conclusion

We summarize our final results for the renormalization exponents: $y_t = 1.587$ (2), $y_h = 2.4815$ (15), $y_i = -0.82$ (6). To allow for any residual dependences on the choice of the fitting formulae, we list error margins of two standard deviations. In Table 3.16 we compare our results with a number of recent estimates obtained by various methods. Our result for the temperature exponent is markedly lower than those of Baillie *et al.* [22] and Gupta and Tamayo [14], which were both obtained by the Monte Carlo renormalization-group method. This could be explained by a violation of hyperscaling. However, the accurate agreement between our result and those of coupling-constant expansion [2], ε -expansion [6], series expansions [8, 9] and the coherent-anomaly method [12] makes this explanation less likely. Gupta and Tamayo view their result as support for the notion that the exponents are ratio-

Table 3.16: Some recent results for the renormalization exponents. The estimate for y_i from Ref. [3] has been calculated from the value for $\theta = -y_i/y_t$ presented in this reference and the value for y_t as calculated in the present work.

	y_t	y_h	y_i
Present work	1.587 (2)	2.4815 (15)	-0.82 (6)
Hasenbusch and Pinn [26]	1.585 (3)		
Butera and Comi [11] (biased)	1.584 (2)	2.481 (2)	
Butera and Comi (unbiased)	1.577 (5)	2.481 (5)	
Talapov and Blöte [25]		2.4808 (16)	-0.81 (4)
Gupta and Tamayo [14]	1.600 (3)	2.488 (3)	-0.7
Blöte <i>et al.</i> [13]	1.585 (3)	2.481 (1)	
Kolesik and Suzuki [12]	1.586 (4)	2.482 (4)	
Guttman and Enting [10]	1.580 (3)		
Landau [24]	1.590 (2)	2.482 (7)	
Baillie <i>et al.</i> [22]	1.602 (5)	2.4870 (15)	-0.8 to -0.85
Nickel [9]	1.587	2.4823	-0.84
Nickel and Rehr [8]	1.587 (4)	2.4821 (4)	-0.83 (5)
Le Guillou and Zinn-Justin [6]	1.584 (4)	2.4813 (13)	
Chen, Fisher and Nickel [3]			-0.86 (8)
Le Guillou and Zinn-Justin [2]	1.587 (4)	2.485 (2)	-0.79 (3)

nal numbers. However, we remark that at least the simple value $y_t = 8/5$ is incompatible with our estimate. We notice that our result for y_t is somewhat higher than the recent series-expansion result of Guttman and Enting [10]. Also the thermal exponent of Butera and Comi [11] lies markedly lower, but this discrepancy shrinks considerably when the critical coupling of Ref. [25] is used (see the entry labeled “biased”). The result for the magnetic exponent is also in good agreement with most other estimates, although again the results of Baillie *et al.* and of Gupta and Tamayo lie significantly higher than the majority of the results. Also the result of Le Guillou and Zinn-Justin obtained by coupling-constant expansion [2] seems somewhat too high. The results for the leading irrelevant exponent are not very accurate, but mostly consistent. In Ref. [14] no explicit error estimate is given for y_i , but the numerical data suggest that it is of the order of 0.04. This implies a considerable deviation from the remaining estimates. For easy reference, Table 3.17 summarizes the exponents α , β , γ , δ , η , ν and θ as calculated from our results for y_t , y_h and y_i , on the assumption that the hypotheses of scaling and hyperscaling are valid.

Table 3.17: The standard critical exponents as well as Wegner’s correction-to-scaling exponent θ as calculated from our best estimates for y_t , y_h and y_i .

Exponent	Expressed in RG exp.	Value
α	$2 - d/y_t$	0.110 (2)
β	$(d - y_h)/y_t$	0.3267 (10)
γ	$(2y_h - d)/y_t$	1.237 (2)
δ	$y_h/(d - y_h)$	4.786 (14)
η	$2 - 2y_h + d$	0.037 (3)
ν	$1/y_t$	0.6301 (8)
θ	$-y_i/y_t$	0.52 (4)

Furthermore, we can calculate the Binder cumulant B (see Sec. 3.4) from our estimate for Q , which yields $B = -1.3956$ (10). Only few accurate results are available for this quantity (see, e.g., Ref. [48] for a review) and one of the most accurate estimates until now is $B = -1.403$ (7) [49]. Our result is in agreement with this and other estimates, but its accuracy is markedly higher.

Table 3.18 presents a comparison of recent results for K_c of the spin- $\frac{1}{2}$ nearest-neighbour Ising model. Again, it should be noted that the error margin of the result obtained in the present work amounts to two standard deviations. It can be seen that the amplitude ratio Q , which is used in this work, provides a good means of obtaining an accurate estimate for the critical coupling. We conclude that the conjecture of Rosengren [50] is not correct (see also Ref. [51]). The result of Ferrenberg and Landau deviates by 1.8 combined standard errors, but the newest estimate of

Table 3.18: Summary of recent results for the critical point of the spin- $\frac{1}{2}$ Ising model with nearest-neighbour couplings.

Reference	Value
Present work	0.2216546 (10)
Butera and Comi [11]	0.221663 (9)
Talapov and Blöte [25]	0.2216544 (3)
Gupta and Tamayo [14]	0.221655 (1)
Landau [24]	0.2216576 (22)
Blöte and Kamieniarz [23]	0.221648 (4)
Baillie <i>et al.</i> [22]	0.221652 (3)
Livet [52]	0.2216544 (10)
Ferrenberg and Landau [21]	0.2216595 (26)
Ito and Suzuki [20]	0.221657 (3)
Blöte <i>et al.</i> [17]	0.221652 (5)
Rosengren (conjecture) [50]	0.2216586 (0)

Landau differs by only 1.2 standard deviations from the result presented here. The difference with Ref. [23] is 1.6 standard errors and is partly due to statistical errors (the data used in this work include those of Ref. [23] but are much more accurate and include $L = 40$ data) and partly because a term with exponent γ_2 was not included in the scaling formula for the ratio Q . The result of Ref. [25] is based on a superset of the data used in this chapter.

In summary, we have presented strong evidence that the three models investigated in this chapter belong to the same universality class. Thus, for the determination of universal quantities, one has the freedom to choose a model in which the corrections to scaling are small. For this purpose the spin-1 model has proven to be particularly useful. Also the introduction of additional third-neighbour couplings in the spin- $\frac{1}{2}$ model is a viable route, although the change of sign of the leading corrections to scaling (compared to those in the nearest-neighbour Ising model) suggests that the ratio between the third-neighbour and nearest-neighbour couplings should be somewhat smaller than 0.4.

References

- [1] G. A. Baker, B. G. Nickel and D. I. Meiron, Phys. Rev. B **17**, 1365 (1978).
- [2] J. C. Le Guillou and J. Zinn-Justin, Phys. Rev. B **21**, 3976 (1980).
- [3] J.-H. Chen, M. E. Fisher and B. G. Nickel, Phys. Rev. Lett. **48**, 630 (1982).
- [4] J. Adler, J. Phys. A **16**, 3585 (1983).

- [5] J. C. Le Guillou and J. Zinn-Justin, *J. Physique Lett.* **46**, L137 (1985).
- [6] J. C. Le Guillou and J. Zinn-Justin, *J. Phys. (Paris)* **48**, 19 (1987).
- [7] A. J. Liu and M. E. Fisher, *Physica A* **156**, 35 (1989).
- [8] B. G. Nickel and J. J. Rehr, *J. Stat. Phys.* **61**, 1 (1990).
- [9] B. G. Nickel, *Physica A* **177**, 189 (1991).
- [10] A. J. Guttmann and I. G. Enting, *J. Phys. A* **27**, 8007 (1994).
- [11] P. Butera and M. Comi, *Phys. Rev. B* **56**, 8212 (1997).
- [12] M. Kolesik and M. Suzuki, *Physica A* **215**, 138 (1995).
- [13] H. W. J. Blöte, J. R. Heringa, A. Hoogland, E. W. Meyer and T. S. Smit, *Phys. Rev. Lett.* **76**, 2613 (1996).
- [14] R. Gupta and P. Tamayo, *Int. J. Mod. Phys. C* **7**, 305 (1996).
- [15] H. W. J. Blöte and R. H. Swendsen, *Phys. Rev. B* **20**, 2077 (1979).
- [16] G. S. Pawley, R. H. Swendsen, D. J. Wallace and K. G. Wilson, *Phys. Rev. B* **29**, 4030 (1984).
- [17] H. W. J. Blöte, J. A. de Bruin, A. Compagner, J. H. Croockewit, Y. T. J. C. Fonk, J. R. Heringa, A. Hoogland and A. L. van Willigen, *Europhys. Lett.* **10**, 105 (1989).
- [18] H. W. J. Blöte, A. Compagner, J. H. Croockewit, Y. T. J. C. Fonk, J. R. Heringa, A. Hoogland, T. S. Smit and A. L. van Willigen, *Physica A* **161**, 1 (1989).
- [19] N. A. Alves, B. A. Berg and R. Villanova, *Phys. Rev. B* **41**, 383 (1990).
- [20] N. Ito and M. Suzuki, *J. Phys. Soc. Jpn.* **60**, 1978 (1991).
- [21] A. M. Ferrenberg and D. P. Landau, *Phys. Rev. B* **44**, 5081 (1991).
- [22] C. F. Baillie, R. Gupta, K. A. Hawick and G. S. Pawley, *Phys. Rev. B* **45**, 10438 (1992).
- [23] H. W. J. Blöte and G. Kamieniarz, *Physica A* **196**, 455 (1993).
- [24] D. P. Landau, *Physica A* **205**, 41 (1994).
- [25] A. L. Talapov and H. W. J. Blöte, *J. Phys. A* **29**, 5727 (1996).
- [26] M. Hasenbusch and K. Pinn, preprint cond-mat/9706003.
- [27] E. W. Meyer, Master's thesis, Delft University, 1991, unpublished.
- [28] A. Hoogland, J. Spaa, B. Selman and A. Compagner, *J. Comp. Phys.* **51**, 250 (1983).
- [29] A. Hoogland, A. Compagner and H. W. J. Blöte, *The Delft Ising System Processor*, in *Special Purpose Computers*, edited by B. J. Alder (Academic, San Diego, 1988).
- [30] R. H. Swendsen and J. S. Wang, *Phys. Rev. Lett.* **58**, 86 (1987).
- [31] C. F. Baillie and P. D. Coddington, *Phys. Rev. B* **43**, 10617 (1991).
- [32] U. Wolff, *Phys. Rev. Lett.* **60**, 1461 (1988).
- [33] M. N. Barber, R. B. Pearson, D. Toussaint and J. L. Richardson, *Phys. Rev. B* **32**, 1720 (1985).
- [34] G. Parisi and F. Rapuano, *Phys. Lett. B* **157**, 301 (1985).
- [35] A. Hoogland, A. Compagner and H. W. J. Blöte, *Physica A* **132**, 593 (1985).

- [36] G. Bhanot, D. Duke and R. Salvador, *Phys. Rev. B* **33**, 7841 (1986).
- [37] A. M. Ferrenberg, D. P. Landau and Y. J. Wong, *Phys. Rev. Lett.* **69**, 3382 (1992).
- [38] T. G. Lewis and W. H. Payne, *J. Ass. Comp. Mach.* **20**, 456 (1973).
- [39] H. W. J. Blöte, E. Luijten and J. R. Heringa, *J. Phys. A* **28**, 6289 (1995).
- [40] L. N. Shchur, J. R. Heringa and H. W. J. Blöte, *Physica A* **241**, 579 (1997).
- [41] K. Binder, *Z. Phys. B* **43**, 119 (1981).
- [42] M. Suzuki, *Prog. Theor. Phys.* **58**, 1142 (1977).
- [43] E. Brézin, *J. Phys. (Paris)* **43**, 15 (1982).
- [44] L. P. Kadanoff, *Phys. Rev. Lett.* **23**, 1430 (1969).
- [45] K. G. Wilson, *Phys. Rev.* **179**, 1499 (1969).
- [46] D. J. Amit, *Field Theory, the Renormalization Group, and Critical Phenomena*, second edition (World Scientific, Singapore, 1984).
- [47] J. Zinn-Justin, *Quantum Field Theory and Critical Phenomena*, third edition (Oxford University Press, Oxford, 1996).
- [48] V. Privman, P. C. Hohenberg and A. Aharony, *Universal Critical-Point Amplitude Relations*, in *Phase Transitions and Critical Phenomena*, Vol. 14, edited by C. Domb and J. L. Lebowitz (Academic, London, 1991).
- [49] P.-Y. Lai and K. K. Mon, *Phys. Rev. B* **40**, 11120 (1989).
- [50] A. Rosengren, *J. Phys. A* **19**, 1709 (1986).
- [51] M. E. Fisher, *J. Phys. A* **28**, 6323 (1995); **29**, 1145 (1996).
- [52] F. Livet, *Europhys. Lett.* **16**, 139 (1991).

Chapter 4

Critical behaviour of spin models with algebraically decaying interactions I *At and above the upper critical dimension*

4.1 Introduction

As a first application of the algorithm presented in Chapter 2 we investigate spin models with algebraically decaying interactions. The critical behaviour of these models has attracted much attention during the last three decades. For the one-dimensional case, some analytical results have been obtained [1–11], as well as a number of numerical results. The numerical results apply to both inverse-square interactions [12–15] and general algebraically decaying interactions [16–27]. Special mention deserves the work by Anderson, Yuval and Hamann [28–31], which greatly stimulated the interest in spin chains with long-range interactions. These authors also developed a renormalization-like approach to the one-dimensional inverse-square model [30, 31]. Further renormalization-group studies of this particular case are presented in Refs. [12, 32–34]. A major contribution was made by Fisher, Ma and Nickel [35] and Sak [36], who obtained renormalization predictions for the critical exponents of models of general dimensionality $d < 4$ with algebraically decaying interactions (obtained independently by Suzuki *et al.* [37]). Other works concerning $d > 1$ are two conjectures on, respectively, the boundary between long-range and short-range behaviour and the boundary between classical

(mean-field) and nonclassical behaviour, both by Stell [38], a (refuted) conjecture by Griffiths [39], a rigorous confirmation of the upper critical dimension by Aizenman and Fernández [10] and a variational approach to the Ising model with long-range interactions [40]. Furthermore, Monte Carlo simulations have been carried out for one particular choice of the spin–spin interaction in a two-dimensional model [41]. However, to our knowledge, neither any further verifications of the renormalization predictions nor any other results are available for higher-dimensional ($d > 1$) models. To conclude this summary, we mention that the one-dimensional q -state Potts model with long-range interactions has been studied analytically [9, 11], numerically [42, 43] and in a mean-field approximation on the Bethe lattice [44].

Why are these models interesting? In the first place from a fundamental point of view: they enable us to study the influence of the interaction range on the critical behaviour, which is the main subject of this thesis. For example, in one-dimensional systems long-range order is only possible in the presence of spin–spin interactions which decay sufficiently slowly. In the borderline (inverse-square) case, the 1D model displays a remarkable behaviour: at the critical temperature the order parameter exhibits a finite jump (see Sec. 4.2), but the free energy has an essential singularity such that all thermal properties are smooth. In this sense, the phase transition can be regarded as the one-dimensional analog of a Kosterlitz–Thouless transition [45, 46], although the jump in the magnetization is not present there, as follows from the Mermin–Wagner theorem [47]. Just as $d = 2$ is the lower critical dimension for the two-dimensional XY model with short-range interactions, $\sigma = 1$ is a critical decay rate in a one-dimensional system with interactions decaying as $r^{-(1+\sigma)}$, see Ref. [32]. With respect to higher-dimensional systems, we note that the decay rate of van der Waals forces in realistic three-dimensional systems is only slightly faster than at the boundary between short-range (Ising-like) and long-range critical behaviour. The question of criticality in ionic systems, where the (screened) Coulomb interactions might lead to effectively algebraically decaying interactions, appears still open to debate [48–50]. It has also been claimed that exponents in the long-range universality class have been observed experimentally in a ferromagnetic phase transition [51]. Recently, it has been derived that critical fluctuations may give rise to long-range Casimir forces (decaying much more slowly than van der Waals interactions) between uncharged particles immersed in a critical fluid [52]. Furthermore, it was shown by Anderson and Yuval [28, 29] that the Kondo problem corresponds to a one-dimensional Ising model with a combination of inverse-square and nearest-neighbour interactions. Yet another application follows from Ref. [22], where it was shown that random exchange (Lévy-flight) processes can generate effective interactions which decay algebraically. Hence, the universal critical properties of the nonequilibrium steady state of these systems are those of the long-range equilibrium Ising models studied in this and the following chapter. Finally, these models allow us to use low-dimensional systems to study

phenomena above the upper critical dimension, since the upper critical dimension can be varied by tuning the decay rate of the interaction.

Below, we present accurate numerical results for Ising systems with algebraically decaying interactions in one, two and three dimensions. Until now, the long-range character of the spin–spin interactions has been the main bottleneck for the examination of these systems by means of numerical methods (and, in fact, also for their analytical solution). All previously published numerical results therefore rely on various extrapolations based on data for small systems. However, our novel Monte Carlo algorithm for the first time enables us to efficiently simulate these systems. The high accuracy of the results opens several perspectives: i) verification of the renormalization predictions for the critical exponents; ii) accurate observation of logarithmic corrections at the upper critical dimension; iii) first estimates of the critical temperatures of two- and three-dimensional systems with long-range interactions; iv) verification of previously obtained estimates of the critical temperatures of one-dimensional systems, which in addition implies a check on the various extrapolation methods that have been developed; v) verification of predicted bounds on the critical temperatures; vi) verification of a conjecture on the behaviour of the critical temperature as a function of the decay parameter. Another problem one encounters in the simulations is the large parameter space: the simulations for a set of different temperatures and system sizes have to be repeated for a range of values of the decay parameter and for $d = 1, 2, 3$. The total computing time dedicated to the results presented here amounts to approximately two CPU years on a modern workstation.

The outline of this chapter is as follows. In Sec. 4.2, we sum up the known rigorous results for the Ising chain with long-range interactions. We review the renormalization-group (RG) scenario of these models in Sec. 4.3 and derive the finite-size scaling behaviour of several quantities. These scaling functions include the corrections to scaling, both at and above the upper critical dimension. Our numerical results are presented and analyzed in Sec. 4.4 and compared with previously obtained results. Finally, we summarize our conclusions in Sec. 4.5.

4.2 Rigorous results for the one-dimensional case

For the one-dimensional case, the Hamiltonian is given by

$$\mathcal{H} = \sum_{ij} J(i-j) s_i s_j, \quad (4.1)$$

where the sum runs over all spin pairs. Since we are interested in algebraically decaying interactions, we have $J(n) \propto n^{-\alpha}$. To ensure that the energy of the system does not diverge, it is required that $\alpha > 1$. In 1968, Ruelle [1] rigorously proved the

absence of long-range order in a spin chain with ferromagnetic spin–spin couplings $J(i - j)$ such that the sum

$$\sum_{n=1}^N nJ(n) \tag{4.2}$$

does not diverge in the limit $N \rightarrow \infty$. In the case of algebraically decaying interactions, this implies the absence of a phase transition for $\alpha > 2$. Shortly later, Dyson [2] proved the *existence* of a phase transition if the sums $\sum_{n=1}^N J(n)$ and $\sum_{n=1}^N (\ln \ln n) [n^3 J(n)]^{-1}$ both converge, for positive and monotonically decreasing $J(n)$. In particular, a phase transition occurs for $J(n) \propto n^{-\alpha}$ with $1 < \alpha < 2$. This *partly* corroborated the conjecture of Kac and Thompson [53], *viz.* that there is a phase transition for $1 < \alpha \leq 2$. Furthermore, Dyson [3] was (as were—much later—also Rogers and Thompson [6]) able to replace Ruelle’s condition with a stronger one, which however still left the case $\alpha = 2$ undecided. This also holds for an even more stringent criterion by Thouless [4], who generalized the argument of Landau and Lifshitz [54] for the absence of a phase transition in an Ising chain with short-range interactions. However, Thouless argued on entropic grounds that *if* a phase transition exists for $\alpha = 2$, the magnetization must have a *discontinuity* at the transition point. This was later dubbed the “Thouless effect” by Dyson, who proved it to occur in the closely related hierarchical model [55]. Simon and Sokal made Thouless’ argument partially rigorous [5], but later Aizenman *et al.* [9] showed that, although a discontinuity in the order parameter *is indeed present* if there is a phase transition, his argument does *not* account for this. Namely, Thouless had assumed that the spin–spin correlation function $\langle s_0 s_r \rangle - \langle s_0 \rangle \langle s_r \rangle$ vanishes in the limit $r \rightarrow \infty$, whereas actually the critical exponent η is equal to 1 in this case. Meanwhile, Fröhlich and Spencer [7] had been able to rigorously prove the *existence* of a phase transition in the borderline case and thus to corroborate the Kac–Thompson conjecture for $\alpha = 2$ as well. Another interesting point is the rigorous proof for the existence of an intermediate ordered phase in the one-dimensional model with inverse-square interactions, where the two-point correlation function exhibits power-law decay with an exponent that varies continuously in a finite temperature range below the critical temperature [11].

4.3 Renormalization-group study of the critical behaviour

Already in a very early stage of the history of the ε -expansion, Fisher, Ma and Nickel analyzed the critical behaviour of d -dimensional systems ($d < 4$) with long-range interactions decaying as $r^{-(d+\sigma)}$, with $\sigma > 0$. [35] They concluded that the upper critical dimension is given by $d_u = 2\sigma$, as was previously conjectured by Stell [38]

and later rigorously proven by Aizenman and Fernández [10]. For more slowly decaying interactions, $0 < \sigma < d/2$, the critical behaviour is classical, whereas the critical exponents assume nonclassical, continuously varying values for $d/2 < \sigma < 2$. For $\sigma > 2$ they take their short-range (Ising) values. Sak [36], however, found that already for $\sigma > 2 - \eta_{\text{sr}}$ the critical behaviour is Ising-like, where η_{sr} denotes the exponent η in the corresponding model with short-range interactions. Several authors have in turn contested the correctness of Sak's scenario. We will pay ample attention to this issue in the next chapter. Here we concentrate on the classical range, for which we have performed extensive Monte Carlo simulations of spin models in $d = 1, 2, 3$. For completeness, we mention that several of the RG results had already been anticipated by Joyce, who generalized the spherical model (exactly solved by Berlin and Kac [56]) to the case of long-range interactions [57].

First, we outline the renormalization-group scenario for these models, in order to derive the finite-size scaling relations required to analyze the numerical data. In particular we discuss some specific issues arising above the upper critical dimension. We start from the following Landau–Ginzburg–Wilson Hamiltonian in momentum space,

$$\begin{aligned} \mathcal{H}(\phi_{\mathbf{k}})/k_{\text{B}}T = & \frac{1}{2} \sum_{\mathbf{k}} (j_{\sigma} k^{\sigma} + j_2 k^2 + r_0) \phi_{\mathbf{k}} \phi_{-\mathbf{k}} \\ & + \frac{u}{4N} \sum_{\mathbf{k}_1} \sum_{\mathbf{k}_2} \sum_{\mathbf{k}_3} \phi_{\mathbf{k}_1} \phi_{\mathbf{k}_2} \phi_{\mathbf{k}_3} \phi_{-\mathbf{k}_1 - \mathbf{k}_2 - \mathbf{k}_3} - h \sqrt{N} \phi_{\mathbf{k}=\mathbf{0}}, \end{aligned} \quad (4.3)$$

where the $\phi_{\mathbf{k}}$ are the Fourier components of the order parameter $\phi(\mathbf{r})$. In the case of the Ising model, $\phi(\mathbf{r})$ is just a real scalar field, but the formulation can straightforwardly be extended to the case of an n -component order parameter. In Chapter 6 we will discuss the underlying ideas of the renormalization-group theory in some more detail. The $j_{\sigma} k^{\sigma}$ term arises from the Fourier transform of the interactions decaying as $r^{-(d+\sigma)}$. The $j_2 k^2$ term normally representing the short-range interactions is included because it will appear anyway in the renormalization process and will compete with the long-range term [36]. h is the magnetic field, r_0 is a measure for the temperature distance to the critical point and the term proportional to u keeps the spin ϕ finite when $r_0 \leq 0$. Under a renormalization transformation with a rescaling factor $b = e^l$, the term $j_{\sigma} k^{\sigma}$ is transformed into $j_{\sigma} k'^{\sigma}$, with $\mathbf{k}' = \mathbf{k}b$. When the long-range forces determine the critical behaviour, we must keep the coefficient of the k^{σ} term fixed and rescale the field $\phi_{\mathbf{k}}$ to $\phi'_{\mathbf{k}'} = b^{-\sigma/2} \phi_{\mathbf{k}}$. Thus, the k^2 term changes as $b^{\sigma-2}$, which indeed suggests the conclusion that for $\sigma < 2$ the long-range forces dominate (here we ignore the subtleties discussed in Chapter 5, which may modify this conclusion near $\sigma = 2$). The coefficient of the ϕ^4 term changes proportional to $b^{2\sigma-d}$. Hence, the Gaussian fixed point dominates the renormalization flow for $\sigma \leq d/2$. This is the situation treated in this chapter. Figure 4.1 displays the regions

of classical and nonclassical critical behaviour as a function of d and σ . We now proceed to discuss the renormalization equations. These equations describe how the coefficients r_0 and u appearing in Eq. (4.3) change under a renormalization transformation with a rescaling factor b . For a detailed derivation we refer to, e.g., Ref. [58]. While it is possible to formulate these equations in terms of a discrete rescaling, we have adopted the (more convenient) formulation in differential form.

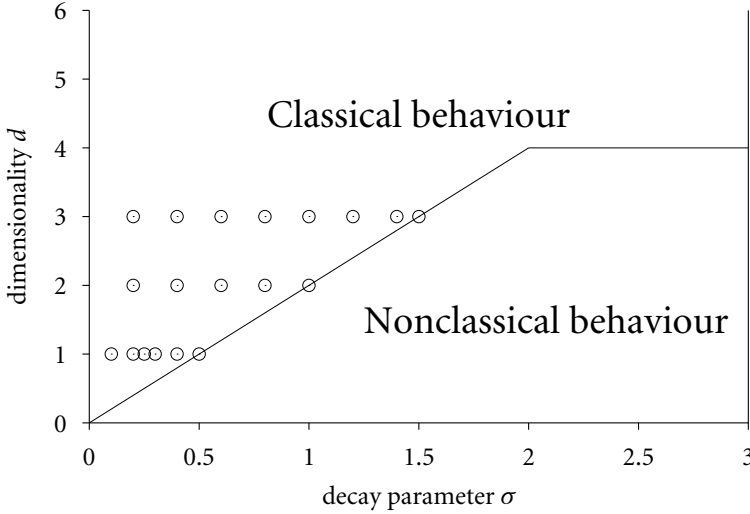


Figure 4.1: Dimensionality versus decay parameter σ . The full lines mark the upper critical dimension, i.e., they separate the classical from the nonclassical critical behaviour. Short-range models are described by $\sigma \geq 2$. The open circles indicate the models investigated in this chapter.

For the sake of generality we treat here the case of an n -component order parameter with $O(n)$ symmetry, which implies that the parameter u in Eq. (4.3) is replaced by a tensor of the form $(u/3)(\delta_{ij}\delta_{kl} + \delta_{ik}\delta_{jl} + \delta_{il}\delta_{jk})$, and of course summations over the indices appear. The renormalization equations are then given by (recall that $l = \ln b$)

$$\frac{dr_0}{dl} = \sigma r_0 + a(n+2)u(c - r_0), \quad (4.4a)$$

$$\frac{du}{dl} = \varepsilon u - a(n+8)u^2, \quad (4.4b)$$

where $(n+2)$ and $(n+8)$ are the usual factors arising from the tensorial structure of the interaction part of the Hamiltonian [59], $\varepsilon \equiv 2\sigma - d$ and a and c are constants. These equations are not complete to second order, because the $\mathcal{O}(u^2)$ term is missing

in Eq. (4.4a). The rescaling factor of the field,¹ $b^{-\sigma/2}$, is not changed by higher-order terms and hence we see from the last term in (4.3) that the magnetic field rescales as $h' = hb^{(d+\sigma)/2}$, yielding the magnetic exponent $\gamma_h = (d + \sigma)/2$.

We first consider the case $\varepsilon < 0$, i.e., strictly above the upper critical dimension. The solution of the second equation is given by

$$u(l) = \bar{u}e^{\varepsilon l} \frac{1}{1 + \bar{u} \frac{a(n+8)}{\varepsilon} (e^{\varepsilon l} - 1)}, \quad (4.5)$$

where \bar{u} denotes the value of u at $l = 0$. This yields, to leading order in u , the following solution for the first equation,

$$r_0(l) = [\bar{r}_0 + ac(n+2)\bar{u}/(d-\sigma)] e^{\sigma l} \left[\frac{1}{1 + \frac{a(n+8)}{\varepsilon} \bar{u} (e^{\varepsilon l} - 1)} \right]^{(n+2)/(n+8)} - \frac{ac(n+2)\bar{u}e^{\varepsilon l}/(d-\sigma)}{1 + \frac{a(n+8)}{\varepsilon} \bar{u} (e^{\varepsilon l} - 1)}, \quad (4.6)$$

with $\bar{r}_0 \equiv r_0(l=0)$. The first factor between square brackets is proportional to the reduced temperature $t \equiv (T - T_c)/T_c$ and the last term is the so-called *shift* of the critical temperature. The factors $[1 + a(n+8)\bar{u}(e^{\varepsilon l} - 1)/\varepsilon]^{-1}$ in Eqs. (4.5) and (4.6) are higher-order corrections in u . Under successive renormalization transformations, u approaches the value $u^* = 0$ and the Gaussian fixed point $(0, 0)$ is thus indeed stable. The pertinent renormalization exponents can immediately be read off from Eqs. (4.5) and (4.6), respectively: the leading irrelevant exponent $\gamma_l = \varepsilon = 2\sigma - d$ and the thermal exponent $\gamma_t = \sigma$.

At $\varepsilon = 0$, the Gaussian fixed point becomes marginally stable. Solving Eq. (4.4b) leads to

$$u^{\text{uc}}(l) = \frac{\bar{u}}{1 + a(n+8)\bar{u}l}, \quad (4.7)$$

where the superscript “uc” indicates that we are operating at the upper critical dimension. This solution can be used to solve, again to leading order in u , Eq. (4.4a), yielding

$$r_0^{\text{uc}}(l) = [\bar{r}_0 + ac(n+2)\bar{u}/(d/2)] e^{\sigma l} \left[\frac{1}{1 + a(n+8)\bar{u}l} \right]^{(n+2)/(n+8)} - \frac{ac(n+2)\bar{u}/(d/2)}{1 + a(n+8)\bar{u}l} \quad (4.8)$$

¹Unless explicitly stated otherwise, the term “field” refers to the order parameter ϕ .

or, in terms of the rescaling factor b ,

$$r_0^{\text{uc}} = [\bar{r}_0 + ac(n+2)\bar{u}/(d/2)] b^\sigma \left[\frac{1}{1 + a(n+8)\bar{u} \ln b} \right]^{(n+2)/(n+8)} - \frac{ac(n+2)\bar{u}/(d/2)}{1 + a(n+8)\bar{u} \ln b}. \quad (4.9)$$

Since σ is fixed at $d/2$ the factor $d/2$ in the last term is identical to the corresponding factor $(d - \sigma)$ in Eq. (4.6). Further comparison of Eqs. (4.6) and (4.8) shows that above the upper critical dimension the leading shift of the critical temperature is proportional to b^ε , whereas this factor vanishes at the upper critical dimension itself and the factor $(e^{\varepsilon l} - 1)/\varepsilon$ in the second-order terms turns into a $\ln b$ term, yielding a logarithmic shift of the form $1/(A \ln b + B)$.

From the solutions of the renormalization equations we can derive the scaling behaviour of the free energy and of (combinations of) its derivatives. For the case $\varepsilon < 0$ the free-energy density f scales, to leading order, as

$$f(t, h, u, 1/L) = b^{-d} f(b^{y_t} [t + \tilde{\alpha} u b^{y_i - \gamma_t}], b^{y_h} h, b^{y_u} u, b/L) + g_0(b), \quad (4.10)$$

where $\tilde{\alpha} = -ac(n+2)/(d - \sigma)$ and we have included a finite-size field L^{-1} . $g_0(b)$ denotes the analytic part of the transformation. We abbreviate the first term on the right-hand side as $b^{-d} f(t', h', u', b/L)$. However, we must take into account the fact that, for $T \leq T_c$, the free energy is singular at $u = 0$. This makes u a so-called *dangerous* irrelevant variable; see, e.g., Ref. [60]. It leads to the breakdown of finite-size scaling as noticed in Ref. [61]. The correct finite-size scaling properties can now be obtained by renormalizing the system to size 1, i.e., by setting $b = L$. The number of degrees of freedom then reduces to one and the free energy to

$$f(t', h', u', 1) = \ln \int_{-\infty}^{+\infty} d\phi \exp \left[h'\phi - \frac{1}{2} r'_0 \phi^2 - \frac{1}{4} u' \phi^4 \right]. \quad (4.11)$$

The substitution $\phi' = \phi/u'^{1/4}$ then leads to a new universal function, \tilde{f} , with

$$f(t', h', u', 1) + g_0(L) = \tilde{f}(\tilde{t}, \tilde{h}) + g_1, \quad (4.12)$$

where $\tilde{t} = t'/u'^{1/2}$ and $\tilde{h} = h'/u'^{1/4}$. The analytic part of the transformation also contributes to the singular dependence of the free energy on t : despite the regularity of this term in each single renormalization step, the infinite number of steps still leads to the build-up of a singularity. This often neglected point was emphasized for the first time by Ma [62] and is discussed in some detail in Ref. [58, Ch. VI, § 3]. Since this contribution, contained in $g_0(L)$, has the same degree of singularity as the singular part of the free energy, we absorb it in \tilde{f} . The truly analytic contribution in $g_0(L)$ [cf. Eq. (3.8)] is denoted by g_1 on the right-hand side of Eq. (4.12). This latter

term is ignored for the moment, but we will return to it shortly. Setting $b = L$ in Eq. (4.10) and combining it with Eq. (4.12) yields

$$f\left(t, h, u, \frac{1}{L}\right) = L^{-d} \tilde{f}\left(L^{y_t - y_i/2} \frac{1}{u^{1/2}} [t + \tilde{\alpha} u L^{y_i - y_t}], L^{y_h - y_i/4} \frac{h}{u^{1/4}}\right) \quad (4.13a)$$

$$= L^{-d} \tilde{f}\left(L^{y_t^*} \frac{1}{u^{1/2}} [t + \tilde{\alpha} u L^{y_i - y_t}], L^{y_h^*} \frac{h}{u^{1/4}}\right). \quad (4.13b)$$

Here, we have introduced the exponents $y_t^* \equiv y_t - y_i/2 = d/2$ and $y_h^* \equiv y_h - y_i/4 = 3d/4$. The first argument on the right-hand side is the scaled temperature

$$\tilde{t} = L^{d/2} \frac{1}{\sqrt{u}} \left(t + \tilde{\alpha} u L^{\sigma-d}\right). \quad (4.14)$$

Interpreting the term $\tilde{\alpha} u L^{\sigma-d}$ as a shift of the “effective critical temperature” for a finite system, we recover for $\sigma = 2$ the result obtained by Brézin and Zinn-Justin for high-dimensional systems with short-range interactions [63]. Below we will come back to this shift of the critical temperature. The critical exponents corresponding to y_t^* and y_h^* indeed assume their fixed, classical values; $\alpha = 0$, $\beta = 1/2$, $\gamma = 1$, $\delta = 3$. The exponent γ is singled out here as a special case; even without taking into account the modification of y_t and y_h due to the dangerous irrelevant variable one obtains the classical value $\gamma = 1$. Since the correlation length exponent $\nu = 1/y_t$ (it is not affected by the singular dependence of the free energy on u), we see that hyperscaling is violated, which is a well-known result for systems above their upper critical dimension [60]. The rescaling of the pair-correlation function $g(|\mathbf{r}|)$ (decaying proportional to $1/r^{d-2+\eta}$) relates the exponent η to the rescaling factor of the field ϕ . Indeed, the Fourier-transformed correlation function $\langle \phi_{\mathbf{k}} \phi_{-\mathbf{k}} \rangle$ is proportional to $k^{\eta-2}$, which is expressed in rescaled wave vectors as $(k'/b)^{\eta-2}$. But we also have $\langle \phi_{\mathbf{k}} \phi_{-\mathbf{k}} \rangle = b^\sigma \langle \phi'_{\mathbf{k}'} \phi'_{-\mathbf{k}'} \rangle$ (no higher-order terms contribute to the rescaling of the correlation function) and hence $b^\sigma = b^{2-\eta}$ or $\eta = 2 - \sigma$. Note that this contrasts with the short-range case ($\sigma = 2$), where η assumes its mean-field value for all dimensionalities $d \geq 4$. This implies that direct experimental measurement of either ν or η offers a way to discern whether the interactions in a system are mean-field-like ($\nu = 1/2$, $\eta = 0$) or have the form of a slowly decaying power-law. Below the upper critical dimension, however, the finite-size scaling behaviour of the spin-spin correlation function is (apart from a volume factor) identical to that of the magnetic susceptibility χ , as we have seen in the previous chapter. This relation yields a contradiction above the upper critical dimension, since χ depends on the scaled combination $tL^{y_t^*}$, instead of tL^{y_t} . Indeed, the susceptibility diverges as $t^{-\gamma}$ and the finite-size behaviour of χ is thus $\chi(L) \propto L^{\gamma y_t^*} = L^{d/2}$, corresponding to $g(L) \propto L^{-d/2}$. On the other hand, if one assumes that the finite-size behaviour of the correlation function is identical to its r dependence, one expects that $g(L) \propto L^{-(d-2+\eta)} = L^{-(d-\sigma)}$.

Only at the upper critical dimension, $d_u = 2\sigma$, these two predictions coincide. We will return to this point at the end of this section. Furthermore, we will examine the behaviour of the spin–spin correlation function in Sec. 4.4.

At the upper critical dimension itself, i.e., at $\varepsilon = 0$, the free-energy density scales as

$$\begin{aligned} f\left(t, h, u, \frac{1}{L}\right) &= b^{-d} f\left(\frac{b^{y_t}}{(1 + \tilde{\beta}u \ln b)^{(n+2)/(n+8)}} \left[t + \tilde{\alpha} b^{-y_t} \frac{u}{(1 + \tilde{\beta}u \ln b)^{6/(n+8)}} \right], \right. \\ &\quad \left. b^{y_h} h, \frac{u}{1 + \tilde{\beta}u \ln b}, \frac{b}{L}\right) + g \end{aligned} \quad (4.15a)$$

$$\begin{aligned} &= L^{-d} \tilde{f}\left(\frac{L^{y_t}}{(1 + \tilde{\beta}u \ln L)^{(n+2)/(n+8)-1/2}} \frac{1}{u^{1/2}} \left[t + \tilde{\alpha} L^{-y_t} \frac{u}{(1 + \tilde{\beta}u \ln L)^{6/(n+8)}} \right], \right. \\ &\quad \left. L^{y_h} \frac{h}{u^{1/4}} [1 + \tilde{\beta}u \ln L]^{1/4}\right), \end{aligned} \quad (4.15b)$$

where $\tilde{\beta} = a(n+8)$ and we have set $b = L$ in the last line. u is now a marginal variable and although we again have to perform the substitution $\phi \rightarrow \phi'$ (the Gaussian fixed point is marginally stable), the exponents y_t and y_h coincide with y_t^* and y_h^* , respectively, because y_1 vanishes. Thus, the scaling relations (4.13b) and (4.15b) differ to leading order only in the logarithmic factors arising in the arguments of \tilde{f} .

Just as in Chapter 3, the finite-size scaling relations are now found by taking derivatives of the free-energy density with respect to the appropriate scaling fields. In the Monte Carlo simulations we have sampled the second and the fourth moment of the magnetization density, the dimensionless amplitude ratio $Q \equiv \langle m^2 \rangle^2 / \langle m^4 \rangle$ (introduced in Sec. 3.4) and the spin–spin correlation function over half the system size (for even system sizes). The second moment of the magnetization density is (apart from a volume factor) equal to the second derivative of the free-energy density with respect to h ,

$$\langle m^2 \rangle = L^{-d} \frac{\partial^2 f}{\partial h^2}(t, h, u, 1/L) = L^{2y_h^* - 2d} u^{-1/2} \tilde{f}^{(2)}\left(L^{y_t^*} \frac{\hat{t}}{u^{1/2}}, L^{y_h^*} \frac{h}{u^{1/4}}\right), \quad (4.16)$$

where $\tilde{f}^{(2)}$ stands for the second derivative of \tilde{f} with respect to its second argument and $\hat{t} \equiv t + \tilde{\alpha} u L^{y_t - y_t}$. At $\varepsilon = 0$, logarithmic factors do arise not only in the arguments of $\tilde{f}^{(2)}$, but also in the prefactor,

$$\langle m^2 \rangle = L^{2y_h - 2d} \left(\frac{1 + \tilde{\beta}u \ln L}{u}\right)^{1/2} \times$$

$$\times \tilde{f}^{(2)} \left(\frac{L^{y_t}}{(1 + \tilde{\beta}u \ln L)^{(n+2)/(n+8)-1/2}} \frac{1}{u^{1/2}} \left[t + \tilde{\alpha} L^{-y_t} \frac{u}{(1 + \tilde{\beta}u \ln L)^{6/(n+8)}} \right], \right. \\ \left. L^{y_h} \frac{h}{u^{1/4}} [1 + \tilde{\beta}u \ln L]^{1/4} \right). \quad (4.17)$$

For the fourth magnetization moment similar expressions hold and in the amplitude ratio Q all prefactors divide out, both for $\varepsilon < 0$ and $\varepsilon = 0$. Thus we find that the ratio Q is given by a universal function \tilde{Q} ,

$$Q_L(T) = \tilde{Q} \left(L^{y_t^*} \frac{\hat{t}}{u^{1/2}} \right) + q_1 L^{d-2y_h^*} + \dots, \quad (4.18)$$

where we have omitted the h dependence of \tilde{Q} , since we are only interested in the case $h = 0$. The additional term proportional to q_1 arises from the h dependence of the analytic part of the free energy [the contribution g_1 in Eq. (4.12)], as discussed in Sec. 3.4, and the ellipsis stands for higher powers of $L^{d-2y_h^*}$ (faster-decaying terms). At $\varepsilon = 0$, \hat{t} must be replaced by the first argument within square brackets in Eq. (4.15b), multiplied by the factor $(1 + \tilde{\beta}u \ln L)^{1/2-(n+2)/(n+8)}$.

An additional result we can derive from Eq. (4.13b) is the shift and rounding of critical singularities in finite systems. If we ignore the corrections to scaling due to the analytic part of the free energy, we can express observables in terms of *universal functions* of the two arguments that appear in the right-hand side of (4.13b). For example, the specific heat can be written as the product of a power of the system size and a *universal function* of the scaled fields. Let the maximum of this function occur at $\tilde{t} = c$ (c a constant). Then, the specific-heat maximum occurs at a temperature which differs, to leading orders in L , from the critical temperature by

$$\Delta t = c\sqrt{u}L^{-d/2} - \tilde{\alpha}uL^{\sigma-d} = c\sqrt{u}L^{-d/2} \left[1 - \frac{\tilde{\alpha}}{c}\sqrt{u}L^{\sigma-d/2} \right]. \quad (4.19)$$

Note that this expression holds for $\sigma < d/2$. For $\sigma = d/2$ we find

$$\Delta t = c\sqrt{u}L^{-d/2} \frac{1}{(1 + \tilde{\beta}u \ln L)^{(4-n)/[2(n+8)]}} \left[1 - \frac{\tilde{\alpha}}{c} \sqrt{\frac{u}{1 + \tilde{\beta}u \ln L}} \right], \quad (4.20)$$

where we have assumed $n \neq 4$. Also in Eq. (4.19) n -dependent factors arise, but only in higher-order terms. For example, the analog of the logarithmic prefactor in Eq. (4.20) is a factor $[1 + \tilde{\beta}u(L^{y_i} - 1)/y_i]^{(n-4)/[2(n+8)]}$.

Interestingly, the finite-size properties of the spherical model with long-range interactions have been studied in Refs. [64, 65], where it was found that the finite-size shift of the (pseudo)critical temperature is proportional to $L^{\sigma-d}$. This analytical result precisely agrees with the renormalization prediction (4.19) [i.e., the last term

of (4.14)]. Indeed, the form of the shift term does not change in the $n \rightarrow \infty$ limit, which corresponds to the spherical model [66].

Clearly, also the function \tilde{Q} [Eq. (4.18)] has a universal value Q at criticality and it was shown in Ref. [63] that this quantity can be calculated exactly: $Q = 8\pi^2/\Gamma^4(\frac{1}{4}) = 0.456947\dots$. This is just the value of Q in the mean-field model as calculated in Appendix A.

Finally, let us reconsider the finite-size scaling behaviour of the spin–spin correlation function $g(|\mathbf{r}|)$, where we may explicitly indicate the L dependence by writing $g(r, L)$. In Sec. 3.5.3, we derived this scaling behaviour by differentiating the free-energy density to two *local* magnetic fields, which couple to the spins at positions $\mathbf{0}$ and \mathbf{r} , respectively, and assuming that the finite-size behaviour is identical to the r dependence of g . However, it turns out that above the upper critical dimension one must distinguish between two different limits, *viz.* $\lim_{L \rightarrow \infty} g(r, L)$ (where r is kept finite) and $\lim_{L \rightarrow \infty} g(\lambda L, L)$, where $0 < \lambda < 1$. If we do not take into account the dangerous-irrelevant-variable mechanism, we find $g(L) \propto L^{2\gamma_h - 2d} = L^{-(d-\sigma)}$, just as we found before from $\eta = 2 - \sigma$. However, replacing γ_h by γ_h^* yields $g(L) \propto L^{-d/2}$, in agreement with the L dependence of the magnetic susceptibility. This clarifies the difference between the two predictions: at short distances (large wave vectors), the $j_\sigma k^\sigma \phi_{\mathbf{k}} \phi_{-\mathbf{k}}$ term will be the dominant term in the Landau–Ginzburg–Wilson Hamiltonian and there is no “dangerous” dependence on u . Hence, the finite-size behaviour of the spin–spin correlation function will be given by $L^{-(d-2+\eta)}$. For $\mathbf{k} = \mathbf{0}$ (which corresponds to the second limit), the coefficient of the ϕ^2 term vanishes and thus the $u\phi^4$ term is required to act as a bound on the magnetization. To account for this singular dependence on u , we rescale the field, which implies that γ_h is replaced by γ_h^* and $g(L)$ scales as $L^{2\gamma_h^* - 2d}$. In a finite system, the wave vectors assume discrete values, $\mathbf{k} = (n_x, n_y, n_z)2\pi/L$, and thus it is easily seen that even for the lowest nonzero wave vectors (i.e., large but finite r) $j_\sigma k^\sigma \phi_{\mathbf{k}} \phi_{-\mathbf{k}}$ constitutes the dominant bounding term on the magnetization. Namely, the coefficient of the ϕ^4 term contains a volume factor L^{-d} [cf. Eq. (4.3)] and this term is thus (above the upper critical dimension) a higher-order contribution decaying as $L^{2\sigma-d}$.

4.4 Numerical results and comparison with earlier results

4.4.1 Simulations

We have carried out Monte Carlo simulations for systems described by the Hamiltonian

$$\mathcal{H}/k_B T = - \sum_{\langle ij \rangle} J(|\mathbf{r}_i - \mathbf{r}_j|) s_i s_j, \quad (4.21)$$

where the sum runs over all spin pairs and periodic boundaries were employed. The precise form of the (long-range) spin–spin interaction $J(r)$ as used in the simulations was chosen dependent on the dimensionality. For $d = 1$ we have followed the conventional choice $J(r) = K/r^{d+\sigma}$ (with *discrete* values for r), as this allows us to compare *all* our results (including nonuniversal quantities) to previous estimates. However, as explained in Chapter 2, this discrete form requires the construction of a look-up table, which becomes inefficient for higher dimensionalities. For $d = 2$ we have thus applied an interaction which is the integral of a continuously decaying function,

$$J(|\mathbf{r}|) = K \int_{r_x - \frac{1}{2}}^{r_x + \frac{1}{2}} dx \int_{r_y - \frac{1}{2}}^{r_y + \frac{1}{2}} dy (x^2 + y^2)^{-(d+\sigma)/2}, \quad (4.22)$$

where $\mathbf{r} = (r_x, r_y)$. In $d = 3$ the corresponding volume integral was used for $J(|\mathbf{r}|)$. This modification of the interaction does only change nonuniversal quantities like the critical temperature, but should not influence the universal critical properties like the critical exponents and dimensionless amplitude ratios, since the difference between the continuous and the discrete interaction consists of faster decaying terms that are irrelevant according to renormalization-group theory.

The following system sizes have been examined: chains of length $10 \leq L \leq 150\,000$, square systems of linear size $4 \leq L \leq 240$, and cubic systems of linear size $4 \leq L \leq 64$. At the upper critical dimension simulations for even larger systems have been carried out in order to obtain accurate results from the analyses: $L = 300\,000$ in $d = 1$ and $L = 400$ in $d = 2$. (Thus, in terms of numbers of particles the largest system size for $d = 2$ is considerably smaller than for $d = 1$ and $d = 3$.) The efficiency gain due to the application of the algorithm described in Chapter 2 is of the order of 10^8 for the largest system sizes. For each data point we have generated between 10^6 and 4×10^6 Wolff clusters.

4.4.2 Determination of the critical temperatures, the amplitude ratio Q and the thermal exponent

The critical couplings K_c of these systems have been determined using an analysis of the amplitude ratio Q . The finite-size scaling analysis was based on the Taylor expansion of Eq. (4.18), which for $\varepsilon < 0$ reads [cf. Eq. (3.14)]:

$$\begin{aligned} Q_L(T) = & Q + p_1 \hat{t} L^{y_t^*} + p_2 \hat{t}^2 L^{2y_t^*} + p_3 \hat{t}^3 L^{3y_t^*} + \dots \\ & + q_1 L^{d-2y_h^*} + \dots + q_3 L^{y_i} + \dots \end{aligned} \quad (4.23)$$

The term proportional to $\tilde{\alpha}$ in \hat{t} yields a contribution $q_2 L^{y_i/2} = q_2 L^{\sigma-d/2}$, as follows from Eq. (4.14). Such a correction, with an exponent that is only half of the leading irrelevant exponent, is specific for finite-size scaling above the upper critical

Table 4.1: The amplitude ratio Q and the thermal exponent y_t^* for systems with long-range interactions in one, two and three dimensions, for several values of the decay parameter $0 < \sigma \leq d/2$. The values in the fifth column have been obtained with Q fixed at the theoretically predicted value (see text) and the last column lists the renormalization predictions for y_t^* .

d	σ	Q	y_t^*	y_t^*	RG
1	0.1	0.4566 (8)	0.507 (7)	0.507 (7)	$\frac{1}{2}$
1	0.2	0.455 (4)	0.54 (4)	0.504 (12)	$\frac{1}{2}$
1	0.25	0.457 (3)	0.500 (8)	0.500 (5)	$\frac{1}{2}$
1	0.3	0.454 (2)	0.519 (14)	0.506 (12)	$\frac{1}{2}$
1	0.4	0.457 (3)	0.50 (2)	0.50 (2)	$\frac{1}{2}$
1	0.5	0.462 (6)	0.51 (5)	0.49 (2)	$\frac{1}{2}$
2	0.2	0.4574 (10)	1.01 (2)	1.01 (2)	1
2	0.4	0.455 (2)	1.02 (2)	1.009 (15)	1
2	0.6	0.450 (6)	1.04 (4)	1.008 (17)	1
2	0.8	0.454 (6)	1.03 (9)	1.03 (3)	1
2	1.0	0.450 (10)	1.02 (3)	1.03 (2)	1
3	0.2	0.4581 (11)	1.51 (3)	1.513 (18)	$\frac{3}{2}$
3	0.4	0.4561 (10)	1.521 (18)	1.512 (15)	$\frac{3}{2}$
3	0.6	0.453 (3)	1.53 (4)	1.521 (14)	$\frac{3}{2}$
3	0.8	0.458 (2)	1.48 (2)	1.487 (10)	$\frac{3}{2}$
3	1.0	0.453 (10)	1.52 (7)	1.508 (9)	$\frac{3}{2}$
3	1.2	0.447 (8)	1.56 (2)	1.519 (10)	$\frac{3}{2}$
3	1.4	0.454 (5)	1.48 (3)	1.48 (3)	$\frac{3}{2}$
3	1.5	0.449 (8)	1.53 (5)	1.46 (3)	$\frac{3}{2}$

dimension. The next correction, $q_3 L^{y_i}$, comes from the denominator in Eq. (4.5). The coefficients p_i and q_i are nonuniversal. In addition to the corrections to scaling in Eq. (4.23) we have also included higher powers of $q_3 L^{y_i}$, which become particularly important when y_i is small (i.e., when σ is close to $d/2$), higher powers of $q_1 L^{d-2y_h^*} = q_1 L^{-d/2}$ and the crossterm proportional to $L^{y_t^*+y_i}$.

Several analyses have been carried out in order to determine the thermal exponent y_t , the amplitude ratio Q and the critical couplings as a function of the decay parameter σ . First, we have only kept fixed the exponents in the correction terms, y_i and y_h^* . The corresponding estimates for Q and y_t^* are shown in the third and fourth

column of Table 4.1. One observes that the Monte Carlo results for both Q and γ_t^* are in quite good agreement with the renormalization predictions $Q = 0.456947\dots$ and $\gamma_t^* = d/2$. However, the uncertainties in the estimates increase considerably with increasing σ , because the leading irrelevant exponent becomes very small. An exception is the relatively large uncertainty in γ_t^* ($d = 1, \sigma = 0.2$), which originates from the fact that the Monte Carlo data were taken in a rather narrow temperature region around the critical point. Furthermore, an accurate simultaneous determination of Q and γ_t^* is very difficult, because of the correlation between the two quantities. Therefore we have repeated the same analysis with Q fixed at its theoretical prediction—as appears justified by the values for Q in Table 4.1—in order to obtain more accurate estimates for γ_t^* . The results, shown in the fifth column of Table 4.1, are indeed in good agreement with the theoretically expected values (last column). Thus, we have kept the thermal exponent fixed at its theoretical value in the further analysis. The corresponding results for Q and K_c are shown in Table 4.2. Over the full range of σ and d the Monte Carlo results for Q show good agreement with the renormalization prediction, thus confirming the universality of this quantity above the upper critical dimension.

The universality of Q is illustrated graphically in Figs. 4.2(a)–4.2(c), where the increasing importance of corrections to scaling upon approaching the upper critical dimension clearly follows from the size of the error bars. At the upper critical dimension itself ($\varepsilon = 0$) this culminates in the appearance of logarithmic corrections, where the finite-size scaling form of Q_L is given by

$$\begin{aligned}
 Q_L(T) = & Q + p_1 L^{\gamma_t} (\ln L)^{1/6} \left[t + v \frac{L^{-\gamma_t}}{(\ln L)^{2/3}} \right] \\
 & + p_2 L^{2\gamma_t} (\ln L)^{1/3} \left[t + v \frac{L^{-\gamma_t}}{(\ln L)^{2/3}} \right]^2 + \dots \\
 & + q_1 L^{d-2\gamma_h} + \dots + \frac{q_3}{\ln L} + \dots .
 \end{aligned} \tag{4.24}$$

The ellipses denote terms containing higher powers of $L^{d-2\gamma_h}$ and $1/\ln L$. The extremely slow convergence of this series is reflected in the uncertainty in the resulting estimates for Q at the upper critical dimension. To illustrate the dependence of the finite-size corrections on ε more directly, Fig. 4.3(a) displays (for equally-spaced values of σ) the finite-size scaling functions as they follow from a least-squares fit of the data for $d = 1$ to Eqs. (4.23) and (4.24), respectively. Although one clearly observes the increase of finite-size corrections when $\sigma \rightarrow d/2$, the true nature of the logarithmic corrections in (4.24) cannot be appreciated from this graph. To emphasize the difference between $\varepsilon = 0$ and $\varepsilon < 0$, we therefore also show [Fig. 4.3(b)] the same plot for the enormous range $0 < L < 10^{10}$. Now it is evident how strongly the case $\varepsilon = 0$ differs even from a case with strong (i.e., slowly decaying) power-law

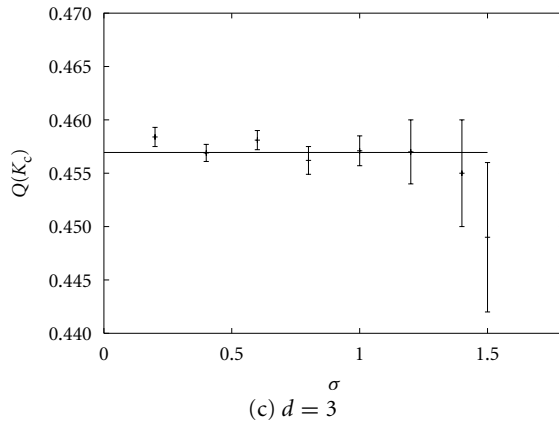
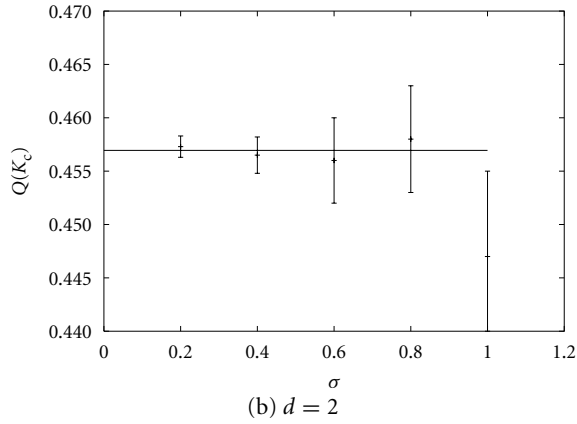
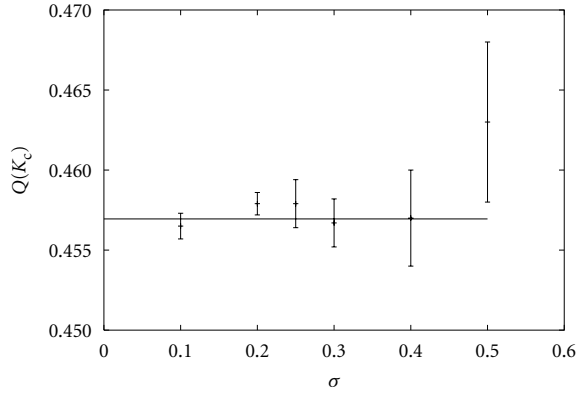


Figure 4.2: The amplitude ratio Q as a function of the decay parameter σ in $d = 1$, $d = 2$ and $d = 3$ dimensions. The solid line marks the renormalization prediction.

corrections, such as $\sigma = 0.4$ ($\varepsilon = -0.2$).

We have used the universality of Q to considerably narrow the error margins on K_c by fixing Q at its theoretical value in the least-squares fit. The corresponding couplings are shown in Table 4.2 as well. The relative accuracy of the critical couplings lies between 1.5×10^{-5} and 5.0×10^{-5} . For the one-dimensional case, we can compare these results to earlier estimates, see Table 4.3. One notes that the newest estimates are more than two orders of magnitude more accurate than previous estimates. The first estimates [18] were obtained by carrying out exact calculations for chains of 1 to 20 spins and subsequently extrapolating these results using Padé approximants. Note that the estimates for T_c in Ref. [18] are expressed in units of the inverse of the Riemann zeta function and thus must be multiplied by $\zeta(1 + \sigma)$. All couplings are somewhat too high, but still in fair agreement with our estimates. The results of Doman [19] have no error bars. Still, his results are worry-

Table 4.2: The amplitude ratio Q and critical couplings K_c for systems with long-range interactions in one, two and three dimensions, for several values of the decay parameter $0 < \sigma \leq d/2$. The thermal exponent (see Table 4.1) was kept fixed at its theoretical value in all analyses. The estimates for K_c in the last column have been obtained by fixing Q at its renormalization prediction. The numbers between parentheses represent the errors in the last decimal places.

d	σ	Q	K_c	K_c
1	0.1	0.4565 (8)	0.0476162 (13)	0.0476168 (6)
1	0.2	0.4579 (7)	0.092234 (2)	0.0922314 (15)
1	0.25	0.4579 (15)	0.114143 (4)	0.1141417 (19)
1	0.3	0.4567 (15)	0.136113 (4)	0.136110 (2)
1	0.4	0.457 (3)	0.181151 (8)	0.181150 (3)
1	0.5	0.463 (5)	0.229157 (8)	0.229155 (6)
2	0.2	0.4573 (10)	0.028533 (3)	0.0285324 (14)
2	0.4	0.4565 (17)	0.051824 (4)	0.0518249 (14)
2	0.6	0.456 (4)	0.071364 (7)	0.071366 (2)
2	0.8	0.458 (5)	0.088094 (7)	0.088094 (2)
2	1.0	0.447 (8)	0.102556 (5)	0.102558 (5)
3	0.2	0.4584 (9)	0.0144361 (10)	0.0144354 (6)
3	0.4	0.4569 (8)	0.0262927 (16)	0.0262929 (7)
3	0.6	0.4581 (9)	0.036050 (2)	0.0360469 (11)
3	0.8	0.4562 (13)	0.044034 (2)	0.0440354 (10)
3	1.0	0.4571 (14)	0.050515 (2)	0.0505152 (12)
3	1.2	0.457 (3)	0.055682 (3)	0.0556825 (14)
3	1.4	0.455 (5)	0.059666 (2)	0.0596669 (11)
3	1.5	0.449 (7)	0.061251 (2)	0.061253 (2)

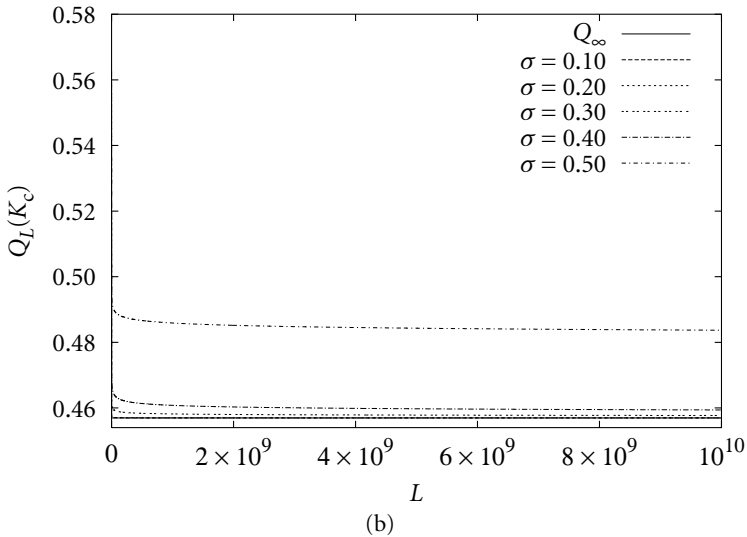
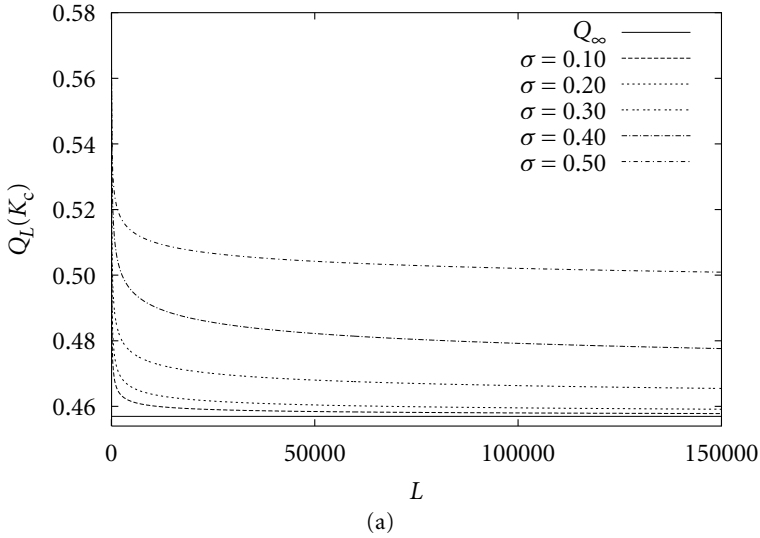


Figure 4.3: The amplitude ratio Q in a one-dimensional system as a function of the system size L for various values of σ . Figure (a) illustrates the increase of the finite-size corrections when the upper critical dimension ($\sigma = d/2$) is approached. Figure (b) emphasizes the difference between finite-size corrections *above* the upper critical dimension (power-law) and at the upper critical dimension itself (logarithmic).

ing, since he carries out a cluster approach, obtaining critical couplings which start at the mean-field value for cluster size zero and increase monotonically with increasing cluster size, as they should, since mean-field theory yields a lower bound on the critical couplings (see below). Thus, he argues that the true couplings will lie *higher* than his best estimates (obtained for cluster size 10). However, all these best estimates lie already *above* our estimates, which seems to indicate a problem inherent in his approach. Reference [20] presents results of an approximation coined “finite-range scaling” with error margins of 1%. For $\sigma = 0.1$ the error is underestimated, but for the other values of the decay parameter the couplings agree with our results well within the quoted errors. The same technique was applied in Ref. [42], but now the uncertainty in the couplings was estimated to be less than 10%, for small σ a few times larger. This is clearly a conservative estimate, as the difference with our results is only a few percent for $\sigma = 0.1$ and considerably less for larger σ . In Ref. [21], the coherent-anomaly method was used to obtain two different estimates without error margins. We have quoted the average of the two results, with their difference as a crude measure for the uncertainty. The agreement is quite good, although all results lie systematically above our values. Yet another approach has been formulated in Ref. [27], where the Onsager reaction-field theory was applied to obtain a general expression for the critical coupling,

$$K_c(\sigma) = \frac{\Gamma(1 + \sigma) \sin(\pi\sigma/2)}{(1 - \sigma)\pi^{1+\sigma}}. \quad (4.25)$$

Unfortunately, no estimate for the accuracy of this expression is given, but it seems to generally underestimate the critical coupling by a few percent. Finally, some estimates have recently been obtained by means of the real-space renormalization-group technique [43].

In addition, Monroe has calculated various *bounds* on the critical couplings as shown in Table 4.4. The Bethe lattice approximation [24] was used to obtain both upper and lower bounds, to which our results indeed conform, although it must be said that the upper bounds do not constitute a very stringent criterion (they amount to roughly twice the actual values). Furthermore, the application of Vigfusson’s method [25] has yielded even closer lower bounds for $\sigma = 0.1$ and $\sigma = 0.2$.

Apart from these approximations, one may also use mean-field theory to make some predictions concerning the critical coupling in the limit $\sigma \downarrow 0$. It was shown by Brankov [67] that in this limit the d -dimensional system with an interaction potential $\propto \sigma/r^{d+\sigma}$ is equivalent to the Husimi–Temperley mean spherical model. (Remark that actual mean-field-like couplings are only recovered for $\sigma = -d$.) More specifically, it was conjectured by Cannas [26] that for the one-dimensional case $\lim_{\sigma \rightarrow 0} K_c \sim \sigma/2$, which is also the first term in the Taylor expansion of Eq. (4.25). Indeed, in mean-field theory one has $zK_c^{\text{MF}} = 1$, where z is the coordination num-

Table 4.3: Comparison between our best estimates of the critical couplings K_c for the one-dimensional system and earlier estimates.

σ	This work	Ref. [18]	Ref. [19]	Ref. [20]	Ref. [42]	Ref. [21]	Ref. [27]	Ref. [43]
0.1	0.0476168 (6)	—	0.0478468	0.0505 (5)	0.04635	0.04777 (12)	0.0469	0.0481
0.2	0.0922314 (15)	0.0926 (5)	0.0933992	0.0923 (9)	0.09155	0.0928 (3)	0.0898	—
0.25	0.1141417 (19)	—	—	—	—	—	0.1106	—
0.3	0.136110 (2)	0.1370 (7)	0.138478	0.1362 (14)	0.1359	0.1375 (10)	0.1314	0.144
0.4	0.181150 (3)	0.1825 (10)	0.184081	0.1815 (18)	0.1813	0.183 (2)	0.1750	—
0.5	0.229155 (6)	0.2307 (14)	0.230821	0.230 (2)	0.2295	0.231 (4)	0.2251	0.250

Table 4.4: Comparison of our best estimates of the critical couplings for the one-dimensional system with some lower and upper bounds.

σ	This work	Ref. [24]	Ref. [24]	Ref. [25]
0.1	0.0476168 (6)	≥ 0.04726	≤ 0.09456	≥ 0.04753
0.2	0.0922314 (15)	≥ 0.08947	≤ 0.1792	≥ 0.09162
0.3	0.136110 (2)	≥ 0.1273	≤ 0.2558	—
0.4	0.181150 (3)	≥ 0.1615	≤ 0.3258	—
0.5	0.229155 (6)	≥ 0.1923	≤ 0.3903	—

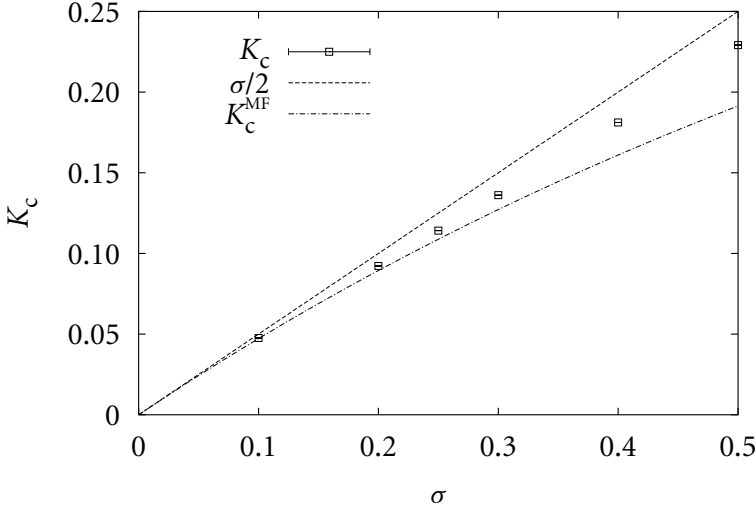


Figure 4.4: The critical coupling K_c as a function of the decay parameter σ for $d = 1$. Also shown is the asymptotic behaviour for $\sigma \downarrow 0$ as predicted by mean-field theory and mean-field values for K_c over the full range of $0 < \sigma < 1/2$.

ber. For $d = 1$ this corresponds to the requirement

$$2K_c^{\text{MF}}(\sigma) \sum_{n=1}^{\infty} \frac{1}{n^{1+\sigma}} = 2K_c^{\text{MF}}(\sigma)\zeta(1+\sigma) = 1, \quad (4.26)$$

where $\zeta(x)$ denotes the Riemann zeta function. The expansion of $\zeta(x)$ around $x = 1$ yields the conjectured relation $\lim_{\sigma \downarrow 0} K_c^{\text{MF}} = \sigma/2$.

Figure 4.4 shows the Monte Carlo results for the critical coupling as a function of the decay parameter σ along with $K_c^{\text{MF}}(\sigma)$ from Eq. (4.26) and the asymptotic behaviour for $\sigma \downarrow 0$. One observes that $K_c(\sigma)$ indeed approaches $K_c^{\text{MF}}(\sigma)$ when σ approaches zero. Furthermore, $K_c^{\text{MF}}(\sigma)$ is smaller than $K_c(\sigma)$ for all σ , as one expects from the fact that mean-field theory *overestimates* the critical temperature. It is interesting to note that for $\sigma = 0.1$ ($K_c^{\text{MF}} \approx 0.047239$) this lower bound already excludes the estimates given in Refs. [42] and [27] (cf. Table 4.3). Replacing zK_c^{MF} by the integrated interaction, we can generalize Eq. (4.26) to higher dimensionalities,

$$K_c^{\text{MF}}(\sigma) \frac{2\pi^{d/2}}{\Gamma\left(\frac{d}{2}\right)} \int_{m_0}^{\infty} dr \frac{1}{r^{1+\sigma}} = 1. \quad (4.27)$$

For $d > 1$, the lower-distance cutoff m_0 of the integral, i.e., the minimal interaction distance with the nearest neighbours, does not have an isotropic value, since there

is no interaction within an elementary *cube* around the origin. Nevertheless, a constant value m_0 , e.g., $m_0 = 1/2$, is a good approximation. Furthermore, for $d = 1$ the integral is only a first-order approximation of Eq. (4.26), but for $d = 2$ and $d = 3$ it precisely (except for the constant value of m_0) corresponds to the interaction (4.22) and its generalization to $d = 3$, respectively. As a first estimate one thus obtains

$$\lim_{\sigma \downarrow 0} K_c^{\text{MF}}(\sigma) = \frac{\Gamma\left(\frac{d}{2}\right)}{2\pi^{d/2}} \sigma m_0^\sigma. \quad (4.28)$$

An expansion in terms of σ shows that the first term is independent of m_0 . For $d = 1, 2, 3$ one finds, respectively, $K_c^{\text{MF}} \sim \sigma/2$, $K_c^{\text{MF}} \sim \sigma/(2\pi)$, $K_c^{\text{MF}} \sim \sigma/(4\pi)$. Figures 4.5(a) and 4.5(b) show $K_c(\sigma)$ for $d = 2$ and $d = 3$, the corresponding asymptotes and Eq. (4.28) with $m_0 = 1/2$.

The deviation of $K_c(\sigma)$ from $K_c^{\text{MF}}(\sigma)$ is also expressed by the last term in the renormalization expression (4.6). However, in order to assess the σ dependence of this term one has to calculate the σ dependence of the coefficients a and c , arising from the integrals of the σ -dependent propagators.

4.4.3 Determination of critical exponents

Magnetic susceptibility

At criticality, the spontaneous magnetization vanishes and hence the magnetic susceptibility χ is directly proportional to the average square magnetization density,

$$\chi = L^d \langle m^2 \rangle. \quad (4.29)$$

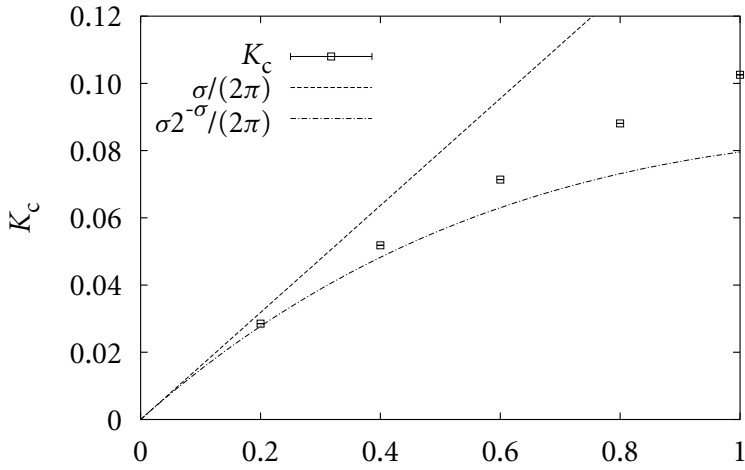
Thus, we can use Eq. (4.16) to analyze the finite-size data. Expanding this equation in t and u we obtain for $\varepsilon < 0$

$$\chi = L^{2y_h^* - d} \left(a_0 + a_1 \hat{t} L^{y_t^*} + a_2 \hat{t}^2 L^{2y_t^*} + \dots + b_1 L^{y_i} + \dots \right) \quad (4.30)$$

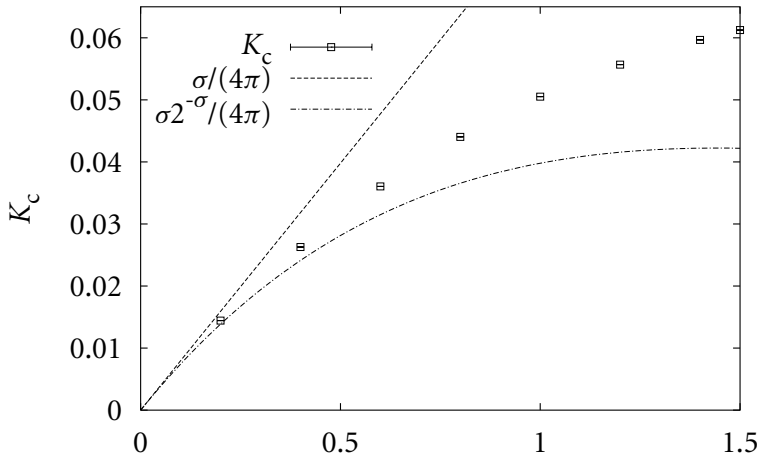
and for $\varepsilon = 0$

$$\begin{aligned} \chi &= L^{2y_h - d} \sqrt{\ln L} \\ &\times \left[a_0 + a_1 L^{y_t} (\ln L)^{1/6} \left(t + v \frac{L^{-y_t}}{(\ln L)^{2/3}} \right) \right. \\ &\quad \left. + a_2 L^{2y_t} (\ln L)^{1/3} \left(t + v \frac{L^{-y_t}}{(\ln L)^{2/3}} \right)^2 + \dots + \frac{b_1}{\ln L} + \dots \right]. \quad (4.31) \end{aligned}$$

The analytic part of the free energy might give rise to an additional constant, but this could not be observed in our simulations, because it is dominated by the corrections to scaling. In Table 4.5 we list the results of an analysis of the numerical data.



(a) $d = 2$



(b) $d = 3$

Figure 4.5: The critical coupling K_c as a function of the decay parameter σ for $d = 2$ and $d = 3$. Also shown is the asymptotic behaviour for $\sigma \downarrow 0$ as predicted by mean-field theory and approximate mean-field values for K_c over the full range of $0 < \sigma < d/2$, as discussed in the text.

Table 4.5: Estimates for the critical coupling K_c and the exponent y_h^* as obtained from the analysis of the magnetic susceptibility. The values for y_h^* in the fifth column have been obtained by fixing K_c at their best estimates from Table 4.2; the error margins include the uncertainty in these values for K_c .

d	σ	K_c	y_h^*	y_h^*	RG
1	0.1	0.0476161 (19)	0.7487 (14)	0.7493 (10)	$\frac{3}{4}$
1	0.2	0.092239 (4)	0.752 (2)	0.7504 (18)	$\frac{3}{4}$
1	0.25	0.114145 (4)	0.7477 (15)	0.747 (2)	$\frac{3}{4}$
1	0.3	0.136110 (5)	0.747 (3)	0.749 (2)	$\frac{3}{4}$
1	0.4	0.181170 (10)	0.749 (5)	0.746 (3)	$\frac{3}{4}$
1	0.5	0.229153 (6)	0.748 (2)	0.7490 (18)	$\frac{3}{4}$
2	0.2	0.028537 (5)	1.500 (6)	1.495 (3)	$\frac{3}{2}$
2	0.4	0.051830 (6)	1.498 (9)	1.496 (3)	$\frac{3}{2}$
2	0.6	0.071370 (5)	1.497 (6)	1.498 (3)	$\frac{3}{2}$
2	0.8	0.088095 (10)	1.496 (5)	1.495 (3)	$\frac{3}{2}$
2	1.0	0.102556 (3)	1.495 (4)	1.497 (3)	$\frac{3}{2}$
3	0.2	0.0144347 (9)	2.249 (2)	2.2504 (14)	$\frac{9}{4}$
3	0.4	0.026296 (2)	2.250 (6)	2.246 (4)	$\frac{9}{4}$
3	0.6	0.036046 (3)	2.246 (7)	2.244 (5)	$\frac{9}{4}$
3	0.8	0.0440349 (17)	2.243 (4)	2.246 (4)	$\frac{9}{4}$
3	1.0	0.050516 (3)	2.239 (9)	2.243 (8)	$\frac{9}{4}$
3	1.2	0.055679 (2)	2.247 (11)	2.251 (8)	$\frac{9}{4}$
3	1.4	0.0596636 (18)	2.27 (3)	2.26 (2)	$\frac{9}{4}$
3	1.5	0.061251 (2)	2.257 (12)	2.249 (7)	$\frac{9}{4}$

For all examined systems we have determined the exponent y_h^* and the critical coupling. The estimates for the latter are in good agreement with those obtained from the analysis of the universal amplitude ratio Q . Furthermore, the exponents agree nicely, for all dimensionalities, with the renormalization prediction $y_h^* = 3d/4$. Just as before, the uncertainties increase with increasing σ , although the analyses at the upper critical dimension itself seem to yield better results than those just above it. Compare in particular the results for $\sigma = 1.4$ ($y_1 = -0.2$) and $\sigma = 1.5$. The logarithmic prefactor in Eq. (4.31) can be clearly observed in the sense that the quality of the least-squares fit decreases considerably when this factor is omitted. To reduce the uncertainty in the exponents we have repeated the analysis with K_c fixed at the

Table 4.6: The correlation length exponent ν for the one-dimensional model as a function of σ , together with earlier estimates and the renormalization predictions.

σ	This work	Ref. [20]	Ref. [42]	Ref. [43]	RG
0.1	9.3 (6)	9.12	9.9	10.48	10.0
0.2	4.9 (3)	4.90	4.95	—	5.0
0.25	4.00 (8)	—	—	—	4.0
0.3	3.27 (12)	3.41	3.32	3.90	3.3...
0.4	2.50 (13)	2.71	2.68	—	2.5
0.5	2.04 (8)	2.34	2.33	2.81	2.0

Table 4.7: The magnetization exponent β for the one-dimensional model as a function of σ , together with earlier estimates and the renormalization predictions.

σ	This work	Ref. [18]	Ref. [21]	RG
0.1	0.494 (8)	—	0.495	$\frac{1}{2}$
0.2	0.495 (13)	0.5	0.482	$\frac{1}{2}$
0.25	0.506 (8)	—	—	$\frac{1}{2}$
0.3	0.497 (15)	0.48	0.460	$\frac{1}{2}$
0.4	0.51 (2)	0.45	0.435	$\frac{1}{2}$
0.5	0.51 (2)	0.39	0.408	$\frac{1}{2}$

best values in Table 4.2, i.e., those obtained with fixed Q . The corresponding estimates of y_h^* are also shown in Table 4.5 and are indeed in good agreement with the renormalization predictions.

Now we can calculate the critical exponents and compare them to earlier estimates for $d = 1$. We do this for the correlation length exponent $\nu = 1/(y_t^* + y_i/2)$ and the magnetization exponent $\beta = (d - y_h^*)/y_t^*$. The exponent y_t^* is taken from Table 4.1 and the exponent y_h^* from Table 4.5. The irrelevant exponent y_i , which is required to calculate y_t (the inverse of ν) from y_t^* , is assumed to take its theoretical value $2\sigma - 1$. The results are shown in Tables 4.6 and 4.7. Since all our estimates for y_t^* and y_h^* agree with the renormalization values, also ν and β are in agreement with the classical critical exponents. Unfortunately, the accuracy in both exponents is seriously hampered by the uncertainty in y_t^* , which has only been determined from the temperature-dependent term in Q . In particular the results for ν from Ref. [42] are, for small σ , in better agreement with the theoretically predicted values than our estimates. However, all previous results, both for ν and for β , deviate seriously from the predicted values when σ approaches $1/2$, which is not the case for our values. This can probably be attributed to the fact that corrections to scaling have been taken into account more adequately.

Spin–spin correlation function

In Sec. 4.3 two different decay modes for the spin–spin correlation function were derived. The relative magnitude of r and L determines which of the modes applies. In the bulk of our simulations we have restricted r in $g(|\mathbf{r}|)$ to $r = L/2$. Since this quantity reflects the $\mathbf{k} = \mathbf{0}$ mode of the correlation function, we write for $\varepsilon < 0$ an expression analogous to that for the magnetic susceptibility,

$$g(L/2) = L^{2y_h^* - 2d} \left[c_0 + c_1 \hat{t} L^{y_t^*} + c_2 \hat{t}^2 L^{2y_t^*} + \dots + d_1 L^{y_i} + \dots \right] \quad (4.32)$$

and for $\varepsilon = 0$

$$g(L/2) = L^{2y_h - 2d} \sqrt{\ln L} \times \left[c_0 + c_1 L^{y_t} (\ln L)^{1/6} \left(t + v \frac{L^{-y_t}}{(\ln L)^{2/3}} \right) + c_2 L^{2y_t} (\ln L)^{1/3} \left(t + v \frac{L^{-y_t}}{(\ln L)^{2/3}} \right)^2 + \dots + \frac{d_1}{\ln L} + \dots \right]. \quad (4.33)$$

For values of r such that $g(|\mathbf{r}|)$ does *not* correspond to this mode of the correlation function, the σ -dependent exponent y_h will appear in (4.32) instead of y_h^* . Furthermore, the logarithmic prefactor in (4.33) will be absent, as it arises from the dangerous irrelevant variable [cf. Eq. (4.17)]. The results of our analysis are shown in Table 4.8. They evidently corroborate that the exponent y_h^* coincides with that appearing in the susceptibility. Also the factor $\sqrt{\ln L}$ in (4.33) was clearly visible in the least-squares analysis. The critical couplings agree with the estimates from Q and χ and we have again tried to increase the accuracy in y_h^* by repeating the analysis with K_c fixed at their best values in Table 4.2. The accuracy of the results is somewhat less than of those obtained from the magnetic susceptibility, because we have now only used numerical data for even system sizes. The fact that the L dependence of $g(L/2)$ is determined by the $\mathbf{k} = \mathbf{0}$ mode raises the question whether one can also observe the power-law decay described by η in finite systems, i.e., the short-distance behaviour which is determined by the $\mathbf{k} \neq \mathbf{0}$ modes (cf. the discussion at the end of Sec. 4.3). To this end, we have sampled $g(r)$ as a function of r in the one-dimensional model. In order to clearly distinguish between the two predictions for the decay of $g(r)$ we have examined a system far from the upper critical dimension, *viz.* with $\sigma = 0.1$. It turned out to be necessary to sample *very* large system sizes to observe the regime where $g(r) \propto r^{-(d-\sigma)}$. Figure 4.6 displays the spin–spin correlation function scaled with $L^{d/2}$ versus r/L . The scaling makes the results collapse for r of the order of the system size. Here, the correlation function levels off. This is the mean-field-like contribution to the correlation function, which dominates in the spatial integral yielding the magnetic susceptibility. For small r the data do not collapse at

Table 4.8: Estimates for the critical coupling K_c and the exponent y_h^* as obtained from the analysis of the spin–spin correlation function. The values for y_h^* in the fifth column have been obtained by fixing K_c at their best estimates from Table 4.2; the error margins include the uncertainty in these values for K_c .

d	σ	K_c	y_h^*	y_h^*	RG
1	0.1	0.047619 (3)	0.750 (2)	0.7488 (13)	$\frac{3}{4}$
1	0.2	0.092233 (7)	0.749 (3)	0.751 (2)	$\frac{3}{4}$
1	0.25	0.114148 (10)	0.750 (5)	0.747 (3)	$\frac{3}{4}$
1	0.3	0.136116 (7)	0.753 (5)	0.752 (4)	$\frac{3}{4}$
1	0.4	0.181158 (15)	0.747 (7)	0.750 (5)	$\frac{3}{4}$
1	0.5	0.229150 (7)	0.749 (2)	0.7503 (15)	$\frac{3}{4}$
2	0.2	0.028535 (7)	1.499 (9)	1.496 (4)	$\frac{3}{2}$
2	0.4	0.051831 (6)	1.505 (6)	1.499 (4)	$\frac{3}{2}$
2	0.6	0.071369 (6)	1.507 (4)	1.502 (4)	$\frac{3}{2}$
2	0.8	0.088091 (6)	1.495 (7)	1.497 (4)	$\frac{3}{2}$
2	1.0	0.102554 (4)	1.490 (6)	1.496 (4)	$\frac{3}{2}$
3	0.2	0.0144348 (16)	2.256 (6)	2.254 (4)	$\frac{9}{4}$
3	0.4	0.026296 (3)	2.257 (8)	2.245 (6)	$\frac{9}{4}$
3	0.6	0.036053 (4)	2.262 (10)	2.246 (5)	$\frac{9}{4}$
3	0.8	0.044035 (4)	2.252 (11)	2.250 (7)	$\frac{9}{4}$
3	1.0	0.050511 (5)	2.228 (15)	2.249 (10)	$\frac{9}{4}$
3	1.2	0.055680 (3)	2.253 (14)	2.257 (10)	$\frac{9}{4}$
3	1.4	0.059667 (2)	2.22 (4)	2.30 (4)	$\frac{9}{4}$
3	1.5	0.061251 (5)	2.26 (3)	2.248 (9)	$\frac{9}{4}$

all, which shows that $g(r)$ exhibits a different scaling behaviour in this regime. Indeed, the correlation function decays here as $r^{-(d-\sigma)} = r^{-0.9}$ and not as $r^{-d/2}$. Note, however, that this regime is restricted to a small region of r and can only be observed for very large system sizes.

It is interesting to note that already Nagle and Bonner [18] have tried to calculate η in a spin chain with long-range interactions from finite-size data for the susceptibility. Because this calculation relied on the assumption that $\chi(L, K_c) - \chi(L - 1, K_c) \sim g(L) \sim L^{-(d-2+\eta)}$, they called the corresponding exponent $\tilde{\eta}$. The results for $\tilde{\eta}$ turned out to assume a constant value approximately equal to 1.50 for $0 < \sigma \leq 0.5$. Thus, the identification of $\tilde{\eta}$ with η was assumed to be invalid in

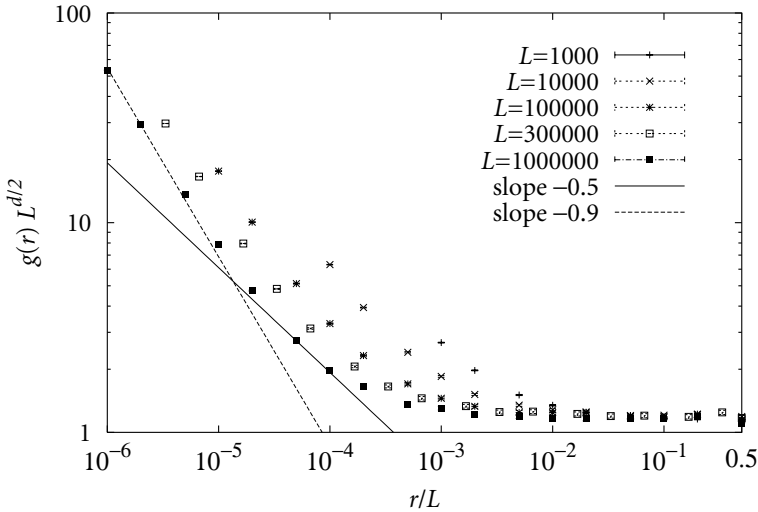


Figure 4.6: The spin–spin correlation function versus r/L in the one-dimensional model with $\sigma = 0.1$. Results for various system sizes are shown. For a discussion see the text.

Ref. [35]. Now we see that $\tilde{\eta}$ is in excellent agreement with $\eta^* \equiv d+2-2y_h^* = 2-d/2$.

4.5 Conclusions

In this chapter we have studied systems with long-range interactions decaying as $r^{-(d+\sigma)}$ in one, two and three dimensions in the regime where these interactions lead to classical critical behaviour, i.e., for $0 < \sigma \leq d/2$. From the renormalization equations we have derived the scaling behaviour, including the corrections to scaling, for various quantities. These predictions, in particular the critical exponents and the scaling behaviour of the amplitude ratio $\langle m^2 \rangle^2 / \langle m^4 \rangle$, have been verified by accurate Monte Carlo results. At the upper critical dimension, the logarithmic factors appearing in the finite-size scaling functions could be accurately observed. Our analysis has also yielded estimates for the critical couplings. For $d = 1$ these values have an accuracy which is more than two orders of magnitude better than previous estimates and could thus serve as a check for half a dozen different approximations. For $d = 2$ and $d = 3$ we have, to our best knowledge, obtained the first estimates for the critical couplings. Finally, we have given both theoretical and numerical arguments that above the upper critical dimension the decay of the critical spin–spin correlation function in finite systems consists of two regimes: one where it decays as $r^{-(d-2+\eta)}$ and one where it is independent of the distance.

References

- [1] D. Ruelle, *Comm. Math. Phys.* **9**, 267 (1968).
- [2] F. J. Dyson, *Comm. Math. Phys.* **12**, 91 (1969).
- [3] F. J. Dyson, *Comm. Math. Phys.* **12**, 212 (1969).
- [4] D. J. Thouless, *Phys. Rev.* **187**, 732 (1969).
- [5] B. Simon and A. D. Sokal, *J. Stat. Phys.* **25**, 679 (1980).
- [6] J. B. Rogers and C. J. Thompson, *J. Stat. Phys.* **25**, 669 (1981).
- [7] J. Fröhlich and T. Spencer, *Comm. Math. Phys.* **84**, 87 (1982).
- [8] J. Z. Imbrie, *Comm. Math. Phys.* **85**, 491 (1982).
- [9] M. Aizenman, J. T. Chayes, L. Chayes and C. M. Newman, *J. Stat. Phys.* **50**, 1 (1988).
- [10] M. Aizenman and R. Fernández, *Lett. Math. Phys.* **16**, 39 (1988).
- [11] J. Z. Imbrie and C. M. Newman, *Comm. Math. Phys.* **118**, 303 (1988).
- [12] J. Bhattacharjee, S. Chakravarty, J. L. Richardson and D. J. Scalapino, *Phys. Rev. B* **24**, 3862 (1981).
- [13] G. V. Matvienko, *Teor. Mat. Fiz.* **63**, 465 (1985) [*Theor. Math. Phys.* **63**, 635 (1985)].
- [14] B. Siu, *J. Stat. Phys.* **38**, 519 (1985).
- [15] J. O. Vignfusson, *Phys. Rev. B* **34**, 3466 (1986).
- [16] D. Rapaport and N. E. Frankel, *Phys. Lett. A* **28**, 405 (1968).
- [17] J. F. Dobson, *J. Math. Phys.* **10**, 40 (1969).
- [18] J. F. Nagle and J. C. Bonner, *J. Phys. C* **3**, 352 (1970).
- [19] B. G. S. Doman, *Phys. Stat. Sol. (b)* **103**, K169 (1981).
- [20] Z. Glumac and K. Uzelac, *J. Phys. A* **22**, 4439 (1989).
- [21] J. L. Monroe, R. Lucente and J. P. Hourlland, *J. Phys. A* **23**, 2555 (1990).
- [22] B. Bergersen and Z. Rácz, *Phys. Rev. Lett.* **67**, 3047 (1991).
- [23] R. Manieri, *Phys. Rev. A* **45**, 3580 (1992).
- [24] J. L. Monroe, *Phys. Lett. A* **171**, 427 (1992).
- [25] J. L. Monroe, *J. Stat. Phys.* **76**, 1505 (1994).
- [26] S. A. Cannas, *Phys. Rev. B* **52**, 3034 (1995).
- [27] A. S. T. Pires, *Phys. Rev. B* **53**, 5123 (1996).
- [28] P. W. Anderson and G. Yuval, *Phys. Rev. Lett.* **23**, 89 (1969).
- [29] G. Yuval and P. W. Anderson, *Phys. Rev. B* **1**, 1522 (1970).
- [30] P. W. Anderson, G. Yuval and D. R. Hamann, *Phys. Rev. B* **1**, 4464 (1970).
- [31] P. W. Anderson and G. Yuval, *J. Phys. C* **4**, 607 (1971).
- [32] J. M. Kosterlitz, *Phys. Rev. Lett.* **37**, 1577 (1976).
- [33] J. L. Cardy, *J. Phys. A* **14**, 1407 (1981).
- [34] S. A. Bulgadaev, *Phys. Lett. A* **102**, 260 (1984).
- [35] M. E. Fisher, S.-k. Ma and B. G. Nickel, *Phys. Rev. Lett.* **29**, 917 (1972).
- [36] J. Sak, *Phys. Rev. B* **8**, 281 (1973).

- [37] M. Suzuki, Y. Yamazaki and G. Igarashi, *Phys. Lett. A* **42**, 313 (1972).
- [38] G. Stell, *Phys. Rev. B* **1**, 2265 (1970).
- [39] R. B. Griffiths, *Phys. Rev. Lett.* **24**, 1479 (1970).
- [40] M. J. Wragg and G. A. Gehring, *J. Phys. A* **23**, 2157 (1990).
- [41] H.-J. Xu, B. Bergersen and Z. Rácz, *Phys. Rev. E* **47**, 1520 (1993).
- [42] Z. Glumac and K. Uzelac, *J. Phys. A* **26**, 5267 (1993).
- [43] S. A. Cannas and A. C. N. de Magalhães, *J. Phys. A* **30**, 3345 (1997).
- [44] L. B. Bernardes and S. Goulart Rosa, Jr., *Phys. Lett. A* **191**, 193 (1994).
- [45] J. M. Kosterlitz and D. J. Thouless, *J. Phys. C* **6**, 1181 (1973).
- [46] J. M. Kosterlitz, *J. Phys. C* **7**, 1046 (1974).
- [47] N. D. Mermin and H. Wagner, *Phys. Rev. Lett.* **17**, 1133 (1966).
- [48] B. Hafskjold and G. Stell, *The Equilibrium Statistical Mechanics of Simple Ionic Liquids*, in *The Liquid State of Matter: Fluids, Simple and Complex*, edited by E. W. Montroll and J. L. Lebowitz (North-Holland, Amsterdam, 1982).
- [49] M. E. Fisher, *J. Stat. Phys.* **75**, 1 (1994).
- [50] R. Folk and G. Moser, *Int. J. Thermophys.* **16**, 1363 (1995).
- [51] O. Boxberg and K. Westerholt, *J. Magn. Magn. Mat.* **140–144**, 1563 (1995).
- [52] T. W. Burkhardt and E. Eisenriegler, *Phys. Rev. Lett.* **74**, 3189 (1995).
- [53] M. Kac and C. J. Thompson, *J. Math. Phys.* **10**, 1373 (1969).
- [54] L. D. Landau and E. M. Lifshitz, *Statistical Physics* (Pergamon, London, 1959).
- [55] F. J. Dyson, *Comm. Math. Phys.* **21**, 269 (1971).
- [56] T. H. Berlin and M. Kac, *Phys. Rev.* **86**, 821 (1952).
- [57] G. S. Joyce, *Phys. Rev.* **146**, 349 (1966).
- [58] S.-k. Ma, *Modern Theory of Critical Phenomena* (Addison–Wesley, Redwood, California, 1976).
- [59] D. J. Amit, *Field Theory, the Renormalization Group, and Critical Phenomena*, second edition (World Scientific, Singapore, 1984).
- [60] V. Privman and M. E. Fisher, *J. Stat. Phys.* **33**, 385 (1983).
- [61] E. Brézin, *J. Phys. (Paris)* **43**, 15 (1982).
- [62] S.-k. Ma, *Rev. Mod. Phys.* **45**, 589 (1973).
- [63] E. Brézin and J. Zinn-Justin, *Nucl. Phys. B* **257** [FS14], 867 (1985).
- [64] J. G. Brankov and N. S. Tonchev, *J. Stat. Phys.* **52**, 143 (1988).
- [65] H. Chamati and N. S. Tonchev, *J. Stat. Phys.* **83**, 1211 (1996).
- [66] H. E. Stanley, *Phys. Rev.* **176**, 718 (1968).
- [67] J. G. Brankov, *Physica A* **168**, 1035 (1990).

Chapter 5

Critical behaviour of spin models with algebraically decaying interactions II

Below the upper critical dimension

5.1 Introduction

In this chapter we continue the study of the models with long-range interactions introduced in the previous chapter. Until now, we have restricted ourselves to the regime where the spin–spin interactions decay sufficiently slowly, such that the systems exhibit essentially classical critical behaviour. Here, however, we focus on interactions decaying as $r^{-(d+\sigma)}$ with $d < 2\sigma$. Although in reality the dimensionality d is discrete (and fixed) and only the decay rate σ can be varied continuously (at least in a numerical simulation), an insightful view is obtained by allowing for noninteger d as well. As shown in Sec. 4.3, the upper critical dimension is then given by $d_u = 2\sigma$ and the Gaussian fixed point reigns the renormalization flow for $d \geq d_u$. For $d < d_u$, on the other hand, this fixed point is unstable and a nontrivial fixed point takes over. Just as in the “conventional” ε -expansion, critical properties for these models can be calculated from a perturbation expansion in the distance $\varepsilon \equiv d_u - d$ to the upper critical dimension. The possibility to vary d_u offers an interesting extension of the well-known expansion in powers of $4 - d$. Indeed, this expansion is divergent for all $\varepsilon > 1$ and a Borel summation is required to obtain accurate results for the physically relevant cases $d = 2, 3$. For integer d , Borel summability has indeed been proven rigorously [1], but still a direct test of this expansion for $\varepsilon \ll 1$ would be useful. This holds even stronger for the ε -expansion of finite-size scaling functions. Brézin

and Zinn-Justin [2] demonstrated that such an expansion indeed exists in terms of powers of $\sqrt{\varepsilon}$ and they calculated the series for the amplitude ratio $\langle m^2 \rangle^2 / \langle m^4 \rangle$ up to $\mathcal{O}(\varepsilon)$. As for this quantity only numerical results for integer dimensions are available, a real comparison has not been possible until now. Evidently, models in which ε can be varied continuously offer here an interesting opportunity.

However, also further below the upper critical dimension interesting questions arise, at which we have already hinted in Chapter 4. In systems with a discrete order parameter *short-range* forces can maintain long-range order at sufficiently low temperatures provided that $d > 1$. Since we study the cases $d = 1, 2, 3$, we expect to observe a striking difference between $d = 1$ on the one hand and $d = 2, 3$ on the other hand when increasing the decay rate of the interactions. In the former model a phase transition will be absent when the interactions decay sufficiently rapidly, whereas the latter two should cross over to the well-known short-range universality classes at some value for σ . Since several contradictory renormalization-group (RG) scenarios for this crossover have been proposed in the literature, it is highly desirable to study this issue with numerical methods. Indeed, a resolution of this question might shed light on much broader theoretical issues underlying the disagreement between the various RG treatments.

Many aspects of these models have been discussed *in extenso* in the preceding chapter: Section 4.1 provides a comprehensive list of earlier studies of systems with long-range interactions, Sec. 4.2 summarizes the steps toward a rigorous determination of the maximum decay rate for which long-range order is possible at nonzero temperatures in the one-dimensional Ising chain and Sec. 4.4.1 introduces the precise spin–spin interactions that have been used in our numerical simulations. Because of the differences between the various dimensionalities, we have opted to treat the three cases separately. Thus, this chapter is organized as follows. In Sec. 5.2 we outline the RG scenario for the critical behaviour of long-range systems below their upper critical dimension and give a detailed treatment of the renormalization considerations concerning the crossover to short-range critical behaviour. Numerical results for the one-dimensional case with $1/2 < \sigma < 1$ are presented in Sec. 5.3. Sections 5.4 and 5.5 treat the nonclassical long-range regime and the short-range regime for two- and three-dimensional systems, respectively. Our conclusions are summarized in Sec. 5.6.

5.2 Renormalization-group study of the nonclassical regime

The framework for an RG treatment of spin models with algebraically decaying interactions has already been set up in Sec. 4.3. The starting point is a conventional Landau–Ginzburg–Wilson (LGW) Hamiltonian (ϕ^4 theory), in which long-range interactions are incorporated, see Eq. (4.3). Clearly, such interactions tend to sup-

press critical fluctuations and may modify the critical behaviour. Thus, if their decay is sufficiently slow (σ sufficiently small) one expects these interactions to dominate over any short-range interactions. Indeed, it was shown in Chapter 4 that for $\sigma < d/2$ (with $d < 4$) the ϕ^4 term in the LGW Hamiltonian is irrelevant, which results in classical critical behaviour, as was confirmed by our numerical results. On the other hand, for $\sigma > 2$ the $r^{-(d+\sigma)}$ interactions decay faster than the gradient term representing the short-range interactions (the k^2 term in the momentum-space representation) such that the latter will dominate. In this case the critical properties are those of the corresponding short-range model, though with additional corrections to scaling due to the irrelevant contribution of the power-law interactions. Our knowledge of the intermediate regime, $d/2 < \sigma < 2$, heavily relies on various RG analyses. Fisher, Ma and Nickel [3] carried out an expansion in $\varepsilon = 2\sigma - d$ and calculated the critical exponents γ and η to order ε^2 ,

$$\gamma = 1 + \frac{n+2}{n+8} \frac{\varepsilon}{\sigma} + \left[\left(\frac{n+2}{n+8} \right)^2 + \frac{(n+2)(7n+20)}{(n+8)^3} \mathcal{A}(\sigma) \right] \left(\frac{\varepsilon}{\sigma} \right)^2 + \mathcal{O}(\varepsilon^3), \quad (5.1a)$$

$$\eta = 2 - \sigma + \mathcal{O}(\varepsilon^3), \quad (5.1b)$$

where $\mathcal{A}(\sigma) \equiv \sigma[\psi(1) - 2\psi(\sigma/2) + \psi(\sigma)]$ and $\psi(x)$ is the Digamma function (logarithmic derivative of the Gamma function). The calculation of the higher-order terms requires considerable computational effort and it is unfortunate that the details have never been published [4]. It was conjectured in Ref. [3] that the expression for η is exact to all orders in ε . Indeed, η follows from the scaling properties of the spin-spin correlation function, which in turn are determined by the rescaling factor of the field ϕ . As long as the long-range interactions dominate the critical behaviour *and* no higher-order terms contribute to the renormalization of $k^\sigma \phi_{\mathbf{k}} \phi_{-\mathbf{k}}$ in the LGW Hamiltonian, η will therefore stick at $2 - \sigma$. Suzuki *et al.* [5] have independently reproduced these results¹ and claimed that also the $\mathcal{O}(\varepsilon^3)$ term vanishes in the expansion for η . The increase of γ with increasing σ is in accordance with the fact that for faster decaying interactions critical fluctuations are less suppressed and hence the susceptibility exhibits a stronger divergence.

It is instructive to show briefly how these results follow from the RG equations (4.4). The solution of the second RG equation, which is still given by Eq. (4.5), shows that for positive ε the Gaussian fixed point is no longer stable. Instead, u flows toward a nonzero value $u^* = \varepsilon/[a(n+8)] + \mathcal{O}(\varepsilon^2)$, as depicted in Fig. 5.1 for both $\tilde{u} < u^*$ and $\tilde{u} > u^*$ and various values of $\varepsilon > 0$. The leading irrelevant exponent γ_1 immediately follows from the decrease of $\tilde{u} \equiv u - u^*$ under successive

¹The reader should beware of misprints in the expression for γ^{-1} in Ref. [5].

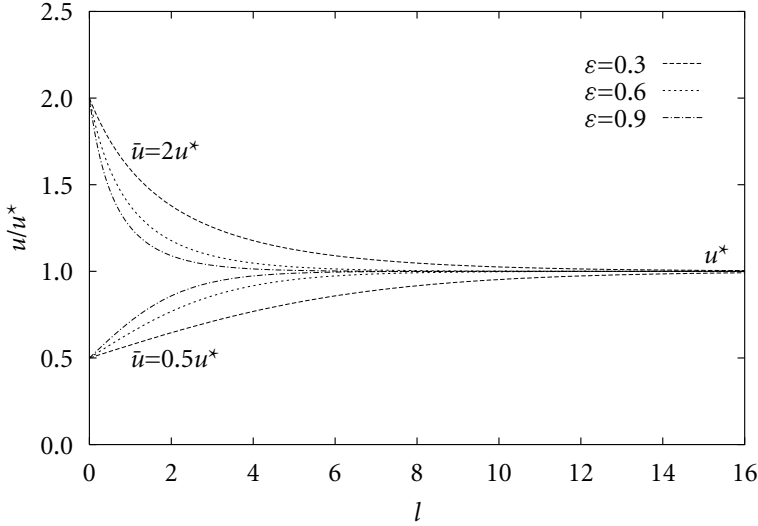


Figure 5.1: The flow of the ϕ^4 coefficient u as a function of the logarithm of the rescaling parameter. The graphs have been normalized by u^* .

RG transformations. Naturally, the equation describing the behaviour of \tilde{u} is very similar to Eq. (4.4b),

$$\frac{d\tilde{u}}{dl} = -\varepsilon\tilde{u} - a(n+8)\tilde{u}^2, \quad (5.2)$$

and to first order we find $y_1 = -\varepsilon$. This is in accordance with the result obtained by Yamazaki and Suzuki [6]. They were the first to address this exponent in systems with long-range interactions and derived it from the β -function appearing in the Callan–Symanzik equations,

$$y_1 \equiv -\omega = -\varepsilon + \frac{2(5n+22)}{(n+8)^2} \frac{\mathcal{A}(\sigma)}{\sigma} \varepsilon^2 + \mathcal{O}(\varepsilon^3). \quad (5.3)$$

The thermal exponent y_t is calculated from Eq. (4.4a), as is easily seen by rewriting this equation as

$$\frac{dr_0}{dl} = [\sigma - a(n+2)u]r_0 + a(n+2)cu. \quad (5.4)$$

The last term leads to a finite renormalization (shift) of the critical temperature [similar to the last term in Eq. (4.6)] and the factor between square brackets yields, upon substitution of u^* , the thermal exponent,

$$y_t = \sigma - \left(\frac{n+2}{n+8} \right) \varepsilon + \mathcal{O}(\varepsilon^2). \quad (5.5)$$

This agrees with the results in Eqs. (5.1), as follows from the scaling relation $\gamma = (2 - \eta)v$,

$$y_t = \sigma - \left(\frac{n+2}{n+8} \right) \varepsilon - \frac{(n+2)(7n+20)}{(n+8)^3} \frac{\mathcal{A}(\sigma)}{\sigma} \varepsilon^2 + \mathcal{O}(\varepsilon^3). \quad (5.6)$$

The magnetic exponent y_h is directly related to the exponent η , which, as mentioned above, follows from the field rescaling factor. We thus find to leading order $y_h = (d + \sigma)/2$, just as in the classical regime. It was conjectured in Ref. [3] that this expression *exactly* holds all the way to $\sigma = 2$, where the short-range term in the LGW Hamiltonian starts to dominate. This implies (for $d < 4$) a discontinuity in η , since $\lim_{\sigma \uparrow 2} \eta = 0$ and $\lim_{\sigma \downarrow 2} \eta = \eta_{\text{SR}} \neq 0$, where η_{SR} stands for the exponent η in the corresponding model with short-range interactions. This intriguing phenomenon was subsequently studied by Sak [7], who included higher-order contributions to the renormalization of the $\phi_{\mathbf{k}}\phi_{-\mathbf{k}}$ term in Eq. (4.3). The leading

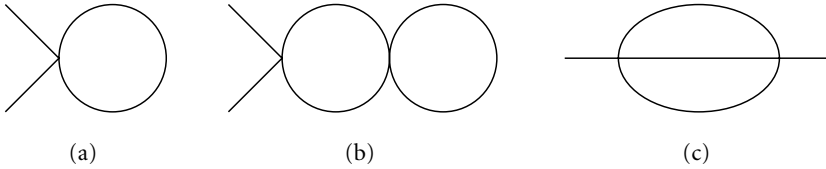


Figure 5.2: The diagrams representing the first-order [(a)] and second-order [(b), (c)] contributions to the renormalization of the ϕ^2 term.

contributions come from the Feynman graphs shown in Fig. 5.2. The first one, proportional to u , yields the last term in Eq. (5.4) and evidently does not carry any k dependence. However, of the second and third graphs, which are of order u^2 , the last one does depend on k , as it leads to an integral of the form

$$\int \frac{d^d q_1}{(2\pi)^d} \int \frac{d^d q_2}{(2\pi)^d} \frac{1}{(j_2 q_1^2 + j_\sigma q_1^\sigma + r_0)(j_2 q_2^2 + j_\sigma q_2^\sigma + r_0)} \times \frac{1}{[j_2(k - q_1 - q_2)^2 + j_\sigma(k - q_1 - q_2)^\sigma + r_0]}, \quad (5.7)$$

where the integrals run over the outer momentum shell. It was argued by Sak that while this yields no contributions proportional to k^σ —in agreement with the conclusions of both Ref. [3] and Ref. [5]—there is a contribution quadratic in k . From the fact that the exponents in (5.1) have been calculated to second order, we conclude that these diagrams must have been considered for the calculation of the results presented in Refs. [3, 5] (they are required for y_t), but that their consequences for the renormalization of the $j_2 k^2$ term in (4.3) have been ignored. Sak obtained an

interesting result: due to the k^2 contribution, short-range forces will always appear in the renormalization process and compete with the long-range forces. Thus, u^* depends on the fixed-point values of both j_σ and j_2 . This dependence, which originates from the integration of propagators [similar to Eq. (5.7)], is immaterial in a situation where only one type of interaction is present, but now we explicitly incorporate it in our notation. The coefficient a in Eq. (4.4b) is hence replaced by $(j_\sigma + j_2)^{-2}$ and to first order $u^* = \varepsilon(j_\sigma + j_2)^2/(n + 8)$. Generalizing Sak's recursion relation for the coefficient j_2 (which was derived from integrations over a momentum shell of fixed size) we find, for a rescaling parameter $b = e^l$,

$$\frac{dj_2}{dl} = (\sigma - 2)j_2 + \frac{n + 2}{2(j_\sigma + j_2)^3}u^2, \quad (5.8)$$

and substitution of the fixed-point value u^* yields

$$\frac{dj_2}{dl} = \left[\sigma - 2 + \frac{n + 2}{2(n + 8)^2}\varepsilon^2 \right] j_2 + \frac{n + 2}{2(n + 8)^2}\varepsilon^2 j_\sigma. \quad (5.9)$$

At the fixed point, j_2 indeed takes a nonzero value

$$j_2^* = \frac{\tilde{\eta} j_\sigma^*}{2 - \sigma - \tilde{\eta}}, \quad (5.10)$$

where we have written j_σ^* because this parameter is kept invariant and we have introduced $\tilde{\eta} \equiv (n + 2)\varepsilon^2/[2(n + 8)^2] + \mathcal{O}(\varepsilon^3)$.² Clearly, this fixed point is only stable for $\sigma < 2 - \tilde{\eta}$, as also follows from the solution of Eq. (5.9),

$$j_2(l) = j_2^* + (\bar{j}_2 - j_2^*)e^{[\sigma - (2 - \tilde{\eta})]l}, \quad (5.11)$$

with $\bar{j}_2 = j_2(l = 0)$. For $\sigma > 2 - \tilde{\eta}$, j_2 will grow without bound under the RG transformation and we conclude that it is the $j_2 k^2$ term that determines the critical behaviour. Indeed, Sak noted that the parameter $\tilde{\eta}$ determining the crossover location agrees to this order with the exponent η_{SR} . Namely, in terms of $\varepsilon' \equiv 4 - d$ we have [8]

$$\eta_{\text{SR}} = \frac{n + 2}{2(n + 8)^2}\varepsilon'^2 + \mathcal{O}(\varepsilon'^3) \quad (5.12)$$

and the difference between ε and ε' is of order ε^2 (we assume ε' to be small, which in turns implies ε small). At first sight this result may seem a remarkable coincidence, but actually it is quite natural, as the diagrams are identical to those in the ε' -expansion. This result led Sak to the conclusion that the crossover occurs at $\sigma = 2 - \eta_{\text{SR}}$. However, we note that no higher-order contributions to Eq. (5.9) have

²We include the $\mathcal{O}(\varepsilon^3)$ term to anticipate higher-order contributions in a later stage.

been calculated which confirm this conclusion. Let us explicitly verify the consistency of this renormalization scenario. Thus, we return to the original LGW Hamiltonian and choose a different rescaling factor for the field [cf. the discussion below Eq. (4.3)], $\phi'_{\mathbf{k}} = b^{-1+\eta_{\text{SR}}/2}\phi_{\mathbf{k}}$. This choice ensures that the coefficient j_2 remains constant. Due to the absence of higher-order terms, the RG equation for j_σ is exact and we indeed find that this coefficient rescales as $j'_\sigma = b^{2-\eta_{\text{SR}}-\sigma}j_\sigma$ and the long-range term vanishes at the fixed point. Indeed, this is fully consistent with Eq. (5.9): all j_σ -dependent contributions vanish for $\sigma > 2 - \eta_{\text{SR}}$ if one replaces j_σ by its fixed-point value (this is similar to the replacement in Eq. (5.9); for a further discussion see, e.g., Ref. [9]). Furthermore, our new choice of the rescaling parameter implies that $\sigma - 2$ between the square brackets is replaced by $-\eta_{\text{SR}}$, which precisely cancels the remaining higher-order terms. At $\sigma = 2$, the LGW Hamiltonian (in momentum space) does not coincide with that of a short-range system, since the k^σ term is replaced by $j_\sigma k^2 \ln k$ [3]. We note that, due to the logarithmic factor, which upon renormalization is split into two parts, the long-range term directly contributes to the short-range term. As one may set j_σ equal to zero in the renormalization equation for j_2 , this contribution does not modify our conclusions concerning the dominance of the short-range term, but it *does* lead to a logarithmic correction to scaling. However, this logarithmic factor is subdominant, as it is multiplied by the contribution of the long-range interactions, which decays as $b^{-\eta_{\text{SR}}}$.

Interestingly, the situation at the crossover point itself, $\sigma = 2 - \eta_{\text{SR}}$, seems to have received little attention. Here, the renormalization equations should not depend on the choice of the rescaling of the field (cf. also Ref. [9]) and we find $j'_\sigma = j_\sigma$ as we had already obtained in the regime $\sigma < 2 - \eta_{\text{SR}}$. Usually, logarithmic corrections appear if an operator becomes marginal and also in this case the existence of such corrections is expected [10]. As such corrections are not implied by the RG equation for j_σ , we expect them to appear in the renormalization equation for j_2 . Indeed, also for this parameter the choice of rescaling factor should not matter at $\sigma = 2 - \eta_{\text{SR}}$ and we thus may use Eq. (5.9). Diagrammatic considerations show that for all graphs the number of propagators is one less than the number of factors ($j_\sigma + j_2$) coming from the first-order term in u^* . So they all contribute to terms which are at least linear in j_σ or j_2 . More generally, we note that, by necessity, all higher-order terms in j_2 contribute to η_{SR} and since the short-range part and the long-range part of the spin–spin interaction appear together in all propagators, we conjecture the full equation to be

$$\frac{dj_2}{dl} = (\sigma - 2 + \eta_{\text{SR}})j_2 + \eta_{\text{SR}}j_\sigma. \quad (5.13)$$

If this conjecture holds (or even if higher-order terms in j_σ appear), we see that j_2 is unbounded at $\sigma = 2 - \eta_{\text{SR}}$, due to the nonvanishing character of j_σ . Indeed, j_2

diverges logarithmically: $j_2 = \eta_{\text{SR}} j_\sigma l = \eta_{\text{SR}} j_\sigma \ln b$ and the ratio j_σ / j_2 decreases as $1/(\eta_{\text{SR}} \ln b)$.

We note that Sak's argument hinges on the observation that all propagators in the higher-order terms can be Taylor-expanded, thus yielding only integer powers of k . In the regime where σ is very close to 2, one must be careful to use such an expansion to distinguish between k^σ and k^2 . Nevertheless, the scenario outlined here has some attractive features. The original discontinuity in the exponent η at $\sigma = 2$ is removed. Furthermore, it is in agreement with Ref. [11], where arguments were given that long-range interactions do not modify the dominant behaviour of the spin-spin correlation function if the resulting η is smaller than η_{SR} . Finally, in the one-dimensional case (with $n = 1$) the absence of a phase transition for $\sigma > 1$ precisely corresponds to a crossover at $\sigma = 2 - \eta_{\text{SR}}$, because $\eta_{\text{SR}} = 1$, reflecting the fact that the correlation function does not decay algebraically above the critical temperature. However, it is by no means evident that this permits us to draw any conclusions for higher-dimensional models: $d = 1$ is a class on its own, with a nonzero transition temperature for $\sigma = 1$ but $T_c = 0$ for any $\sigma > 1$. The properties of the fixed point at $d = \sigma = 1$ are completely different from that of any other long-range system with a one-component order parameter. Nevertheless, all this has led to a rather wide acceptance of a crossover at $\sigma = 2 - \eta_{\text{SR}}$, despite the absence of any further evidence. The implications of this issue extend far beyond the mere question as to where the crossover occurs: it is relevant to the study of long-range correlated random impurities [12] and the more general question of dimensional regularization in systems with interaction terms with different critical dimensionalities [13]. Furthermore, related techniques have been applied to study the relevance of long-range interactions in spin glasses [14] and other ϕ^3 theories [15]. An expansion around the lower critical dimension has been carried out for n -component models ($n > 2$) with long-range interactions [9], which also yielded $2 - \eta_{\text{SR}}$ as the dividing line.

Yet, Sak's scenario does not get away uncriticized. An interesting contribution has been made by van Enter [16], who showed that it cannot hold for the XY model with $d \geq 3$. He proved that a long-range perturbation, which is considered irrelevant for $\sigma > 2 - \eta_{\text{SR}}$, still restores a broken rotational symmetry for any $\sigma < 2$ and thus modifies the critical behaviour. Yamazaki devoted several papers to the study of long-range systems by renormalized perturbation theory and found that the results depended on the precise normalization conditions for the vertex functions. In Refs. [17, 18], the regime $d/2 < \sigma < 2$ was divided into three regions: (i) the region $\sigma < 2 - \tilde{\epsilon}$, where the critical behaviour is strictly determined by the long-range interactions and $\eta = 2 - \sigma$; (ii) an intermediate region $2 - \tilde{\epsilon} < \sigma < 2 - \eta_{\text{SR}}$, where η starts to deviate from the classical value; (iii) the so-called *weakly long-range* region $2 - \eta_{\text{SR}} < \sigma < 2$, where the obtained value for η depends on the choice of the propagator. Indeed, in case (iii), Sak's result $\eta = \eta_{\text{SR}}$ was recovered if the short-range (k^2) propagator is applied, whereas for the long-range (k^σ) propagator

a continuously varying exponent η was found which at $\sigma = 2$ coincides with η_{SR} . Thus, η varies continuously as a function of σ . The parameter $\tilde{\varepsilon}$ has not been rigorously defined, but was said to depend on the relative magnitude of ε , $\varepsilon' = 4 - d$ and $2 - \sigma$. Reference [19] extends this treatment with ε -expansions for other critical exponents and in Refs. [20, 21] it is applied to the study of long-range models with a cubic anisotropy. In Ref. [22] the same scenario is outlined again. We find it difficult to get a consistent picture from Yamazaki's approach, as he carries out all calculations twice: either all propagators are expanded in terms of k^2 or in terms of k^σ , independent of the question which fixed point is the stable one. For example, the above-mentioned continuously varying η was found with a k^σ propagator, whereas at the same time it is admitted that $j_\sigma^* = 0$. However, if this implies that we must reject this result, we encounter a mismatch at $\sigma = 2 - \eta_{\text{SR}}$, unless the size of region (ii) shrinks to zero. But in the latter case, the entire Sak scenario is recovered.

The validity of the various renormalization approaches was reconsidered by Gusmão and Theumann [23]. According to their analysis, $2 - \sigma$ is not a valid ex-

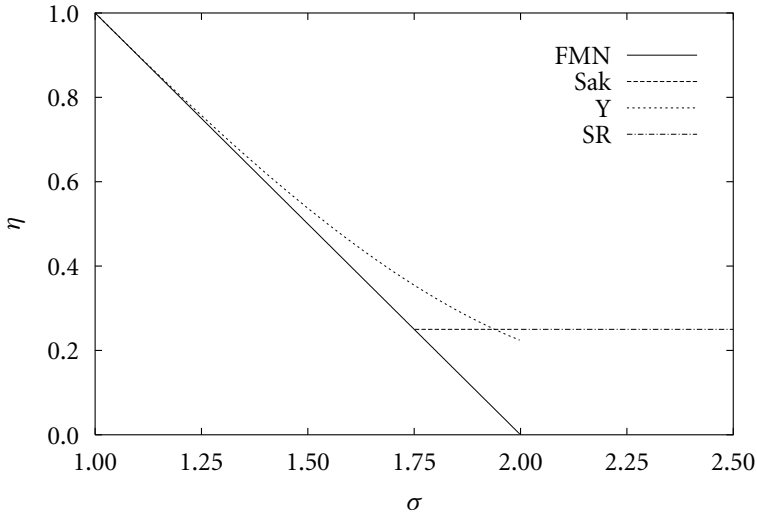


Figure 5.3: The exponent η as a function of the decay rate σ in the two-dimensional case. The solid line (“FMN”) denotes the exponent $2 - \sigma$, which is assumed to hold for any $\sigma < 2$ and hence implies a discontinuity at $\sigma = 2$; the dashed line (“Sak”) marks η according to Sak’s prediction of crossover at $\sigma = 2 - \eta_{\text{SR}}$, the dotted line (“Y”) indicates Yamazaki’s prediction of a smoothly varying exponent and the dash-dotted line (“SR”) indicates the short-range (2D Ising) exponent $1/4$. The small mismatch between “Y” and “SR” at $\sigma = 2$ is caused by the fact that the former is an ε -expansion result: if all higher-order terms are taken into account, a continuous crossover will be found.

pansion parameter, i.e., one cannot expand the full propagator in terms of k^2 , and hence the calculations of both Sak and Yamazaki are incorrect. They point out an apparent inconsistency in Yamazaki's calculations for the two-point vertex functions and conclude that his observation that η deviates from $2 - \sigma$ already below $\sigma = 2 - \eta_{\text{SR}}$ [the above-mentioned region (ii)] is erroneous. On the other hand, also Sak's result is disputed and different RG equations are obtained for j_2 and j_σ . Instead of Eq. (5.10), the fixed-point value of j_2 would be

$$j_2^* = \frac{\eta_{\text{SR}} R(\sigma) j_\sigma^*}{2 - \sigma}, \quad (5.14)$$

where $\lim_{\sigma \uparrow 2} R(\sigma) = 1$. Then, short-range forces are indeed generated in the renormalization process, but they do not modify the critical behaviour for any $\sigma < 2$. On the other hand, no higher-order terms appear in the recursion relation for j_σ and thus the result $\eta = 2 - \sigma$ holds in this entire region. Thus, the original discontinuity at the crossover location is recovered.

The situation is obscured even further by the notion that the long-range fixed point is only stable if the exponent ω [Eq. (5.3)] is positive [6]. To second order in ε , we find that for $d = 3$ this is the case for any $3/2 < \sigma < 2$. However, in two dimensions, ω first increases when moving away from the upper critical dimension ($\sigma = 1$), but then decreases fairly rapidly and passes (according to the second-order expression) through zero at $\sigma = 1.428 \dots$. In the one-dimensional case the stability region is even restricted to $\sigma \in [0.5, 0.6736]$. Although higher-order terms in the expansion for ω will change the size of this region, the range of validity of the corresponding ε -expansion is still remarkably small, in particular for the case $d = 1$.

In Fig. 5.3 we have collected the various predictions for the exponent η as a function of σ (for $d = 2$). Clearly, the proliferation of renormalization scenarios illustrates that a thorough understanding of the crossover from long-range to short-range critical behaviour is still lacking. Each of the various calculations has its own attractive features and a different approach is desirable to shed some light on this issue. Numerical calculations are an obvious choice, but problems may be expected here as well. As noted before, a one-dimensional model with a one-component order parameter is definitely not a representative case. In three dimensions, the region $2 - \eta_{\text{SR}} < \sigma < 2$ is very small, as are the differences between the various predictions. Moreover, strong corrections to scaling will be present close to the crossover point, which will hamper the numerical analysis. Also in the remaining nonclassical region, $3/2 < \sigma < 2 - \eta_{\text{SR}}$, one may hardly expect that the numerical error on the exponent η can be made sufficiently small to distinguish between $\eta = 2 - \sigma$ on the one hand and Yamazaki's slightly different prediction on the other hand. This leaves the two-dimensional case (with a one-component order parameter) as the most promising one. Here, the value of $\eta_{\text{SR}} = 1/4$ is relatively large, leading to grossly differing

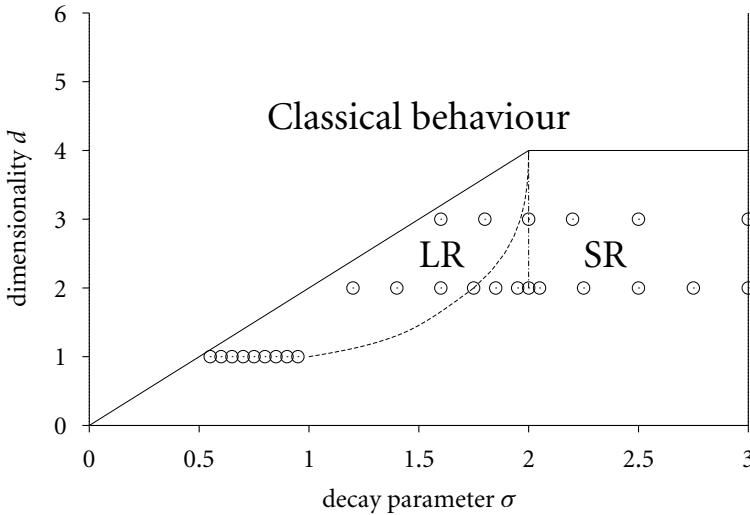


Figure 5.4: Dimensionality versus decay parameter σ . The full lines mark the upper critical dimension. “LR” and “SR” stand for long-range and short-range critical behaviour, respectively. The dashed curve, for which the numerical results of Ref. [24] have been used, marks the separation between these two regimes according to the renormalization scenario of Sak. The dotted vertical line denotes the separation as it follows from the original renormalization treatment by Fisher, Ma and Nickel, recovered by Gusmão and Theumann. For a further discussion see the text. The open circles indicate the models investigated in this chapter.

predictions as σ approaches 2 from below, whereas also the range of σ where the predictions disagree has an appreciable size. On the other hand, the remaining nonclassical region $1 < \sigma < 7/4$ may be sufficiently large to allow for the detection of any deviations from the conjectured value $\eta = 2 - \sigma$ without being plagued by strong corrections to scaling due to the proximity of either of the endpoints.

In conclusion, we note that some rigorous bounds have been derived in Ref. [25] for general spin models with algebraically decaying interactions. For the present discussion, the most important result is the bound

$$\frac{d}{1 - \eta/2} \geq \frac{d}{\min\{1, \sigma/2\}}, \quad (5.15)$$

which for $\sigma \leq 2$ reduces to $\eta \geq 2 - \sigma$ and thus cannot serve to pinpoint the crossover location.

Figure 5.4, which is the counterpart of Fig. 4.1, shows the various regimes as a function of both d and σ , including Sak’s crossover criterion. Also the models for which we have made numerical calculations are indicated.

5.3 The one-dimensional Ising model with long-range interactions

We have carried out simulations for spin chains of length $10 \leq L \leq 150\,000$ and a decay parameter $0.55 \leq \sigma \leq 0.95$, in intervals of 0.05. For each value of σ we have determined various critical properties. In contrast with the systems discussed in Chapter 4, no precise predictions exist for the correction-to-scaling exponents in this regime. Thus, these exponents have to be determined in the least-squares fits as well. We have applied the following general scheme for the analysis of the data:

1. Determine the exponent γ_i of the leading correction to scaling from a least-squares fit of the amplitude ratio Q and/or the magnetic susceptibility χ . As this estimate varies somewhat as a function of the minimal system size, we increase the error bars to cover this variation.
2. Make an analysis of both Q and the magnetic susceptibility with this exponent fixed at its best value. These analyses are then repeated with γ_i fixed at a value that lies one standard deviation above and below the best estimate, to determine the influence of the uncertainty in γ_i . The advantage of keeping γ_i fixed is that one can include more (nonlinear) correction terms and thus include smaller system sizes in the analysis.
3. Finally, the susceptibility is analyzed with the magnetic exponent fixed at its conjectured value, where again the uncertainty in γ_i is taken into account. The resulting estimate for the critical coupling is then used in an analysis of the amplitude ratio Q , to make a more precise estimate of this quantity. The thermal exponent is left free in all analyses.

Table 5.1: Results of least-squares analyses of the magnetic susceptibility. Apart from the Monte Carlo estimates, also the RG conjecture for the magnetic exponent is included.

σ	γ_i	γ_h	γ_h (RG)	γ_t	K_c
0.55	-0.15 (5)	0.777 (5)	0.775	0.499 (10)	0.254775 (14)
0.60	-0.15 (5)	0.798 (4)	0.800	0.502 (8)	0.281793 (10)
0.65	-0.20 (4)	0.826 (3)	0.825	0.503 (10)	0.310503 (10)
0.70	-0.23 (5)	0.848 (3)	0.850	0.491 (10)	0.341226 (12)
0.75	-0.24 (5)	0.875 (2)	0.875	0.469 (15)	0.374530 (15)
0.80	-0.25 (5)	0.896 (4)	0.900	0.457 (10)	0.41104 (3)
0.85	-0.26 (5)	0.9243 (15)	0.925	0.413 (14)	0.45209 (3)
0.90	-0.35 (5)	0.9508 (10)	0.950	0.379 (15)	0.49968 (6)
0.95	-0.32 (2)	0.9754 (7)	0.975	0.287 (6)	0.55870 (15)

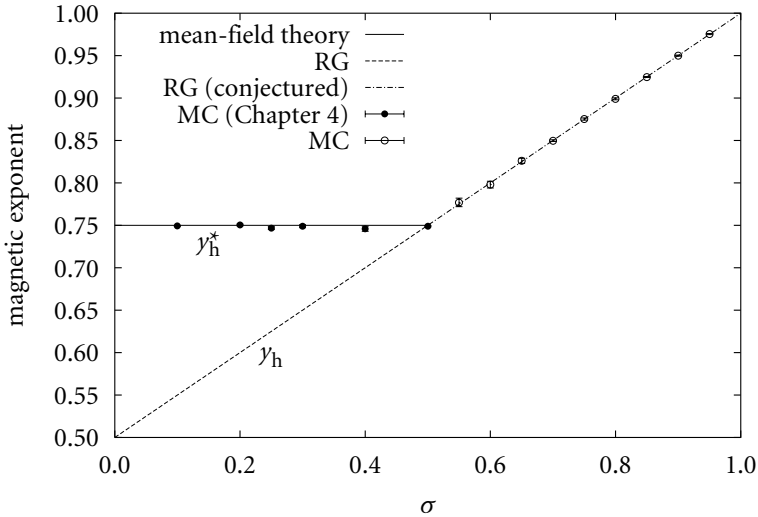


Figure 5.5: Monte Carlo results for the magnetic exponent. The full circles denote estimates for γ_h^* (the classical regime, see Chapter 4) and the open circles indicate values for γ_h (the nonclassical regime). The dash-dotted line marks the RG prediction below the upper critical dimension, which is conjectured to hold exactly to all orders in the ε -expansion.

Table 5.1 shows the results for γ_i and for the analyses of the magnetic susceptibility as described in step 2. Here, an expression of the form (4.30) was used to describe the data, where γ_h^* and γ_t^* were replaced by γ_h and γ_t , respectively. As usual, a cross term proportional to $L^{\gamma_t + \gamma_i}$ had to be included in the scaling formula as well. Evidently, over the full range of σ , there is an excellent agreement between the Monte Carlo estimates for γ_h and the renormalization-group conjecture $\gamma_h = (d + \sigma)/2$. This is illustrated graphically in Fig. 5.5. Furthermore, we note that the second-order expression (5.3) yields a poor description of the irrelevant exponent.

For Q , an expression similar to Eq. (4.23) was applied. Since the analysis is insensitive to the precise exponent in the subdominant correction $q_1 L^{d-2\gamma_h}$, the exponent γ_h could be kept fixed at its conjectured value, which is also justified by the results from the susceptibility. The corresponding results are collected in Table 5.2. The estimates for K_c as obtained from the susceptibility and Q are in mutual agreement. One observes that the critical coupling monotonically increases with increasing σ , as one would expect. Also for the thermal exponent γ_t the agreement between Tables 5.1 and 5.2 is quite good.

Next, we have carried out step 3. For later comparison, the results for the critical coupling, which are our most accurate estimates, are collected in Table 5.5. The estimates for γ_t (both from the analyses of χ and from the analyses of Q) and for Q are

Table 5.2: Results of analyses of the amplitude ratio Q for different values of the decay parameter σ .

σ	Q	γ_t	K_c
0.55	0.50 (2)	0.494 (19)	0.254754 (17)
0.60	0.54 (2)	0.497 (8)	0.281781 (14)
0.65	0.590 (8)	0.501 (8)	0.310481 (12)
0.70	0.639 (3)	0.491 (10)	0.341226 (11)
0.75	0.689 (3)	0.491 (14)	0.374517 (11)
0.80	0.742 (2)	0.460 (10)	0.411071 (17)
0.85	0.8019 (11)	0.416 (9)	0.452090 (15)
0.90	0.8637 (8)	0.371 (10)	0.49964 (3)
0.95	0.9302 (12)	0.286 (6)	0.55866 (8)

Table 5.3: Estimates for the thermal exponent and the amplitude ratio from analyses in which either the magnetic exponent was kept fixed (second column) or the critical coupling (third and fourth column).

σ	$\gamma_t (\chi)$	$\gamma_t (Q)$	Q
0.55	0.502 (16)	0.49 (3)	0.507 (8)
0.60	0.496 (10)	0.505 (10)	0.550 (3)
0.65	0.505 (10)	0.510 (10)	0.595 (3)
0.70	0.485 (9)	0.498 (10)	0.641 (2)
0.75	0.469 (13)	0.484 (10)	0.6911 (15)
0.80	0.450 (14)	0.460 (8)	0.7442 (11)
0.85	0.411 (13)	0.416 (7)	0.8026 (6)
0.90	0.380 (12)	0.372 (14)	0.8634 (6)
0.95	0.289 (4)	0.287 (6)	0.9298 (3)

listed in Table 5.3. All results are consistent with those obtained from the previous analyses, but for the thermal exponent the new estimates are not necessarily more accurate. This is caused by the uncertainty in γ_t , which is now the main source of the error margins. However, for the amplitude ratio the accuracy has clearly improved.

In Fig. 5.6 we have plotted the most accurate estimates for the thermal exponent along with the Monte Carlo estimates from the previous chapter and the first- and second-order ε -expansion results [see Eqs. (5.5) and (5.6), respectively]. Until $\sigma = 0.8$ ($\varepsilon = 0.6$) the agreement is quite good. For larger values of σ , on the other hand, the Monte Carlo data approach the dash-dotted curve indicating the first-order expansion around the Kosterlitz–Thouless point at $\sigma = 1$: $\gamma_t = \sqrt{2(1 - \sigma)}$ [26]. In addition, we have plotted the behaviour of Q as a function of the decay parameter in Fig. 5.7. For ε small, the results quite accurately follow a straight line, which can roughly be described by the expression $Q_{MF}(1 + \varepsilon)$. Naturally, this is only an ap-

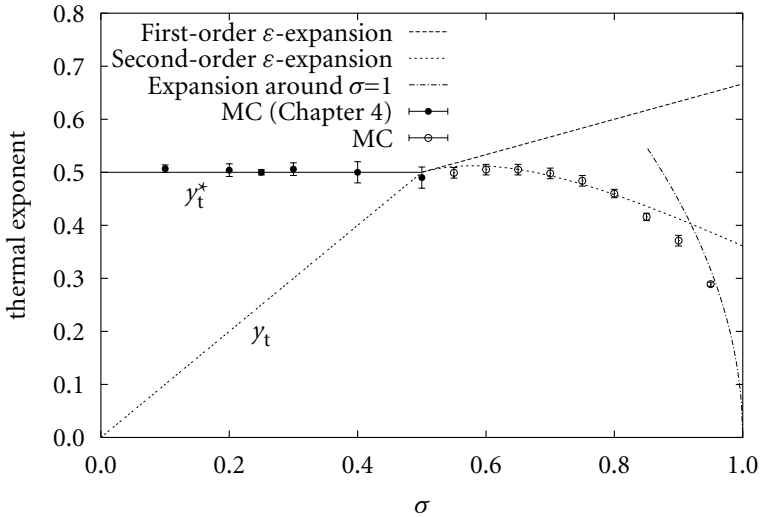


Figure 5.6: Monte Carlo results for the thermal exponent. The full circles denote estimates for γ_t^* (the classical regime, see Chapter 4) and the open circles indicate values for γ_t (the nonclassical regime). The dashed line and curve mark the first- and second-order ε -expansions. We have also included an expansion around $\sigma = 1$ (dash-dotted curve).

proximation, since there is no *a priori* reason for the amplitude of the $\mathcal{O}(\varepsilon)$ term to be identical to Q_{MF} . Further below the upper critical dimension (larger σ), the estimates for Q start to deviate from the straight line, which is in full harmony with the prediction of a Kosterlitz–Thouless transition at $\sigma = 1.0$. Namely, it is predicted that the order parameter exhibits a jump discontinuity at this point, which in turn suggests that the critical value of the amplitude ratio Q must be equal to 1 there. Indeed, the deviations of Q from the straight line are compatible with this value. Below we will come back to the behaviour of Q as a function of ε .

In Table 5.4 we have collect various earlier estimates for the correlation-length exponent. The approximations of Refs. [27, 28] apparently break down when σ ap-

Table 5.4: The correlation length exponent ν for the one-dimensional model as a function of σ , together with earlier estimates and the renormalization predictions.

σ	This work	Ref. [27]	Ref. [29]	Ref. [28]	Ref. [30]	Ref. [31]
0.6	1.98 (2)	1.9	2.16	2.12	2.00	—
0.7	2.01 (4)	1.8	2.123	2.17	1.93	2.66
0.8	2.17 (5)	1.9	2.208	2.24	2.07	—
0.9	2.70 (7)	2.0	2.63	2.30	2.47	3.90

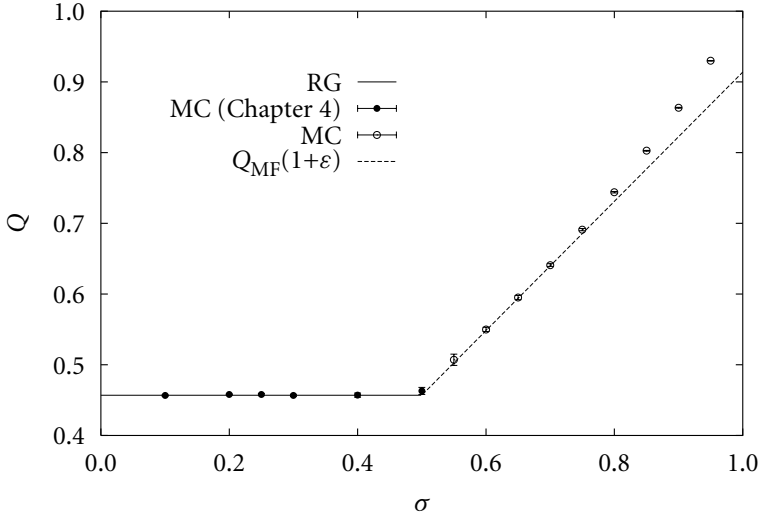


Figure 5.7: Monte Carlo results for the amplitude ratio Q . The full circles denote estimates for Q in the classical regime (see Chapter 4) and the open circles indicate the values for Q obtained in this chapter. The dashed line indicates a simple guess for the behaviour of Q just below the upper critical dimension.

proaches 1. The agreement with the results of Refs. [29, 30] is generally quite good.

Finally, we compare our best estimates for the critical couplings with earlier estimates, see Table 5.5. Just as in Sec. 4.4, our results supersede all other values by about two orders of magnitude. Both the series-expansion results of Nagle and Bonner [27] and the finite-range extrapolations of Glumac and Uzelac [29, 30] agree with our results. The estimates of Ref. [32] now lie *below* our values, in contrast with the classical region. The agreement with the coherent-anomaly results [28] decreases for increasing σ . This is also true for the approximations from Ref. [33], cf. Eq. (4.25), which confirms that this is essentially a mean-field-like approach. The discrepancies (for $\sigma \gg 0$) with the real-space renormalization-group results were already predicted in Ref. [31]. Furthermore, we see from Table 5.6 that our results conform to all predicted bounds. Comparing these bounds with Table 4.4, we find that the lower bounds become less tight with increasing σ , whereas the upper bounds become more tight.

Table 5.5: Comparison between our best estimates of the critical couplings K_c for the one-dimensional system and earlier estimates.

σ	This work	Ref. [27]	Ref. [32]	Ref. [29]	Ref. [34]	Ref. [30]	Ref. [28]	Ref. [33]	Ref. [31]
0.55	0.254772 (9)	—	—	—	—	—	—	0.2547	—
0.60	0.281800 (5)	0.2832 (18)	0.279092	0.282 (3)	—	0.2822	0.282 (6)	0.2894	—
0.65	0.310500 (5)	—	—	—	—	—	—	0.3317	—
0.70	0.341237 (4)	0.343 (2)	0.329139	0.341 (3)	—	0.3417	0.338 (7)	0.3855	0.391
0.75	0.374531 (5)	—	—	—	0.388 (5)	—	—	0.4582	—
0.80	0.411090 (8)	0.412 (3)	0.381071	0.411 (4)	—	0.4116	0.401 (7)	0.5642	—
0.85	0.452101 (8)	—	—	—	—	—	—	0.7374	—
0.90	0.49963 (2)	0.499 (4)	0.434861	0.499 (5)	—	0.4987	0.4728 (4)	1.079	0.65
0.95	0.55862 (4)	—	—	—	—	—	—	2.096	—

Table 5.6: Comparison of our best estimates of the critical couplings for the one-dimensional system with lower and upper bounds.

σ	This work	Ref. [35]	Ref. [35]
0.60	0.281800 (5)	≥ 0.2203	≤ 0.4502
0.70	0.341237 (4)	≥ 0.2458	≤ 0.5066
0.80	0.411090 (8)	≥ 0.2691	≤ 0.5596
0.90	0.49963 (2)	≥ 0.2903	≤ 0.6101

5.4 The two-dimensional Ising model with long-range interactions

5.4.1 Introduction

As indicated in Sec. 5.2, the two-dimensional case is the most suitable candidate for resolving the contradicting scenarios for the crossover from nonclassical long-range critical behaviour to short-range critical behaviour. We recall that the classical regime ends at $\sigma = d/2 = 1$ and the intermediate long-range regime is predicted to end either at $\sigma = 2 - \eta_{\text{SR}} = 7/4$ or at $\sigma = 2$. We have simulated models with $\sigma \in \{1.20, 1.40, 1.60, 1.75, 1.85, 1.95, 2.00, 2.05, 2.25, 2.50, 2.75, 3.00\}$ and determined the amplitude ratio Q , the magnetic and thermal exponent and the critical coupling. Just as in the one-dimensional case, the absence of precise predictions for the correction-to-scaling exponents considerably reduces the accuracy that can be obtained in the analyses. In effect, for each value of σ an individual approach is required. Thus, we have divided the models into three categories: (A) $1 < \sigma < 7/4$; (B) $7/4 \leq \sigma \leq 2$; (C) $\sigma > 2$. In the following subsections we discuss these categories separately.

5.4.2 Regime A: $1 < \sigma < 7/4$

These models ($\sigma = 1.20, 1.40, 1.60$), for which we have simulated linear system sizes $4 \leq L \leq 400$, closely resemble those analyzed in the one-dimensional case. Thus, we have followed the scheme outlined in Sec. 5.3. As can be seen from Table 5.7, for $\sigma = 1.20$ the irrelevant exponent is in good agreement with the first-order ε -expansion ($-\varepsilon = -0.4$). At $\sigma = 1.40$ the irrelevant exponent has further increased (in the absolute sense), but at $\sigma = 1.60$ it has decreased again. This might indicate the presence of the short-range fixed point. We cannot exclude that the irrelevant exponents as listed in the table are only “effective” exponents, representing the combined effects of various corrections to scaling. The magnetic exponent γ_h is for all three cases in very good agreement with the renormalization prediction, so it appears as if for this regime the expression $\gamma_h = (d + \sigma)/2$ indeed holds exactly. Repeating the analysis of the susceptibility with γ_h fixed yields an accurate prediction for the critical coupling, which we have used in the analysis of Q . The corresponding results are shown in Table 5.8.

5.4.3 Regime B: $7/4 \leq \sigma \leq 2$

This regime is by far the most difficult to analyze due to very slow convergence of the numerical data. For the models with $\sigma = 1.75, 1.85, 1.95, 2.00$ we have simulated

Table 5.7: Results of least-squares analyses of the magnetic susceptibility in regime A. Apart from the Monte Carlo estimates, also the RG conjecture for the magnetic exponent is included.

σ	γ_i	γ_h	γ_h (RG)	γ_t	K_c
1.20	-0.41 (7)	1.597 (8)	1.600	1.00 (2)	0.114966 (4)
1.40	-0.60 (8)	1.693 (8)	1.700	1.00 (2)	0.125297 (4)
1.60	-0.43 (3)	1.795 (15)	1.800	0.98 (3)	0.133397 (7)

Table 5.8: The amplitude ratio Q and the thermal exponent γ_t in regime A, as obtained with the critical coupling fixed at the estimates in Table 5.7.

σ	Q	γ_t
1.20	0.560 (3)	1.02 (3)
1.40	0.6534 (10)	1.04 (3)
1.60	0.759 (2)	1.03 (2)

linear system sizes up to $L = 600, 1000, 600, 400$, respectively. Here, we discuss the four cases separately.

For $\sigma = 1.75$, the choice of the scaling formula depends on the pertinent renormalization scenario. If the crossover between long-range and short-range critical behaviour indeed occurs at this location (the ‘‘Sak’’ scenario), logarithmic corrections should be present. On the other hand, if the scenario of either Gusmão and Theumann (GT) or Yamazaki is correct, such corrections are not to be expected here. However, Sak and GT agree on a magnetic exponent equal to $15/8$, whereas Yamazaki has predicted that this value is only reached in the limit $\sigma \uparrow 2$. First, we have analyzed the amplitude ratio Q using an expression which contains only algebraically decaying corrections to scaling. This yielded the following estimates for the universal quantities: $Q = 0.804$ (9), $\gamma_t = 1.007$ (5) and $\gamma_i = -0.41$ (6). The χ^2 criterion gave no reason to doubt the reliability of this analysis. Subsequently we used the estimate for γ_i to analyze the magnetic susceptibility. The resulting estimate for the magnetic exponent was $\gamma_h = 1.831$ (12), which yields an inconsistency for the GT scenario. Thus, we fitted an expression containing both logarithmically decaying terms *and* an algebraic correction to the numerical data for Q . This gave $Q = 0.842$ (19), $\gamma_t = 1.003$ (9) and $\gamma_i = -1.1$ (6). Since both Q and the thermal exponent are in agreement with the 2D Ising universality class, we repeated the analysis with $Q = 0.856216$ fixed: $\gamma_t = 1.000$ (7) and $\gamma_i = -0.86$ (8). The resulting irrelevant exponent was then used for an analysis of the susceptibility, yielding $\gamma_h = 1.84$ (3). Fixing K_c at the estimate from the last analysis of Q gave $\gamma_h = 1.86$ (3). While these values are not very accurate, they are in full agreement with the Sak scenario.

Next, we considered $\sigma = 1.85$. The usual analysis of Q to determine the expo-

ment of the leading correction to scaling resulted in a remarkably large value: $y_i = -0.48$ (8). Furthermore, we found $y_t = 0.990$ (7) and $Q = 0.827$ (8). The latter estimate would—in combination with the first estimate of Q at $\sigma = 1.75$ —suggest an amplitude ratio that gradually increases upon the approach of $\sigma = 2$. However, to allow for the situation that this is only an effective correction exponent, we re-analyzed Q with an additional correction decaying as $L^{-0.10}$, as predicted for the decay of coefficient j_σ in the Sak scenario. This yielded $Q = 0.86$ (4), $y_i = -0.51$ (5) and $y_t = 0.99$ (5). As this suggests at least a consistency with crossover at $\sigma = 1.75$, we fixed Q to obtain a better estimate of K_c and y_i . For the latter we found $y_i = -0.501$ (12), which we used in an analysis of the magnetic susceptibility, yielding $y_h = 1.86$ (4). By fixing K_c we could improve this to $y_h = 1.87$ (3).

For $\sigma = 1.95$ we have already approached the point $\sigma = 2$ very closely, which makes it difficult to distinguish the predictions of Sak and Yamazaki. However, it is a very suitable system to judge the GT scenario, as the discrepancy in η (or y_h) increases with the distance to $\sigma = 7/4$. An analysis of Q yielded: $Q = 0.86$ (3), $y_t = 0.991$ (5) and $y_i = -0.31$ (4). With Q fixed at its 2D Ising value, we found $y_i = -0.34$ (4). This exponent presumably incorporates the effects of both the decaying long-range term (exponent -0.20) and higher correction terms. The magnetic exponent then resulted from an analysis of the susceptibility: $y_h = 1.873$ (16), which lies already six standard deviations from GT's prediction $y_h = 1.975$. Fixing the critical coupling reinforced this conclusion: $y_h = 1.878$ (7).

Finally, we considered the case $\sigma = 2$. In fact, this is the counterpart of $\sigma = 1.75$, since now the scenarios of both GT and Yamazaki predict logarithmic corrections, whereas in Sak's case they only occur in subdominant correction terms. However, in all three scenarios Q is expected to take its 2D Ising value. An analysis with only algebraic corrections gave $Q = 0.859$ (14) and $y_i = -0.41$ (9). Including logarithmic corrections led to the inconclusive result $Q = 0.79$ (6), so that we made a new analysis with Q fixed. Without logarithmic corrections we found $y_i = -0.42$ (3) and inclusion of logarithms hardly modified this estimate; $y_i = -0.41$ (4). Furthermore, the coefficient of the logarithmic term was zero within less than one standard deviation. This suggests that the logarithms are at least very weak. Fitting the susceptibility with only algebraic corrections then gave $y_h = 1.871$ (14) and with a fixed coupling even $y_h = 1.875$ (3).

In summary, we have handled this regime as follows. For each system, the corrections to scaling were determined from the amplitude ratio Q . Since Q was in all four cases consistent with the 2D Ising value, we obtained a better estimate for the correction exponent by assuming that Q indeed takes this value. A subsequent analysis of the susceptibility with this correction then yielded a magnetic exponent which is in agreement with the 2D Ising value, which corroborates the consistency of our assumption. In Table 5.9 we have collected our estimates for Q , y_h , y_t and K_c , where the latter was obtained with Q fixed.

Table 5.9: Estimates for the amplitude ratio Q , the magnetic and the thermal exponent and the critical coupling in regime B.

σ	Q	y_h	y_t	K_c
1.75	0.842 (19)	1.86 (3)	1.003 (9)	0.137870 (3)
1.85	0.86 (4)	1.87 (3)	0.99 (5)	0.140074 (2)
1.95	0.86 (3)	1.878 (7)	0.991 (5)	0.141646 (2)
2.00	0.859 (14)	1.875 (3)	0.980 (10)	0.142203 (3)

Table 5.10: Our best estimates for Q , y_t , y_i and K_c in regime C.

σ	Q	y_t	y_i	K_c
2.05	0.861 (9)	0.97 (2)	-0.51 (4)	0.142611 (4)
2.25	0.854 (6)	0.97 (15)	-0.68 (4)	0.142832 (3)
2.50	0.859 (3)	0.99 (2)	-0.73 (2)	0.140392 (3)
2.75	0.855 (3)	0.997 (15)	-0.78 (4)	0.135640 (4)
3.00	0.857 (3)	1.01 (2)	-1.01 (7)	0.129266 (4)

5.4.4 Regime C: $\sigma > 2$

This regime, which contains the systems with $\sigma = 2.05, 2.25, 2.50, 2.75$ and 3.00 , posed much less problems than the preceding one. The analyses of Q in which the correction-to-scaling exponent was included as a free parameter left little doubt that the amplitude ratio indeed takes its 2D Ising value for these systems. This in turn allowed for an accurate determination of y_i . Table 5.10 lists the results for Q and the estimates for y_t , y_i and K_c obtained with Q fixed. When judging the accuracy of these estimates, one should keep in mind that the largest linear system sizes decrease with increasing σ ; they are given by $L = 400, 400, 300, 200, 200$, respectively. Close to $\sigma = 2$, the exponent y_i also includes the effect of the correction to scaling caused by the presence of the long-range term, but for larger σ this is a subdominant correction. The critical coupling shows a remarkable behaviour: starting from $\sigma = 0$ it increases monotonically with σ , although slower and slower when $\sigma = 2$ is approached. Even in regime C, the increase continues, until between $\sigma = 2.25$ and $\sigma = 2.50$ the critical coupling starts to decrease. This can be explained from the fact that we have simulated systems with an interaction that is an integral over a square around each lattice site (see Sec. 4.4.1). For interactions which decay very fast, the large value of the integrand near the lower-distance cutoff leads to a strong nearest-neighbour coupling, explaining the decrease of K_c .

Next, the correction exponents were used in an analysis of the susceptibility, with K_c both free and fixed. The results are collected in Table 5.11. Clearly, there is strong evidence that all these models belong to the 2D Ising universality class, although with much stronger corrections to scaling than the two-dimensional nearest-neighbour

Ising model itself.

Table 5.11: The exponents y_h and y_t in regime C. The estimates in the third column were obtained with the critical couplings fixed at their best estimates from Table 5.10.

σ	y_h	y_h	y_t
2.05	1.873 (11)	1.875 (4)	0.96 (3)
2.25	1.875 (4)	1.8748 (15)	0.97 (2)
2.50	1.876 (3)	1.8749 (10)	0.99 (4)
2.75	1.874 (4)	1.8745 (10)	0.97 (2)
3.00	1.873 (2)	1.8748 (8)	1.01 (2)

5.4.5 Discussion and conclusion

In Fig. 5.8 we have collected the results for Q for all two-dimensional systems investigated in this and the preceding chapter. Clearly, the region $1.75 < \sigma < 2.00$ is the most problematic one, but all data are consistent with the 2D Ising value. The data in the region $1.0 < \sigma < 1.6$ are remarkably well described by a straight line, just as in the one-dimensional case (cf. Fig. 5.7). The remarkable point concerning this apparently linear dependence on ε is that (as mentioned in Sec. 5.1) in Ref. [2] the dependence of Q on $\varepsilon' = 4 - d$ has been calculated for short-range models, for which a series expansion in $\sqrt{\varepsilon'}$ was found (see Fig. 5.9). In this series the coefficient of the first ε' -dependent term was by no means small compared to higher-order terms. In view of the close resemblance between the expansions around $d_u = 2\sigma$ and $d_u = 4$ one would thus expect a clearly observable square-root dependence of Q on ε , especially because the source of these square roots seems a very general feature. This indicates an unclarified peculiarity for the ε -expansion around $d_u = 2\sigma$.

Figure 5.10 shows the magnetic exponent for all examined long-range models. Clearly, our results exclude the renormalization scenario of Gusmão and Theumann, which we considered as the most serious opponent of Sak's scenario. In the region $1.00 \leq \sigma \leq 1.75$ the conjecture $y_h = 1 + \sigma/2$ is confirmed to a considerable accuracy. The predictions of Yamazaki are more difficult to discern from this conjecture. Apart from the inconsistencies pointed out in Sec. 5.2, we note the following. First, we consider the expansions given in Ref. [22]. From Fig. 5.3 one observes that the discrepancies in η reach their maximum around $\sigma = 1.75$, so this is the best location to test the predictions of the ε -expansion. At $\sigma = 1.60$, the second-order ε -expansion predicts $y_h \approx 1.77$ and at $\sigma = 1.75$ $y_h \approx 1.82$. These values agree less well with our values (while we notice that for the entire region $1.0 < \sigma < 2.0$ the deviations of Sak's scenario must be small), but the differences are insufficient to be reliably excluded. Secondly, we have not observed any logarithmic corrections to scaling at $\sigma = 2.0$, which contradicts the predictions of Yamazaki.

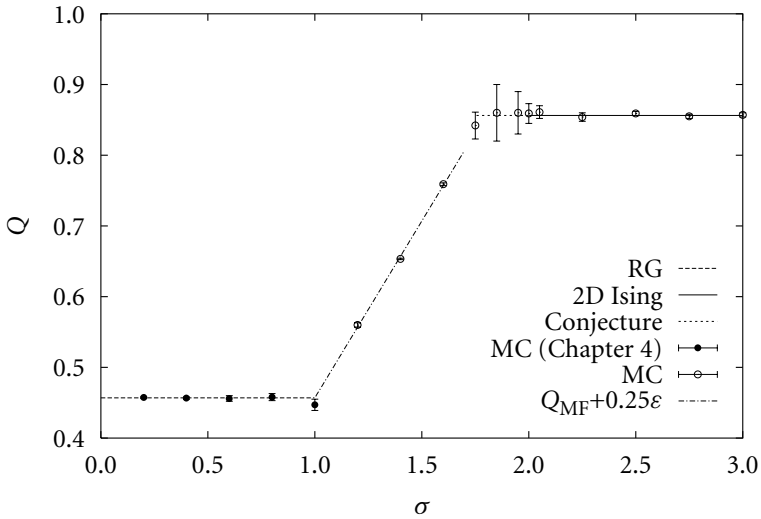


Figure 5.8: Monte Carlo results for the amplitude ratio Q . The full circles denote estimates for Q in the classical regime (see Chapter 4) and the open circles indicate the values for Q obtained in this chapter. The dash-dotted line indicates a simple guess for the behaviour of Q just below the upper critical dimension.

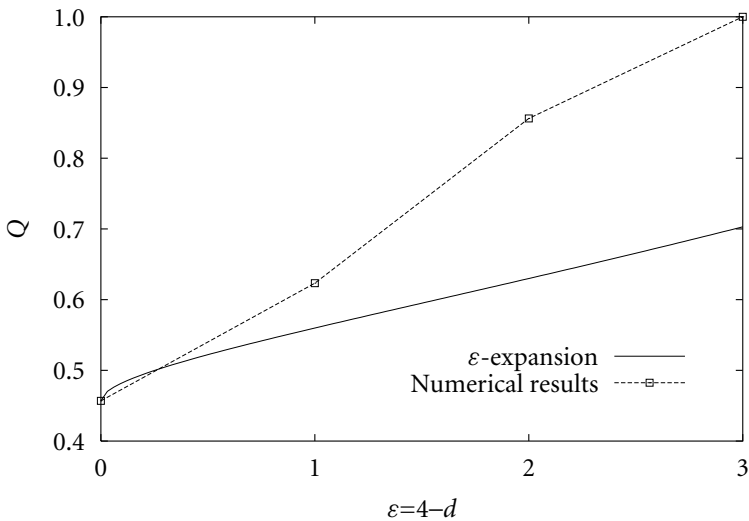


Figure 5.9: The $\sqrt{\epsilon'}$ -expansion result (to order ϵ') of Ref. [2] for the amplitude ratio Q , along with the results for discrete dimensionalities.

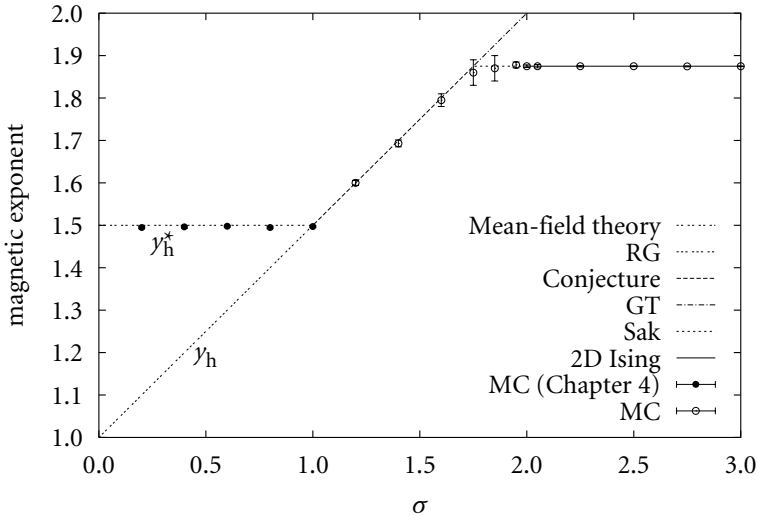


Figure 5.10: Monte Carlo results for the magnetic exponent. The full circles denote estimates in the classical regime (see Chapter 4) and the open circles indicate the values obtained in this chapter. Our numerical data clearly exclude the prediction of Gusmão and Theumann (dash-dotted line) of a crossover at $\sigma = 2.0$.

5.5 The three-dimensional Ising model with long-range interactions

5.5.1 Introduction

As predicted at the end of Sec. 5.2, the strong corrections to scaling pose considerable problems for the analysis of the numerical results in three dimensions, where we have carried out simulations for linear system sizes up to $L = 64$. From the situation in two dimensions we expect long-range critical behaviour for $3/2 < \sigma \lesssim 1.963$ and short-range critical behaviour for larger values of σ . Simulations have been carried out for $\sigma \in \{1.6, 1.8, 2.0, 2.2, 2.5, 3.0\}$. Whereas the latter three systems yield quite satisfactory estimates for the universal quantities, the results of the former three are rather poor. For this reason, we treat these two categories separately.

5.5.2 Systems with a decay parameter $\sigma = 1.6, 1.8, 2.0$

As in Sec. 5.4.3, we outline the analysis of the numerical results in some detail for each of these systems individually.

The case $\sigma = 1.6$ suffers from the proximity of the upper critical dimension, which leads to a small correction-to-scaling exponent. From the comparable one-

and two-dimensional models, we conclude that this exponent in good approximation is given by $y_i = -\varepsilon = -0.20$. Thus, we have analyzed the amplitude ratio Q with this exponent fixed, which yielded $Q = 0.54$ (4) and $y_t = 1.50$ (2). A similar analysis of the magnetic susceptibility yielded $y_h = 2.29$ (2), in agreement with the conjectured value 2.30. Thus, we fixed this exponent in order to get an accurate estimate of the critical coupling, which was then used to obtain more precise results for the amplitude ratio and the thermal exponent; $Q = 0.522$ (19) and $y_t = 1.523$ (16). Because of the close agreement between the latter value and the second-order ε -expansion result $y_t = 1.527$, we have repeated the same analysis with the thermal exponent fixed, but this did not improve the results.

For $\sigma = 1.8$ it proved difficult to determine the leading irrelevant exponent from the analysis, so we made the rough estimate $y_i = -0.5$ (1) and kept it fixed in the least-squares fits. For the magnetic susceptibility this yielded $y_h = 2.37$ (3) and $y_t = 1.54$ (4). The magnetic exponent is consistent with the conjecture $y_h = 2.40$ and the thermal exponent agrees with the ε -expansion result $y_t \approx 1.55$. The value of the amplitude ratio varies considerably with the value of y_i and we found $Q = 0.56$ (2). Next we determined the critical coupling from a fit of the susceptibility for $y_i = -0.4, -0.5, -0.6$. The three resulting, rather different estimates were then used for three analyses of Q , each with y_i fixed at the corresponding value. Surprisingly, the variation in the results for the amplitude ratio turned out to be much weaker and our final estimate is $Q = 0.554$ (12).

At $\sigma = 2.0$ the convergence is extremely slow, which can be understood from the presence of the crossover point. The corrections are predicted to decay as $L^{-\eta_{SR}} \sim L^{-0.037}$. An accurate confirmation of the universal 3D Ising quantities can therefore not be obtained from the current numerical data. We found $Q = 0.71$ (16), $y_t = 1.59$ (4) and $y_h = 2.39$ (8). Especially the magnetic exponent has a strong tendency to drop below the expected value $y_h = 2.4815$.

5.5.3 Systems with a decay parameter $\sigma = 2.2, 2.5, 3.0$

When σ is moved away from the crossover location, the situation rapidly improves. For $\sigma = 2.2$ and $\sigma = 2.5$ we clearly observed a correction to scaling which is not present in the 3D Ising model, but for $\sigma = 3.0$ this could not be discerned from the usual corrections. The general procedure of the analysis was as follows. First we analyzed Q without fixing any parameters. Since in all cases this yielded estimates for the amplitude ratio and the thermal exponent which are consistent with the 3D Ising values (cf. Chapter 3), we subsequently kept these parameters fixed in a least-squares fit of Q to determine y_i and K_c more accurately. These values were then used to analyze the susceptibility. For $\sigma = 2.2$ we found $y_i = -0.411$ (10), which is most likely an effective exponent, as it is twice as large as one would expect. In the susceptibility the correction with this exponent was only very weak. At $\sigma = 2.5$ the correction

exponent was -0.48 (3), which agrees very well with $2 - \eta_{\text{SR}} - \sigma$.

5.5.4 Discussion and conclusions

In Table 5.12 we have collected our estimates for Q , y_t , y_h and K_c , for the three-dimensional models considered in Secs. 5.5.2 and 5.5.3. All results are consistent with a crossover at $\sigma = 2 - \eta_{\text{SR}}$, but the accuracy of the estimates is too low to detect subtle deviations from the predicted scenario. We note that both y_t and y_h increase monotonically from their classical values to the 3D Ising values. The same holds from the fourth-order amplitude ratio, but it is not possible to confirm the linear dependence on ε as convincing as in Figs. 5.7 and 5.8. The critical coupling exhibits the same nonmonotonicity as could be observed in Table 5.10, again between $\sigma = 2.2$ and $\sigma = 2.5$.

Table 5.12: Our best estimates for the amplitude ratio Q , the thermal and the magnetic exponent and the critical coupling K_c in a number of three-dimensional systems with long-range interactions.

σ	Q	y_t	y_h	K_c
1.6	0.522 (19)	1.523 (16)	2.29 (2)	0.0625861 (10)
1.8	0.554 (12)	1.54 (4)	2.37 (3)	0.0645353 (4)
2.0	0.71 (16)	1.59 (4)	2.39 (8)	0.0655958 (18)
2.2	0.62 (2)	1.60 (3)	2.466 (10)	0.0658720 (10)
2.5	0.606 (11)	1.597 (12)	2.479 (3)	0.0650179 (11)
3.0	0.6229 (8)	1.61 (4)	2.476 (6)	0.0610918 (9)

5.6 Conclusion

Let us briefly summarize the results of this chapter. We have analyzed the nonclassical critical behaviour of Ising models with long-range interactions. In the one-dimensional case, we covered the entire region between the upper critical dimension and the Kosterlitz–Thouless point. Apart from accurate estimates for the critical couplings, we showed that the thermal exponent is well described by the second-order ε -expansion of Fisher, Ma and Nickel, up to $\varepsilon \approx 0.6$. Close to $\sigma = 1$, our numerical results indeed approach the expansion of Kosterlitz. Our data provide strong evidence that the renormalization conjecture for the magnetic exponent indeed holds exactly up to $\sigma = 1$. The universal fourth-order amplitude ratio is quite well described by a linear function of ε .

For the two-dimensional case, we covered not only the entire nonclassical long-range regime, but also part of the short-range regime. Again, our results are in good

agreement with the conjectured value for y_h and for Q we observe the linear dependence on ε . Most importantly, however, we provide strong evidence that the crossover from long-range to short-range critical behaviour occurs at $\sigma = 1.75$, i.e., at $\sigma = 2 - \eta_{SR}$. Herewith, we have resolved a long-standing disagreement between various renormalization-group scenarios for the location of this crossover.

Finally, we have also presented results for the three-dimensional case. Here, the analyses are greatly hampered by the strong corrections to scaling, but still we could show that our estimates for the universal properties are consistent with the predicted values.

References

- [1] J. Zinn-Justin, *Quantum Field Theory and Critical Phenomena*, third edition (Oxford University Press, Oxford, 1996).
- [2] E. Brézin and J. Zinn-Justin, Nucl. Phys. B 257 [FS14], 867 (1985).
- [3] M. E. Fisher, S.-k. Ma and B. G. Nickel, Phys. Rev. Lett. 29, 917 (1972).
- [4] M. E. Fisher, private communication.
- [5] M. Suzuki, Y. Yamazaki and G. Igarashi, Phys. Lett. A 42, 313 (1972).
- [6] Y. Yamazaki and M. Suzuki, Prog. Theor. Phys. 57, 1886 (1977).
- [7] J. Sak, Phys. Rev. B 8, 281 (1973).
- [8] K. G. Wilson, Phys. Rev. Lett. 28, 548 (1972).
- [9] J. Sak, Phys. Rev. B 15, 4344 (1977).
- [10] A. Aharony, *Dependence of Universal Critical Behaviour on Symmetry and Range of Interaction*, in *Phase Transitions and Critical Phenomena*, Vol. 6, edited by C. Domb and M. S. Green (Academic, London, 1976).
- [11] G. Stell, Phys. Rev. B 1, 2265 (1970).
- [12] A. Weinrib and B. I. Halperin, Phys. Rev. B 27, 413 (1983).
- [13] A. Theumann, J. Phys. A 22, 5297 (1989).
- [14] M.-c. Chang and J. Sak, Phys. Rev. B 29, 2652 (1984).
- [15] W. K. Theumann and M. A. Gusmão, Phys. Rev. B 31, 379 (1985).
- [16] A. C. D. van Enter, Phys. Rev. B 26, 1336 (1982).
- [17] Y. Yamazaki, Phys. Lett. A 61, 207 (1977).
- [18] Y. Yamazaki, in *Proceedings of the 13th IUPAP Conference on Statistical Physics (Statphys 13)*, Haifa, 1977, edited by D. Cabib, C. G. Kuper and I. Riess (Annals of the Israel Physical Society, Vol. 2).
- [19] Y. Yamazaki, Physica A 92, 446 (1978).
- [20] Y. Yamazaki, Physica A 90, 535 (1978).
- [21] Y. Yamazaki and A. Holz, Physica A 109, 568 (1981).
- [22] Y. Yamazaki, Nuovo Cimento 55A, 59 (1980).
- [23] M. A. Gusmão and W. K. Theumann, Phys. Rev. B 28, 6545 (1983).

- [24] J. C. Le Guillou and J. Zinn-Justin, *J. Phys. (Paris)* **48**, 19 (1987).
- [25] M. Aizenman and R. Fernández, *Lett. Math. Phys.* **16**, 39 (1988).
- [26] J. M. Kosterlitz, *Phys. Rev. Lett.* **37**, 1577 (1976).
- [27] J. F. Nagle and J. C. Bonner, *J. Phys. C* **3**, 352 (1970).
- [28] J. L. Monroe, R. Lucente and J. P. Hourlland, *J. Phys. A* **23**, 2555 (1990).
- [29] Z. Glumac and K. Uzelac, *J. Phys. A* **22**, 4439 (1989).
- [30] Z. Glumac and K. Uzelac, *J. Phys. A* **26**, 5267 (1993).
- [31] S. A. Cannas and A. C. N. de Magalhães, *J. Phys. A* **30**, 3345 (1997).
- [32] B. G. S. Doman, *Phys. Stat. Sol. (b)* **103**, K169 (1981).
- [33] A. S. T. Pires, *Phys. Rev. B* **53**, 5123 (1996).
- [34] R. Manieri, *Phys. Rev. A* **45**, 3580 (1992).
- [35] J. L. Monroe, *Phys. Lett. A* **171**, 427 (1992).

Chapter 6

Critical properties of the Ising model in four and five dimensions

6.1 Introduction

After the analysis of the critical behaviour of spin models with algebraically decaying interactions in the previous two chapters, we now return to Ising models with short-range interactions. In fact, these models may be considered as special cases of the systems studied before, as follows from a brief recapitulation of the results of Sec. 4.3. Indeed, d -dimensional systems with interactions decaying as $r^{-(d+\sigma)}$ have an upper critical dimension $d_u = 2\sigma$. For $d \geq d_u$ they display classical critical behaviour and for $d < d_u$ one can obtain information concerning their universal critical properties from an expansion in powers of $\varepsilon = 2\sigma - d$. All these properties hold for systems with short-range interactions if one sets $\sigma = 2$, which also restricts ε to integer values. Whereas the range of the interaction is no longer a free parameter and we again restrict ourselves to systems with a one-component order parameter, the universal critical properties still strongly depend on the dimensionality of the lattice. For the simplest case, $d = 1$, a phase transition is absent [1, § 149]. The two-dimensional Ising model on the square lattice was solved by Onsager in 1944 [2]. He found that the critical exponents strongly deviated from the classical ones. This exact solution was a major achievement and constituted a breakthrough in the study of critical phenomena. Unfortunately, the practically most relevant case, *viz.* the three-dimensional one, has until now defied any analytical solution. Thus we have to rely on numerical calculations in order to obtain information concerning the critical behaviour, see Chapter 3. Increasing the dimensionality beyond three, we reach more solid ground, though exact solutions are probably even more distant. Since the renormalization-group (RG) theory predicts an upper critical dimension $d_u = 4$, we expect classical or mean-field-like critical behaviour for $d \geq 4$. At the upper criti-

cal dimension itself, the power-law behaviour of observables is modified by multiplicative logarithmic corrections, which we already encountered in Chapter 4. Even though the form of these corrections is predicted by renormalization-group theory, none of these results is rigorous and hence an independent verification is necessary. Conversely, accurate verification of the predicted universal properties of systems at and above their upper critical dimension constitutes an important confirmation of the renormalization scenario, especially because the RG equations for $d = 4$ involve no approximation schemes (such as the ε -expansion). Thus, if this scenario is correct, the RG results should hold exactly. Furthermore, the critical behaviour of the four-dimensional Ising model is directly associated with the Gaussian fixed point, which serves as the basis of the ε -expansion. In this sense, it acts as the focal point of the modern theory of critical phenomena. Any conceivable error or incompleteness of the renormalization theory would be likely to surface near this fixed point. For this reason we assign a high priority to a precise verification of the predicted scaling behaviour of the Ising model in four dimensions. Besides, since we have studied systems with long-range interactions on either side of their upper critical dimension and also three-dimensional systems with short-range interactions, the investigation of Ising models with $d \geq 4$ emerges naturally. One might raise the objection that these high-dimensional models are not very realistic. Although their fundamental interest is an adequate justification, we may add that there exist several models with $d_u < 4$, where the various issues might be of experimental relevance. For example, the tricritical Ising model has $d_u = 3$ and the long-range models in Chapter 4 have an upper critical dimension that can take any value below four. The nature of finite-size scaling for $d > d_u$ has led to some debate in the past. It was shown by Brézin [3] that conventional finite-size scaling does not hold above four dimensions, since an additional length scale comes into play. Thereafter Botet *et al.* [4, 5] presented a phenomenological approach to scaling in mean-field-like systems, but a deeper understanding was provided by Privman and Fisher [6], who showed that the finite-size scaling hypothesis can be extended to $d > d_u$ if a so-called dangerous irrelevant variable is taken into account. The dangerous character of this irrelevant variable is responsible for the violation of hyperscaling as well, as has also been shown within the context of real-space renormalization [7].

Yet another motivation comes from the intimate connection between quantum field theory (QFT) and critical phenomena, mentioned in Chapter 1. Indeed, the former operates at $d = 4$, which makes the four-dimensional Ising model particularly relevant. The expected logarithmic corrections to the mean-field critical behaviour arise from the presence of a marginal operator, which corresponds to asymptotic (ultraviolet) freedom in nonabelian gauge theories. However, no rigorous proof exists for this so-called triviality of QFT at the upper critical dimension and additional evidence is therefore required. As logarithmic corrections constitute the hallmark of a marginal operator, their numerical observation may be viewed as

such evidence.

The actual amount of available numerical results for high-dimensional systems turns out to be limited, which can be explained from the fact that the required computing time for a given (linear) system size increases exponentially with increasing dimensionality. The majority of the research has been focused on four- and five-dimensional models, which are also the cases studied in this chapter. The main interest in the *four*-dimensional Ising model stems from its central position in the study of critical phenomena and the logarithmic factors expected in the scaling functions. Yet, in most studies until now the numerical accuracy and available system sizes were such that one could only *assume* the predicted scaling equations to be correct and check for consistency with the finite-size data. Indeed, the logarithmic factors lead to anomalously slow finite-size convergence, which makes this model difficult to analyze. Actually, the most accurate simulations until now had considerable difficulty to distinguish between different logarithmic factors. The *five*-dimensional model, on the other hand, is the first one in which $d > d_u$ and as such it is well suited to study the violation of hyperscaling [8]. Interest in this model rapidly grew when large-scale simulations were reported [9] to have yielded a fourth-order cumulant (see Sec. 3.4) in striking disagreement with the renormalization prediction [10]. As such incompatible results for this quantity, which is closely related to the renormalized coupling constant, might signal a problem with the renormalization scenario above the upper critical dimension, it is important to investigate this issue in more detail. In this chapter we present the results of large-scale simulations of both the four- and the five-dimensional Ising model, for which we have determined the critical properties with an unprecedented accuracy. An important difference to the simulations discussed in Chapter 4 is that we have also sampled energy-like quantities. In systems with long-range interactions this is—despite the new Monte Carlo algorithm—a very expensive operation, but in high-dimensional systems with short-range interactions it is still affordable. This offers the possibility of an accurate determination of the thermal exponent, because it is this exponent that determines the singular behaviour of temperature derivatives of the free energy. Whereas for the three-dimensional Ising model (Chapter 3) we only considered the energy and the specific heat, we have sampled two further quantities for the four- and five-dimensional Ising model, *viz.* two higher derivatives of the energy with respect to the temperature. Since these quantities display a more singular behaviour, one might hope for a better determination of the thermal exponent.

Let us make here some general comments with respect to the analysis of the numerical data. The finite-size scaling formulae that will be derived from RG theory serve as the basis for the least-squares fits. Clearly, an independent confirmation of the predicted parameters appearing in the scaling formulae constitutes a confirmation of the validity of the theory. However, often the total number of parameters in a formula is so large that an insufficient accuracy is obtained when all parameters are

left free. In such cases, we have fixed *some* of the parameters at their predicted values. If the fit then reproduces the theoretical values for the remaining parameters, this is still an independent verification of the theory, as there would be no reason for these remaining parameters to take their predicted values if the theory were incorrect. In all analyses, the χ^2 criterion was used to judge the quality of the fits.

The simulations required of the order of one year of (single-processor) CPU time on a Cray T3E parallel computer, but could in principle also have been obtained using a cluster of workstations. The outline of this chapter is as follows. In Sec. 6.2 we examine the renormalization-group predictions for systems with $d \geq d_u$ and rederive various results. For the purpose of illustration, we briefly discuss some finite-size properties of the specific heat of the mean-field model in Sec. 6.3. The next two sections are devoted to a detailed analysis of the numerical results for $d = 5$ and $d = 4$, respectively. In this analysis we apply the scaling functions as derived within the RG framework. Finally, the results are discussed within the context of earlier studies in Sec. 6.6.

6.2 Theory

The idea that for $d \geq 4$ the classical or mean-field exponents become exact (for short-ranged systems) predates the renormalization-group theory. Indeed, the requirement of self-consistency already indicates the breakdown of Landau theory below four dimensions, where fluctuations can no longer be neglected [11, 12]. Also the logarithmic factors appearing in the critical singularities at $d = 4$ have been calculated before the advent of the RG theory by means of the parquet method [13]. However, the seminal papers of Wilson [14, 15] provided a firm basis for the notion of the “upper critical dimension”. Even the particular scaling behaviour of four-dimensional systems was already mentioned in the second of these papers, although the consequential logarithmic factors were not pursued in detail. We first give a brief outline of the renormalization scenario. Indeed, this scenario is very closely related to that presented in Sec. 4.3, but here we will put somewhat more emphasis on the underlying ideas and refer to Chapter 4 for the actual solutions of the renormalization equations.

As before, we assume that the universal properties of the system under investigation can be described by a Landau–Ginzburg–Wilson (LGW) Hamiltonian,

$$\mathcal{H}(\phi)/k_B T = \int_V d^d x \left\{ \frac{1}{2} (\nabla \phi)^2 - h \phi + \frac{1}{2} r_0 \phi^2 + \frac{1}{4} u \phi^4 \right\}. \quad (6.1)$$

Here, the first term in the integrand represents the nearest-neighbour coupling between the spins, h denotes the magnetic field and the terms proportional to r_0 and u are used to determine the probability for the spin (represented by the continuous

field ϕ) to have a particular value [15]. Although we consider a system containing N particles placed on a lattice, we have followed the convention¹ and written an integral running over the volume V instead of a sum over the lattice sites. The renormalization of this Hamiltonian is most conveniently carried out in momentum space, so we first Fourier-transform it,

$$\begin{aligned} \mathcal{H}(\phi_{\mathbf{k}})/k_{\text{B}}T &= \frac{1}{2} \sum_{\mathbf{k}} (k^2 + r_0) \phi_{\mathbf{k}} \phi_{-\mathbf{k}} \\ &+ \frac{u}{4N} \sum_{\mathbf{k}_1} \sum_{\mathbf{k}_2} \sum_{\mathbf{k}_3} \phi_{\mathbf{k}_1} \phi_{\mathbf{k}_2} \phi_{\mathbf{k}_3} \phi_{-\mathbf{k}_1-\mathbf{k}_2-\mathbf{k}_3} - h\sqrt{N} \phi_{\mathbf{k}=0}. \end{aligned} \quad (6.2)$$

The wave vectors are discrete because we have adopted periodic boundary conditions. In addition, the original lattice structure with lattice spacing a provides a natural momentum cutoff: the wave vectors are restricted to the first Brillouin zone. The long-wavelength fluctuations (small wave vectors) are responsible for the critical singularities, but at the same time we may not neglect the fluctuations with shorter wavelengths. The RG theory takes this into account by successively integrating out the outer momentum shells. This yields an analytic contribution, whereas the remaining part of the Hamiltonian is rescaled such that it again covers the full Brillouin zone. Under successive renormalization steps the Hamiltonian will approach a so-called fixed-point Hamiltonian. In general a renormalization transformation will have several fixed points and it depends on the original Hamiltonian which of these will be approached. If the spin–spin coupling decreases at each renormalization step we will finally end up at the so-called “high-temperature” fixed point. Here the Hamiltonian corresponds to a system in which all spins are independent of each other. On the other hand, a spin–spin coupling that *increases* at each step leads to the low-temperature fixed point, where the system has a uniform magnetization. Finally, if the strength of the spin–spin coupling stays invariant under a rescaling of the Hamiltonian we approach the nontrivial fixed point. It is a fundamental hypothesis of the renormalization-group theory that this fixed point corresponds to the critical point of the spin model that we want to describe. The change of the coefficients r_0 and u in Eq. (6.2) under the renormalization transformation is expressed by the renormalization equations. For a rescaling factor $b = e^l$ these equations are, to first order in r_0 and u , given in differential form by

$$\frac{dr_0}{dl} = \gamma_1 r_0 + \alpha u, \quad (6.3a)$$

$$\frac{du}{dl} = \gamma_1 u, \quad (6.3b)$$

¹This dates back to Landau and Ginzburg and was adopted by Wilson in his original formulation of the renormalization-group theory [15].

in which $y_t = 2$ and $y_i = 4 - d$. For $d > 4$ the coefficient u of the quartic term will decrease and hence is an *irrelevant* variable, and y_i is the leading irrelevant exponent. Since r_0 is a measure for the temperature distance to the critical point, y_t is called the *thermal* exponent. This exponent is positive, indicating that the temperature is a relevant variable. Thus the Hamiltonian will only flow to the nontrivial fixed point if the temperature is precisely tuned at its critical value. The parameter α is a constant that depends on the dimensionality d . These equations coincide with Eqs. (4.4) if one sets $\sigma = 2$, except that we have completely omitted second-order terms here. Thus, upon integration they yield, to first order in u ,

$$r_0(b) = b^{y_t} [(\bar{r}_0 - \tilde{\alpha}\bar{u}) + \tilde{\alpha}\bar{u}b^{y_i - y_t}] , \quad (6.4a)$$

$$u(b) = b^{y_i}\bar{u} , \quad (6.4b)$$

where $\tilde{\alpha} = \alpha/(y_i - y_t)$, $\bar{r}_0 = r_0(b = 1)$ and $\bar{u} = u(b = 1)$. The term $(\bar{r}_0 - \tilde{\alpha}\bar{u})$ can now be identified with the reduced temperature $t \equiv (T - T_c)/T_c$ and the term proportional to $b^{y_i - y_t}$ is the so-called shift of the critical temperature with respect to the mean-field critical temperature (see, e.g., Ref. [16, Ch. 6] and Chapter 4). The rescaling of the last term on the right-hand side of Eq. (6.2) yields the magnetic exponent $y_h = 1 + d/2$. Thus, one observes that one exactly reproduces the results of Sec. 4.3 for systems with algebraically decaying interactions in the classical regime. This also holds for the mechanism of the dangerous irrelevant variable, which leads to modified renormalization exponents $y_t^* = y_t - y_i/2 = d/2$ and $y_h^* = y_h - y_i/4 = 3d/4$. These starred exponents coincide with those introduced in Eq. (4.13b) and yield the classical critical exponents $\alpha = 0$ [not to be confused with the coefficient in (6.3a)], $\beta = 1/2$, $\gamma = 1$, $\delta = 3$. The correlation length exponent $\nu = 1/y_t = 1/2$ and hence the hyperscaling relation $d\nu = 2 - \alpha$ is violated for $d > 4$. The exponent η can again be obtained from the rescaling of the pair-correlation function, from which we find $\eta = 0$. As already remarked in Chapter 4, this reveals a remarkable difference between models with short-range interactions, which have a constant η for $d \geq d_u$, and those with long-range interactions, for which η depends on σ , i.e., on the distance to the upper critical dimension.

In addition to the critical exponents, also the amplitude ratio Q takes a universal (although for $d < d_u$ geometry-dependent) value at criticality. Brézin and Zinn-Justin [10] were the first to realize that for hypercubic systems this quantity can easily be calculated at the tree level (i.e., by ignoring contributions from nonzero modes) and that for $d \geq 4$ (in short-range models) all loop corrections decay as powers of L^{-1} , so that the mean-field value is exact for all systems at and above the upper critical dimension.

The derivation of the scaling relations now proceeds along the same lines as in Sec. 4.3. Thus, for $d > 4$ we find the following scaling behaviour of the free-energy

density,

$$f\left(t, h, u, \frac{1}{L}\right) = b^{-d} \tilde{f}\left(b^{\gamma_t^*} \frac{1}{u^{1/2}} [t + \tilde{\alpha} u b^{\gamma_t - \gamma_t}], b^{\gamma_h^*} \frac{h}{u^{1/4}}, \frac{b}{L}\right). \quad (6.5)$$

As demonstrated in Chapters 3 and 4, the finite-size scaling functions for various observables are obtained by differentiating with respect to the appropriate scaling fields and setting $b = L$. For example, for the average square magnetization density we find Eq. (4.16) and the scaling behaviour of Q is given by Eq. (4.18). Similarly, for the four-dimensional Ising model we recover Eq. (4.15) for the scaling behaviour of the free-energy density,

$$\begin{aligned} f\left(t, h, u, \frac{1}{L}\right) &= b^{-d} \tilde{f}\left(\frac{b^{\gamma_t}}{(1 + \tilde{\beta} u \ln b)^{(n+2)/(n+8)-1/2}} \frac{1}{u^{1/2}} \left[t + \tilde{\alpha} b^{-\gamma_t} \frac{u}{(1 + \tilde{\beta} u \ln b)^{6/(n+8)}}\right], \right. \\ &\quad \left. b^{\gamma_h} \frac{h}{u^{1/4}} [1 + \tilde{\beta} u \ln b]^{1/4}, \frac{b}{L}\right), \end{aligned} \quad (6.6)$$

where, for the sake of generality, we consider again the $O(n)$ symmetric case and the exponents now take the values $\gamma_t = 2$ and $\gamma_h = 3$. Equation (4.17) gives the corresponding finite-size scaling function for $\langle m^2 \rangle$.

However, the scaling functions for the free-energy density also provide the key to the scaling relations in the thermodynamic limit. To this end, the rescaling factor b must be chosen such that the t dependence is removed from the first argument of \tilde{f} .² We will now derive these relations for several quantities, thereby illustrating that Eqs. (6.5) and (6.6) form a compact formulation encompassing many known results. The derivations focus on the situation in $d = 4$, since in this case logarithmic factors appear in all the observables. For $d > 4$ we only quote the resulting expressions.

The order parameter, or magnetization density, is given by the first derivative of the free-energy density with respect to the magnetic scaling field,

$$\begin{aligned} \langle m \rangle &= \frac{\partial f}{\partial h}(t, h, u, 1/L) = b^{\gamma_h - d} \left(\frac{1 + \tilde{\beta} u \ln b}{u}\right)^{1/4} \\ &\quad \times \tilde{f}^{(0,1)}\left(\frac{b^{\gamma_t}}{(1 + \tilde{\beta} u \ln b)^{(n+2)/(n+8)-1/2}} \frac{1}{u^{1/2}} \left[t + \tilde{\alpha} b^{-\gamma_t} \frac{u}{(1 + \tilde{\beta} u \ln b)^{6/(n+8)}}\right], \right. \\ &\quad \left. b^{\gamma_h} \frac{h}{u^{1/4}} [1 + \tilde{\beta} u \ln b]^{1/4}, \frac{b}{L}\right), \end{aligned} \quad (6.7)$$

²In the same way, one can also derive the h dependence of observables at $t = 0$, see Sec. 6.6.2.

where $\tilde{f}^{(k,l)}(t, h, 1/L) = \partial^{k+l} \tilde{f}(t, h, 1/L) / \partial^k t \partial^l h$. In the absence of an external magnetic field, $h = 0$ and we can omit the second argument of the scaling function. Since we are, for the moment, interested in the thermodynamic limit, the third argument vanishes and we also omit it. Then, the temperature dependence of $\langle m \rangle$ is found by choosing the scaling parameter b such that the first argument takes some constant value. This requirement yields, to leading order,

$$b = t^{-1/\gamma_t} |\ln |t||^{(n-4)/[2\gamma_t(n+8)]} = t^{-1/2} |\ln |t||^{-\zeta_n}, \quad (6.8)$$

where we have also omitted the shift of the critical temperature and introduced the exponent $\zeta_n \equiv (4 - n)/[4(n + 8)]$. Without going into further detail we note that $n = 4$ constitutes a particular case. Substituting (6.8) in Eq. (6.7) we find that close to T_c the leading temperature dependence of the order parameter is (for $t < 0$) given by

$$\langle m \rangle = (-t)^{1/2} |\ln(-t)|^{3/(n+8)} \tilde{m}(c, 0, 0). \quad (6.9)$$

Here, the universal function \tilde{m} is directly proportional to $\tilde{f}^{(0,1)}$ and c is a constant. Remark that we indeed obtain the mean-field exponent $\beta = 1/2$ and a multiplicative logarithmic correction that agrees with the result obtained by both Wegner and Riedel [17] and Brézin, Le Guillou and Zinn-Justin [18] within different renormalization schemes. Corrections to the leading scaling behaviour decaying as powers of $1/\ln |t|$ arise from, e.g., the additive term equal to unity in the prefactor of Eq. (6.7) or a multiplicative constant in the right-hand side of Eq. (6.8). Above the upper critical dimension, the logarithmic factors disappear and we simply find $\langle m \rangle \propto (-t)^{(d-\gamma_h^*)/\gamma_t^*} \propto (-t)^{1/2}$.

From the relation (4.29) between the average square magnetization density and the magnetic susceptibility we see that the latter is given by Eq. (4.17), in which all occurrences of L are replaced by b , multiplied by a volume factor. Using Eq. (6.8) we thus find

$$\chi = t^{-1} |\ln |t||^{(n+2)/(n+8)} \tilde{\chi}(c, 0, 0), \quad (6.10)$$

where $\tilde{\chi}$ is directly proportional to $\tilde{f}^{(0,2)}$. For $d > 4$ the temperature dependence is given by $\chi \propto t^{-1}$. Similarly, the specific heat is proportional to the second derivative of the free-energy density with respect to the temperature (see Sec. 3.5.2) and to leading order we find

$$\begin{aligned} C \propto \frac{\partial^2 f}{\partial t^2}(t, h, u, 1/L) &= b^{2\gamma_t - d} \frac{1}{u} (1 + \tilde{\beta} u \ln b)^{(4-n)/(n+8)} \\ &\times \tilde{f}^{(2,0)} \left(\frac{b^{\gamma_t}}{(1 + \tilde{\beta} u \ln b)^{(n+2)/(n+8) - 1/2}} \frac{1}{u^{1/2}} \left[t + \tilde{\alpha} b^{-\gamma_t} \frac{u}{(1 + \tilde{\beta} u \ln b)^{6/(n+8)}} \right], \right. \\ &\left. b^{\gamma_h} \frac{h}{u^{1/4}} [1 + \tilde{\beta} u \ln b]^{1/4}, \frac{b}{L} \right), \end{aligned} \quad (6.11)$$

yielding

$$C \propto |\ln |t||^{(4-n)/(n+8)} \quad (n \neq 4). \quad (6.12)$$

Equations (6.10) and (6.12) agree with the results obtained from diagrammatic techniques (parquet resummation) by Larkin and Khmel'nitskiĭ [13] and were obtained for the first time using the renormalization group by Wegner and Riedel [17]. For higher dimensionalities, the fluctuations not even bring about a logarithmic divergence in the specific heat, but this quantity just reaches a maximum at criticality (see also Sec. 6.3).

As mentioned above, the finite-size scaling relations can be derived in a similar fashion. Several of these relations have already been given in Chapter 4 and therefore we restrict ourselves to one final example. Kenna and Lang [19] studied the scaling of the zeroes of the partition function of the four-dimensional ϕ^4 model in the complex temperature plane, in the absence of an external magnetic field. These zeroes occur at locations $\tau \equiv |(K - K_c)/K_c|$ such that the temperature argument of the free-energy density takes a certain value and hence we find to leading order

$$\tau \propto L^{-2}(\ln L)^{-2\zeta_n}, \quad (6.13)$$

which for $n = 1$ indeed reduces to the result $\tau \propto L^{-2}(\ln L)^{-1/6}$ found in Ref. [19]. Furthermore, to leading order this expression is identical to Eq. (4.20) with $d = 4$.

6.3 The specific heat of the mean-field model

An instructive illustration of the finite-size behaviour of the specific heat above the upper critical dimension is given by the mean-field model, which can be identified with the $d \rightarrow \infty$ limit of the Ising model. The Hamiltonian for this mean-field model is given in Sec. 2.4. Equation (6.12) shows that for $d = 4$ the specific heat diverges, albeit slowly, at the critical point. In the mean-field model, however, where fluctuations are completely suppressed, C only exhibits a jump discontinuity at T_c . This is illustrated in Fig. 6.1, in which the specific heat per spin for this model is plotted as a function of the spin-spin coupling for systems containing $10^2 \leq N \leq 10^9$ particles. One observes that the maxima of the curves shift toward the critical coupling $K_c = 1$ with increasing system size. Indeed, this is the shift described by Eq. (4.19), which can be written in terms of N ,

$$\Delta t = c\sqrt{u}N^{-1/2} - \tilde{\alpha}uN^{-1}, \quad (6.14)$$

where we have also taken the limit $d \rightarrow \infty$.

The $N \rightarrow \infty$ limit of the specific heat $C(K, N)$ at criticality can now be taken in three different ways:

1. $\lim_{K \downarrow K_c} \lim_{N \rightarrow \infty} C(K, N)$.
2. $\lim_{N \rightarrow \infty} C_{\max}(N)$, where C_{\max} denotes the maximum of the specific heat for a given system size.
3. $\lim_{N \rightarrow \infty} C(K_c, N)$.

The first case yields the specific-heat maximum in the thermodynamic limit, $C/k_B = 3/2$. For the second case, it can be seen from Fig. 6.1 that the peaks of the curves sharpen up with increasing system size and reach a maximum that, for sufficiently large systems, clearly exceeds the value $3/2$. The excess peak, which has a vanishing width for $N \rightarrow \infty$, reaches a *finite* maximum of approximately $1.657 \dots$ in this limit. This overshoot could already be observed in Fig. 1 of Ref. [20], where it however received no further attention. It may be associated with the onset of critical fluctuations in finite systems. The third case, finally, corresponds to the crossing points of the finite-size curves at $K = 1$. As shown in Appendix A, the specific heat at this point can be calculated exactly as $\frac{3}{4} - 3[\Gamma(\frac{3}{4})/\Gamma(\frac{1}{4})]^2 = 0.407290 \dots$ [Eq. (A.17)]. Neither this value nor the specific-heat maximum are universal quantities, although one can easily define dimensionless ratios involving the specific heat which take a universal value at criticality, cf. Ref. [21, Ch. 28].

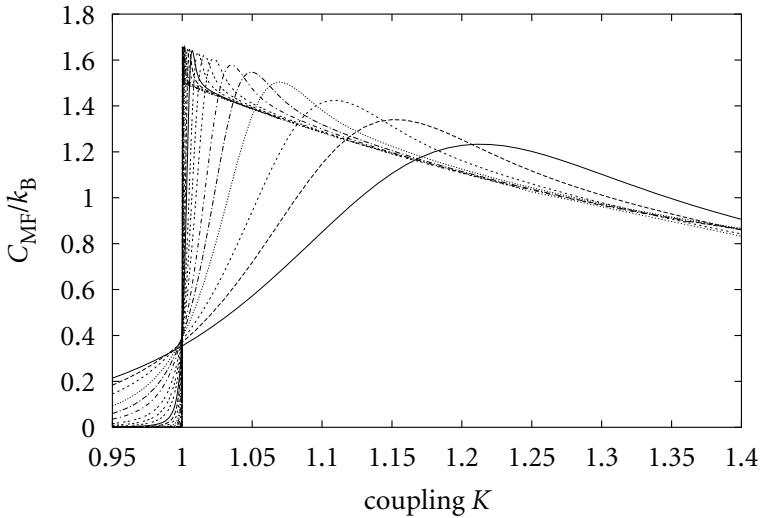


Figure 6.1: The specific heat per spin in the mean-field model for systems containing between 10^2 and 10^9 particles.

6.4 Numerical results for the case $d = 5$

6.4.1 General considerations

Before considering the four-dimensional model, we first turn our attention to the five-dimensional case, just as we approached the upper critical dimension from above in Chapter 4. For this model we have carried out quite extensive Monte Carlo simulations for hypercubic systems with linear system sizes up to $L = 22$, which corresponds to more than 5×10^6 spins. Periodic boundaries were employed. All simulations were carried out using the Wolff cluster method [22]. Practical details are collected in Table 6.1. In order to fix the definition of the nearest-neighbour coupling K_{nn} , we explicitly give the Hamiltonian describing the model under investigation,

$$\mathcal{H}/k_{\text{B}}T = -\frac{J}{k_{\text{B}}T} \sum_{\langle ij \rangle} s_i s_j = -K_{\text{nn}} \sum_{\langle ij \rangle} s_i s_j, \quad (6.15)$$

where the sum runs over all nearest-neighbour pairs on the five-dimensional lattice. Note that in the temperature derivatives that we will encounter below, both the Boltzmann constant k_{B} and the parameter J have been set to unity.

The procedure is quite similar to that in Chapter 3: we have sampled ten different quantities, from which we will determine the universal amplitude ratio Q , the critical coupling and the thermal and magnetic exponents. In Sec. 6.4.2 we will also attempt to determine the exponent in the leading correction to scaling. For conciseness, all finite-size expansions are expressed in terms of the reduced temperature t . However, in the actual least-squares analyses, this parameter was (in concordance with Chapter 3) replaced by $(K_{\text{nn}} - K_c)$. One of the main consequences is that the sign of the coefficients of the linear temperature-dependent terms has been reversed. Furthermore, it should be noted that, unless explicitly stated otherwise, all the coefficients appearing in the expansions of the scaling functions are defined *locally*, i.e., no relationship is implied between identically named coefficients in finite-size expansions for different observables.

6.4.2 The amplitude ratio Q

Our interest in the dimensionless amplitude ratio $Q = \langle m^2 \rangle^2 / \langle m^4 \rangle$ is twofold: in the first place we want to verify whether it indeed takes the predicted (universal) value in the five-dimensional Ising model and in the second place it is very well suited for accurately determining the critical coupling. The scaling behaviour for Q is given by Eq. (4.18) and the corresponding finite-size expansion by Eq. (4.23). For easy reference we repeat the latter formula here,

$$Q_L(T) = Q + p_1 \hat{t} L^{\gamma_i^*} + p_2 \hat{t}^2 L^{2\gamma_i^*} + p_3 \hat{t}^3 L^{3\gamma_i^*} + \dots$$

$$+ q_1 L^{d-2y_h^*} + \dots + q_3 L^{y_i} + \dots, \quad (6.16)$$

with $\hat{t} \equiv t + s_1 L^{y_i - y_t^*}$, where the last term is referred to as the *shift* of the critical temperature. This expansion leaves considerable freedom with respect to the number of corrections to scaling that are included in the least-squares analysis. In all analyses we have included two thermal terms, proportional to p_1 and p_2 , and the correction proportional to q_1 with fixed exponent $-d/2$. Furthermore we included the shift term in \hat{t} and at least one irrelevant contribution q_3 , with $y_i \equiv 4 - d = -1$ fixed. Finally we also included one cross term in the expansion, *viz.* $t L^{y_i^* + y_i}$. With this formula we have first tried to determine Q , y_t^* and the critical point, which we will express in $K_c = J/k_B T_c$. All data points for $L \geq 5$ were included in the analysis. As noted in Sec. 4.4.2, simultaneous determination of Q and y_t^* poses some problems due to the correlation between the two quantities. Table 6.2 summarizes our results. Analysis 1 contained both the correction term $q_3 L^{y_i}$ and the above-mentioned cross term. The result for y_t^* agrees quite well with the theoretical prediction $5/2$ and the agreement for Q is clearly excellent. In order to improve the accuracy for y_t^* we replaced the cross term by a second correction term proportional to L^{2y_i} , which yielded analysis 2. The result for the thermal exponent lies indeed closer to the expected

Table 6.1: Details of the Monte Carlo simulations of the five-dimensional Ising model. The table shows both the number of Wolff clusters per sample and the total number of samples taken for each system size.

System size	Clusters/sample	Million Samples
2	5	40
3	10	36
4	20	21
5	30	13
6	50	13
7	70	5.3
8	100	5.8
9	120	3.0
10	200	2.7
11	200	1.6
12	250	1.9
13	320	0.77
14	400	0.95
15	500	0.51
16	600	0.64
17	700	0.38
18	800	0.32
19	900	0.29
20	1000	0.26
22	1400	0.19

Table 6.2: Results of the various analyses of the amplitude ratio Q in the five-dimensional Ising model. The best fits are indicated in boldface.

Analysis	y_t^*	Q	K_c
1	2.46 (9)	0.456 (6)	0.1139149 (7)
2	2.52 (4)	0.462 (9)	0.1139160 (12)
3	2.44 (5)	0.459 (6)	0.1139157 (9)
4	2.5 (fixed)	0.454 (5)	0.1139147 (6)
5	2.5 (fixed)	0.464 (7)	0.1139161 (12)
6	2.5 (fixed)	0.455 (5)	0.1139153 (9)
7	2.5 (fixed)	0.45694658... (fixed)	0.1139150 (4)

value, but Q tends to slightly shift away from the theoretical prediction, which is due to the higher value of K_c . In the third analysis, we included both the cross term and the second correction term, which allowed us to include the data points for $L = 4$ as well. The resulting Q and y_t^* are in agreement with the theoretical predictions, but do not constitute an improvement compared to analysis 1. All three analyses yielded a least-squares fit of comparable quality. Given the fact that Q is by no means the best quantity for an accurate determination of y_t^* , we consider the current results as a sufficient justification for keeping this exponent fixed at its theoretical value. Thus, we have repeated the three analyses, for which the results are again shown in Table 6.2. Except for slightly smaller error margins, the results 4, 5 and 6 closely resemble 1, 2 and 3, respectively. The quality (in terms of the χ^2 criterion) of the analyses which included a cross term was somewhat better than of analyses 2 and 5 and hence we choose our best fit from analyses 4 and 6. Given the somewhat smaller uncertainty in K_c in analysis 4, we consider this as the best one.

Since the numerical result for the amplitude ratio Q is in good agreement with the RG prediction, we may make two more analyses. First, we can also keep Q fixed in order to obtain an accurate estimate for the critical coupling; see analysis 7. Next, we have attempted to determine the exponent of the leading correction. In practice one can only include this exponent as a free parameter if there is just one correction term present. This, in turn, requires omitting the smallest system sizes. Using $L \geq 10$ and again keeping Q fixed, we found that the leading correction has an exponent -0.56 (9), which is in quite good agreement with the exponent $y_i/2$ predicted from the shift of the critical temperature (cf. also Sec. 4.4.2). Actually, this result in itself already constitutes a confirmation of the renormalization scenario. Indeed, pure mean-field theory would have predicted a much weaker finite-size correction $\propto 1/\sqrt{N} = L^{-5/2}$ [see Eq. (A.14)]. Note that, conversely, in the $d \rightarrow \infty$ limit the corrections proportional to $L^{y_i/2}$ and $L^{d-2y_h^*}$ coincide.

6.4.3 The magnetic susceptibility

While the amplitude ratio Q allows for an accurate determination of the critical coupling and provides valuable information concerning the universality class, the magnetic susceptibility is most suitable for the determination of the magnetic exponent γ_h^* . For the analysis we have used Eq. (4.30), which included the two leading corrections and one cross term (just as for the amplitude ratio). To incorporate the latter we have replaced t by $t(1 + a_4 L^{\gamma_i})$. A possible analytic contribution was omitted, since it would have been masked by the corrections to scaling. Also the coefficient of the shift of the critical temperature was insignificant and has therefore been fixed at zero. All system sizes $L \geq 5$ have been included in the analysis. First, the magnetic exponent and the critical coupling were determined (see Table 6.3): the former is in good agreement with the theoretical prediction $15/4$ and the latter is identical to the coupling from our best fit (analysis 7) of Q . Since also the error margins are nearly the same, the estimate for γ_h^* can only slightly be improved by fixing K_c at the value obtained from Q , see again Table 6.3 (in the error margins quoted in the last column the uncertainty in K_c has been included).

Table 6.3: Results of two analyses of the magnetic susceptibility.

	Analysis 1	Analysis 2
γ_h^*	3.748 (13)	3.748 (9)
K_c	0.1139150 (5)	0.1139150 (fixed)
a_0	1.85 (17)	1.85 (12)
a_1	14.2 (11)	14.2 (9)
a_2	66 (7)	67 (6)
a_4	-0.55 (18)	-0.55 (16)
b_1	0.8 (6)	0.8 (5)
b_2	-5.3 (9)	-5.4 (8)

6.4.4 The spin–spin correlation function

In Sec. 4.3 and 4.4.3 we already noted the existence of two different decay modes for the spin–spin correlation function $g(|\mathbf{r}|)$ above the upper critical dimension. Namely, the short-distance behaviour is ruled by the exponent η which is not affected by the modification of γ_h into γ_h^* , while the large-distance behaviour is identical to that of the magnetic susceptibility, which depends on γ_h^* . For the five-dimensional Ising model this implies that at short distances $g(r) \propto r^{-(d-2+\eta)} = r^{-3}$ and at large distances $g(r) \propto r^{2\gamma_h^*-2d} = r^{-5/2}$. As we have calculated the spin–spin correlation function over half the system size (for even system sizes), we expect to observe the latter behaviour. We have analyzed our results for $L \geq 6$ using Eq. (4.32) and listed the

Table 6.4: Results of two analyses of the spin–spin correlation function over half the system size.

	Analysis 1	Analysis 2
γ_h^*	3.75 (2)	3.74 (2)
K_c	0.1139154 (5)	0.1139150 (fixed)
c_0	1.8 (3)	1.9 (3)
c_1	14 (2)	15 (2)
c_2	56 (5)	58 (4)
d_1	0.8 (4)	0.8 (4)
d_2	−5.8 (12)	−6.0 (13)

results in Table 6.4. Indeed, the exponent γ_h^* agrees with the prediction $3d/4$, corresponding to the large-distance decay mode. The critical coupling agrees with that found from either Q or χ and hence we have repeated the analysis with K_c fixed (see again Table 6.4). A cross term proportional to $L^{\gamma_i^* + \gamma_i}$ could not accurately be identified. The coefficients c_0, c_1, c_2, d_1 and d_2 agree with a_0, a_1, a_2, b_1 and b_2 (Table 6.3), respectively, as one expects from the fact that the susceptibility is the spatial integral of the correlation function. The statistical uncertainty in the results presented here, however, is considerably larger than for χ . This is due to two effects: first, we have employed only even system sizes in the current analysis and secondly, the intrinsic uncertainty in the Monte Carlo results for the correlation function is larger than in those for the susceptibility.

6.4.5 The fourth power of the magnetization density

The fourth power of the magnetization density, $\langle m^4 \rangle$, which we have sampled for the calculation of Q , can also be analyzed independently. We have applied a finite-size

Table 6.5: Results of two analyses of the fourth power of the magnetization density.

	Analysis 1	Analysis 2
γ_h^*	3.739 (11)	3.743 (10)
K_c	0.1139148 (5)	0.1139150 (fixed)
p_0	8.4 (13)	8.0 (11)
p_1	107 (14)	102 (12)
p_2	800 (140)	760 (130)
p_4	−1.3 (3)	−1.2 (2)
q_1	−2 (5)	0 (4)
q_2	−26 (8)	−28 (7)

scaling formula analogous to that for the magnetic susceptibility,

$$\langle m^4 \rangle = L^{4y_h^* - 4d} \left[p_0 + p_1 \hat{t} (1 + p_4 L^{y_i}) L^{y_t^*} + p_2 \hat{t}^2 (1 + p_4 L^{y_i})^2 L^{2y_t^*} + \dots \right. \\ \left. + q_1 L^{y_i} + q_2 L^{2y_i} + \dots \right], \quad (6.17)$$

where the cross term (with coefficient p_4) has now been written out explicitly. No relationship with the coefficients in Eq. (6.16) is implied. Using all system sizes $L \geq 5$ we found (Table 6.5) a quite accurate value for the magnetic exponent and a value for the critical coupling that closely agrees with the estimate from the amplitude ratio. Analysis 2 shows the result of the same least-squares fit with K_c fixed. The cross term in the finite-size expansion was indispensable for an acceptable fit result.

Table 6.6: Results of least-squares fits of the nearest-neighbour sum S_{nn} .

	Analysis 1	Analysis 2
y_t^*	2.504 (11)	2.499 (9)
K_c	0.113917 (2)	0.1139150 (fixed)
c_0	0.67568 (10)	0.67559 (3)
a_0	5.59 (16)	5.69 (14)
a_1	59 (3)	60 (3)
a_2	220 (20)	230 (20)
a_4	-0.41 (13)	-0.44 (13)
b_1	-1.3 (4)	-1.5 (3)

6.4.6 The energy

As mentioned in Sec. 6.1, we have sampled several energy-like quantities. We first consider the nearest-neighbour sum S_{nn} , which is directly proportional to the energy. The scaling behaviour of this quantity has been derived in Sec. 3.5.1. We have used the finite-size expansion

$$S_{nn} = c_0 + \dots \\ + L^{y_t^* - d} \left[a_0 + a_1 \hat{t} (1 + a_4 L^{y_i}) L^{y_t^*} + a_2 (1 + a_4 L^{y_i})^2 \hat{t}^2 L^{2y_t^*} \right. \\ \left. + \dots + b_1 L^{y_i} + \dots \right], \quad (6.18)$$

where the various coefficients should not be confused with those introduced for the magnetic susceptibility. In the analysis we have kept y_i fixed and included all system sizes $L \geq 5$. Table 6.6 lists the results. Just as for the three-dimensional models, the analytic background is determined very accurately. Note, however, that here we have not fixed the critical coupling in the first analysis. The resulting estimate (which has

a moderate accuracy) is in agreement with values obtained before and hence we have repeated the least-squares fit with K_c fixed. This mainly improved the accuracy in c_0 . The most important result is of course the value for γ_t^* , which has a much higher precision than in Table 6.2 and is in close agreement with the predicted value $5/2$.

6.4.7 The specific heat

We have also sampled the fluctuations in the energy, which determine the specific heat,

$$C \equiv -\frac{\partial S_{\text{nn}}}{\partial T} = K_{\text{nn}}^2 [\langle S_{\text{nn}}^2 \rangle - \langle S_{\text{nn}} \rangle^2] . \quad (6.19)$$

The corresponding finite-size expansion is (cf. Sec. 3.5.2)

$$C = p_0 + \dots + L^{2\gamma_t^* - d} \left[q_0 + q_1 \hat{t} (1 + q_4 L^{\gamma_i}) L^{\gamma_t^*} + q_2 \hat{t}^2 (1 + q_4 L^{\gamma_i})^2 L^{2\gamma_t^*} + \dots + r_1 L^{\gamma_i} + r_2 L^{2\gamma_i} + \dots \right] , \quad (6.20)$$

where the analytic contribution could not be separated from the ‘‘singular’’ part and hence has been omitted in our analyses. This is justified by the first analysis in Table 6.7 (obtained from $L \geq 5$), which shows that the specific heat conforms to the predicted scaling behaviour with a thermal exponent close to $d/2$. The critical coupling lies one standard deviation below the best estimate in Table 6.2. Indeed, if K_c is kept fixed at the latter value the thermal exponent lies even closer to the renormalization prediction, see the last column of Table 6.7. The coefficients for C can be related to those for S_{nn} , if one realizes that all expansions are formulated in terms of $(K_{\text{nn}} - K_c)$ and differentiation of (6.18) with respect to T thus entails an additional factor $\partial K_{\text{nn}} / \partial T = -K_{\text{nn}}^2$. Indeed, $a_1 K_c^2 = 0.78$ (4) (Table 6.6), in good agreement with $q_0 = 0.76$ (8) (Table 6.7), and $2a_2 K_c^2 = 6.0$ (5), to be compared with $q_1 = 6.5$ (11).

Table 6.7: Results of least-squares fits of the specific heat C .

	Analysis 1	Analysis 2
γ_t^*	2.47 (2)	2.491 (17)
K_c	0.1139142 (8)	0.1139150 (fixed)
q_0	0.87 (12)	0.76 (8)
q_1	7.7 (14)	6.5 (11)
q_2	40 (11)	31 (7)
q_4	-1.0 (4)	-0.6 (3)
r_1	-0.2 (5)	0.2 (3)
r_2	-1.7 (8)	-2.2 (6)

6.4.8 The first temperature derivative of the specific heat

In the introductory section, the sampling of higher temperature derivatives of the energy was justified by the hope for a better determination of the thermal exponent γ_t^* . Unfortunately, the advantage offered by their more singular behaviour is annulled by the lower statistical accuracy from which correlated quantities suffer. Still, it is interesting to study their scaling behaviour.

In the Monte Carlo simulations we have sampled the quantity

$$C' \equiv K_{\text{nn}}^3 [\langle S_{\text{nn}}^3 \rangle - 3\langle S_{\text{nn}}^2 \rangle \langle S_{\text{nn}} \rangle + 2\langle S_{\text{nn}}^3 \rangle] . \quad (6.21)$$

We will refer, somewhat loosely, to C' as the “first temperature derivate of the specific heat”. Strictly speaking this is incorrect, because we have only differentiated the term between square brackets in Eq. (6.19). The actual relation between C and C' is

$$C' = K_{\text{nn}}^3 \frac{\partial}{\partial K_{\text{nn}}} \left(\frac{C}{K_{\text{nn}}^2} \right) . \quad (6.22)$$

Due to the limited numerical accuracy it suffices for the finite-size scaling analysis to take into account the leading singular behaviour and the analytic contribution. From Eq. (6.20) we find

$$\begin{aligned} C' = & u_0 + \dots \\ & + L^{3\gamma_t^* - d} \left[v_0 + v_1 \hat{t} (1 + v_4 L^{\gamma_i}) L^{\gamma_i^*} + v_2 \hat{t}^2 (1 + v_4 L^{\gamma_i})^2 L^{2\gamma_i^*} \right. \\ & \left. + \dots + w_1 L^{\gamma_i} + w_2 L^{2\gamma_i} + \dots \right] , \end{aligned} \quad (6.23)$$

The background u_0 is difficult to separate from the correction to scaling $w_2 L^{2\gamma_i}$ and hence we have only included the latter in the analysis. If u_0 is included as a free parameter instead, comparable results are obtained. As usual we have made the analysis (for $L \geq 5$) with K_c either free or fixed, see Table 6.8. In both cases, good agreement with the expected scaling behaviour is found. Equation (6.22) shows that corresponding coefficients in C and C' differ by a factor K_{nn} . For the leading coefficients the agreement is quite close: $q_1 K_c = 0.74$ (13) and $2q_2 K_c = 7.1$ (16) (Table 6.7), whereas $v_0 = 0.69$ (18) and $v_1 = 7$ (2) (Table 6.8).

6.4.9 The second temperature derivative of the specific heat

By also sampling the fourth power of the energy, we have been able to calculate one more derivative, which—in analogy with C' —will be referred to as the second temperature derivative of the specific heat,

$$C'' \equiv K_{\text{nn}}^4 [\langle S_{\text{nn}}^4 \rangle - 4\langle S_{\text{nn}}^3 \rangle \langle S_{\text{nn}} \rangle - 3\langle S_{\text{nn}}^2 \rangle^2 + 12\langle S_{\text{nn}}^2 \rangle \langle S_{\text{nn}} \rangle^2 - 6\langle S_{\text{nn}} \rangle^4] . \quad (6.24)$$

Table 6.8: Results of least-squares fits of the first temperature derivative of the specific heat.

	Analysis 1	Analysis 2
y_t^*	2.50 (3)	2.49 (2)
K_c	0.1139152 (11)	0.1139150 (fixed)
ν_0	0.7 (2)	0.69 (18)
ν_1	7 (3)	7 (2)
ν_2	15 (9)	17 (7)
ν_4	-1.3 (8)	-1.4 (5)
w_1	0.4 (9)	0.3 (8)
w_2	-3.2 (13)	-3.1 (11)

Table 6.9: Results of least-squares fits of the second temperature derivative of the specific heat.

	Analysis 1	Analysis 2
y_t^*	2.491 (13)	2.491 (13)
K_c	0.113915 (2)	0.1139150 (fixed)
ν_0	0.76 (19)	0.76 (19)
ν_1	7.4 (15)	7.3 (9)
ν_2	-80 (50)	-80 (50)
ν_4	-0.7 (16)	-0.7 (17)
s_1	-0.09 (6)	-0.09 (7)
w_1	-1.7 (3)	-1.7 (3)

Actually this quantity is proportional to the derivative of the term between square brackets in Eq. (6.21),

$$C'' = K_{nn}^4 \frac{\partial}{\partial K_{nn}} \left(\frac{C'}{K_{nn}^3} \right) = K_{nn}^4 \frac{\partial^2}{\partial K_{nn}^2} \left(\frac{C}{K_{nn}^2} \right). \quad (6.25)$$

Evidently, the statistical accuracy decreases quite dramatically when such involved correlations are sampled. Compared to the magnetic susceptibility, the relative uncertainties have increased by approximately one order of magnitude, which imposes a serious limitation on the quality of the least-squares analysis. We have made two fits for $L \geq 5$, using a scaling formula of the same form as Eq. (6.23), but a leading scaling behaviour proportional to $L^{4y_t^* - d}$. The results are shown in Table 6.9. In view of the uncertainties in the coefficients and in K_c , the result for the thermal exponent is rather precise, which can be attributed to the strong divergence of this observable. The shift term in \hat{t} could indeed be observed in this quantity, but its amplitude s_1 is difficult to determine. The fixation of K_c does hardly influence the estimates for the various parameters. Comparing the coefficient of the linear temperature depen-

dence in C' with the leading coefficient in C'' , we find from Table 6.8 $\nu_1 K_c = 0.8$ (2), in agreement with $\nu_0 = 0.76$ (19) in Table 6.9.

6.4.10 The temperature derivative of the magnetic susceptibility

As in Chapter 3, we have sampled the correlation between $\langle m^2 \rangle$ and S_{nn} , which gives us the temperature derivative of the magnetic susceptibility [see Eq. (3.30)]. The analysis of this quantity yields estimates for $2\gamma_h^* + \gamma_t^*$, as follows from the scaling formula,

$$\begin{aligned} \frac{\partial \chi}{\partial K_{nn}} &= L^{2\gamma_h^* + \gamma_t^* - d} \\ &\times \left[a_0 + a_1 \hat{t} (1 + a_4 L^{\gamma_i}) L^{\gamma_t^*} + a_2 \hat{t}^2 (1 + a_4 L^{\gamma_i})^2 L^{2\gamma_t^*} \right. \\ &\quad \left. + \dots + b_1 L^{\gamma_i} + b_2 L^{2\gamma_i} + \dots \right]. \end{aligned} \quad (6.26)$$

Due to the strong divergence of the leading power of L , a possible analytic contribution could not be distinguished in the analysis. Table 6.10 lists the results of the least-squares fits, in which all system sizes $L \geq 4$ could be included. The estimate for γ_t^* is calculated under the assumption that γ_h^* takes its theoretical value $15/4$. Comparing the coefficients in (6.26) with those in the expansion for χ , we find from Table 6.3 $a'_1 = 14.2$ (9) and $2a'_2 = 134$ (12) (where primes have been appended for distinction). Taking into account the error margins, the agreement between a'_1 and a_0 is quite reasonable and between $2a'_2$ and a_1 it is even very good.

Table 6.10: Results of least-squares fits of the temperature derivative of the magnetic susceptibility.

	Analysis 1	Analysis 2
γ_t^*	2.51 (3)	2.51 (2)
K_c	0.1139151 (4)	0.1139150 (fixed)
a_0	12.3 (13)	12.5 (13)
a_1	130 (25)	130 (25)
a_2	580 (180)	600 (170)
a_4	-0.9 (4)	-0.9 (4)
b_1	11 (5)	10 (6)
b_2	-63 (5)	-62 (6)

6.4.11 The temperature derivative of Q

The last quantity we have studied in our simulations of the five-dimensional Ising model is the temperature derivative of the fourth-order amplitude ratio. As demonstrated in Sec. 3.5.6, this derivative can be calculated from correlations between the energy and the magnetization distribution. By differentiating Eq. (6.16) and dividing out a factor Q [see Eq. (3.32)] we arrive at the finite-size scaling formula [cf. also Eq. (3.33)],

$$\frac{1}{Q} \frac{\partial Q}{\partial K_{\text{nn}}} = L^{y_t^*} \left[a_0 + a_1 \hat{t} L^{y_t^*} + a_2 \hat{t}^2 L^{2y_t^*} + \dots \right. \\ \left. + b_1 L^{d-2y_h^*-y_t^*} + \dots + d_1 L^{y_i} + d_2 L^{2y_i} + \dots \right]. \quad (6.27)$$

The correction proportional to b_1 is very weak (it decays as L^{-5}) and has been omitted in the fit (which used $L \geq 5$). In contrast to the situation in $d = 3$, the resulting thermal exponent is not very precise, but it agrees with the theoretical prediction. The coefficients a_0 and a_1 (Table 6.11) agree quite well with the corresponding coefficients in Eq. (6.16) divided by Q . For example, for analysis 4 in Table 6.2, $p_1 = 1.02$ (6) and $2p_2 = 8.6$ (7), yielding $a_0 = 2.23$ (13) and $a_1 = 18.8$ (16), respectively.

Table 6.11: Results of least-squares fits of the temperature derivative of the amplitude ratio Q .

	Analysis 1	Analysis 2
y_t^*	2.55 (8)	2.50 (5)
K_c	0.1139160 (13)	0.1139150 (fixed)
a_0	1.9 (6)	2.3 (5)
a_1	11 (6)	15 (5)
a_2	-7 (8)	-11 (8)
d_1	3 (2)	2.3 (18)
d_2	-8 (3)	-7 (3)

6.5 Numerical results for the case $d = 4$

6.5.1 General considerations

We now proceed with the Ising model at its upper critical dimension. We have simulated hypercubic systems with periodic boundaries containing up to 48^4 spins, which amounts to roughly the same number of spins as for our largest system in five dimensions. Also the further aspects of the simulations closely resemble those

of the previous section: we have applied the Wolff cluster algorithm (details are given in Table 6.12) and invested approximately the same amount of computing time. The Hamiltonian is given by Eq. (6.15), which now of course applies to a four-dimensional lattice. Again, a considerable number of quantities has been sampled. According to the renormalization scenario, the singular behaviour of each of these quantities exhibits its own specific multiplicative logarithm correction. Thus, an independent determination of these corrections would constitute an important test of the renormalization predictions. However, since these logarithmic factors vary extremely slowly, their numerical determination poses considerable problems. For example, the correction factor in the energy varies as $(\ln L)^{(1/6)}$ [see Eq. (6.31) below]. Therefore, only very few numerical tests have been carried out until now, for a limited number of observables. It is the purpose of this section to present an exhaustive analysis of the scaling behaviour of various observables in the four-dimensional Ising model. In particular we aim for an independent assessment of the logarithmic correction factors. This is possible thanks to the (relatively) large range of system sizes we have studied *and* the large statistical accuracy of our results. For convenience, we define ζ_t and ζ_h as the exponents appearing in the logarithmic factors in the thermal and magnetic argument, respectively, of the free-energy density \tilde{f} [Eq. (6.6)], for $n = 1$. Thus, the theoretical predictions for these exponents are $\zeta_t = 1/6$ and $\zeta_h = 1/4$. In the analysis of systems with long-range interactions at their upper critical dimension (Chapter 4), these exponents have been held fixed at their theoretical values.

The practical aspects of the analysis, such as the replacement of t by $(K_{nn} - K_c)$, are identical to those mentioned in Sec. 6.4.1.

6.5.2 The amplitude ratio Q

The finite-size scaling behaviour of the dimensionless amplitude ratio Q at the upper critical dimension is described by a universal function \tilde{Q} , as has already been discussed in Chapter 4,

$$Q_L(T) = \tilde{Q} \left(L^{\zeta_t} \left[1 + \tilde{\beta} u \ln L \right]^{\zeta_t} \frac{t}{u^{1/2}} \right) + q_1 L^{d-2\zeta_h} + \dots, \quad (6.28)$$

where for brevity we have omitted here the shift of the critical temperature, which exhibits a logarithmic factor as well. Just like this shift yields a correction decaying as the square root of the correction L^{ζ_t} for systems above the upper critical dimension, it leads to a correction term proportional to $1/\sqrt{\ln L}$ at $d = d_u$. This correction decays very slowly as a function of L , but due to its small coefficient (within one standard deviation from zero for most observables) it is generally not the dominant correction to scaling. For a system with a scalar order parameter, the full finite-size expansion of Eq. (6.28) is given by Eq. (4.24). We have fitted this formula to our

Table 6.12: Details of the Monte Carlo simulations of the four-dimensional Ising model. The table shows both the number of Wolff clusters per sample and the total number of samples taken for each system size.

System size	Clusters/sample	Million Samples
2	4	41
3	6	33
4	8	20
5	10	16
6	16	10
7	20	8.2
8	25	6.7
9	30	5.3
10	40	4.2
11	50	3.3
12	60	3.0
13	70	2.5
14	80	2.1
15	80	2.0
16	100	1.7
17	100	1.6
18	120	1.3
19	125	1.3
20	140	1.1
21	150	1.1
22	160	0.86
23	180	0.88
24	180	0.88
26	200	0.87
28	240	0.72
30	280	0.56
32	320	0.48
34	360	0.38
36	400	0.40
38	500	0.32
40	600	0.26
44	600	0.26
48	750	0.22

data, in which we included all data points for $4 \leq L \leq 48$. The exponent ζ_t in the temperature-dependent term was kept fixed, as was the thermal exponent γ_t . Furthermore we included the corrections $q_3/\ln L$ and $q_4/(\ln L)^2$ and the term proportional to q_1 . The results are shown in Table 6.13. The estimate for Q has a remarkably small error margin and agrees well with the renormalization prediction. Thus it constitutes a precise confirmation of the calculation by Brézin and Zinn-Justin [10]. Also the accuracy of the critical temperature is encouraging. Fixing Q at its theoretical value (analysis 2) did not yield a further improvement of the results.

Table 6.13: Results of the analysis of the amplitude ratio Q in the four-dimensional Ising model.

	Analysis 1	Analysis 2
Q	0.454 (2)	0.45694658... (fixed)
K_c	0.1496928 (3)	0.1496927 (3)
p_1	0.999 (9)	0.999 (9)
p_2	2.4 (4)	2.4 (4)
q_1	0.56 (16)	0.34 (9)
q_3	0.267 (18)	0.239 (6)
q_4	-0.26 (4)	-0.20 (2)

6.5.3 The magnetic susceptibility

Unlike the amplitude ratio Q , the magnetic susceptibility exhibits a multiplicative logarithmic correction in the prefactor of the scaling function. It arises from the differentiation of the free energy with respect to the magnetic scaling field, which in turn has picked up a power of the marginal variable, see Eq. (4.17). We have analyzed our data (again for $L \geq 4$) using Eq. (4.31), in which we included two temperature-dependent terms and both a linear and a quadratic term in $1/\ln L$. For reference we repeat the formula here, without the shift of the critical temperature,

$$\chi = L^{2\gamma_h-d} (\ln L)^{2\zeta_h} \times \left[a_0 + a_1 t L^{\gamma_t} (\ln L)^{\zeta_t} + a_2 t^2 L^{2\gamma_t} (\ln L)^{2\zeta_t} + \dots + \frac{b_1}{\ln L} + \frac{b_2}{(\ln L)^2} + \dots \right]. \quad (6.29)$$

Table 6.14 summarizes the results of our analyses. First, we have determined γ_h and K_c , while keeping $\zeta_h = 1/4$, $\gamma_t = 2$ and $\zeta_t = 1/6$. The resulting estimate for the magnetic exponent lies somewhat above the theoretical value $\gamma_h = 3$, but the difference is not disturbing and can probably be traced back to an (unavoidable) arbitrariness in the scaling formula. The critical coupling is also somewhat higher than

Table 6.14: Results of three analyses of the magnetic susceptibility.

	Analysis 1	Analysis 2	Analysis 3
γ_h	3.009 (4)	3 (fixed)	3 (fixed)
γ_t	2 (fixed)	1.93 (4)	2 (fixed)
ζ_h	1/4 (fixed)	0.31 (4)	0.260 (14)
K_c	0.1496937 (3)	0.1496935 (3)	0.1496930 (1)
a_0	1.30 (7)	1.1 (2)	1.39 (9)
a_1	8.0 (3)	9.4 (2)	8.6 (2)
a_2	25.3 (8)	33 (3)	28.3 (18)
b_1	1.18 (11)	1.6 (4)	1.10 (15)
b_2	-1.09 (11)	-0.98 (11)	-0.82 (6)

that obtained from the analysis of Q . Next (analysis 2), we kept γ_h fixed and allowed ζ_h to vary instead. We also included γ_t as a free parameter. While the resulting K_c lies close to the first estimate, γ_t has a clear tendency to drop below 2. This change is reflected in the variation of a_1 , which differs considerably from its earlier value. Only the analysis of an observable with γ_t in its leading singular behaviour will yield a thermal exponent that is sufficiently accurate to observe any deviations from the theoretical prediction. The uncertainty in ζ_h is rather large and hence any conclusions appear premature. Thus, we have made a third analysis in which we kept γ_t fixed as well. Apart from an accurate estimate for K_c (in agreement with the result from Q), this yielded a very precise value for ζ_h , in close agreement with the theoretically predicted value. Since the error margin for K_c is already smaller than in the analysis of Q , fixing K_c cannot further improve the precision for ζ_h .

Approaching this case from a different angle, we have also analyzed the susceptibility under the assumption that the four-dimensional Ising model exhibits purely classical behaviour, without any multiplicative logarithmic corrections. This turned out to wreak havoc: apart from a much too high χ^2 in the least-squares fit, it also yielded a magnetic exponent that differed by many standard deviations from the classical value. This is another strong indication for the presence of such corrections.

6.5.4 The spin–spin correlation function

The analysis of the spin–spin correlation function has proceeded along the same lines as that of the magnetic susceptibility. Whilst the two different decay modes as they were discerned *above* the upper critical dimension (cf. Sec. 6.4.4) now have the same power-law behaviour (since γ_h and γ_h^* coincide), the large-distance behaviour exhibits a logarithmic factor that is absent in the short-distance behaviour. Again, we have calculated the spin–spin correlation function over half the system size and we thus have used Eq. (6.29) multiplied by a factor L^{-d} . The results from an analysis

for $L \geq 4$, collected in Table 6.15, closely resemble those for the susceptibility. Including y_t as a free parameter gives rather inaccurate results, but for fixed y_h and y_t an estimate for ζ_h is obtained that lies close to $1/4$.

Table 6.15: Results of three analyses of the spin–spin correlation function over half the system size.

	Analysis 1	Analysis 2	Analysis 3
y_h	3.008 (7)	3 (fixed)	3 (fixed)
y_t	2 (fixed)	1.94 (4)	2 (fixed)
ζ_h	$1/4$ (fixed)	0.29 (5)	0.229 (18)
K_c	0.1496931 (4)	0.1496931 (3)	0.1496925 (2)
a_0	1.19 (12)	1.1 (3)	1.44 (12)
a_1	8.0 (5)	9.7 (2)	9.1 (3)
a_2	26.6 (10)	34 (4)	31 (2)
b_1	0.9 (2)	1.2 (4)	0.6 (2)
b_2	-1.3 (2)	-1.1 (2)	-0.83 (10)

6.5.5 The fourth power of the magnetization density

A promising approach to a precise determination of ζ_h is the study of the fourth power of the magnetization density. Namely, the free energy has to be differentiated four times with respect to the magnetic scaling field in order to obtain the scaling function, which thus exhibits an accordingly high power of $\ln L$ in the prefactor:

$$\begin{aligned}
 \langle m^4 \rangle &= L^{4y_h-d} (\ln L)^{4\zeta_h} \\
 &\times \left[p_0 + p_1 t L^{y_t} (\ln L)^{\zeta_t} + p_2 t^2 L^{2y_t} (\ln L)^{2\zeta_t} \right. \\
 &\quad \left. + \dots + \frac{q_1}{\ln L} + \frac{q_2}{(\ln L)^2} + \dots \right]. \tag{6.30}
 \end{aligned}$$

We have carried out three different analyses (for $L \geq 4$). The first one was aimed at a precise determination of the magnetic exponent y_h . Hence, both ζ_h and y_t were kept fixed at their theoretical values. Table 6.16 illustrates the excellent agreement with the renormalization prediction. In the second analysis we have therefore kept $y_h = 3$ and allowed ζ_h to vary. Also the thermal exponent in the temperature-dependent terms was included as a free variable. This yielded not only a value for ζ_h with an accuracy comparable to the best estimate in Table 6.14, but also a value for y_t that does not suffer from the deviations observed in the analyses of the previous two quantities. Thus, we made a third analysis in which both the magnetic and the thermal

Table 6.16: Results of three analyses of the fourth power of the magnetization density.

	Analysis 1	Analysis 2	Analysis 3
γ_h	3.0023 (15)	3 (fixed)	3 (fixed)
γ_t	2 (fixed)	1.99 (3)	2 (fixed)
ζ_h	1/4 (fixed)	0.261 (18)	0.254 (4)
K_c	0.1496933 (2)	0.1496932 (2)	0.1496931 (1)
p_0	4.37 (18)	4.2 (8)	4.45 (17)
p_1	46.7 (6)	47.3 (10)	47.0 (6)
p_2	200 (5)	208 (19)	201 (4)
q_1	4.7 (3)	5.0 (12)	4.6 (3)
q_2	-4.08 (19)	-4.1 (4)	-3.94 (13)

exponent were held at their theoretical values. The result for ζ_h , one standard deviation above the theoretical value, definitely is the best estimate obtained so far, with an uncertainty of approximately 1.5%.

6.5.6 The energy

The nearest-neighbour sum S_{nn} , directly proportional to the energy, is very well suited for determination of both γ_t and ζ_t . Analogous to Eq. (6.18) we obtain the following scaling formula,

$$S_{nn} = c_0 + \dots + L^{\gamma_t - d} (\ln L)^{\zeta_t} \times \left[a_0 + a_1 t L^{\gamma_t} (\ln L)^{\zeta_t} + a_2 t^2 L^{2\gamma_t} (\ln L)^{2\zeta_t} + \dots + \frac{b_1}{\ln L} + \dots \right], \quad (6.31)$$

where a possible temperature dependence of the irrelevant field (cf. Sec. 3.5.1) is indistinguishable from the $1/\ln L$ corrections. Because a simultaneous determination of γ_t and ζ_t yields inaccurate results, we have made two separate analyses, in which either of them was kept fixed. As can be seen in Table 6.17, the thermal exponent could be confirmed with an accuracy that lies on the promille level, whereas even for the very weakly varying power of $\ln L$ the error lies below the 10% level. Thus, the deviations in γ_t as found in the (much less accurate) analyses of χ and $g(L/2)$ are not confirmed by the current analysis. However, a remarkable point concerning this analysis is the too low estimate for the critical coupling, which lies two standard deviations below the previously obtained values. Since the uncertainty in the coupling is an order of magnitude larger than in the earlier values (similar to our experiences for $d = 5$), the importance of this discrepancy is limited. Such a deviation can usually be traced back to the neglect of a correction to scaling, although we have not been able to do so in the present case.

Table 6.17: Results of least-squares fits for $L \geq 4$ of the nearest-neighbour sum S_{nn} .

	Analysis 1	Analysis 2
γ_t	2.002 (4)	2 (fixed)
ζ_t	1/6 (fixed)	0.175 (14)
K_c	0.149687 (3)	0.149686 (3)
c_0	0.77005 (19)	0.77002 (17)
a_0	3.67 (5)	3.65 (8)
a_1	34.2 (7)	34.6 (5)
a_2	112 (15)	98 (11)
b_1	0.09 (4)	0.12 (8)

6.5.7 The specific heat

In order to increase the accuracy of our estimate of the exponent ζ_t we have also sampled quantities which are higher derivatives of the free-energy density with respect to the temperature and hence exhibit a prefactor that is a higher power of $\ln L$. Unfortunately, the possible improvement in the accuracy of ζ_t is to a large extent cancelled by the larger statistical uncertainty in these quantities, cf. Sec. 6.4.8. Nevertheless, we will attempt to determine their scaling behaviour. The first of these observables is the specific heat, which follows from the fluctuations in the nearest-neighbour sum S_{nn} . A detailed derivation of the finite-size scaling function of the specific heat is given in Sec. 3.5.2. Clearly, in the four-dimensional analog of Eq. (3.20) logarithms abound and tend to mutually interfere. Thus, it is difficult to include many different corrections to scaling. For the analysis we have applied the following finite-size expansion

$$\begin{aligned}
 C = p_0 + \dots \\
 + L^{2\gamma_t-d} (\ln L)^{2\zeta_t} \left[q_0 + q_1 t L^{\gamma_t} (\ln L)^{\zeta_t} + q_2 t^2 L^{2\gamma_t} (\ln L)^{2\zeta_t} + \dots \right. \\
 \left. + \frac{r_1}{\ln L} + \frac{r_2}{(\ln L)^2} + \dots \right]. \quad (6.32)
 \end{aligned}$$

The analytic background p_0 cannot be resolved clearly from the leading additive logarithmic correction $r_1/\ln L$, which leads to an overall contribution decaying as $1/(\ln L)^{2/3}$. Thus we have omitted p_0 in the first two analyses. Just as for the energy, we have kept ζ_t fixed in the first analysis (Table 6.18). This yielded an accurate confirmation of the theoretical value of the thermal exponent and hence we see that, apart from the logarithmic factor, the L dependence of the prefactor of the singular part in Eq. (6.32) indeed vanishes. The exponent of the logarithmic factor could be determined rather precisely in the second analysis and agrees well with the predicted value. Finally we have made a least-squares fit in which we omitted the slowly varying term $r_1/\ln L$ and included the constant contribution p_0 instead. Table 6.18

Table 6.18: Results of least-squares fits for $L \geq 4$ of the specific heat.

	Analysis 1	Analysis 2	Analysis 3
y_t	2.002 (4)	2 (fixed)	2.002 (5)
ζ_t	1/6 (fixed)	0.16 (2)	1/6 (fixed)
K_c	0.1496930 (4)	0.1496927 (3)	0.1496926 (3)
p_0	0.0 (fixed)	0.0 (fixed)	0.28 (9)
q_0	0.75 (4)	0.80 (7)	0.63 (8)
q_1	3.76 (11)	3.88 (12)	3.78 (14)
q_2	10.2 (12)	10.4 (12)	10.2 (13)
r_1	0.25 (7)	0.16 (13)	0.0 (fixed)
r_2	-0.41 (4)	-0.36 (6)	-0.31 (2)

shows that the results are in good agreement with that of the first analysis and that the coefficient p_0 has taken over the rôle of r_1 . This merely illustrates the difficulty of separating the various corrections to the leading scaling behaviour. The results for the critical coupling agree well with the estimates from Q , χ and $g(L/2)$, which corroborates that the results for the energy (Table 6.17) are an exception. Also the coefficient q_0 is in accordance with a_1 from Table 6.17: for the first analysis we have $a_1 K_c^2 = 0.766$ (16) and $q_0 = 0.75$ (4).

6.5.8 The first temperature derivative of the specific heat

The next derivative of the energy that we have sampled is C' , the so-called first temperature derivative of the specific heat (see Sec. 6.4.8). The previous remarks concerning interfering logarithmic corrections apply here *a fortiori*. The finite-size expansion that has served as the starting point for our analysis reads

$$\begin{aligned}
 C' = & u_0 + \dots \\
 & + L^{3y_t-d} (\ln L)^{3\zeta_t} \left[v_0 + v_1 \hat{t} L^{y_t} (\ln L)^{\zeta_t} + v_2 \hat{t}^2 L^{2y_t} (\ln L)^{2\zeta_t} + \dots \right. \\
 & \left. + \frac{w_1}{\ln L} + \frac{w_2}{(\ln L)^2} + \dots \right], \tag{6.33}
 \end{aligned}$$

where $\hat{t} \equiv t + s_1/(\ln L)^{2/3}$. In contrast with the previously analyzed observables for this model, the shift s_1 of the critical temperature, which leads to an additional finite-size correction decaying as $1/\sqrt{\ln L}$ (see Sec. 6.5.2), could be observed rather clearly. Omitting this shift in the analysis of C' led to a somewhat high χ^2 in the least-squares analysis and to a critical temperature that differed markedly from the previous estimates. Furthermore, we also expect less singular contributions differing from the leading one by factors $L^{y_t} (\ln L)^{\zeta_t}$, cf. Eq. (3.20). The first of these terms, with coefficient u_1 , has been included in the analysis. This yielded a slightly better

fit than with the (very similar) term u_0 . Table 6.19 shows the results of two analyses for $L \geq 6$.

Table 6.19: Results of two least-squares analyses of the first temperature derivative of the specific heat.

	Analysis 1	Analysis 2
y_t	2.00 (2)	2 (fixed)
ζ_t	1/6 (fixed)	0.17 (3)
K_c	0.1496928 (7)	0.1496927 (7)
ν_0	0.2 (3)	0.2 (2)
ν_1	5.3 (18)	5.6 (12)
ν_2	-13 (16)	-16 (12)
s_1	-0.16 (13)	-0.13 (7)
u_1	-2.64 (12)	-2.63 (14)

6.5.9 The second temperature derivative of the specific heat

As already remarked in Sec. 6.4.9, the limited statistical accuracy of the second temperature derivative of the specific heat, C'' , makes the analysis rather problematic. Indeed, for the four-dimensional case it proved to be difficult to obtain sensible results from the least-squares fit. The expected scaling behaviour of this quantity is

$$\begin{aligned}
 C'' = & u_0 + \dots \\
 & + L^{4y_t-d} (\ln L)^{4\zeta_t} \left[\nu_0 + \nu_1 \hat{t} L^{y_t} (\ln L)^{\zeta_t} + \nu_2 \hat{t}^2 L^{2y_t} (\ln L)^{2\zeta_t} + \dots \right. \\
 & \left. + \frac{w_1}{\ln L} + \frac{w_2}{(\ln L)^2} + \dots \right]. \quad (6.34)
 \end{aligned}$$

The analytic contribution is very weak compared to the singular part and has therefore been omitted. The quality of the fit (in terms of the χ^2 criterion) was not very sensitive to the particular choice of the various logarithmic corrections that were included. However, the resulting estimate of the critical coupling rather strongly depended on the inclusion of a shift term $s_1/(\ln L)^{2/3}$. Indeed, the agreement of K_c with the values obtained from other quantities turned out to be a reasonably good indication for the quality of the analysis. Thus, we included the shift term and the correction proportional to $1/(\ln L)^2$. The correction $w_1/\ln L$ had to be omitted to allow for a determination of s_1 . Table 6.20 lists the results for analyses that included system sizes $L \geq 6$. The agreement with the theoretical predictions is satisfactory.

Table 6.20: Results of two least-squares analyses of the second temperature derivative of the specific heat.

	Analysis 1	Analysis 2
γ_t	1.995 (8)	2 (fixed)
ζ_t	1/6 (fixed)	0.16 (3)
K_c	0.149693 (4)	0.149693 (3)
ν_0	0.1 (3)	0.1 (3)
ν_1	8 (2)	8 (2)
ν_2	-44 (13)	-42 (12)
s_1	-0.16 (6)	-0.17 (6)
w_2	-0.48 (16)	-0.45 (19)

6.5.10 The temperature derivative of the magnetic susceptibility

A temperature derivative which allowed for a less cumbersome analysis is that of the magnetic susceptibility. Its scaling formula is given by

$$\begin{aligned} \frac{\partial \chi}{\partial K_{\text{nn}}} &= L^{2\gamma_h + \gamma_t - d} (\ln L)^{2\zeta_h + \zeta_t} \\ &\times \left[a_0 + a_1 t L^{\gamma_t} (\ln L)^{\zeta_t} + a_2 t^2 L^{2\gamma_t} (\ln L)^{2\zeta_t} \right. \\ &\quad \left. + \dots + \frac{b_1}{\ln L} + \frac{b_2}{(\ln L)^2} + \dots \right]. \end{aligned} \quad (6.35)$$

Table 6.21 lists the results of two analyses for $L \geq 4$. In the first one, the power of $\ln L$ in the prefactor was kept fixed. This yields an estimate for $2\gamma_h + \gamma_t$. The value for γ_t in the table is calculated under the assumption that $\gamma_h = 3$. In the second fit, both the magnetic and the thermal exponent were held fixed, yielding $2\zeta_h + \zeta_t$ in agreement with the expected scaling behaviour.

6.5.11 The temperature derivative of Q

Finally, we consider the temperature derivative of the amplitude ratio Q . Like for the temperature derivative of the specific heat, inclusion of the finite-size correction due to the shift of the critical temperature proved very beneficial for the quality of the analysis. The following finite-size expansion was applied,

$$\begin{aligned} \frac{1}{Q} \frac{\partial Q}{\partial K_{\text{nn}}} &= L^{\gamma_t} (\ln L)^{\zeta_t} \\ &\times \left[a_0 + a_1 \hat{t} L^{\gamma_t} (\ln L)^{\zeta_t} + a_2 \hat{t}^2 L^{2\gamma_t} (\ln L)^{2\zeta_t} + \dots + \frac{b_1}{\ln L} + \dots \right]. \end{aligned} \quad (6.36)$$

Table 6.21: Results of two least-squares analyses of the temperature derivative of the magnetic susceptibility.

	Analysis 1	Analysis 2
γ_t	2.004 (10)	2 (fixed)
$2\zeta_h + \zeta_t$	2/3 (fixed)	0.68 (9)
K_c	0.1496934 (3)	0.1496934 (3)
a_0	6.4 (4)	6.4 (15)
a_1	55 (4)	54 (7)
a_2	140 (17)	135 (26)
b_1	9.7 (7)	9.5 (15)
b_2	-6.8 (6)	-6.9 (15)

Table 6.22: Results of two least-squares analyses of the temperature derivative of the amplitude ratio Q .

	Analysis 1	Analysis 2
γ_t	1.998 (7)	2 (fixed)
ζ_t	1/6 (fixed)	0.151 (19)
K_c	0.1496925 (6)	0.1496926 (7)
a_0	0.94 (19)	0.99 (17)
a_1	9.9 (6)	9.7 (6)
a_2	-19 (2)	-19 (2)
s_1	-0.24 (4)	-0.24 (3)

The results in Table 6.22 show that both γ_t and ζ_t have been determined quite accurately and are in good agreement with the renormalization predictions.

6.6 Discussion and conclusions

6.6.1 The five-dimensional Ising model

First, we summarize our best estimates for some universal critical properties of the five-dimensional Ising model: $Q = 0.454$ (5), $\gamma_t^* = 2.499$ (9) and $\gamma_h^* = 3.748$ (9), in excellent agreement with the renormalization predictions $Q = 8\pi^2/\Gamma^4(\frac{1}{4}) = 0.4594658\dots$, $\gamma_t^* = 5/2$ and $\gamma_h^* = 15/4$. Our best value for the critical coupling is $K_c = 0.113950$ (4). In this section we compare these results to those from earlier studies. Whereas quite some estimates for the critical coupling exist, only few papers are concerned with the remaining critical properties. In Ref. [23], only the order parameter for system size $L = 6$ has been studied in a small temperature range below T_c . Reference [24] constitutes the first extensive study, but since its numerical content has largely been superseded by Ref. [9] we will consider the latter in-

stead. Also Ref. [25] contains several finite-size scaling results for this model; series-expansion results for critical exponents are given in Refs. [26, 27].

The most accurate estimate in Ref. [9] for the dimensionless amplitude ratio is $Q = 0.489$ (6), which differs more than five standard deviations from the renormalization prediction. This rather disturbing discrepancy led to various new studies. Mon [28] has argued that neglected finite-size effects might be the cause of the deviation. In Ref. [25] only finite-size data for Q are given, because the statistical accuracy of the numerical results was insufficient for an extrapolation to the $L \rightarrow \infty$ limit. Whereas the results of Chapter 4 confirmed the renormalization scenario above the upper critical dimension with a considerable accuracy, one might object that these results were obtained within a different class of models. Hence, the result obtained in this chapter is the first confirmation of the renormalization prediction for Q in the five-dimensional Ising model itself. Our data have much smaller statistical errors than in Ref. [9] and span a larger range of system sizes. Still, the error margin in our estimate of Q is of the same order as in Ref. [9], which reflects the fact that we have taken into account more corrections to scaling. Indeed, the earlier found discrepancy may well be explained from the neglect of the correction to scaling proportional to L^{ν_i} in Eq. (6.16).

In order to gain some additional insight in the nature of the finite-size corrections affecting Q , we have studied $Q(K_c, L)$ as a function of the system size. Most of the data were taken at $K = 0.1139100$, slightly below our best estimate for K_c . Therefore we have corrected these data for the difference in coupling strength using Eq. (6.16). Figure 6.2 shows both $Q(K = 0.1139100, L)$ and $Q(K_c, L)$ as a function of L . This turns out to be a surprisingly instructive plot. First, one notices that for the larger values of L the finite-size data for Q are *strongly* dependent on the coupling, which is due to the large value of γ_t^* . This implies that an incorrect estimate of K_c has a considerable effect on the resulting estimate of the amplitude ratio. Secondly, one observes that the dashed curve indicating the finite-size corrections as predicted by renormalization theory gives a good description of the data down to system sizes as small as 4 or 5 (cf. Ref. [28]). The overall approach to the $L \rightarrow \infty$ limit is very slow, given the huge number of spins in the largest system. Returning to the original discrepancy, we have repeated the least-squares fits with a smaller number of correction terms. Apart from an increase in χ^2 , indicating the importance of the higher-order terms, this leads to a higher estimate of the critical coupling and a correspondingly higher value for Q , although it was by no means as high as the result in [9].

No independent determination of the thermal exponent has been attempted in Ref. [9]: instead, it was checked graphically that the finite-size scaling behaviour of several observables is consistent with $\gamma_t^* = 5/2$. In Ref. [25] the shift of the temperature at which the connected susceptibility $\langle m^2 \rangle - \langle m \rangle^2$ takes its maximum was studied as a function of the system size (for $L \leq 16$). As follows from Eq. (4.19), this shift is ruled by γ_t^* , which is consistent with the result 2.32 (16) found in [25].

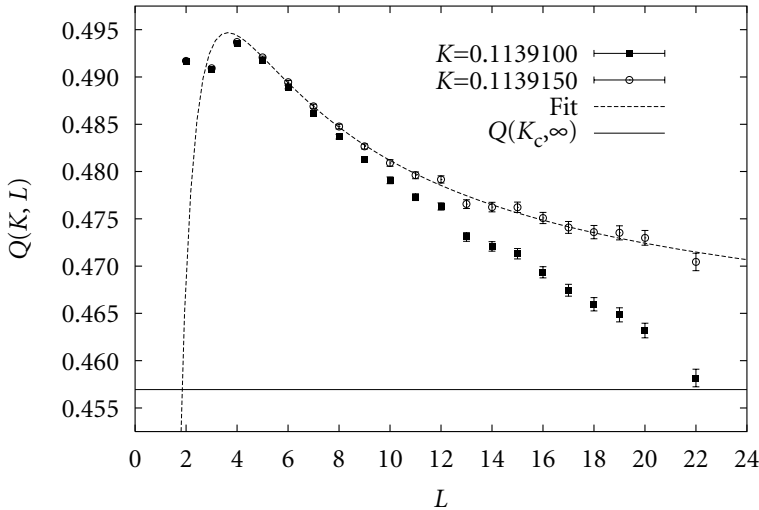


Figure 6.2: The amplitude ratio Q at $K = 0.1139100$, where most of our data were taken, and $K = 0.1139150$, our best estimate of K_c , versus the system size L . The points at the latter coupling were calculated from those at the former coupling. Furthermore the function describing the finite-size corrections at criticality (dashed curve) and the $L \rightarrow \infty$ limit of the Binder cumulant (solid line) are shown.

The magnetic exponent has been determined in Refs. [9, 25] from the height of the maximum of the connected susceptibility. Equation (4.30) shows that this height diverges as $L^{2\gamma_h^* - d}$. Expressed in terms of the magnetic exponent the results are: 3.81 (Ref. [9], no error given) and 3.74 (2) (Ref. [25]).

In order to compare our results to series-expansion results, we calculate the critical exponents β and γ from the renormalization exponents (cf. Table 3.17, where γ_t and γ_h must be replaced by their starred counterparts). This yields $\beta = 0.501$ (5) and $\gamma = 0.999$ (10). The accuracy in γ is not as good as in the series-expansion result of Ref. [27], $\gamma = 1.005$ (5), but the accuracy in β surpasses that of the estimate $\beta = 0.50$ (5) from Ref. [26] by an order of magnitude, where it should be remarked that this series-expansion result was obtained while keeping $\gamma = 1$ fixed.

Table 6.23 shows a compilation of estimates for the critical coupling. We briefly compare these estimates to the value obtained in this chapter. The early result by Fisher and Gaunt [29] already has a remarkable accuracy, but the quoted uncertainty turns out to be almost ten times too small. Other series-expansion results [26, 27] agree with our prediction; in particular the result of Guttman (which was obtained by fixing the critical exponent γ at its mean-field value) is very close. Still, the uncertainty in this estimate is more than an order of magnitude larger than in the newest Monte Carlo result. The most accurate result until now from equilibrium

Monte Carlo simulations was obtained by Parisi and Ruiz-Lorenzo [25] and lies one standard deviation below our estimate. Since this value was obtained with y_t^* fixed, the uncertainty has to be compared to that of analysis 4 in Table 6.2. Finally, two (coinciding) estimates were obtained by studying the critical dynamics of the five-dimensional Ising model [27, 30] for very large system sizes and requiring that the effective dynamical critical exponent approaches its asymptotic value $z = 2$. These results are also in good agreement with our estimate and the latter may hence be used to make a more accurate study of the critical dynamics of the five-dimensional Ising model.

Table 6.23: Critical couplings for the five-dimensional Ising model as obtained in various studies.

Reference	Year	K_c	Method	Remarks
[29]	1964	0.114035 (13)	series exp.	
[23]	1979	0.1149 (7)	Monte Carlo	$L = 6$
[26]	1981	0.113917 (7)	series exp.	γ fixed
[8], [24]	1985	0.1140	Monte Carlo	$L \leq 7$
[27]	1993	0.113935 (15)	series exp.	
[27]	1993	0.11391 (1)	dynamic MC	$L \leq 48$
[9]	1994	0.113929 (45)	Monte Carlo	$L \leq 17$
[28]	1996	0.11389 (13)	Monte Carlo	$L \leq 14$
[25]	1996	0.11388 (3)	Monte Carlo	$L \leq 16, y_t^*$ fixed
[30]	1996	0.11391 (1)	dynamic MC	$L = 112$
This work	1997	0.1139149 (7)	Monte Carlo	$L \leq 22$
This work	1997	0.1139150 (4)	Monte Carlo	$L \leq 22, Q$ and y_t^* fixed

Two other nonuniversal quantities for which estimates exist in the literature are the internal energy U at criticality and the specific-heat maximum. Whereas the former vanishes in mean-field theory [31], it does not in the five-dimensional Ising model, since fluctuations are not completely suppressed. Our best estimate is $|U| = 0.67559 (3)$ (Table 6.6), to be compared with the value $0.67 (1)$ [24]. Fluctuations are also responsible for the fact that the maximum of the specific heat, $C_{\max}/k_B = 2.0 (2)$ [9], exceeds the mean-field value. The height of this maximum, $\lim_{T \uparrow T_c} C(T)/k_B$, cannot be found from our analysis, since the parameter q_0 (Table 6.7) represents the value of C right at criticality and therefore takes a value between 0 and C_{\max}/k_B , cf. Fig. 6.1 on page 116. Indeed, q_0 is the analog of the exact value mentioned at the end of Sec. 6.3. Unfortunately, the temperature range around T_c within which our data have been taken is for the largest system sizes too small to observe an excess peak of the type discussed in Sec. 6.3.

In conclusion we remark that we have presented accurate results for several critical properties of the five-dimensional Ising model, which could be obtained thanks

to precise numerical results for a large range of system sizes. Various renormalization predictions for universal quantities have been confirmed, as well as the finite-size scaling hypothesis for systems above their upper critical dimension.

6.6.2 The four-dimensional Ising model

In summary, our best estimates for some universal critical properties of the four-dimensional Ising model are given by: $Q = 0.454$ (2), $\gamma_t = 2.002$ (4), $\gamma_h = 3.0023$ (15), $\zeta_t = 0.175$ (14) and $\zeta_h = 0.254$ (4). We recall that the last two exponents are defined as the powers of the logarithmic factors appearing in the right-hand side of Eq. (6.6), for $n = 1$. The theoretical prediction for Q is the same as in the five-dimensional model and the exponents are predicted to be $\gamma_t = 2$, $\gamma_h = 3$, $\zeta_t = 1/6$ and $\zeta_h = 1/4$. Both the value for Q and the thermal and magnetic exponents are a strong indication that the four-dimensional model displays classical critical behaviour. Moreover, the results for the exponents ζ_t and ζ_h , which we consider to belong to the main feats of this chapter, accurately confirm the presence of multiplicative logarithmic corrections.

While no other estimates for Q are known to us, several results for the exponents exist, to which we may compare our values. The first series-expansion results which did take into account the possibility of logarithmic factors are those by Moore [32]. He found that the agreement of the critical exponents with the classical values depended on the inclusion of such logarithms. Also Kadanoff *et al.* [33] found agreement with the classical exponents in an RG treatment. Baker [34], however, claimed from series expansions that hyperscaling was violated in $d = 4$. The first determination of the power appearing in a logarithmic factor was then made by Guttman [35], for ($d = 4, n = 0$). From a high-temperature expansion for the susceptibility he found $\chi \propto t^{-1} |\ln |t||^p$ with $p = 0.23$ (4), in agreement with Eq. (6.10). Subsequently, the case $n = 1$ was studied by several authors. In Ref. [23], the temperature dependence of the order parameter close to T_c was determined by Monte Carlo simulation of a 12^4 system, where the temperature region was chosen such that finite-size effects were absent. Good agreement with a factor $|\ln |t||^p$ was found, but the graph in Ref. [23] describing the quality of a least-squares fit as a function of p suggests unlikely strong evidence for $p = 1/3$ (no explicit estimate is given). Both the neglect of any finite-size effects up to $t = 0.005$ and the curves in Fig. 2 of Ref. [23] point to a considerable error margin in p . Gaunt *et al.* [36] carried out a series analysis for the susceptibility. Making the same assumption for the temperature dependence as Guttman (i.e., assuming the presence of a logarithmic factor and keeping γ fixed), they found $p = 0.33$ (7). For comparison we calculate p from the renormalization exponents. Expressing p in terms of ζ_t and ζ_h , we find $p = [(d - 2\gamma_h)/\gamma_t]\zeta_t + 2\zeta_h = -\gamma\zeta_t + 2\zeta_h$ and for fixed γ our best estimates thus yield $p = 0.33$ (2). The same collaboration also considered the critical isotherm of

the four-dimensional Ising model [37]. From the critical equation of state one expects the magnetization to vary as $h^{1/\delta} |\ln |h||^q$, where the exponent q was estimated as 0.30 (5) (for fixed $\delta = 3$). Also this relation can be calculated from Eq. (6.6). Indeed, the rescaling parameter b must be chosen such that the argument involving h takes some constant value,

$$b = h^{-1/\gamma_h} |\ln |h||^{-\zeta_h/\gamma_h} . \quad (6.37)$$

Upon substitution in Eq. (6.7) we find

$$\langle m \rangle \propto h^{1/3} |\ln |h||^{4\zeta_h/3} , \quad (6.38)$$

yielding $q = 0.339$ (5).

A subsequent determination of the critical exponents using the Monte Carlo RG technique [38] again yielded estimates in agreement with the classical ones. However, logarithmic corrections to scaling could not be observed in this analysis. Reference [19] is the first work that was actually concerned with a finite-size scaling analysis of the four-dimensional Ising model. As mentioned in Sec. 6.2, in this paper the location of the zeroes of the partition function in the absence of an external magnetic field is studied as a function of the system size. This yields the exponent ζ_t . Similarly, the location of Lee–Yang zeroes, which for real temperatures lie on the imaginary field axis, yields the exponent ζ_h . Since the numerical results obtained in Ref. [19] are presented (with minor differences) in a more extensive form in Ref. [39], together with results for the Lee–Yang zeroes, we will quote the results of the second paper. The simulations have been carried out for system sizes $L \leq 24$. Using $L \geq 4$, the authors found $\zeta_t = 0.217$ (12), more than four standard deviations from the renormalization prediction. An analysis for $12 \leq L \leq 24$ yielded $\zeta_t = 0.21$ (4), which is consistent with the theoretical value $1/6$. For ζ_h the two analyses yielded, respectively, 0.204 (9) (five standard deviations from the predicted value) and 0.22 (3). The latter value is consistent with $1/4$. While the actual observation of logarithmic factors in a finite-size scaling analysis is a promising result, we conclude that only a rather crude agreement with the predicted values is obtained. In fact, the simulations are hardly able to distinguish between the scaling of the two types of partition-function zeroes.

Finally, we consider several estimates for the critical coupling, see Table 6.24. The oldest estimates [29, 32] are somewhat high, where in particular the error quoted in Ref. [29] is much too small. The deviation for Ref. [23] is due to the fact that the critical coupling was estimated from the maximum in the (connected) susceptibility for a system with $L = 12$, without the application of any finite-size scaling techniques. The series-expansion result found in Ref. [36] is already in rather good agreement with the best estimates. The first result of Kenna and Lang lies approximately two standard deviations too high, but in their second, slightly lower

Table 6.24: Critical couplings for the four-dimensional Ising model as obtained in various studies. The remarks regarding fixed exponents concern both the critical exponents and the powers in the logarithmic factors.

Reference	Year	K_c	Method	Remarks
[29]	1964	0.14988 (3)	series exp.	
[32]	1970	0.14981 (7)	series exp.	
[23]	1979	0.15020 (18)	Monte Carlo	$L = 12$
[36]	1979	0.14966 (3)	series exp.	exponents fixed
[19]	1991	0.149709 (8)	Monte Carlo	$L \leq 24$
[39]	1992	0.149703 (15)	Monte Carlo	$L \leq 24$
[41]	1996	0.1497 (2)	Monte Carlo	$L \leq 14$
[40]	1997	0.149696 (4)	series exp.	exponents fixed
[40]	1997	0.149694 (5)	dynamic MC	$L = 480$, exponents fixed
This work	1997	0.1496930 (3)	Monte Carlo	$L \leq 48$

result they have doubled the error estimate. The newest, consistent results obtained from a large-scale Monte Carlo study of the critical dynamics and a reanalysis of series expansions [40] lie very close to our best estimate. This estimate, which is shown in the table as well, was obtained from the following considerations. The most precise values emerged from the analyses of the susceptibility and the fourth power of the magnetization. However, accurate estimates have also been obtained from the analyses of the amplitude ratio Q and the specific heat, in which all theoretically predicted quantities were kept fixed. The latter estimates lie one standard deviation below the former ones. Such differences can be explained from an arbitrariness in the choice of the scaling formula. To account for this, we have quoted the best values, but increased the error estimate such that the values from Q and the specific heat are included. Still, this implies an improvement of more than an order of magnitude compared to earlier estimates. As a side remark we note that the critical coupling predicted by mean-field theory, which is the inverse of the coordination number, lies 12% too low for the five-dimensional model and 16% for the four-dimensional model.

In conclusion, we note that we have presented an accurate confirmation of the renormalization scenario at the upper critical dimension. The predicted logarithmic factors have not only been determined with an appreciable precision, but their occurrence has also been demonstrated in a considerable number of observables.

References

- [1] L. D. Landau and E. M. Lifshitz, *Statistical Physics* (Pergamon, London, 1959).
- [2] L. Onsager, *Phys. Rev.* **65**, 117 (1944).

- [3] E. Brézin, *J. Phys. (Paris)* **43**, 15 (1982).
- [4] R. Botet, R. Jullien and P. Pfeuty, *Phys. Rev. Lett.* **49**, 478 (1982).
- [5] R. Botet and R. Jullien, *Phys. Rev. B* **28**, 3955 (1983).
- [6] V. Privman and M. E. Fisher, *J. Stat. Phys.* **33**, 385 (1983).
- [7] H. J. F. Knops, J. M. J. van Leeuwen and P. C. Hemmer, *J. Stat. Phys.* **17**, 197 (1977).
- [8] K. Binder, M. Nauenberg, V. Privman and A. P. Young, *Phys. Rev. B* **31**, 1498 (1985).
- [9] Ch. Rickwardt, P. Nielaba and K. Binder, *Ann. Physik (Leipzig)* **3**, 483 (1994).
- [10] E. Brézin and J. Zinn-Justin, *Nucl. Phys. B* **257** [FS14], 867 (1985).
- [11] S.-k. Ma, *Modern Theory of Critical Phenomena* (Addison-Wesley, Redwood, California, 1976).
- [12] P. Pfeuty and G. Toulouse, *Introduction to the Renormalization Group and to Critical Phenomena* (Wiley, London, 1977).
- [13] A. I. Larkin and D. E. Khmel'nitskiĭ, *Zh. Eksp. Teor. Fiz.* **56**, 2087 (1969) [*Sov. Phys.-JETP* **29**, 1123 (1969)].
- [14] K. G. Wilson, *Phys. Rev. B* **4**, 3174 (1971).
- [15] K. G. Wilson, *Phys. Rev. B* **4**, 3184 (1971).
- [16] D. J. Amit, *Field Theory, the Renormalization Group, and Critical Phenomena*, second edition (World Scientific, Singapore, 1984).
- [17] F. J. Wegner and E. K. Riedel, *Phys. Rev. B* **7**, 248 (1973).
- [18] E. Brézin, J. C. Le Guillou and J. Zinn-Justin, *Phys. Rev. D* **8**, 2418 (1973).
- [19] R. Kenna and C. B. Lang, *Phys. Lett. B* **264**, 396 (1991).
- [20] J. Rudnick, H. Guo and D. Jasnow, *J. Stat. Phys.* **41**, 353 (1985).
- [21] J. Zinn-Justin, *Quantum Field Theory and Critical Phenomena*, third edition (Oxford University Press, Oxford, 1996).
- [22] U. Wolff, *Phys. Rev. Lett.* **62**, 361 (1989).
- [23] O. G. Mouritsen and S. J. Knak Jensen, *Phys. Rev. B* **19**, 3663 (1979).
- [24] K. Binder, *Z. Phys. B* **61**, 13 (1985).
- [25] G. Parisi and J. J. Ruiz-Lorenzo, *Phys. Rev. B* **54**, R3698 (1996); **55**, 6082(E) (1997).
- [26] A. J. Guttmann, *J. Phys. A* **14**, 233 (1981).
- [27] Ch. Munkel, D. W. Heermann, J. Adler, M. Gofman and D. Stauffer, *Physica A* **193**, 540 (1993).
- [28] K. K. Mon, *Europhys. Lett.* **34**, 399 (1996).
- [29] M. E. Fisher and D. S. Gaunt, *Phys. Rev.* **133**, A224 (1964).
- [30] D. Stauffer and R. Knecht, *Int. J. Mod. Phys. C* **7**, 893 (1996).
- [31] R. J. Baxter, *Exactly Solved Models in Statistical Mechanics* (Academic, London, 1982).
- [32] M. A. Moore, *Phys. Rev. B* **1**, 2238 (1970).
- [33] L. P. Kadanoff, A. Houghton and M. C. Yalabik, *J. Stat. Phys.* **14**, 171 (1976).

- [34] G. A. Baker, Jr., *Phys. Rev. B* **15**, 1552 (1977).
- [35] A. J. Guttmann, *J. Phys. A* **11**, L103 (1978).
- [36] D. S. Gaunt, M. F. Sykes and S. McKenzie, *J. Phys. A* **12**, 871 (1979).
- [37] S. McKenzie, M. F. Sykes and D. S. Gaunt, *J. Phys. A* **12**, 743 (1979).
- [38] H. W. J. Blöte and R. H. Swendsen, *Phys. Rev. B* **22**, 4481 (1980).
- [39] R. Kenna and C. B. Lang, *Nucl. Phys. B* **393**, 461 (1992).
- [40] D. Stauffer and J. Adler, *Int. J. Mod. Phys. C* **8**, 263 (1997).
- [41] N. Aktekin, *Physica A* **232**, 397 (1996).

Chapter 7

Crossover from Ising to classical critical behaviour in two-dimensional systems

7.1 Introduction

As shown in the preceding chapters, the critical behaviour of a physical system strongly depends on the range of the interactions. The longer the range, the stronger critical fluctuations will be suppressed. In the limit of infinitely ranged interactions (which decay sufficiently slowly), we recover classical or mean-field-like critical behaviour. For interactions with a finite range, however, fluctuations remain very important and essentially modify the critical behaviour. As follows from the Ginzburg criterion [1], sufficiently close to the critical temperature T_c nonclassical critical exponents apply for any finite interaction range R . This crucial difference between finite and infinite R implies a crossover from one type of critical behaviour to another as a function of R . Such crossover effects are of great interest for a wealth of critical phenomena. They occur, e.g., in polymer mixtures (see Ref. [2] and references therein), as a function of the chain length, and gas-liquid transitions, as a function of the difference between the temperature and the critical temperature. The explanation of these phenomena in terms of competing fixed points of a renormalization-group transformation is one of the important features of the renormalization-group (RG) theory (see, e.g., Ref. [3]).

In Ref. [4], Mon and Binder have already studied crossover as a function of R within the context of finite-size scaling, motivated by the crossover in polymer mixtures. They predicted that the critical amplitudes of scaling functions display a singular dependence on R . The various power-law dependences were obtained from

phenomenological crossover scaling arguments. In this chapter, we will derive this dependence on R from a renormalization description of the crossover from classical to nonclassical critical behaviour. The first part of the renormalization trajectory is governed by the Gaussian fixed point, which is unstable for dimensionalities $d < 4$. The corresponding scaling relations have been derived by Rikvold *et al.* [5]. Sufficiently close to criticality, the final part of the renormalization trajectory is governed by the Ising fixed point. The resulting relations are in complete agreement with the predictions from Ref. [4]. In addition, we obtain the R dependence of the leading corrections to scaling and derive from renormalization arguments a logarithmic factor in the shift of the critical temperature. This factor was already conjectured in Ref. [4].

It is interesting to note that the physical mechanism leading to the singular range dependence of scaling functions is closely related to that leading to the violation of hyperscaling for $d > 4$. The latter effect is caused by a singular dependence of thermodynamic quantities on the coefficient u of the ϕ^4 term for $u \rightarrow 0$ in a Landau–Ginzburg–Wilson (LGW) Hamiltonian. In other words, u is a so-called dangerous irrelevant variable (see Chapter 4 for a more detailed discussion). Here, as we will see, the fact that this coefficient becomes small for large values of R plays again an essential rôle, although u is relevant for $d < 4$.

Furthermore, we present Monte Carlo results for two-dimensional Ising models with an extended range of interaction. A serious problem associated with simulations of such models is that the simulation time tends to increase rapidly with the number of interacting spins. However, a large interaction range is crucial to observe the predicted R dependences, as will follow from the renormalization description. The maximum range that could be accessed in Ref. [4] was too small to verify the theoretical predictions. We overcome this limitation by means of the cluster Monte Carlo algorithm described in Chapter 2, in which the simulation time per spin is practically independent of the range of the interactions.

Subsequently, we use the results of these simulations to determine the scaling functions describing the crossover from Ising-like to classical critical behaviour, both as a function of the system size and as a function of the temperature distance to the critical point. Since this crossover spans several decades in the reduced temperature as well as in the finite-size crossover variable, it has up to now largely evaded a satisfactory numerical determination, while also on the experimental side several open questions remain. Accurate results for sufficiently large interaction ranges are again a crucial ingredient for observing the full crossover region both above and below the critical temperature. We present strong evidence that our data reproduce the universal crossover functions. Also the so-called effective exponents are discussed and we show that these can vary nonmonotonically in the crossover region.

The outline of this chapter is as follows. In Sec. 7.2, we derive the R depen-

dence of critical amplitudes from renormalization theory. These results are verified by Monte Carlo simulations, presented in Sec. 7.3. In the second part of this chapter, Secs. 7.4 to 7.7, we treat crossover scaling functions and effective exponents. We end with our conclusions in Sec. 7.8.

7.2 Renormalization-group derivation of the dependence of critical amplitudes on the interaction range

Chapters 4 and 5 were devoted to models with spin–spin interactions that decay algebraically as a function of the distance r between the spins. By changing the decay parameter in this model, a changeover can be induced from short-range critical behaviour to an intermediate regime with continuously varying critical exponents. For interactions which decay even more slowly, the critical behaviour is classical. In this chapter we focus on a different way to interpolate between the long-range (mean-field) limit and short-range models. Instead, we choose ferromagnetic interactions which are constant within a range R and zero beyond this range. Thus, we have the following Hamiltonian:

$$\mathcal{H}/k_B T = - \sum_i \sum_{j>i} K_d(\mathbf{r}_i - \mathbf{r}_j) s_i s_j - h_0 \sum_i s_i, \quad (7.1)$$

where the spin–spin interaction $K_d(\mathbf{r}) \equiv cR^{-d}$ for $|\mathbf{r}| \leq R$ and the sums run over all spins in the system. This Hamiltonian displays physical behaviour that is different from the power-law case. In particular, the intermediate regime with variable exponents is absent, and mean-field critical behaviour is restricted to the infinite-range limit. We analyze the influence of the range R within the context of renormalization-group theory, starting from a generalized Landau–Ginzburg–Wilson Hamiltonian, where the $[\nabla\phi(\mathbf{r})]^2$ term normally representing the (short-range) interactions is replaced by a term with spin–spin coupling (B.1),

$$\begin{aligned} \mathcal{H}(\phi)/k_B T = \int_V d\mathbf{r} \left\{ -\frac{1}{2} \int_{|\mathbf{r}-\mathbf{r}'| \leq R} d\mathbf{r}' \left[\frac{c}{R^d} \phi(\mathbf{r})\phi(\mathbf{r}') \right] - h_0 \phi(\mathbf{r}) \right. \\ \left. + \frac{1}{2} v \phi^2(\mathbf{r}) + \frac{1}{4} u_0 \phi^4(\mathbf{r}) \right\}. \end{aligned} \quad (7.2)$$

As a consequence of the normalization factor R^{-d} , the critical value of the temperature parameter c depends only weakly on R . The first integral runs over the volume V which contains N particles. We adopt periodic boundary conditions. The Fourier transform of the interaction is calculated in Appendix B. It leads to the following

momentum-space representation of the Hamiltonian

$$\begin{aligned} \mathcal{H}(\phi_{\mathbf{k}})/k_{\text{B}}T &= \frac{1}{2} \sum_{\mathbf{k}} \left[-c \left(\frac{2\pi}{kR} \right)^{d/2} J_{d/2}(kR) + \bar{\nu} \right] \phi_{\mathbf{k}} \phi_{-\mathbf{k}} \\ &+ \frac{u_0}{4N} \sum_{\mathbf{k}_1} \sum_{\mathbf{k}_2} \sum_{\mathbf{k}_3} \phi_{\mathbf{k}_1} \phi_{\mathbf{k}_2} \phi_{\mathbf{k}_3} \phi_{-\mathbf{k}_1-\mathbf{k}_2-\mathbf{k}_3} - h_0 \sqrt{N} \phi_{\mathbf{k}=\mathbf{0}}. \end{aligned} \quad (7.3)$$

J_ν is a Bessel function of the first kind of order ν . The wave vectors are discrete because of the periodic boundary conditions. Furthermore, we restrict the wave vectors to lie within the first Brillouin zone, which is reminiscent of the underlying lattice structure. The term containing the Bessel function can be expanded in a Taylor series containing only even terms in kR . This means that we will be mainly concerned with the term of order $(kR)^2$, because higher-order terms will turn out to be irrelevant. The constant term in the Taylor series is absorbed in $\bar{\nu}$ and the coefficient of the quadratic term as a factor in \bar{c} . This yields a new Hamiltonian

$$\begin{aligned} \mathcal{H}_t(\phi_{\mathbf{k}})/k_{\text{B}}T &= \frac{1}{2} \sum_{\mathbf{k}} [\bar{c}R^2 k^2 + \bar{\nu}] \phi_{\mathbf{k}} \phi_{-\mathbf{k}} \\ &+ \frac{u_0}{4N} \sum_{\mathbf{k}_1} \sum_{\mathbf{k}_2} \sum_{\mathbf{k}_3} \phi_{\mathbf{k}_1} \phi_{\mathbf{k}_2} \phi_{\mathbf{k}_3} \phi_{-\mathbf{k}_1-\mathbf{k}_2-\mathbf{k}_3} - h_0 \sqrt{N} \phi_{\mathbf{k}=\mathbf{0}}. \end{aligned} \quad (7.4)$$

Since we are free to choose the scale on which the fluctuations of the order parameter are measured, we may rescale $\phi \rightarrow \psi \equiv \sqrt{\bar{c}}R\phi$. This is generally the most convenient choice because the dominant k -dependent term becomes independent of R .¹ This leads to

$$\begin{aligned} \tilde{\mathcal{H}}(\psi_{\mathbf{k}})/k_{\text{B}}T &= \frac{1}{2} \sum_{\mathbf{k}} \left[k^2 + \frac{\bar{\nu}}{\bar{c}R^2} \right] \psi_{\mathbf{k}} \psi_{-\mathbf{k}} \\ &+ \frac{u_0}{4\bar{c}^2 R^4 N} \sum_{\mathbf{k}_1} \sum_{\mathbf{k}_2} \sum_{\mathbf{k}_3} \psi_{\mathbf{k}_1} \psi_{\mathbf{k}_2} \psi_{\mathbf{k}_3} \psi_{-\mathbf{k}_1-\mathbf{k}_2-\mathbf{k}_3} - \frac{h_0}{\sqrt{\bar{c}}R} \sqrt{N} \psi_{\mathbf{k}=\mathbf{0}}. \end{aligned} \quad (7.5)$$

The parameter \bar{c} is merely a constant, *independent of the range*, and in order not to be hampered by it in the further analysis, we absorb the various powers of it in $r_0 \equiv \bar{\nu}/\bar{c}$, $u \equiv u_0/\bar{c}^2$, and $h \equiv h_0/\sqrt{\bar{c}}$. Now, r_0 assumes the rôle of the temperature parameter.

If the range R is large, the coefficient of the ψ^4 term is relatively small and hence the critical behaviour of the system is determined by the Gaussian fixed point. Under

¹Naturally, this rescaling is not compulsory and the same results will be obtained without it, provided one keeps track of the dependence of the nontrivial fixed point on $\bar{c}R^2$, arising from the integration of propagators over the outer part of the Brillouin zone.

a renormalization transformation with a rescaling parameter l the Hamiltonian thus transforms as

$$\begin{aligned} \tilde{\mathcal{H}}(\psi'_{\mathbf{k}'})/k_{\text{B}}T' &= \frac{1}{2} \sum_{\mathbf{k}'} \left[k'^2 + \frac{r_0}{R^2} l^2 \right] \psi'_{\mathbf{k}'} \psi'_{-\mathbf{k}'} \\ &+ \frac{u}{4R^4 N'} l^{4-d} \sum_{\mathbf{k}'_1} \sum_{\mathbf{k}'_2} \sum_{\mathbf{k}'_3} \psi'_{\mathbf{k}'_1} \psi'_{\mathbf{k}'_2} \psi'_{\mathbf{k}'_3} \psi'_{-\mathbf{k}'_1 - \mathbf{k}'_2 - \mathbf{k}'_3} \\ &- \frac{h}{R} \sqrt{N'} l^{1+d/2} \psi'_{\mathbf{k}'=0}. \end{aligned} \quad (7.6)$$

Here $\psi'_{\mathbf{k}'} = l^{-1} \psi_{\mathbf{k}}$, $\mathbf{k}' = \mathbf{k}l$, the sums run again over the full Brillouin zone, and $N' = Nl^{-d}$. For $d < 4$, the ψ^4 term grows and the system moves away from the Gaussian fixed point μ_0^* (see Fig. 7.1). At present, we are interested in the flow from the neighbourhood of the Gaussian fixed point to that of the Ising fixed point. Thus we remain close to the critical line connecting the two fixed points and the temperature field parametrized by r_0 remains small. The crossover to Ising-like critical behaviour occurs when the coefficient of the ψ^4 term becomes of the same order as that of the $k^2\psi^2$ term, which is unity, i.e., when $l = l_0 \equiv R^{4/(4-d)}$. We shall refer to l_0 as the *crossover scale*. Upon approach of the Ising fixed point, a further increase of u is then stopped by nonlinear contributions to the renormalization of the ψ^4 coefficient.

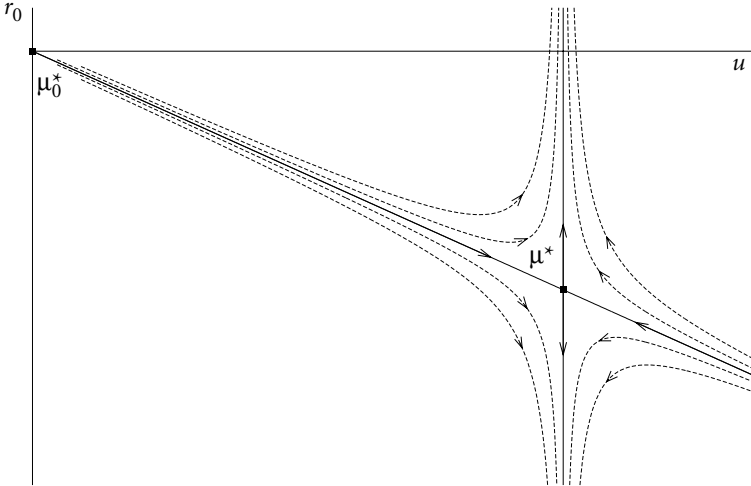


Figure 7.1: A qualitative picture of the renormalization trajectory describing the crossover from the Gaussian fixed point $\mu_0^* = (0, 0)$ to the Ising fixed point $\mu^* = (r_0^*, u^*)$.

By comparing the coefficient of the ψ^4 term to that of the $r_0\psi^2$ term, it is possible to derive a criterion that states for which temperatures the critical behaviour will be Ising-like and for which temperatures it will be classical. This is the well-known Ginzburg criterion [1], which can also be derived from Eq. (7.6) (see, e.g., Ref. [6, p. 107]). One expects the Gaussian fixed point to dominate the renormalization flow if, irrespective of l , the ψ^4 coefficient is small compared to the temperature coefficient. Thus, one requires the scaled combination $uR^{-4}l^{4-d}/(r_0R^{-2}l^2)^{(4-d)/2}$ to be small, or $r_0^{(4-d)/2}R^d u^{-1} \gg 1$ (cf. also Ref. [4, Eq. (3)]).

Since we are now in the neighbourhood of the Ising fixed point, we continue renormalizing our Hamiltonian with *nonclassical* renormalization exponents y_t , y_h and y_i . To leading order, it will transform as follows, where b denotes the rescaling factor of our new transformation,

$$\begin{aligned} \tilde{\mathcal{H}}''(\psi_{\mathbf{k}''})/k_B T'' &= \frac{1}{2} \sum_{\mathbf{k}''} \left[k''^2 + R^{2d/(4-d)} (b^{y_t} \tilde{r}_0 + r_0^*) \right] \psi_{\mathbf{k}''}'' \psi_{-\mathbf{k}''}'' \\ &+ \frac{b^{y_i} \tilde{u} + u^*}{4N''} \sum_{\mathbf{k}_1''} \sum_{\mathbf{k}_2''} \sum_{\mathbf{k}_3''} \psi_{\mathbf{k}_1''}'' \psi_{\mathbf{k}_2''}'' \psi_{\mathbf{k}_3''}'' \psi_{-\mathbf{k}_1''-\mathbf{k}_2''-\mathbf{k}_3''}'' \\ &- hR^{3d/(4-d)} \sqrt{N''} b^{y_h} \psi_{\mathbf{k}''=0}'' . \end{aligned} \quad (7.7)$$

We have introduced the coefficients \tilde{r}_0 and \tilde{u} , which denote the location of the point (r_0, u) in the new coordinates with respect to the nontrivial (Ising) fixed point μ^* which we are now approaching (see Fig. 7.1).

The singular part of the free-energy density, f_s , is after the transformation $\phi \rightarrow \psi$ denoted by \tilde{f}_s ,

$$f_s(r_0, u, h) = \tilde{f}_s \left(\frac{r_0}{R^2}, \frac{u}{R^4}, \frac{h}{R} \right) . \quad (7.8)$$

Furthermore, we introduce the notation $\hat{f}_s(\tilde{r}_0, \tilde{u}, h) \equiv \tilde{f}_s(r_0, u, h)$. Because the total free energy is conserved along the renormalization trajectory, the singular part of the free-energy density changes as

$$\begin{aligned} \tilde{f}_s \left(\frac{r_0}{R^2}, \frac{u}{R^4}, \frac{h}{R} \right) &= l^{-d} \tilde{f}_s \left(\frac{r_0}{R^2} l^2, \frac{u}{R^4} l^{4-d}, \frac{h}{R} l^{1+d/2} \right) \\ &= R^{-4d/(4-d)} \hat{f}_s \left(\tilde{r}_0 R^{2d/(4-d)}, \tilde{u}, hR^{3d/(4-d)} \right) \\ &= b^{-d} R^{-4d/(4-d)} \hat{f}_s \left(tR^{2d/(4-d)} b^{y_t}, \tilde{u} b^{y_i}, hR^{3d/(4-d)} b^{y_h} \right) , \end{aligned} \quad (7.9)$$

where we have used the notation $t \propto [T - T_c(R)]/T_c(R)$ for \tilde{r}_0 . In Fig. 7.1, t stands for the distance to the critical line connecting μ_0^* and μ^* . In the second equality we have substituted the crossover scale, $l = R^{4/(4-d)}$. Of course, this is only a *qualitative*

measure for the location of the crossover, but the renormalization predictions for the scaling exponents are exact. The relation (7.9), which holds for $1 < d < 4$, is the key to the scaling relations obtained on phenomenological grounds in Ref. [4]. We will first illustrate this by deriving the R dependence of the critical amplitudes of the magnetization density m and the magnetic susceptibility χ . The magnetization density can be calculated by taking the first derivative of the free-energy density with respect to the magnetic scaling field h ,

$$\begin{aligned} m &= \frac{\partial f_s}{\partial h}(r_0, u, h) = \frac{\partial \tilde{f}_s}{\partial h} \left(\frac{r_0}{R^2}, \frac{u}{R^4}, \frac{h}{R} \right) \\ &= b^{\gamma_h - d} R^{-d/(4-d)} \hat{f}_s^{(1)} \left(t R^{2d/(4-d)} b^{\gamma_t}, \tilde{u} b^{\gamma_i}, h R^{3d/(4-d)} b^{\gamma_h} \right), \end{aligned} \quad (7.10)$$

where $\hat{f}_s^{(1)}$ denotes the first derivative of \hat{f}_s with respect to its third argument. Here, we have omitted a contribution from the analytic part of the free energy, because h only couples to the $\mathbf{k} = \mathbf{0}$ (uniform) mode. To extract the dependence of m on t and R from Eq. (7.10), we choose the rescaling factor b such that the first argument of the derivative of \hat{f}_s is equal to 1, i.e., $b = t^{-1/\gamma_t} R^{-2d/[\gamma_t(4-d)]}$, and set the irrelevant variable \tilde{u} and the magnetic scaling field h equal to zero,

$$m = t^\beta R^{(2d\beta - d)/(4-d)} \hat{f}_s^{(1)}(1, 0, 0). \quad (7.11)$$

This result agrees with Ref. [4, Eq. (34)]. In the same way we can calculate the magnetic susceptibility from \hat{f}_s by taking the second derivative with respect to h ,

$$\begin{aligned} \chi &= \frac{\partial^2 f_s}{\partial h^2}(r_0, u, h) = \frac{\partial^2 \tilde{f}_s}{\partial h^2} \left(\frac{r_0}{R^2}, \frac{u}{R^4}, \frac{h}{R} \right) \\ &= b^{2\gamma_h - d} R^{2d/(4-d)} \hat{f}_s^{(2)} \left(t R^{2d/(4-d)} b^{\gamma_t}, \tilde{u} b^{\gamma_i}, h R^{3d/(4-d)} b^{\gamma_h} \right). \end{aligned} \quad (7.12)$$

Choosing the arguments of the second derivative of \hat{f}_s as in Eq. (7.11), we find

$$\chi = t^{-\gamma} R^{2d(1-\gamma)/(4-d)} \hat{f}_s^{(2)}(1, 0, 0), \quad (7.13)$$

in agreement with Ref. [4, Eq. (39)]. In Eqs. (7.11) and (7.13) we have used the well-known relations between the renormalization exponents and the critical exponents (see Table 3.17 on page 45).

The finite-size scaling behaviour of thermodynamic functions can also be derived from this renormalization scenario by including a finite-size field $1/L$ as an additional argument of the free-energy density in Eq. (7.9). Under the first renormalization transformation this scaling field will scale as $1/L$ and under the second

renormalization transformation as $lb/L = bR^{4/(4-d)}L^{-1}$. The finite-size scaling behaviour is found by choosing b such that $lb/L = 1$, i.e., $b = LR^{-4/(4-d)}$. Substituting this in Eqs. (7.10) and (7.12), we obtain for m

$$m = L^{y_h-d} R^{(3d-4y_h)/(4-d)} \times \hat{f}_s^{(1)} \left(tL^{y_t} R^{-2(2y_t-d)/(4-d)}, \tilde{u}L^{y_i} R^{-4y_i/(4-d)}, hL^{y_h} R^{(3d-4y_h)/(4-d)} \right), \quad (7.14)$$

and for χ ,

$$\chi = L^{2y_h-d} R^{2(3d-4y_h)/(4-d)} \times \hat{f}_s^{(2)} \left(tL^{y_t} R^{-2(2y_t-d)/(4-d)}, \tilde{u}L^{y_i} R^{-4y_i/(4-d)}, hL^{y_h} R^{(3d-4y_h)/(4-d)} \right). \quad (7.15)$$

These results agree with Ref. [4], where the prefactors of the magnetization density and the magnetic susceptibility were predicted as, respectively, $L^{-\beta/\nu} R^{(2\beta-\gamma)/[\nu(4-d)]}$ and $L^{\gamma/\nu} R^{(4\beta-2\gamma)/[\nu(4-d)]}$. Furthermore, the first argument of the scaling functions was predicted as $tL^{1/\nu} R^{\mathcal{H}}$, with $\mathcal{H} = -(2\alpha)/[\nu(4-d)]$ (Ref. [4, Eq. (25)]). This is indeed equivalent with our result $\mathcal{H} = -2(2y_t - d)/(4 - d)$. However, the predicted range dependence of the critical amplitudes [i.e., of the prefactors in Eqs. (7.14) and (7.15)] is only valid in the limit of infinite range. For smaller ranges, R -dependent correction terms are present. These correction terms can be calculated as well. They do *not* come from the dependence of the scaling functions on the irrelevant fields, as corrections to scaling normally do: such corrections vanish in the thermodynamic limit. However, they come from higher-order contributions to the renormalization of the ψ^4 coefficient which were previously neglected in the derivation of the crossover scale l_0 . Note that in the neighbourhood of the Gaussian fixed point, the terms ψ^n with $n < 2d/(d-2)$ are relevant and that for $d = 2$ all higher-order terms are equally relevant. However, the coefficients of these terms are, after the rescaling $\phi \rightarrow \psi$, proportional to R^{-n} , so the leading contribution comes from the term $wR^{-6}\psi^6$. Under a spatial rescaling with a factor $l = e^s$, the renormalization equation for this term is, to leading order,

$$\frac{dw'}{ds} = (6 - 2d)w'. \quad (7.16)$$

The solution of this equation, $w'(s) = we^{(6-2d)s}$, can be substituted into the renormalization equation for the ψ^4 coefficient,

$$\frac{1}{R^4} \frac{du'}{ds} = (4-d) \frac{u'}{R^4} + a \frac{w'}{R^6}. \quad (7.17)$$

To first order in w , this yields

$$\begin{aligned} \frac{u'}{R^4} &= e^{(4-d)s} \frac{1}{R^4} \left[u + \frac{a}{2-d} \frac{w}{R^2} \left(e^{(2-d)s} - 1 \right) \right] \\ &= l^{4-d} \frac{1}{R^4} \left[u + \frac{a}{2-d} \frac{w}{R^2} \left(l^{2-d} - 1 \right) \right], \end{aligned} \quad (7.18)$$

where u and w denote the values of u' and w' at $l = 1$, respectively. This implies that the previously obtained crossover scale $l_0 = R^{4/(4-d)}$ is multiplied by a factor $(1 + \tilde{a}R^{-2})$ and hence all critical amplitudes will exhibit this correction. However, the solution (7.18) is not valid for $d = 2$, where $uR^{-4}\psi^4$ and $wR^{-6}\psi^6$ are equally relevant. The solution of Eq. (7.17) is then given by

$$\frac{u'}{R^4} = e^{2s} \frac{1}{R^4} \left(u + a \frac{w}{R^2} s \right) = l^2 \frac{1}{R^4} \left(u + a \frac{w}{R^2} \ln l \right), \quad (7.19)$$

which yields a (leading) correction factor $[1 + R^{-2}(\tilde{a}_1 + \tilde{a}_2 \ln R)]$ in the crossover scale and the critical amplitudes.

From a similar mechanism we can derive the R dependence of the so-called shift of the critical temperature [4, Eq. (15)]. A detailed treatment of the shift of T_c can be found in, e.g., Sec. 4.3 and Ref. [7]. It arises from the u -dependent contribution in the renormalization equation for the coefficient of the ψ^2 term,

$$\frac{1}{R^2} \frac{dr'_0}{ds} = 2 \frac{r'_0}{R^2} + c \frac{u'}{R^4}, \quad (7.20)$$

where c is some constant. Thus, the first argument on the right-hand side of the first equation in (7.9) should be replaced by

$$\begin{aligned} \frac{r'_0}{R^2} &= l^2 \left[\left(\frac{r_0}{R^2} - \tilde{c} \frac{u}{R^4} \right) + \tilde{c} \frac{u}{R^4} l^{2-d} \right] \\ &= l^2 \frac{1}{R^2} \left[\left(r_0 - \tilde{c} \frac{u}{R^2} \right) + \tilde{c} \frac{u}{R^2} l^{2-d} \right]. \end{aligned} \quad (7.21)$$

The term between round brackets is proportional to the reduced temperature and the last term is the leading shift. Substitution of the crossover scale l_0 shows that this shift in the reduced temperature is proportional to $R^{-2d/(4-d)}$, which indeed vanishes in the mean-field ($R \rightarrow \infty$) limit. In addition, we expect corrections due to a lower-distance cutoff in the spin-spin interaction. As follows from Eq. (B.5), this yields an additional contribution to the ψ^2 term in the Hamiltonian (7.5), proportional to R^{-d} . Thus, in this Hamiltonian \bar{v} is replaced by $\bar{v}(1 + \bar{v}_1 R^{-d})$. This is in agreement with Ref. [4], where a shift $\propto R^{-d}$ was predicted. For $d > 2$ the latter shift dominates the contribution $R^{-2d/(4-d)}$, but for the analysis of the Monte Carlo data in this chapter it is inconsequential, because we only consider $d = 2$, which is a special case. Namely, for $d = 2$ we obtain instead of Eq. (7.21) the following solution of Eq. (7.20),

$$\frac{r'_0}{R^2} = l^2 \left(\frac{r_0}{R^2} + c \frac{u}{R^4} \ln l \right) = l^2 \frac{1}{R^2} \left(r_0 + c \frac{u}{R^2} \ln l \right). \quad (7.22)$$

Thus, we find, upon substitution of the crossover scale, that the shift in the reduced temperature has the form $(p+q \ln R)/R^2$, where the constant p comes from a multiplicative factor introduced by the crossover criterion. In Ref. [4], $d = 2$ was already suggested as a special case, with possibly logarithmic corrections. The renormalization argument shows that such a $\ln R$ term is indeed present.

Now, let us return to Eq. (7.4), where we omitted quartic (and higher) terms in kR . It follows from the renormalization scenario that terms proportional to k^{2n} transform as $k^{2n}l^{2-2n}$ under the first renormalization transformation and hence are irrelevant for $n > 1$. The behaviour of these terms under the second renormalization transformation is less simple, but again quartic and higher terms do not influence the leading terms; see, e.g., Ref. [8, Section VII.6].

Besides, it can be seen that the structure of the coefficient of the ϕ^2 term does not depend on the details of the spin–spin interaction. For example, replacing the interaction (B.1) with $K(\mathbf{r}) = cR^{-d} \exp[-(r/R)^2]$ leads to precisely the same structure of the LGW Hamiltonian and hence to the same scaling relations involving R . This is in agreement with the universality hypothesis.

In addition, the renormalization description explains why the interaction range must be large to observe the predicted powers of R in the critical amplitudes: only for systems with R large the renormalization trajectory starts in the neighbourhood of the Gaussian fixed point and hence only these systems will accurately display the corresponding R dependence. Finally, in the finite-size scaling description, the system size must be sufficiently large in order to observe the crossover to Ising-like critical behaviour: we require that the rescaling factor b is minimal of order unity, or $L = \mathcal{O}(R^{4/(4-d)})$.

7.3 Monte Carlo results and comparison with the theoretical predictions

7.3.1 Definition of the model

We have carried out Monte Carlo simulations for two-dimensional Ising systems consisting of $L \times L$ lattice sites with periodic boundary conditions and an extended range of interaction. Each spin interacts equally with its z neighbours lying within a distance R_m , as defined in Eqs. (7.1) and (B.1) with R replaced by R_m and $d = 2$. The Monte Carlo simulations were carried out using the cluster algorithm described in Chapter 2. Following Ref. [4] we define the effective range of interaction R as

$$R^2 \equiv \frac{\sum_{j \neq i} |\mathbf{r}_i - \mathbf{r}_j|^2 K_{ij}}{\sum_{j \neq i} K_{ij}}$$

$$= \frac{1}{z} \sum_{j \neq i} |\mathbf{r}_i - \mathbf{r}_j|^2 \quad \text{with } |\mathbf{r}_i - \mathbf{r}_j| \leq R_m. \quad (7.23)$$

Table 7.1 lists the values of R_m^2 for which we have carried out simulations, as well as the corresponding values of R^2 . The ratio between R^2 and R_m^2 approaches $1/2$, as can be simply found when the sums in Eq. (7.23) are replaced by integrals. Note that the results for $R_m^2 = 18$ and $R_m^2 = 32$ differ from those presented by Mon and Binder, because in Ref. [4] the interactions were for these two system sizes spatially distributed within a *square*, as can be seen from the number of interacting neighbours and the corresponding effective ranges of interaction.

Table 7.1: The range of interaction R_m , the corresponding number of neighbours z and the effective range of interaction R .

R_m^2	2	4	6	8	10	18	32	50	72	100	140
z	8	12	20	24	36	60	100	160	224	316	436
R^2	$\frac{3}{2}$	$\frac{7}{3}$	$\frac{17}{5}$	$\frac{25}{6}$	6	$\frac{148}{15}$	$\frac{81}{5}$	$\frac{517}{20}$	$\frac{1007}{28}$	$\frac{4003}{79}$	$\frac{7594}{109}$

7.3.2 Determination of the critical temperature

The critical temperatures T_c of these systems have been determined using the well-known universal amplitude ratio $Q_L \equiv \langle m^2 \rangle_L^2 / \langle m^4 \rangle_L$. Both in the Ising and in the mean-field limit the critical-point value of this quantity is accurately known. In the mean-field limit, $Q = Q_{\text{MF}} = 8\pi^2 / \Gamma^4(\frac{1}{4}) \approx 0.456947$; see Ref. [7] and Appendix A. In the Ising limit, $Q = Q_{\text{I}} = 0.856216$ (1) [9].

As was noted in Sec. 7.2 and also in Ref. [4], rather large system sizes [$\mathcal{O}(R^2)$] are required to determine T_c , since Q must approach Q_{I} . For $R_m^2 \leq 10$ we have included linear system sizes up to $L = 500$ and for larger ranges we have used system sizes up to $L = 700$ or even $L = 800$ ($R_m^2 = 100, 140$). For each run we have generated 10^6 Wolff clusters after equilibration of the system. The various thermodynamic quantities were sampled after every tenth Wolff cluster. In Fig. 7.2, $Q_L(K_c)$ for $R_m^2 = 140$ is plotted as a function of the system size. One clearly observes the crossover from Q_{MF} (for $L \ll R_m^2$) to Q_{I} (for $L \gg R_m^2$).

In the Ising limit, the finite-size expansion of Q_L reads [see Eq. (3.14)]

$$Q_L(K) = Q + a_1(K - K_c)L^{y_1} + a_2(K - K_c)^2 L^{2y_1} + \dots \\ + b_1 L^{y_1} + b_2 L^{y_2} + \dots. \quad (7.24)$$

K denotes the spin-spin coupling, K_c the critical coupling, and the a_i and b_i are nonuniversal (range-dependent) coefficients. The term proportional to L^{y_2} , with

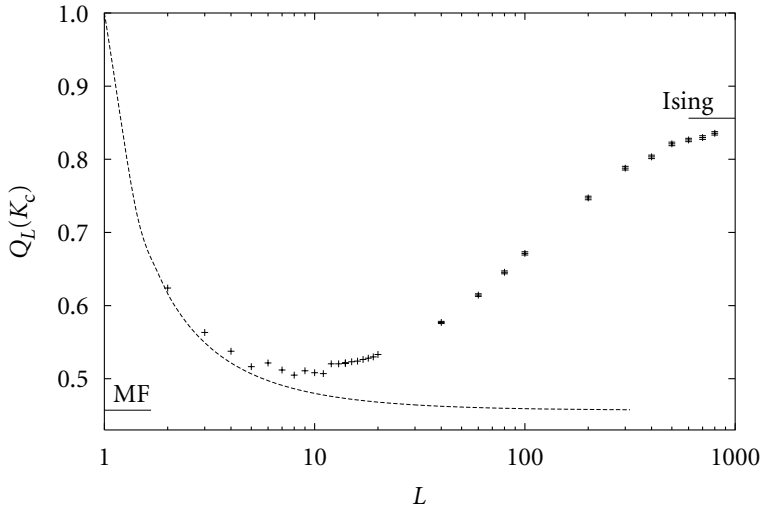


Figure 7.2: The critical-point amplitude ratio $Q_L(K_c)$ for $R_m^2 = 140$ as a function of the system size (discrete points). For large L , $Q_L(K_c)$ approaches the Ising limit $Q_I \approx 0.856216$ (“Ising”). For decreasing L , $Q_L(K_c)$ approaches the mean-field limit $Q_{MF} \approx 0.456947$ (“MF”), until the system size becomes smaller than the range R_m and strong finite-size effects come into play. To illustrate that the system is indeed mean-field-like for these system sizes, we have also plotted Q for finite systems in which all spins interact equally strong (dashed curve, cf. Fig. 2.1). The points for $R_m^2 = 140$ indeed approach this curve for L small.

$y_2 = d - 2y_h$, comes from the field dependence of the analytic part of the free energy. In a ϕ^4 theory this term is absent, as was stated in Sec. 7.2, but in a discrete model it should be allowed for. The exponents y_t , y_h and y_i , which have already been introduced in the previous section, are, respectively, the temperature, magnetic and leading irrelevant exponent for the two-dimensional Ising model; $y_t = 1$, $y_h = \frac{15}{8}$ and $y_i = -2$. Table 7.2 displays the results of a least-squares fit according to Eq. (7.24), where y_t , y_i and y_2 were kept fixed at their theoretical values. For comparison we have included the estimates for K_c from Ref. [4]. Except for $R_m^2 = 10$ there is good agreement between the respective estimates. The discrepancy for $R_m^2 = 10$ may be explained by the limited range of system sizes in Ref. [4]. Furthermore, for $R_m^2 = 2$, which corresponds to the Ising model with nearest and next-nearest neighbour interactions, an accurate transfer-matrix estimate of the critical coupling exists, $K_c = 0.19019269(5)$ [10]. The Monte Carlo result agrees with this value. The results for Q are in good agreement with the expected value Q_I , which confirms not only that universality is satisfied, but also that the maximum system sizes in our simulations are sufficiently large, so that crossover to Ising-like critical behaviour indeed

Table 7.2: The amplitude ratio Q and critical coupling K_c for the various ranges of interaction studied in this section. The numbers in parentheses denote the errors in the last decimal places. The fourth column shows the estimates for K_c obtained with Q fixed at its Ising value. For comparison, we also list the estimates for K_c given in Ref. [4].

R_m^2	Q	K_c	K_c	K_c [4]
2	0.8556 (5)	0.1901908 (19)	0.1901931 (11)	0.190
4	0.8557 (9)	0.1140216 (18)	0.1140225 (7)	0.11402
6	0.8553 (7)	0.0631917 (8)	0.0631926 (4)	
8	0.8553 (13)	0.0510460 (10)	0.0510467 (4)	0.05106
10	0.8563 (9)	0.0324136 (5)	0.03241352 (18)	0.032463
18	0.8555 (14)	0.0185335 (3)	0.01853367 (9)	
32	0.853 (3)	0.01075152 (25)	0.01075182 (7)	
50	0.856 (6)	0.00657274 (26)	0.00657276 (5)	
72	0.854 (4)	0.00464056 (16)	0.00464064 (4)	
100	0.850 (8)	0.00325903 (15)	0.00325905 (5)	
140	0.862 (17)	0.00234637 (19)	0.00234631 (2)	

has taken place, as it should for an accurate determination of K_c . In fact, the error margins on K_c can be reduced significantly by fixing Q at its Ising value in Eq. (7.24) (see Table 7.2). Figure 7.3 illustrates the shift of $1/(zK_c) \propto T_c$ as a function of R^{-2} . Even close the mean-field limit ($R^{-2} \rightarrow 0$), the deviation of $1/(zK_c)$ from 1 appears not truly linear. Therefore we have tried to identify the logarithmic term, which was suggested in Ref. [4] and derived from the renormalization scenario in Sec. 7.2, by writing the following expression for the critical coupling,

$$zK_c = 1 + \frac{p + q \ln R}{R^2}. \quad (7.25)$$

In Fig. 7.4 we have plotted $\Delta \equiv (zK_c - 1)R^2$ versus $\ln R$. Indeed, for large values of R the points lie approximately on a straight line, confirming the presence of the logarithmic correction.

Since an estimate of $T_c(R)$ for (very) large R will be required in the second part of this chapter, we have fitted an expression of the form (7.25) to the numerical data. It turned out to be necessary to add a higher-order correction:

$$T_c = T_c^{\text{MF}} + \frac{a_1}{R^2} [1 + a_2 \ln R^2] + \frac{a_3}{R^4}, \quad (7.26)$$

where $T_c^{\text{MF}} = 1$. A least-squares fit for $16 \lesssim R^2 \lesssim 70$ ($32 \leq R_m^2 \leq 140$) yielded $a_1 = -0.267$ (6), $a_2 = 1.14$ (3) and $a_3 = -0.27$ (3). The curve described by Eq. (7.26) is also shown in Fig. 7.3.

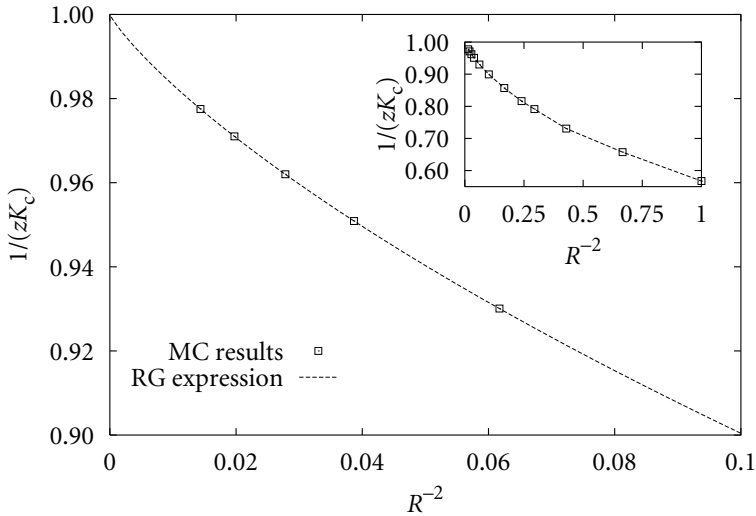


Figure 7.3: Plot of $1/(zK_c)$ versus R^{-2} . The dashed line denotes Eq. (7.26) fitted to the Monte Carlo data. The inset shows $1/(zK_c)$ over the full range of R^{-2} between the Ising and the mean-field limit.

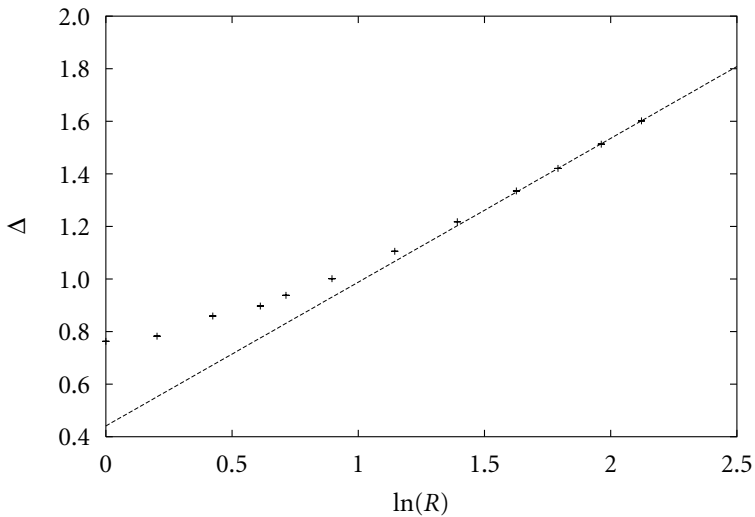


Figure 7.4: $\Delta \equiv (zK_c - 1)R^2$ versus $\ln R$. For large R the graph strongly suggests the presence of a logarithmic correction in the shift of the critical temperature. The error bars do not exceed the symbol size.

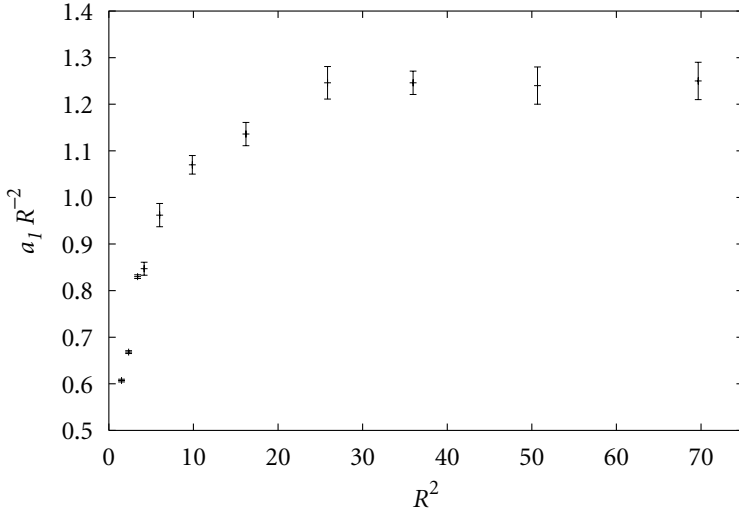


Figure 7.5: Range dependence of the amplitude of the temperature-dependent argument of the finite-size scaling function of the universal amplitude ratio Q .

Another $\ln R$ correction was suspected in Ref. [4] in the temperature-dependent argument of the finite-size scaling functions. This argument is proportional to $R^{-2(2\gamma_t-d)/(4-d)} = R^{-2\alpha/[v(4-d)]}$; see Eqs. (7.14) and (7.15). For $d = 2$, $\alpha = 0$ implies a logarithmic divergence of the specific heat and hence one might expect a similar logarithmic factor here. On the other hand, we have not found a mechanism in the renormalization scenario which could explain such a factor. Therefore, we have numerically examined the range dependence of the coefficient a_1 in Eq. (7.24). Since $(K - K_c)$ is proportional to R^{-2} , we must first divide a_1 by R^2 . Figure 7.5 displays this quantity as a function of the range. For small ranges, there is a strong dependence on R , but the coefficients seem to approach a constant value in the large-range limit. This suggests that a logarithmic correction factor is absent.

7.3.3 Range dependence of the magnetization density

We have sampled the absolute magnetization density, $\langle |m| \rangle$, for which the range dependence is given by Eq. (7.14). This quantity has been fitted to the following finite-size expansion,

$$m_L(K, R) = L^{y_h-d} \left\{ d_0(R) + d_1(R)[K - K_c(R)]L^{y_t} + d_2(R)[K - K_c(R)]^2 L^{2y_t} + \dots + e_1(R)L^{y_i} + \dots \right\}, \quad (7.27)$$

where we now have explicitly indicated the range dependence of the parameters. The critical couplings found from this quantity agree well with those obtained from the

Table 7.3: The exponent γ_h and the critical amplitude $d_0(R)$ of the magnetization for the various ranges of interaction. The third column shows the estimates for γ_h obtained with K_c fixed at the most accurate values shown in Table 7.2.

R_m^2	γ_h	γ_h	$d_0(R)$
2	1.8745 (7)	1.8749 (3)	0.9533 (4)
4	1.8763 (15)	1.8756 (4)	0.8706 (5)
6	1.873 (3)	1.8767 (13)	0.7937 (10)
8	1.873 (3)	1.8754 (8)	0.7523 (7)
10	1.874 (2)	1.8748 (7)	0.6783 (6)
18	1.871 (3)	1.8740 (12)	0.5816 (6)
32	1.875 (6)	1.8744 (9)	0.4929 (11)
50	1.873 (7)	1.876 (2)	0.4181 (18)
72	1.865 (5)	1.8752 (16)	0.3742 (8)
100	1.867 (9)	1.877 (2)	0.3296 (8)
140	1.895 (13)	1.879 (3)	0.2938 (13)

amplitude ratio Q and the exponent γ_h , listed in Table 7.3, is in good agreement with the exact value $15/8$. Furthermore, we have made a least-squares fit with K_c fixed at the most accurate values obtained from Q . The corresponding estimates for γ_h are also shown in Table 7.3. They lie even closer to $15/8$, which again corroborates that all systems belong to the Ising universality class. From the critical amplitudes $d_0(R)$ we can derive the leading R dependence of the magnetization. To increase the accuracy, the values in Table 7.3 were determined with γ_h fixed at its theoretical value. As can be seen from the log-log plot in Fig. 7.6, the approach to the asymptotic scaling behaviour is very slow. Therefore we have determined the scaling exponent in two different ways. A straight line through the points for the three largest ranges yielded $d_0(R) \propto R^{-0.738(13)}$, in agreement with the predicted exponent $-3/4$ [Eq. (7.14)]. Inclusion of the correction factor $[1 + R^{-2}(\tilde{a}_1 + \tilde{a}_2 \ln R)]$, as predicted from Eq. (7.19), allowed us to include *all* data points in the fit and yielded $d_0(R) \propto R^{-0.756(5)}$, also in good agreement with the predicted exponent. The corresponding curve is shown in Fig. 7.6 as well.

7.3.4 Range dependence of the susceptibility

The magnetic susceptibility can be calculated from the average square magnetization,

$$\chi = L^d \langle m^2 \rangle. \quad (7.28)$$

We thus expect the following finite-size scaling behaviour:

$$\chi_L(K, R) = s_0 + L^{2\gamma_h - d} \{ p_0(R) + p_1(R)[K - K_c(R)]L^\nu \}$$

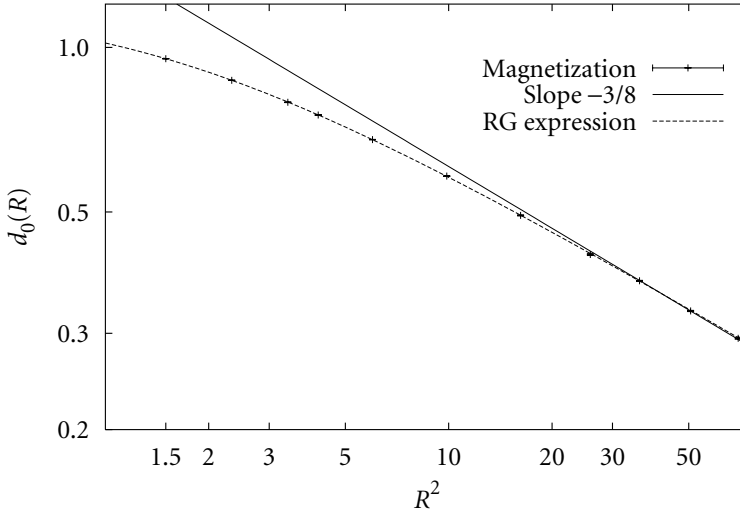


Figure 7.6: The critical amplitude $d_0(R)$ of the absolute magnetization density versus R^2 and the renormalization prediction fitted to the data (dashed line).

$$+ p_2(R)[K - K_c(R)]^2 L^{2y_t} + \dots + q_1(R)L^{y_i} + \dots \} . \quad (7.29)$$

The term s_0 comes from the analytic part of the free energy. Because it tends to interfere with the term proportional to $q_1(R)$, we have ignored it in the further analysis. Again, the critical couplings obtained from a least-squares fit lie close to those in Table 7.2 and the estimates for y_h agree with the Ising value (see Table 7.4). By repeating the fits with K_c fixed at the most accurately known values, the values for y_h lie even closer to $15/8$ (third column of Table 7.4). From the parameter $p_0(R)$, plotted in Fig. 7.7, we can extract the leading range dependence of the susceptibility. A straight line through the amplitudes for the three largest ranges gave $p_0(R) \propto R^{-1.46(3)}$. For a curve (including the first correction term) through the amplitudes it was necessary to include the data for all ranges $R^2 \geq 7/3$ in the fit, in order to determine the coefficient of the $\ln R$ factor. This yielded $p_0(R) \propto R^{-1.47(2)}$. Both exponents are in good agreement with the predicted value $2(3d - 4y_h)/(4 - d) = -3/2$.

7.3.5 Spin–spin correlation function

The finite-size scaling behaviour of the spin–spin correlation function $g(|\mathbf{r}|)$ closely resembles that of the magnetic susceptibility χ , as may be expected from the fact that χ is the spatial integral of g . We also expect the range dependence of the two quantities to be the same. We have sampled the correlation function over half the

Table 7.4: The exponent γ_h and the critical amplitude $p_0(R)$ of the magnetic susceptibility for the various ranges of interaction. The third column shows the estimates for γ_h obtained with K_c fixed at the most accurate values shown in Table 7.2.

R_m^2	γ_h	γ_h	$p_0(R)$
2	1.8754 (9)	1.8748 (2)	0.9743 (9)
4	1.8753 (12)	1.8752 (3)	0.8136 (7)
6	1.8740 (18)	1.8761 (10)	0.6762 (14)
8	1.873 (2)	1.8750 (6)	0.6076 (9)
10	1.874 (3)	1.8741 (6)	0.4943 (7)
18	1.874 (4)	1.8740 (11)	0.3620 (9)
32	1.868 (4)	1.873 (2)	0.2622 (9)
50	1.862 (6)	1.874 (3)	0.1914 (7)
72	1.863 (17)	1.870 (4)	0.1534 (8)
100	1.870 (6)	1.874 (4)	0.1180 (8)
140	1.86 (3)	1.870 (5)	0.0954 (9)

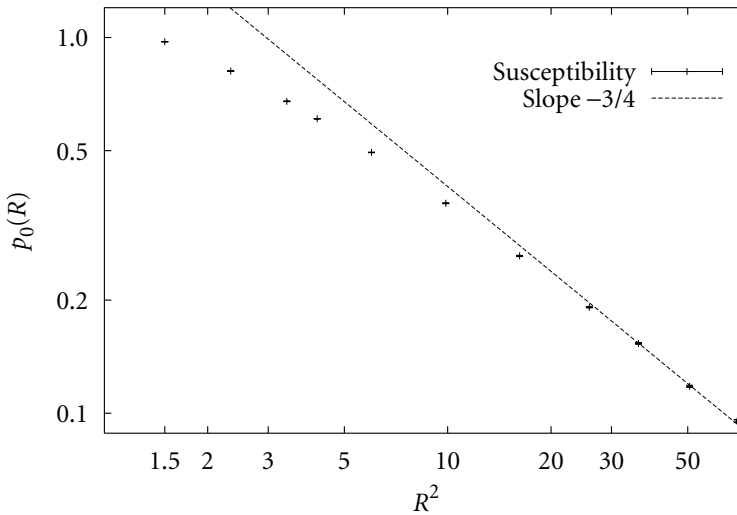


Figure 7.7: The critical amplitude $p_0(R)$ of the magnetic susceptibility as a function of R^2 .

Table 7.5: The exponent γ_h and the critical amplitude $\nu_0(R)$ of the spin–spin correlation function for the various ranges of interaction. The third column shows the estimates for γ_h obtained with K_c fixed at the most accurate values shown in Table 7.2.

R_m^2	γ_h	γ_h	$\nu_0(R)$
2	1.8759 (8)	1.8754 (3)	0.7907 (8)
4	1.8744 (12)	1.8750 (3)	0.6609 (6)
6	1.8748 (19)	1.8765 (11)	0.5489 (12)
8	1.8746 (17)	1.8754 (6)	0.4930 (8)
10	1.875 (3)	1.8741 (7)	0.4011 (7)
18	1.874 (4)	1.8745 (10)	0.2934 (7)
32	1.873 (4)	1.8747 (18)	0.2137 (6)
50	1.864 (7)	1.876 (3)	0.1537 (8)
72	1.860 (8)	1.871 (4)	0.1238 (7)
100	1.872 (9)	1.876 (4)	0.0949 (7)
140	1.86 (3)	1.871 (3)	0.0771 (8)

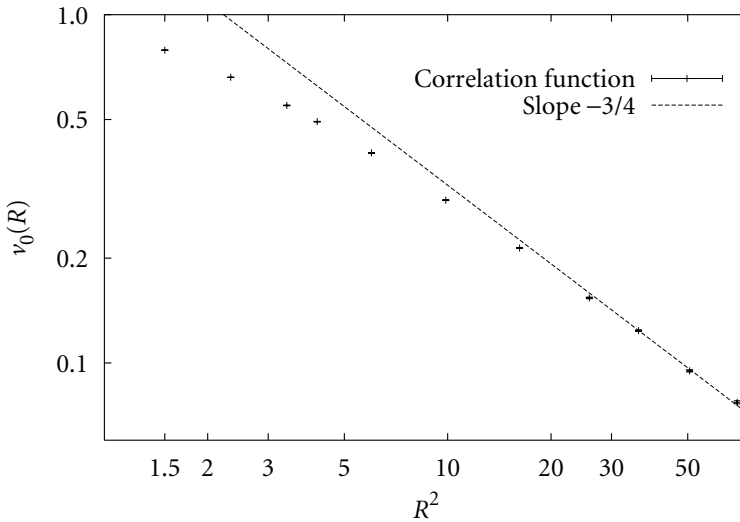


Figure 7.8: The critical amplitude $\nu_0(R)$ of the spin–spin correlation function versus R^2 .

system size and analyzed it using the expansion

$$g_L(K, R) = L^{2y_h - 2d} \{v_0(R) + v_1(R)[K - K_c(R)]L^{y_t} + v_2(R)[K - K_c(R)]^2 L^{2y_t} + \dots + w_1(R)L^{y_i} + \dots\}. \quad (7.30)$$

The constant term in (7.29) is not present here (see Secs. 3.5.3 and 3.5.4). Table 7.5 shows the results for y_h , both with K_c free and fixed. In the latter case, y_h is in accurate agreement with its theoretical value, just as for the magnetization density and the magnetic susceptibility. Figure 7.8 shows a log–log plot of the critical amplitude $v_0(R)$ as a function of the range. A fit of a straight line through the points with $R^2 > 35$ (i.e., $R_m^2 \geq 72$) yielded $v_0(R) \propto R^{-1.46^{(3)}}$, whereas a curve through all points with $R^2 \geq 7/3$ gave $v_0(R) \propto R^{-1.49^{(2)}}$. Both estimates are again in good agreement with the predicted exponent $-3/2$.

7.4 Crossover scaling

In addition to the verification of the range dependences of critical amplitudes, the Monte Carlo results of the previous section also allow a determination of the crossover functions for various quantities. This crossover from Ising-like to classical critical behaviour has attracted renewed attention in recent years. As mentioned in Sec. 7.1, sufficiently close to the critical point the systems under consideration exhibit critical exponents belonging to the Ising universality class. At larger distances from the critical point, but still within the critical region, classical (mean-field-like) critical exponents are observed. Although this appears to be a well-established picture, the precise nature of the crossover between these two universality classes is still subject to investigation. For example, Anisimov *et al.* recently claimed [11] to have observed (in several ionic solutions) an “effective” susceptibility exponent which varied *nonmonotonically* from its classical value $\gamma_{MF} = 1$ to its 3D Ising value $\gamma_1 \approx 1.24$ when the critical point was approached. Later, the possibility of such behaviour within the critical domain was questioned by Bagnuls and Bervillier, see Refs. [12, 13]. On the other hand, Fisher has argued [14] that nonmonotonical variation of effective critical exponents is not necessarily an indication of nonuniversal behaviour. Other questions concern the size of the crossover region, which is expected to span several decades in the crossover variable [15], and the size of the temperature region around T_c within which Ising-like behaviour is observed [16]. Until now it has turned out to be very difficult to accurately observe the full crossover region in numerical simulations. A major effort has been undertaken in Ref. [2] for three-dimensional polymer mixtures, where crossover occurs as a function of the polymer chain length. However, despite chain lengths of up to 512 monomers, the results did not span the full crossover region. This was the original motivation for Mon and Binder [4] to turn their attention to the two-dimensional Ising model

with a variable range of interaction. In two dimensions one can not only access larger interaction ranges, but also both asymptotic regimes are known exactly and the variation of the critical exponents is considerably larger than in the crossover from 3D Ising-like critical behaviour to classical critical behaviour. Nevertheless, even in these two-dimensional systems the mean-field regime turned out to be only barely reachable.

In the next section, we show that our numerical results allow a full mapping of the finite-size crossover curves for various quantities. However, these curves describe the *finite-size* dependences of critical amplitudes, which have (to our knowledge) not been observed experimentally. Therefore we have also carried out simulations at temperatures farther from the critical temperature in order to observe the *thermal* crossover of these quantities. The results of these simulations are presented as well. The fact that in our model both the temperature distance from the critical point and the interaction range can be varied turns out to be essential to observe the full crossover region.

The remainder of this chapter is organized as follows. In Sec. 7.5 we start with finite-size crossover scaling. We discuss the required system sizes and interaction ranges and obtain the crossover curves for the absolute magnetization density, the magnetic susceptibility, the spin–spin correlation function over half the system size and the amplitude ratio Q . Thermal crossover scaling is treated in Sec. 7.6, where we consider the approach of T_c both in the symmetric phase ($T > T_c$) and in the state of broken symmetry ($T < T_c$). Again, crossover curves are obtained for the order parameter and the susceptibility. The various aspects of these curves are discussed in some detail. Graphs of the logarithmic derivatives of the crossover curves, which can be associated with so-called effective critical exponents as measured in experiments, are presented in Sec. 7.7.

7.5 Finite-size crossover scaling

7.5.1 General considerations

It has been shown by Binder and Deutsch [17] that crossover scaling can be combined with finite-size scaling by including the dependence on the crossover variable in the probability distribution function of the order parameter. Indeed, just as crossover in the thermodynamic limit is described as a function of the reduced temperature divided by the Ginzburg number, it can be described as the function of a size-dependent crossover variable G in finite systems. In Ref. [4], this crossover variable was derived as $G = LR^{-4/(4-d)}$. This also follows from the renormalization treatment in Sec. 7.2; cf. in particular Eq. (7.6), in which one requires the coefficient of the ϕ^4 term to be much smaller than that of the ϕ^2 term, $uL^{4-d}/R^4 \ll 1$. This

again leads to the crossover parameter $LR^{-4/(4-d)}$, where for the moment we assume that u is of order unity.

In Sec. 7.3, we focused our attention on the critical finite-size amplitudes in the limit of $L \rightarrow \infty$. Here we will examine the crossover in the corresponding data for *finite* system sizes at $T = T_c$. Since the crossover regime is expected [14, 15] to span several decades in the crossover variable $G = L/R^2$, it is numerically not feasible to observe both asymptotic regimes by merely varying the system size L while keeping the range R fixed. Therefore we construct the curve by combining the results for various values of R , cf. Ref. [2]. Indeed, the Ising regime ($L/R^2 \gg 1$) is easily reachable, although the results for very small ranges do not conform well to the leading R dependence of the critical scaling functions [4] and are thus, at first sight, not well suited for constructing the crossover curve. The mean-field regime ($L/R^2 \ll 1$), however, poses more substantial problems. If the linear system size L is made too small, the numerical results exhibit strong finite-size effects. Therefore L must be at least of the order of the interaction range. More precisely, boundary effects will occur for systems for which $L \approx R_m$ and the smallest possible value of the crossover variable G is roughly equal to $R_m/R^2 \approx \sqrt{2}/R$. Thus, large ranges are required to reach the regime where $G \ll 1$. Although we can handle these in an efficient way using our dedicated cluster algorithm, one problem still remains. Namely, the finite-size crossover scaling is valid *at* the critical temperature. Any deviation from this temperature will lead to systematic errors in the analysis. Since the (range-dependent) critical temperatures are determined in the Ising limit, i.e., from system sizes $L > R^2$, large interaction ranges require *very* large system sizes for an accurate determination of T_c . For example, the most efficient way to obtain data for $G \approx 0.02$ is to simulate a system with $L = 100$ and $R_m = 100$ ($R \approx 70$). However, an accurate determination of $T_c(R = 70)$ requires system sizes of at least $L = 5000$, whereas our simulations were restricted to system sizes up to 1000×1000 lattice sites. This problem was avoided by using expression (7.26) to calculate the critical temperatures for these interaction ranges.

7.5.2 Absolute magnetization density

In the Ising regime, the absolute magnetization density scales (at criticality) asymptotically as $\langle |m| \rangle = L^{-1/8} d_0(R)$, where the critical amplitude d_0 is a function of R , $d_0 \propto R^{-3/4}$ (see Sec. 7.3.3). In the mean-field regime $\langle |m| \rangle$ does not depend on R , but is simply proportional to $L^{-1/2}$. When plotting $\langle |m| \rangle$ as a function of $G = L/R^2$ a data collapse is obtained if it is multiplied by a factor $L^x R^{-(2x-1)}$. This resulting quantity is proportional to $G^{x-1/8}$ in the Ising regime and to $G^{x-1/2}$ in the mean-field regime. A suitable choice is $x = 1/2$, because this yields a quantity which is still independent of R in the mean-field regime. Indeed, it is shown in Appendix A that

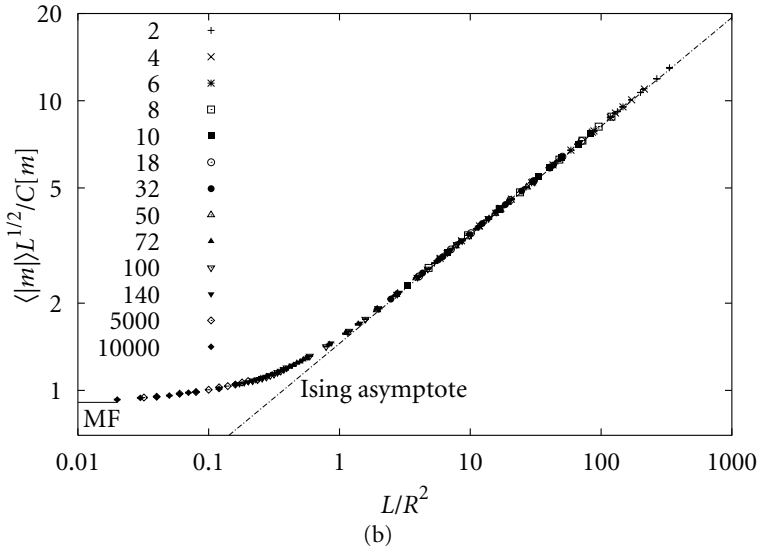
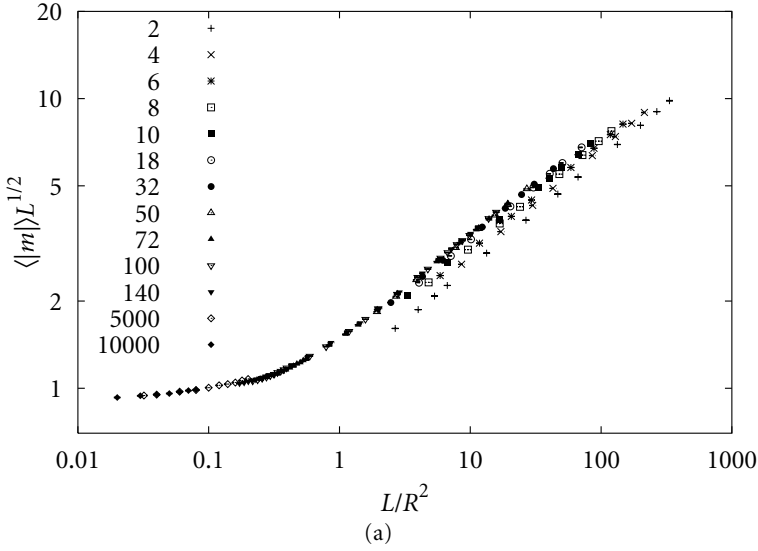


Figure 7.9: (a) Finite-size crossover curve for the absolute magnetization density multiplied by the square root of the system size. (b) The same graph but now the range-dependent corrections predicted by renormalization theory have been divided out. The correction factor abbreviated by $C[m]$ stands for the factor between square brackets in Eq. (7.32). A perfect collapse is obtained for all system sizes and interaction ranges. Both the exact mean-field limit (indicated by “MF”) and the Ising asymptote with slope $3/8$ are confirmed by the data. In this and all following figures the numbers in the key refer to values for R_m^2 .

in a two-dimensional system in which all spin–spin interactions are equally strong,

$$\langle |m| \rangle = 12^{1/4} \frac{\Gamma(\frac{1}{2})}{\Gamma(\frac{1}{4})} \frac{1}{\sqrt{L}} + \mathcal{O}\left(\frac{1}{L^{3/2}}\right) \quad (7.31)$$

and $\langle |m| \rangle \sqrt{L}$ will thus approach $12^{1/4} \Gamma(1/2)/\Gamma(1/4) = 0.909890588\dots$ in the limit of $G \rightarrow 0$. Remark that our requirement $L > \sqrt{2}R$ unambiguously relates the limit $G \rightarrow 0$ to the mean-field ($R \rightarrow \infty$) limit. In Fig. 7.9(a) we have plotted the absolute magnetization density multiplied by the square root of the system size versus the crossover variable. Interaction ranges from $R_m^2 = 2$ to $R_m^2 = 10000$ were included, where the data for $R_m^2 = 5000$ and $R_m^2 = 10000$ (spanning the range $0.02 \lesssim G \lesssim 0.2$) have been obtained at temperatures calculated from Eq. (7.26): $K_c(R_m = \sqrt{5000}) = 6.3746(3) \times 10^{-5}$ and $K_c(R_m = \sqrt{10000}) = 3.18491(9) \times 10^{-5}$. The crossover curve evidently spans approximately three decades in G . In the limit of $G \rightarrow 0$ it gradually approaches a horizontal line. For $G \gg 1$ the picture is not very clear. The data points for each single value of R lie on a straight line with slope $3/8$, corresponding to the Ising asymptote, but the asymptotes only coincide for large ranges (cf. Fig. 4 in Ref. [4]). The reason for this is that, as mentioned above, for small ranges the critical amplitudes do not conform to the leading $R^{-3/4}$ dependence. This can be cured by invoking the renormalization treatment of Sec. 7.2. Indeed, the theory predicts the structure of the corrections to the leading R dependence of the critical amplitude,

$$d_0 = b_0 R^{-3/4} \left[1 + \frac{1}{R^2} (b_1 + b_2 \ln R^2) \right]. \quad (7.32)$$

This “finite-range correction” has been derived in Sec. 7.2; see also Sec. 7.3.3. It is illustrated graphically in Fig. 7.6, where we have plotted the result of a least-squares fit of Eq. (7.32) to the data. The curve clearly yields an excellent description of the critical amplitudes, even for small ranges. We have used this fit to construct a clear crossover curve for the magnetization density on which the data for all values of R collapse. To this end, all data are divided by the correction factor between square brackets in Eq. (7.32). The result is shown in Fig. 7.9(b). One observes that in the Ising regime all data perfectly collapse on a common asymptote with slope $3/8$. For G small, the data indeed approach the mean-field prediction (7.31). The fact that at $G \approx 0.2$ the data for $R_m^2 = 5000$ and $R_m^2 = 10000$ coincide with those for $R_m^2 = 72, 100, 140$ confirms that the critical temperatures for the large ranges have been estimated accurately. The center of the crossover region lies between $G = 0.1$ and $G = 1.0$ which shows that the parameter u is indeed of order unity. Finally, it is particularly encouraging that no remaining finite-size effects, causing deviations from the curve, are visible in Fig. 7.9(b), despite the fact that the correction factor was calculated in the $L \rightarrow \infty$ limit and hence does not compensate for such higher-order finite-size effects.

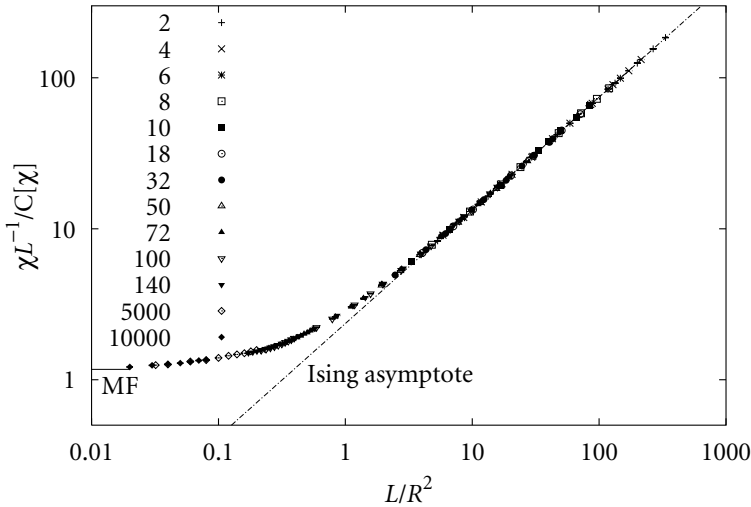


Figure 7.10: Finite-size crossover curve for the magnetic susceptibility divided by the system size. The range-dependent correction factor $C[\chi]$ [the factor between square brackets in Eq. (7.33)] has been divided out, as discussed in the text. Both the mean-field limit and the Ising asymptote (slope 3/4) are confirmed by the data.

7.5.3 Magnetic susceptibility

The procedure described above for the absolute magnetization density can be applied to the magnetic susceptibility χ , which we have calculated from the average square magnetization, $\chi = L^d \langle m^2 \rangle$. At $T = T_c$, the susceptibility is in the Ising regime proportional to $L^{7/4} R^{-3/2}$, and in the mean-field regime it scales proportional to L . To obtain a data collapse for χ as a function of G , one has to multiply the finite-size data by $L^x R^{-(2x+2)}$, where a suitable choice is given by $x = -1$. In the mean-field limit, χ/L approaches $\sqrt{12} \Gamma(3/4) / \Gamma(1/4) = 1.17082866 \dots$ (see Appendix A). As shown in Sec. 7.2, the deviation from the leading range dependence of the critical amplitude is very similar to that of the absolute magnetization density,

$$p_0 = q_0 R^{-3/2} \left[1 + \frac{1}{R^2} (q_1 + q_2 \ln R^2) + \frac{q_3}{R^4} \right], \quad (7.33)$$

where now one additional higher-order correction is required. Therefore we only show the resulting crossover curve for the susceptibility after the data have been divided by the correction factor between square brackets, see Fig. 7.10. Again, both the mean-field asymptotic result and the Ising asymptote (slope 3/4) are clearly reproduced, with a perfect collapse for all ranges.

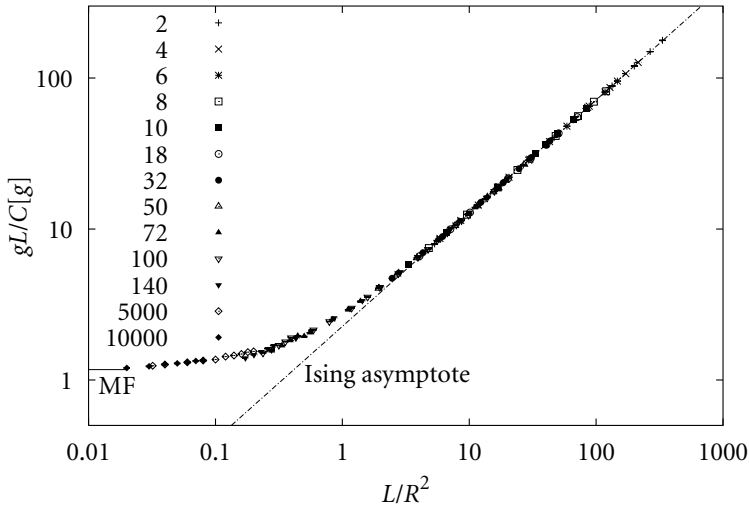


Figure 7.11: Finite-size crossover curve for the spin–spin correlation function multiplied by the system size. A range-dependent correction factor (abbreviated as $C[g]$) has been divided out, as discussed in the text. Both the mean-field limit and the Ising asymptote (slope $3/4$) are confirmed by the data.

7.5.4 Spin–spin correlation function

In our simulations we have sampled the spin–spin correlation function over half the system size, which scales both in the Ising regime and in the mean-field regime as χ/L^2 . Thus, we obtain a data collapse by multiplying the finite-size data by $L^x R^{-(2x-2)}$, in which we have set $x = 1$. After correcting for the higher-order range-dependent corrections in the critical amplitude [which have the same structure as those in Eq. (7.33)] we obtain the graph shown in Fig. 7.11. The full crossover curve can be mapped and shows a close resemblance to that for the susceptibility, including the approach of the asymptotic mean-field value. In the range $0.2 \lesssim L/R^2 \lesssim 1.0$, the data do not precisely coincide on a smooth curve. This is due to nonlinear finite-size effects, which are for the spin–spin correlation function apparently larger than for the absolute magnetization density or the magnetic susceptibility. We will pay more attention to these deviations when discussing the universal amplitude ratio (see below).

7.5.5 Universal amplitude ratio

The amplitude ratio $Q_L \equiv \langle m_L^2 \rangle^2 / \langle m_L^4 \rangle$ is a size-dependent quantity, which takes a universal value Q in the $L \rightarrow \infty$ limit. That is, it is calculated by taking the ratio of the square of the magnetization density and the fourth power of it in a finite geom-

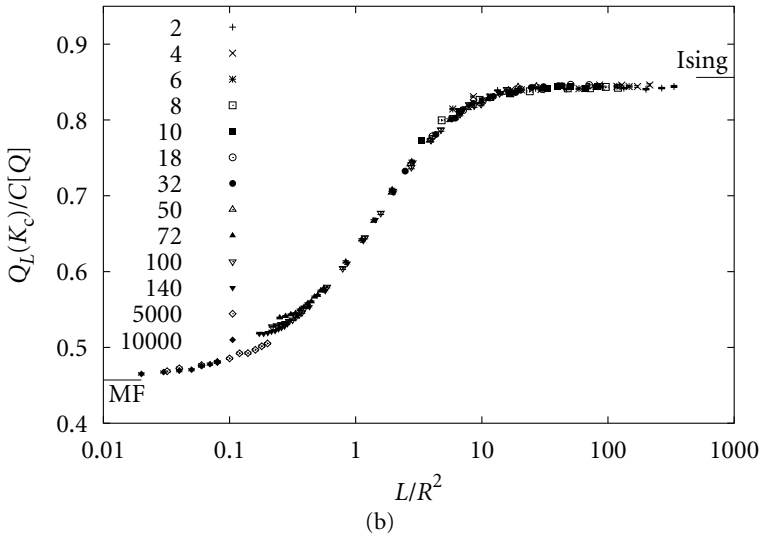
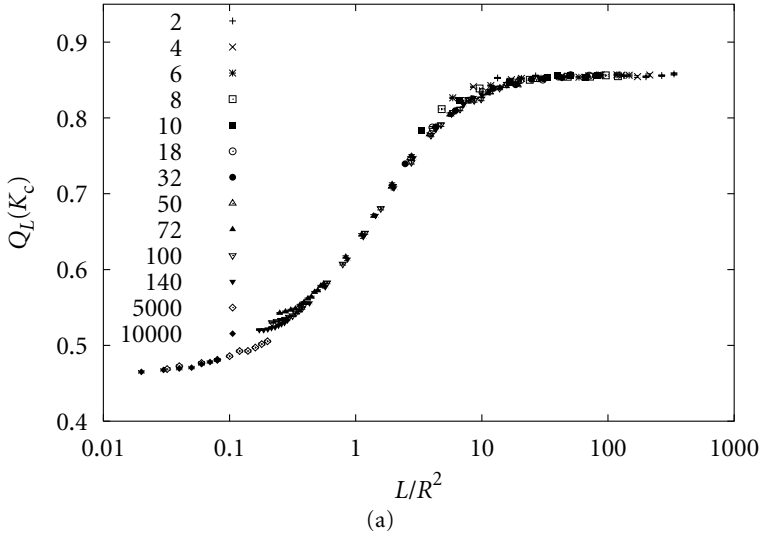


Figure 7.12: Finite-size crossover curves for the amplitude ratio Q . Figure (a) shows the curve without any additional corrections, whereas in (b) a range-dependent correction factor $C[Q]$ [see Eq. (7.34)] has been divided out. For small values of the crossover variable L/R^2 the mean-field limit is reproduced and for large values of L/R^2 the Ising limit is approached. For a further discussion see the text.

entry and subsequently taking the limit $L \rightarrow \infty$. In the disordered phase ($T > T_c$), Q_L approaches the Gaussian value $Q = 1/3$ and in the ordered phase ($T < T_c$) it approaches the maximum value $Q = 1$. At criticality, the amplitude ratio is known exactly in the mean-field case and to a high accuracy in the two-dimensional Ising model, see Sec. 7.3.2. In Fig. 7.2, $Q_L(K_c)$ has been plotted for a large interaction range ($R_m^2 = 140$) as a function of the system size. Although the approach of the Ising value is clearly visible for L large, for small system sizes Q first decreases toward Q_{MF} and then starts to show strong nonlinear finite-size effects. Evidently, it is a better approach to construct the true crossover curve for $Q(K_c)$ by plotting finite-size data for Q for various ranges versus the crossover variable. This is shown in Fig. 7.12(a). Several remarks apply to this graph. In the first place, one notes that L/R^2 is indeed the appropriate crossover variable: a reasonable collapse is obtained for all values of L and R . However, some remarkable deviations from this scaling behaviour are present, which are most clearly visible in the range $0.2 < L/R^2 < 0.6$, but also present around $L/R^2 = 10$. Similar effects were already observed in the results for the spin–spin correlation function, but now the effects stand out much more pronounced because for the amplitude ratio we have employed a linear instead of a logarithmic vertical scale. These deviations are due to nonlinear finite-size corrections, as can be seen clearly by zooming in into the deviations, see Fig. 7.13. The data points for $R_m^2 = 5000$ and $R_m^2 = 10000$ may serve as a reference for the location of the “true” crossover curve. One observes that for each of the ranges $R_m^2 = 72, 100$

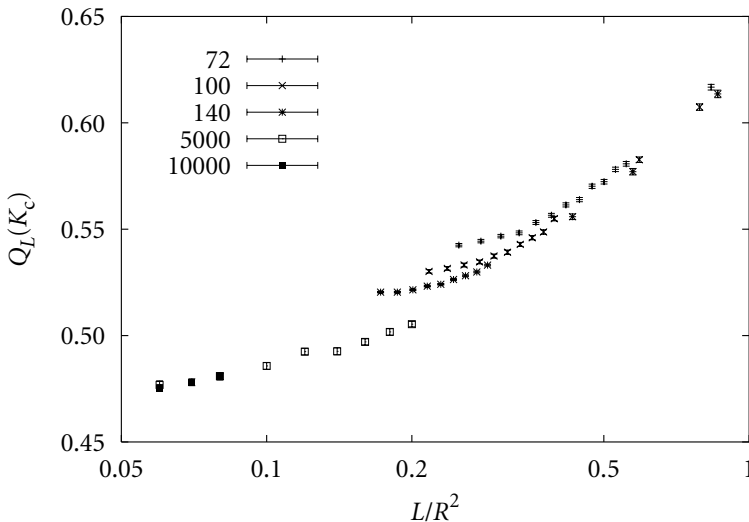


Figure 7.13: A detailed view of Fig. 7.12(a) showing the deviations from the crossover curve for very small system sizes.

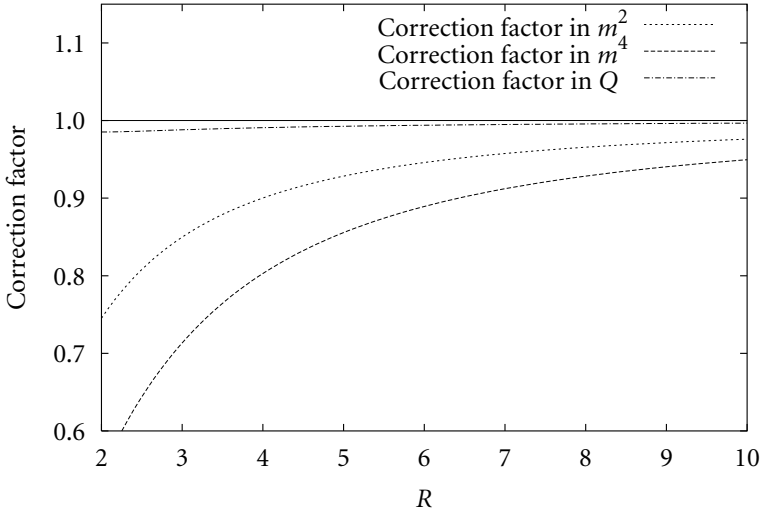


Figure 7.14: The range-dependent correction factors $C[m^2] = C[\chi]$, $C[m^4]$ and $C[Q]$ in $\langle m^2 \rangle$, $\langle m^4 \rangle$ and Q , respectively, as determined by least-squares fits to the critical amplitudes extracted from the Monte Carlo data. The line at height 1 is drawn for reference. One observes that $C[Q]$ lies very close to, although not exactly at, unity.

and 140 the deviations from this curve increase with *decreasing* system size, which indeed shows that the effects are caused by finite-size corrections. For example, if the deviations had been caused by an inaccurate determination of the critical temperature, the effects would have increased with increasing system size. Unfortunately, it is not easy to separate these corrections from the leading crossover behaviour (except graphically), unless the full crossover function is known (which in turn would limit the use of a numerical determination). Of course this problem can be circumvented by determining the crossover curve at these values for G from systems with a larger system size and a larger interaction range. The deviations around $L/R^2 = 10$ are caused by the same effect, but now for systems with small R . Although the amplitude ratio is more sensitive—even if one takes into account the difference in scale—to these finite-size effects than $\langle m^2 \rangle = \chi/L^2$ and $\langle m^4 \rangle$ individually (the curve for the latter is not shown here, but its smoothness is comparable to that of the susceptibility), Q is less sensitive to corrections to the leading range dependence. Indeed, for $\langle m^4 \rangle$ these corrections are again of the form $[1 + R^{-2}(s_1 + s_2 \ln R^2) + R^{-4}s_3]$ and Q must thus be divided by

$$\frac{[1 + R^{-2}(q_1 + q_2 \ln R^2) + R^{-4}q_3]^2}{1 + R^{-2}(s_1 + s_2 \ln R^2) + R^{-4}s_3}. \quad (7.34)$$

The coefficients s_1 , s_2 and s_3 have been determined from a least-squares fit to the critical amplitudes of $\langle m^4 \rangle$ and q_1 , q_2 and q_3 come from Eq. (7.33). Figure 7.14 shows the correction factors for $\langle m^2 \rangle$, $\langle m^4 \rangle$ and Q . Evidently, the latter factor (7.34) is much closer to unity than the former two. Figure 7.12(b) shows $Q_L(K_c)$ divided by the correction factor (7.34), which indeed exhibits only slightly less scatter than the graph without this correction factor. In particular the deviations for the larger ranges do not disappear.

7.6 Thermal crossover scaling

7.6.1 General considerations

The finite-size crossover scaling studied in the previous section is an intrinsic finite-size effect which is not observable in thermodynamic systems. For this reason it is important to study its temperature-dependent counterpart as well. This so-called *thermal* crossover, which was from a phenomenological scaling point of view already considered in Ref. [18], is of course closely related to finite-size crossover: in finite systems crossover to mean-field-like behaviour occurs when the *system size* has been decreased to the appropriate power of the interaction range (i.e., $L \sim R^{4/(4-d)}$ or $L \sim R^2$ for $d = 2$), whereas in the temperature-dependent case this crossover occurs when the temperature distance to the critical point is such the *correlation length* has become of the order of an appropriate power of the interaction range. More precisely, the crossover location in the latter case is determined by the Ginzburg criterion, $t^{(4-d)/2} R^d u^{-1} \approx 1$, where u is the coefficient of the ϕ^4 term in the LGW Hamiltonian. It should be kept in mind that these considerations are valid only *within the critical region*, i.e., care must be exercised to keep the reduced temperature $t = [T - T_c(R)]/T_c(R)$ sufficiently small. When studying thermal crossover in practical simulations one has the additional complication that sufficiently close to T_c the correlation length will always be bounded by the finite system size, which is precisely the situation one wants to avoid. So relatively large system sizes are required.

As follows from the Ginzburg criterion, the appropriate scaling variable in two dimensions is tR^2 and one can therefore study thermal crossover effects by varying the interaction range as well. This is essential because of the following. For small values of R , t has to be made rather large to cross over to classical critical behaviour and it is possible that one leaves the critical region before reaching the classical regime. On the other hand, if one only studies systems with large interaction ranges, t has to be made very small to observe Ising-like critical behaviour. However, for such small values of t extremely large system sizes are required to avoid finite-size effects. Therefore we have constructed, just as in the previous section, crossover curves from data for various ranges. We have carried out simulations for the interaction ranges studied in Sec. 7.3 at temperatures further below T_c and also generated data for the

Table 7.6: Some properties of the additional ranges used to span the full thermal crossover region. $R_m^2 = 5000$ has been included for completeness; it has only been used for the finite-size crossover scaling. The first three columns list the squared range of interaction R_m^2 , the corresponding number of neighbours z and the squared effective range of interaction R^2 . Furthermore the critical coupling K_c as calculated from Eq. (7.26) and the mean-field approximation for the critical coupling $K_c^{\text{MF}} = 1/z$ are shown.

R_m^2	z	R^2	K_c	K_c^{MF}
500	1580	$\frac{99449}{395} \approx 251.770$	$6.379 (2) \times 10^{-4}$	6.3291139×10^{-4}
1000	3148	$\frac{394530}{787} \approx 501.309$	$3.1904 (6) \times 10^{-4}$	3.1766201×10^{-4}
4000	12580	$\frac{1259568}{629} \approx 2002.49$	$7.9594 (5) \times 10^{-5}$	7.9491256×10^{-5}
5000	15704	$\frac{9813759}{3926} \approx 2499.68$	$6.3746 (3) \times 10^{-5}$	6.3678044×10^{-5}
10000	31416	$\frac{6545445}{1309} \approx 5000.34$	$3.18491 (9) \times 10^{-5}$	3.1830914×10^{-5}

interaction ranges $R_m^2 = 500, 1000, 4000$ and 10000 . Table 7.6 summarizes some properties of these systems. Simulations have been carried out down to temperatures as low as $T \approx 0.5T_c$. For the order parameter, crossover can only be studied in the phase of broken symmetry, but for the susceptibility we have also considered the symmetric ($T > T_c$) phase. Since in this phase no saturation effects occur, much smaller interaction ranges suffice to span the full crossover region, as we will show below.

7.6.2 Absolute magnetization density

As derived in Ref. [4] and Sec. 7.2 the absolute magnetization density scales, sufficiently close to the critical point, as $\langle |m| \rangle \propto (-t)^\beta R^{(2d\beta-d)/(4-d)}$ ($t < 0$), which for the two-dimensional case yields $\langle |m| \rangle \propto (-t)^{1/8} R^{-3/4}$. In the mean-field regime, on the other hand, the magnetization density is simply proportional to $(-t)^{1/2}$. When plotted as a function of tR^2 , a data collapse for all ranges is now obtained if the magnetization density is multiplied by R . Figure 7.15(a) shows the corresponding plot. We will discuss the various aspects of this graph in some more detail. The overall picture suggests that the data roughly follow the Ising asymptote (slope 1/8) for small values of tR^2 and then gradually approach the mean-field asymptote (slope 1/2) for large values of tR^2 . Here “small” and “large” refer to the absolute value of tR^2 and “slope” is generally used for the logarithmic derivative, $d \ln \langle |m| \rangle / d \ln |t|$. For very small values of tR^2 the data start to deviate from the Ising asymptote at an L -dependent location and approximately follow (for temperatures closer to T_c) a horizontal line. Here one has entered the finite-size regime, where the correlation length is limited by the system size. This is the case which was studied in the previous sec-

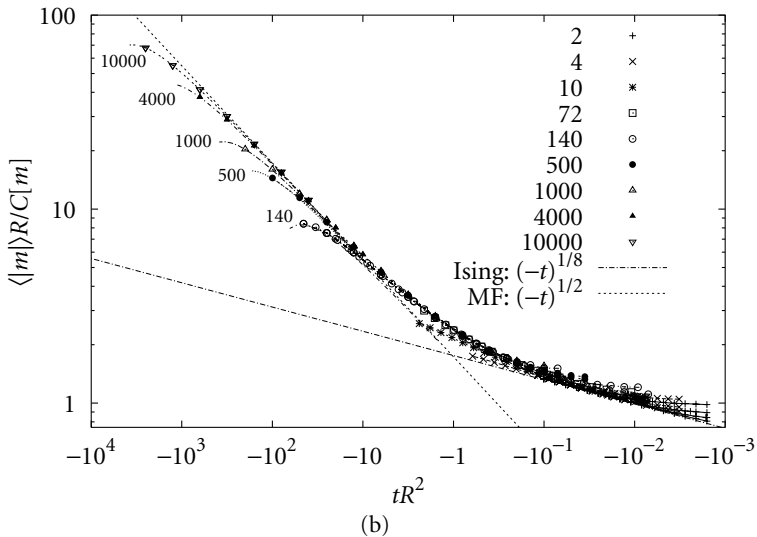
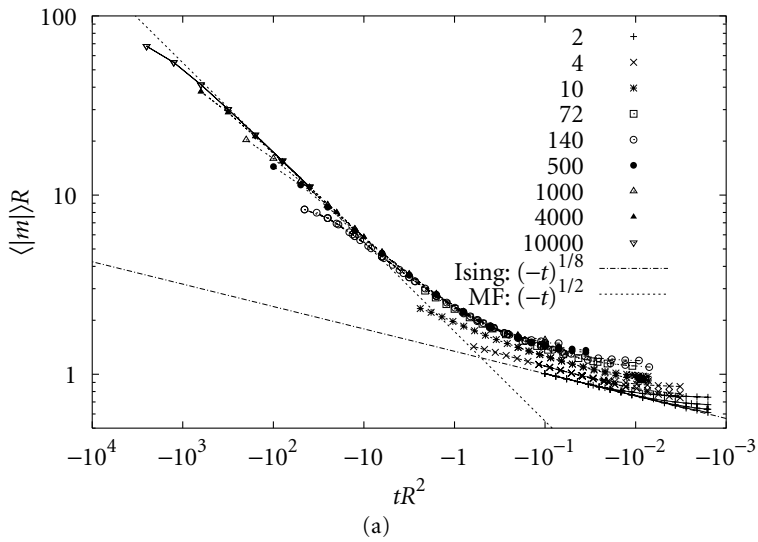


Figure 7.15: Thermal crossover for the absolute magnetization density for various ranges and system sizes, where the range-dependent reduced temperature t is defined as $[T - T_c(R)]/T_c(R)$. In figure (a) no additional correction terms have been used, whereas in (b) the factor $C[m]$ has been divided out. For an extensive discussion of the various features of these graphs the reader is referred to the text.

tion. The width of this regime depends (for general d) both on the system size and the interaction range, as can be read off from the universal scaling functions derived in Sec. 7.2. Indeed, the temperature-dependent argument of these functions is $tL^{y_t}R^{-2(2y_t-d)/(4-d)}$ ($y_t = 1$ in the 2D Ising universality class) and the width of the finite-size regime is thus proportional to $L^{-y_t}R^{2(2y_t-d)/(4-d)} = L^{-1}$. Note that the absence of any range dependence is *not* a general feature and even for the two-dimensional Ising model only true to leading order (cf. Fig. 7.5). Higher-order terms will entail range-dependent factors that involve (for $d = 2$) logarithms of R . Outside the finite-size regime, the data for each individual range first lie approximately on the Ising asymptote, which has been drawn with an amplitude such that it coincides with the data for $R_m^2 = 2$. For the smaller ranges the amplitudes of the asymptotes show a considerable range dependence, whereas for larger ranges the amplitudes converge. Upon further decrease of the temperature (increase of the absolute value of t) several types of behaviour occur: for the smallest range ($R_m^2 = 2$) the data points still lie on the Ising asymptote. For $R_m^2 = 4$ and $R_m^2 = 10$ the data leave the Ising asymptote at sufficiently low temperatures and then follow a nearly straight line with a slope that lies between the Ising and the mean-field asymptote. In these cases one has left the critical region without ever reaching the asymptotic mean-field regime. For each range the data for all system sizes coincide, as they should outside the finite-size regime. For $R_m^2 = 72$ and $R_m^2 = 140$ the mean-field asymptote is approached much closer. However, if the temperature is decreased further below the critical temperature the data points start to deviate from the asymptote again. This effect is caused by saturation of the magnetization and can be quantitatively described with mean-field theory, as we will show below. Turning to even larger ranges, we see that the data now really reach the asymptote with slope $1/2$ and follow it for up to one decade in the crossover variable (for the largest range we have studied) before saturation sets in. Also the exact amplitude $\sqrt{3}$ (see below) of the asymptote is precisely reproduced, which shows again that the critical temperatures of the systems with large interaction ranges have been accurately determined: a deviation would have shifted the graph along the horizontal axis.

We will now first consider the offset of the asymptotes in the Ising regime. Although this effect occurs outside the finite-size regime, we may well hope that the so-called finite-range corrections applied in the previous section [Eq. (7.32)] can be used here as well. Indeed, these corrections are part of the universal scaling functions and although the amplitude $b_0 = \lim_{R \rightarrow \infty} \lim_{L \rightarrow \infty} R^{3/4}L^{1/8} \langle |m_L(K_c)| \rangle$ is a specific limiting value, the range-dependent correction factor does not depend on this limit. Especially the collapse obtained in Fig. 7.9(b) makes it very tempting to apply a similar correction here. On the other hand, these corrections were calculated in the *Ising* regime, which we here are gradually leaving. In Fig. 7.15(b) we show the same data but now divided by the correction factor. Although a perfect collapse is not obtained, the asymptotes lie much closer together than without this correction.

Also the critical amplitude of the Ising asymptote is known exactly. Indeed, by expanding Onsager's expression for the spontaneous magnetization [19, 20],

$$m = \left[1 - \frac{1}{\sinh^4(2J/k_B T)} \right]^{1/8}, \quad (7.35)$$

around the critical point $J/k_B T_c = \frac{1}{2} \operatorname{arcsinh}(1)$ we obtain for $t < 0$

$$m = [4\sqrt{2} \operatorname{arcsinh}(1)(-t) + \mathcal{O}(t^2)]^{1/8} \approx 1.22240995(-t)^{1/8}. \quad (7.36)$$

For the nearest-neighbour Ising model $R = R_m = 1$, so the fact that in Fig. 7.15 along the horizontal axis tR^2 is used instead of t and along the vertical axis $\langle |m| \rangle R$ instead of $\langle |m| \rangle$ does not affect the amplitude of the asymptote. However, the correction factor $C[m]$ [denoting the factor between square brackets in Eq. (7.32)] must of course be taken into account. This correction factor describes the deviation of the critical amplitude $d_0(R)$ from the leading scaling behaviour in terms of a power series in R^{-2} (with coefficients that depend on $\ln R$) and it is not *a priori* clear whether $C[m]$ converges for $R = 1$. It is certainly unlikely that a single term [the term proportional to b_2 in (7.32) vanishes] describes the deviation very well. No exact result for $d_0(R = 1) = \lim_{L \rightarrow \infty} m_L(K_c)L^{1/8}$ is known to us, but from a modest Monte Carlo simulation we found $d_0(R = 1) = 1.0092$ (4). On the other hand, from Eq. (7.32) with $b_0 = 1.466$ (2) and $b_1 = -0.305$ (1) we find $d_0(R = 1) = 1.018$ (4) which differs approximately two standard deviations from the numerical result. Recall that b_0 and b_1 were obtained from a least-squares fit to the critical finite-size amplitudes for $2 \leq R_m^2 \leq 140$. Nevertheless, the relative difference lies below the one-percent level, which cannot be distinguished in our graph. Therefore we have drawn the Ising asymptote with amplitude $[4\sqrt{2} \operatorname{arcsinh}(1)]^{1/8}/(1 + b_1)$ in Fig. 7.15(b) and it indeed turns out to be a precise tangent to the crossover curve.

As mentioned above, also the saturation effects can be described with mean-field theory. Namely, the magnetization follows from the well-known expression [21, 22]

$$m = \tanh\left(\frac{T_c}{T}m\right). \quad (7.37)$$

Rewriting this as $m = (1 + t) \operatorname{arctanh}(m)$ and solving for m one obtains below T_c for small t

$$\begin{aligned} m = & \sqrt{3}(-t)^{1/2} - \frac{2}{5}\sqrt{3}(-t)^{3/2} - \frac{12}{175}\sqrt{3}(-t)^{5/2} - \frac{2}{125}\sqrt{3}(-t)^{7/2} \\ & + \frac{166}{67375}\sqrt{3}(-t)^{9/2} + \mathcal{O}((-t)^{11/2}). \end{aligned} \quad (7.38)$$

The leading term shows the classical value $\beta = 1/2$ and the critical amplitude $\sqrt{3}$. To describe the saturation effects in Fig. 7.15, the first three terms of this series suffice.

Figure 7.15(b) shows for the five largest ranges ($R_m^2 = 140, 500, 1000, 4000, 10000$) the curves

$$\langle |m| \rangle R = \sqrt{3}(-tR^2)^{1/2} \left[1 - \frac{2}{5R^2}(-tR^2) - \frac{12}{175R^4}(-tR^2)^2 \right]. \quad (7.39)$$

For $R_m^2 = 140$ this expression does not precisely coincide with the numerical data, but for the remaining values the curves accurately describe the saturation effects. For these cases the interaction ranges are apparently large enough to suppress the critical fluctuations to a large extent. The lowest temperatures shown in the figure are $T/T_c = 0.52, 0.60, 0.60, 0.68$ and 0.50 for $R_m^2 = 140, 500, 1000, 4000$ and 10000 , respectively. Saturation effects become visible in Fig. 7.15 for $t \lesssim -0.15$, i.e., $T/T_c \lesssim 0.85$. According to Eq. (7.38) the magnetization deviates here approximately five percent from the asymptote. Using Eq. (7.38) we can perform another operation on the numerical data. Namely, the influence of saturation effects in the mean-field model is described by the ratio of the full series expansion on the right-hand side of (7.38) and its first term. As the mean-field expression constitutes an accurate description of the saturation effects for $R_m^2 \geq 500$, the factor between square brackets in Eq. (7.39) will give an accurate description of the *relative* saturation effects (i.e., the ratio of the saturated magnetization and the crossover curve) down to probably even lower interaction ranges. To illustrate this we have divided the data for $R_m^2 \geq 72$ by the corresponding factor. The resulting graph (Fig. 7.16)—in which also the data points in the finite-size regime have been omitted—shows that the data for these large ranges now nicely coincide on one curve, which is the actual crossover curve for the order parameter.

The fact that for different interaction ranges the data (which overlap for considerable intervals of tR^2) coincide on one curve lends strong support to the hypothesis that the crossover curve is universal. Indeed, nonuniversal effects may occur once one has left the critical region. Then, microscopic cutoff effects are no longer negligibly small compared to the *finite* correlation length ξ , which implies that the form of the crossover curve depends on the ratio between ξ and the lattice spacing a . In our simulations we have not measured the correlation length directly, but we can still make a rough estimate from the data. Namely, at the locations marking the boundaries of the finite-size regime for different interaction ranges and system sizes in Fig. 7.15, the correlation length is approximately equal to the system size. From the magnetization densities for $R_m^2 \geq 72$ we conclude that $\xi \approx 0.5/(-t)$, independent of the interaction range. The latter conclusion is in agreement with the above-mentioned renormalization prediction that the width of the finite-size regime is to leading order independent of the interaction range. Thus, at a fixed value of the crossover variable tR^2 the correlation lengths for different ranges have *different* values. However, the crossover curves coincide at fixed tR^2 and hence are independent of the ratio ξ/a .

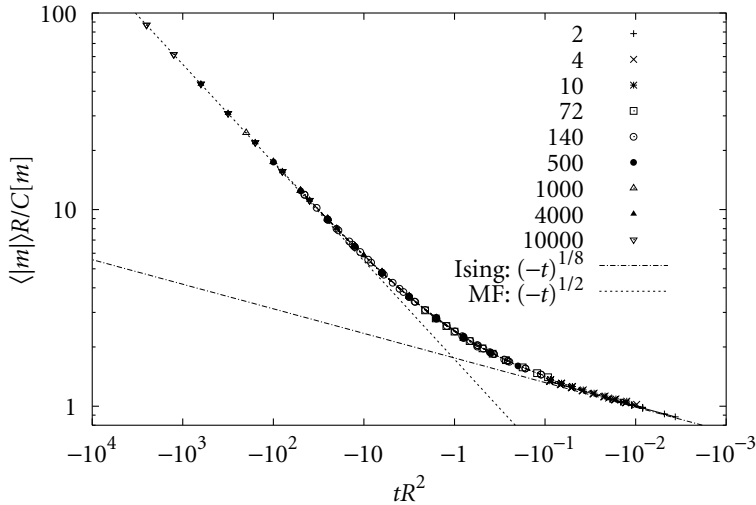


Figure 7.16: Thermal crossover for the absolute magnetization density for various ranges and system sizes, where not only the factor $C[m]$ has been divided out, but also the data for $R_m^2 \geq 72$ have been corrected for saturation effects and data points in the finite-size regime have been omitted.

Finally, we make some observations concerning the size of the crossover region. It is clear that it takes at least between two and three decades in the crossover variable to cross over from Ising-like to classical critical behaviour. Thus, unless one studies systems with a rather large interaction range, one has to go to such a large temperature distance from T_c in order to sufficiently decrease the correlation length compared to the interaction range that one has already left the critical region before observing classical critical behaviour! We note that the center of the crossover region lies in the neighbourhood of $|tR^2| = 1$, which is consistent with a value for u of order unity.

7.6.3 Magnetic susceptibility

Unlike the order parameter, the magnetic susceptibility displays crossover upon approaching the critical point either from below or from above. We will discuss these two situations separately. In the ordered phase, $T \leq T_c$, the magnetic susceptibility is given by the so-called connected susceptibility,

$$\tilde{\chi} = L^d \frac{\langle m^2 \rangle - \langle |m| \rangle^2}{k_B T}. \quad (7.40)$$

In the two-dimensional Ising model with interaction range R this quantity will, close to the critical point, diverge as $(-t)^{-7/4} R^{-3/2}$. Further below T_c it will cross over to

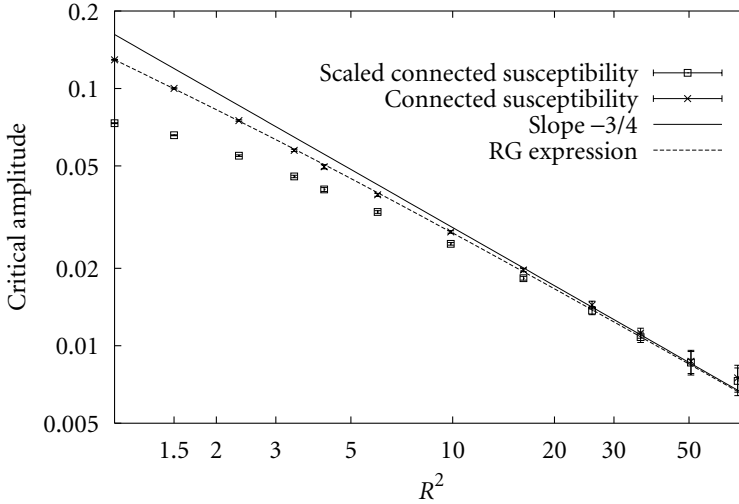


Figure 7.17: Critical amplitude for the connected susceptibility $\tilde{\chi} = L^d(\langle m^2 \rangle - \langle |m| \rangle^2)/k_B T$ as extracted from the thermodynamic limit of $L^{-7/4}\tilde{\chi}_L(K_c)$. The dashed curve indicates the renormalization prediction fitted to the numerical data. Also the critical amplitude of the scaled susceptibility $k_B T_c \tilde{\chi}$ is shown, which for small ranges deviates considerably stronger from the asymptotic behaviour.

classical critical behaviour, where $\tilde{\chi} \propto (-t)^{-1}$. In a graph showing results for various ranges as a function of the crossover variable tR^2 a data collapse is obtained for $\tilde{\chi}/R^2$. However, just as for previous crossover curves, the data for small R will display an offset because of corrections to the leading $R^{-3/2}$ dependence. To determine these deviations we first study the critical amplitude of the connected susceptibility, which was not considered in Sec. 7.3; see Fig. 7.17. The statistical uncertainty of this amplitude is notably larger than for $\langle |m| \rangle$ and $\langle m^2 \rangle$ (cf., e.g., Fig. 7.6), but one can still observe that the asymptotic regime is reached. In this figure we have also plotted the critical amplitude of the so-called scaled susceptibility $k_B T \tilde{\chi}$ which was studied in, e.g., Ref. [4]. Evidently, the latter amplitude shows a much stronger deviation from the leading range dependence, due to the fact that also $T_c(R)$ deviates from T_c^{MF} (Fig. 7.3). Thus, although both amplitudes have the same asymptotic behaviour for large interaction ranges, it is much more difficult to extract this behaviour from medium-range results for $k_B T \tilde{\chi}$ than from the corresponding results for $\tilde{\chi}$. This may partially explain the difficulties experienced in Ref. [4]. The deviations have been fitted to a correction factor of the form $[1 + R^{-2}(\nu_1 + \nu_2 \ln R^2)]$, which we abbreviate as $C[\tilde{\chi}]$.

In Fig. 7.18(a) we show the connected susceptibility, appropriately scaled with R and divided by the correction factor $C[\tilde{\chi}]$, as a function of the crossover variable.

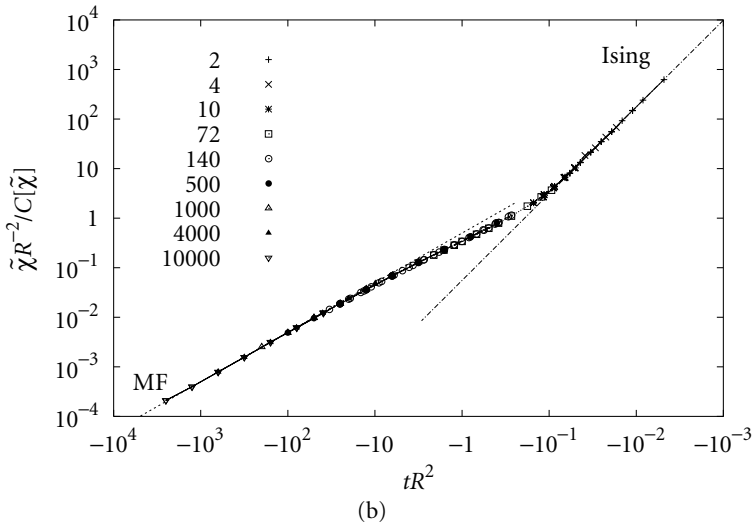
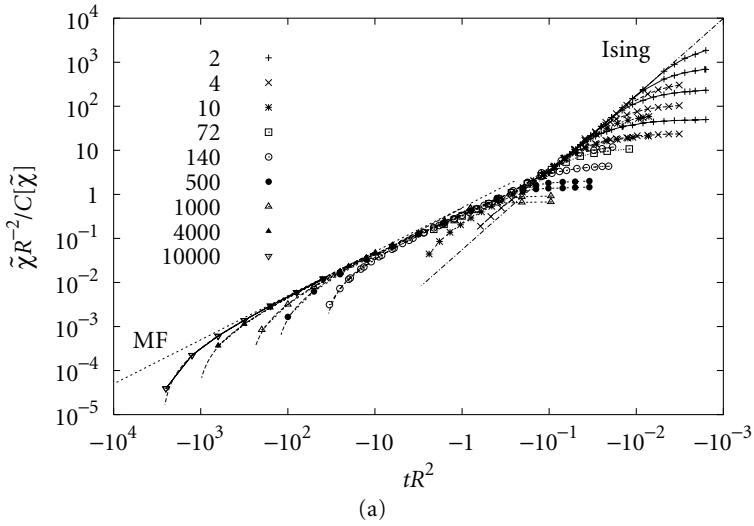


Figure 7.18: Thermal crossover for the connected susceptibility $\tilde{\chi}$ for various ranges and system sizes. A finite-range correction factor $C[\tilde{\chi}]$ has been divided out. Figure (b) has also been corrected for saturation effects for $R_m^2 \geq 72$ and data points in the finite-size regime have been omitted. For a discussion see the text.

Just as for the magnetization density, deviations from the crossover curve are present even after the finite-range corrections have been applied. These effects are either caused by finite-size effects (close to T_c) or by systems that leave the critical region. In the latter case, saturation effects start to come into play. The finite-size effects are clearly recognizable in the rightmost part of the graph, where the curves start to follow horizontal lines. Once the temperature has been sufficiently decreased, the graphs start following an asymptote with slope $-7/4$, on which the data for various ranges quite accurately collapse. The amplitude of this asymptote is simply related to the exactly known amplitude $A^- = 0.025537 \dots$ [23, 24] of the *reduced* susceptibility χ_0 . This reduced susceptibility is defined as $\chi_0 \equiv k_B T \tilde{\chi} / \mu^2$, where μ denotes the magnetic moment of a spin. Also in our calculations this magnetic moment has implicitly been divided out. However, we should keep in mind that we have expressed all temperatures in terms of the mean-field critical temperature, i.e., we have taken $T_c = 1/(zK_c)$, where z denotes the coordination number. For the nearest-neighbour model this yields an additional factor 4 and we thus expect a critical amplitude $2 \operatorname{arcsinh}(1)A^-$. In addition we have to take into account the finite-range correction factor which has been divided out. The question whether this factor is applicable for $R = 1$ has already been discussed in Sec. 7.6.2 [below Eq. (7.36)]. In this case, the difference between the deviation from the leading scaling behaviour as predicted by $C[\tilde{\chi}]$ and the numerical result is approximately 3%, whereas the smallest differences that can be discerned on the logarithmic scale of Fig. 7.18(a) are of the order of 5%. The asymptote with the above-mentioned amplitude divided by $C[\tilde{\chi}]$ indeed lies tangential to the crossover curve, confirming our data. As the temperature is further decreased, the data for systems with small interaction ranges start to follow a line with a slope that lies between that of the Ising and the mean-field asymptotes. This effect is caused by the fact that these systems have left the critical region. For sufficiently large interaction ranges, however, the different curves coincide and have a slope that gradually decreases (in the absolute sense). Although the crossover curve at first varies more rapidly than for the absolute magnetization density, it subsequently only slowly approaches the classical regime and the overall size of the crossover region is again between two and three decades. Remarkably, the slope of the crossover curve passes even *through* the mean-field value -1 before settling at this value for sufficiently low temperatures. In other words, the logarithmic derivative of the connected susceptibility appears to change nonmonotonically from its asymptotic Ising value $-7/4$ to its classical value -1 .

The saturation effects can—just as for the magnetization density—for large ranges be described with mean-field theory. In a mean-field model the magnetic susceptibility is given by

$$\chi = \frac{1 - m^2}{t + m^2}. \quad (7.41)$$

Using Eq. (7.38) we find for $T < T_c$

$$\chi = \frac{1}{-2t} - \frac{9}{10} + \frac{18}{175}(-t) + \frac{18}{175}(-t)^2 + \frac{6714}{67375}(-t)^3 + \mathcal{O}((-t)^4), \quad (7.42)$$

which exhibits the classical value for the susceptibility exponent, $\gamma_{\text{MF}} = 1$ and the critical amplitude $\frac{1}{2}$. Figure 7.18(a) shows the asymptote with this amplitude and one can observe that the crossover curve approaches this asymptote from *below* around $tR^2 = -1$. Also the mean-field curves (7.42) are shown for $R_m^2 = 140, 500, 1000, 4000$ and 10000 and they accurately describe the numerical data. Thus, we have used the ratio between the series expansion (7.42) and the asymptotic behaviour $1/(-2t)$ to remove the saturation effects in Fig. 7.18(a). The resulting graph is shown in Fig. 7.18(b), in which also the data points in the finite-size regime have been omitted in order to obtain a clear crossover curve. The nonmonotonical variation of the slope of this curve is clearly visible.

In the disordered (symmetric) phase, we encounter a different situation. The susceptibility is now given by $\chi' \equiv L^d \langle m^2 \rangle / k_B T$. This is identical to the expression we have used for the finite-size crossover scaling, except that the temperature-dependent factor has been omitted in Sec. 7.5.3. Figure 7.19 shows the critical finite-size amplitudes of both χ' and $\chi = L^d \langle m^2 \rangle$ as a function of the interaction range. We have fitted an expression of the form (7.33) to the data for $R_m^2 \geq 2$. This expression describes the data well, except for the data point at $R_m^2 = 1$, where the deviation is approximately 10%. Just as for the connected susceptibility, the finite-range corrections to the critical amplitude of χ' are much smaller than for χ . In fact, they are so small that they can be completely omitted in the thermal crossover scaling, as illustrated in Fig. 7.20. This graph shows χ'/R^2 as a function of the crossover variable tR^2 for various interaction ranges and system sizes. Outside the finite-size regime, the data follow the Ising asymptote with slope $-7/4$. The exactly known amplitude $2 \operatorname{arcsinh}(1)A^+$, where $A^+ = 0.96258 \dots$ [23, 24], of this asymptote is accurately reproduced by the numerical data. For larger temperatures, the curves gradually approach an asymptote with the mean-field slope -1 . However, some care has to be exercised when interpreting this behaviour. Above T_c , no saturation of the order parameter occurs and the system smoothly passes over to regular (noncritical) behaviour. In this high-temperature region the susceptibility decreases proportional to $1/T$. For small interaction ranges it is this behaviour that one observes in the graph. Only for larger interaction ranges one actually observes classical *critical* behaviour. The latter systems indeed reproduce the mean-field critical amplitude, which is equal to 1 [as follows from Eq. (7.41) with $m = 0$]. Note that, due to the absence of saturation effects, interaction ranges up to $R_m^2 = 1000$ are amply sufficient to observe the full crossover region.

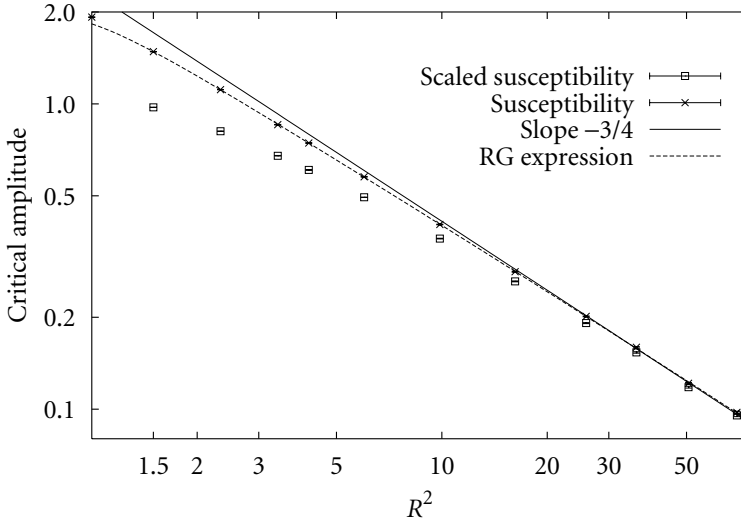


Figure 7.19: Critical amplitude for the susceptibility $\chi' = L^d \langle m^2 \rangle / k_B T$ as extracted from the thermodynamic limit of $L^{-7/4} \chi'_L(K_c)$. The dashed curve indicates the renormalization prediction fitted to the numerical data. The critical amplitude of the scaled susceptibility $k_B T_c \chi'$ (see also Fig. 7.7) is shown as well; for small ranges it deviates considerably stronger from the asymptotic behaviour.

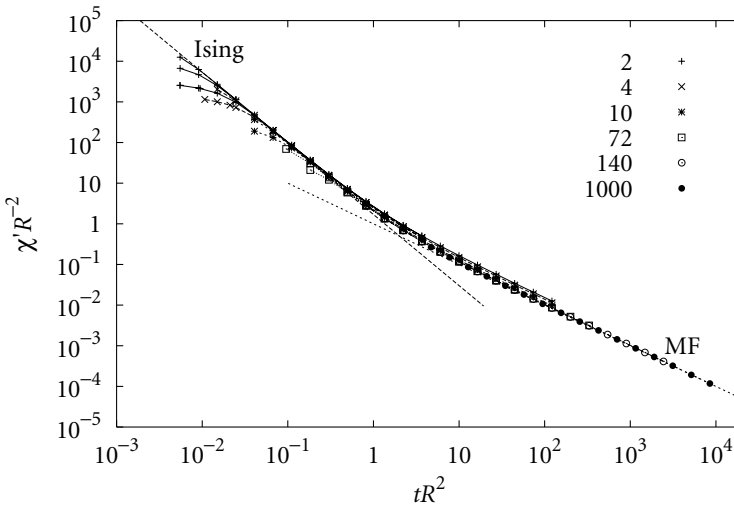


Figure 7.20: Thermal crossover for the susceptibility χ' in the symmetric phase, for various ranges and system sizes. No finite-range corrections have been applied. For a discussion see the text.

7.7 Effective exponents

In several papers (see, e.g., Refs. [11, 14]) the slopes of the crossover functions are described by so-called effective exponents. These exponents can be defined as $\beta_{\text{eff}} \equiv d \ln \langle m \rangle / d \ln |t| = t d \ln \langle m \rangle / dt$ and $\gamma_{\text{eff}} \equiv -d \ln \chi / d \ln |t| = -t d \ln \chi / dt$. In fact, this concept is familiar from the analysis of experimental data since a long time [25], but only a limited amount of theoretical work has addressed these issues. Of course, these exponents change from their Ising values to the classical values in the crossover region. However, the precise variation in the crossover region is unclarified and partially subject to debate. Although these exponents can be read off from the form of the crossover curves presented in the previous section, we consider it worthwhile to present separate graphs displaying β_{eff} , γ_{eff}^- and γ_{eff}^+ , where the superscripts denote the cases $t < 0$ and $t > 0$, respectively. The additional advantage of these exponents is that they follow from data obtained for the same range and hence are not affected by any range-dependent correction factors.

As the graph in Fig. 7.9(b) is particularly smooth, it is tempting to consider its derivative as well. As derived in Sec. 7.2, $\langle |m| \rangle \sqrt{L} \propto (L/R^2)^{\gamma_{\text{h}}-3/2}$. This relation also holds in the mean-field regime, provided that one replaces the magnetic exponent γ_{h} by its starred counterpart $\gamma_{\text{h}}^* \equiv 3d/4 = 3/2$. The asterisk indicates that the exponent is modified due to the dangerous-irrelevant-variable mechanism, as explained in Chapter 4. Thus, while we can rewrite the above-mentioned relation in the Ising regime in terms of conventional critical exponents as $\langle |m| \rangle \sqrt{L} \propto (L/R^2)^{-\beta/\nu+1/2}$, this is not possible in the mean-field regime, since ν_{MF} is not affected by the dangerous-irrelevant-variable mechanism. As an alternative we employ the specific-heat exponent α ; $\langle |m| \rangle \sqrt{L} \propto (L/R^2)^{-2\beta/(2-\alpha)+1/2}$. The fact that the latter relation holds in the mean-field regime while the former does not is a direct manifestation of the violation of hyperscaling. Thus, we define $[2\beta/(2-\alpha)]_{\text{eff}} \equiv \frac{1}{2} - d \ln(\langle |m| \rangle \sqrt{L}) / d \ln(L/R^2)$. This quantity is shown as a function of L/R^2 in Fig. 7.21. Although the size of the error bars is considerable, the crossover from the Ising value $1/8$ (for large values of L/R^2) to the classical value $1/2$ (for small values of L/R^2) is clearly visible.

Turning to thermal crossover, we display in Figs. 7.22, 7.23 and 7.24 the exponents β_{eff} , γ_{eff}^- and γ_{eff}^+ as defined above. The effective magnetization exponent β_{eff} increases monotonically from its Ising value $1/8$ to the classical value $1/2$. In particular do the data for different interaction ranges roughly fall onto the same curve, which supports the hypothesis that the crossover curve is universal. However, one observes that for systems with relatively small interaction ranges the effective exponent does *not* follow this curve. This effect, caused by saturation of the order parameter, can clearly lead to misleading results in experiments! In Fig. 7.23 the non-monotonical variation of γ_{eff}^- between $7/4$ and 1 is clearly visible. This may be considered as a manifestation of what Fisher [14] calls an “underswing”. The occurrence

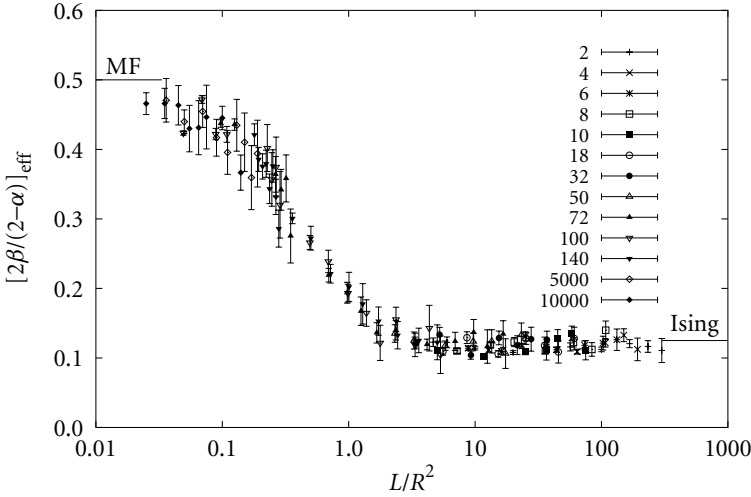


Figure 7.21: The effective exponent $[2\beta/(2 - \alpha)]_{\text{eff}}$ as obtained from the finite-size crossover curve for $\langle |m| \rangle \sqrt{L}$.

of such a nonmonotonical crossover has been predicted by various renormalization calculations for the crossover from Ising to XY and Heisenberg critical behaviour *above* T_c , see, e.g., Refs. [26–28] and references therein. Furthermore, an exponent $\gamma_{\text{eff}} = 0.88$ (3) has been measured in the symmetric phase in micellar solutions [29]. Fisher [14] has suggested that an effective susceptibility exponent that takes a value $\gamma_{\text{eff}} < 1$ in the crossover region might be a general feature of crossover from 3D Ising to classical critical behaviour and noted that concrete calculations yielding such an effective exponent would be valuable. In Ref. [14], a first-order ε -expansion is quoted for the exponent crossover function,

$$\gamma_{\text{eff}} = 1 + (\gamma_1 - \gamma_{\text{MF}})E(\ln[|t/G|]), \quad (7.43)$$

where G is the crossover temperature or Ginzburg number and

$$E(\ln y) = 1/(1 + y^{\varepsilon/2}). \quad (7.44)$$

In our case, the ratio t/G is directly proportional to the crossover variable tR^2 . To describe the experimental results from Ref. [29], Fisher used the following extension of Eq. (7.44),

$$E(\ln y) = (1 + py^{\varepsilon/2})/[1 + (p + 1)y^{\varepsilon/2} + qy^{\varepsilon}]. \quad (7.45)$$

Even though one may not expect such an expansion to converge for $d = 2$, we have drawn expression (7.43) in Fig. 7.23, where we have taken the function $E(\ln y)$ from

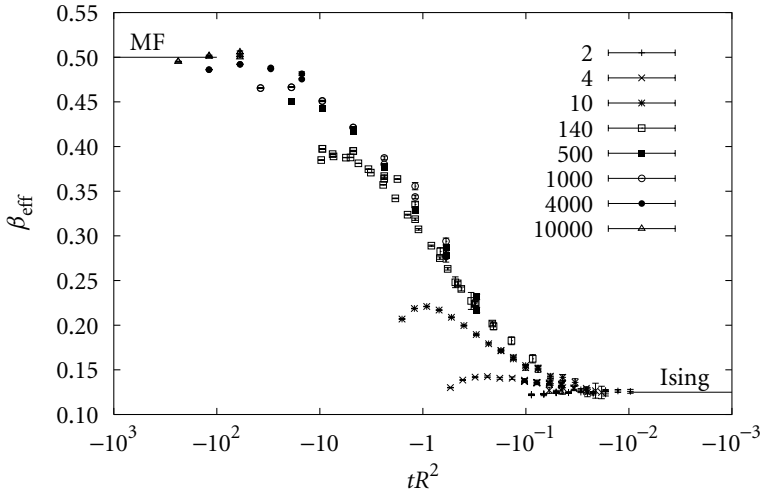


Figure 7.22: The effective magnetization exponent β_{eff} describing the logarithmic derivative of the crossover function for the magnetization density.

Eq. (7.45), set $\varepsilon = 2$ and adjusted p and q such that the curve constituted a reasonable description of the data. Clearly, no conclusions should be drawn from this curve, especially because Eq. (7.45) has been proposed for the symmetric phase. In addition, for $d = 2$ the exponent $\varepsilon/2$ is a very poor approximation for the exponent $\theta \equiv -y_i/y_t = 2$, which is actually expected to appear in the function $E(\ln y)$. As follows from Fig. 7.24, the behaviour above T_c is completely different. Here we have used expression (7.43) with Eq. (7.44) to describe the data. Except for a shift along the horizontal axis (a proportionality constant in the Ginzburg number), no adjustable parameter is present and it is surprising how well the data agree with the theoretical prediction. It would be interesting to calculate the amplitude of the first Wegner correction as a function of R . However, even with the present techniques this would, for the large values of R , require prohibitively large system sizes (to avoid finite-size effects) and thus has not been attempted.

Sometimes experiments have yielded effective exponents in disagreement with the known [3] universality classes, but still satisfying the scaling relations, such as $\gamma_{\text{eff}} + 2\beta_{\text{eff}} = 2 - \alpha_{\text{eff}}$. Here α_{eff} denotes the effective exponent of the specific heat, which in our case is expected to be always (close to) zero, as both the classical and the 2D Ising value of α are equal to zero. This is also confirmed by the close resemblance between Figs. 7.21 and 7.22. Thus, it is interesting to note that this scaling relation is strongly violated in the present case: from Figs. 7.22 and 7.23 we can estimate that $\gamma_{\text{eff}} + 2\beta_{\text{eff}}$ reaches a minimum of approximately 1.4 at $tR^2 \approx -1$.

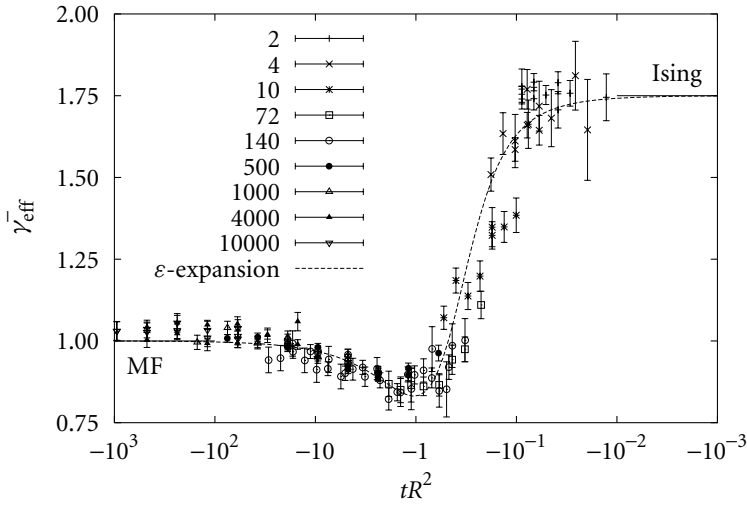


Figure 7.23: The effective susceptibility exponent γ_{eff}^- describing the logarithmic derivative of the crossover function for the connected susceptibility. The results on the left-hand side lie somewhat above the mean-field exponent due to saturation effects.

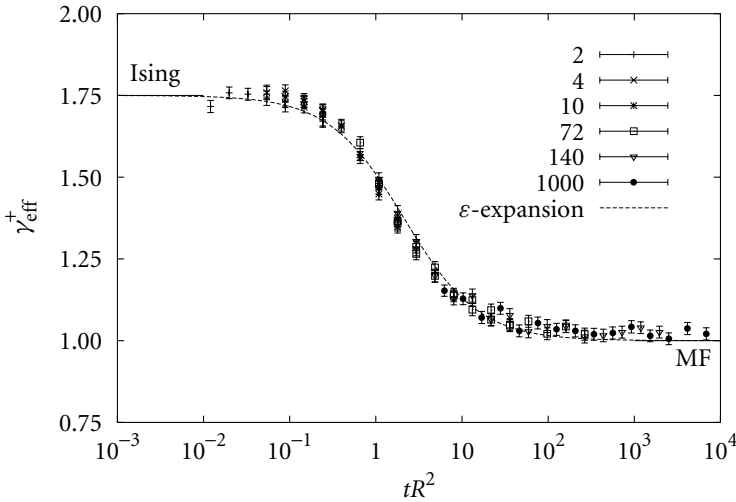


Figure 7.24: The effective susceptibility exponent γ_{eff}^+ describing the logarithmic derivative of the crossover function for the susceptibility above T_c .

7.8 Conclusions

In this chapter, we have derived the dependence of scaling functions on the range of interactions from renormalization-group arguments. The results agree with the predictions of Mon and Binder and yield in addition the corrections to the leading scaling behaviour, including the previously conjectured logarithmic factor in the shift of the critical temperature of two-dimensional systems.

We have also carried out Monte Carlo simulations for systems in which the range of the interactions was large enough to verify the theoretical predictions. It was confirmed with high precision that all examined systems belong to the 2D Ising universality class. Besides the range dependence of critical amplitudes, we also observed the predicted range dependence of the corrections to scaling.

Furthermore, we have presented numerical results for scaling functions describing the crossover from Ising-like to classical critical behaviour in two-dimensional systems. While the general concepts describing this crossover have been developed many years ago, only a limited amount of progress has been made for a long time. Here, it is demonstrated, for the first time, that one can obtain accurate quantitative information on crossover scaling from computer simulations. The full crossover region was covered both for finite-size crossover and thermal crossover above and below T_c . A data collapse has been obtained for all system sizes and interaction ranges, which supports the hypothesis that these crossover functions are universal. Deviations from this curve are present but can be understood from finite-size and saturation effects. The results are in agreement with the previously derived renormalization scenario for these systems.

Working in two dimensions offers the advantage that the exponents and the critical amplitudes are known exactly. More importantly, critical fluctuations are very large in two dimensions, which leads to critical behaviour that strongly differs from classical behaviour and hence to a clearly visible crossover between the two universality classes. We have shown that the magnetization density is described by a smooth crossover curve. The effective exponent, defined as the logarithmic derivative of this curve, increases monotonically from the Ising value to the classical value over two or three decades in the reduced temperature. On the other hand, the effective exponent for the susceptibility has a logarithmic derivative which varies monotonically above the Curie temperature and nonmonotonically below it. The occurrence of nonmonotonic behaviour in the symmetric phase has been inferred from renormalization-group calculations in three dimensions and found long-standing interest. An extension of the present study to $d = 3$ is therefore highly desirable.

References

- [1] V. L. Ginzburg, *Fiz. Tverd. Tela* **2**, 2031 (1960) [*Sov. Phys. Solid State* **2**, 1824 (1960)].
- [2] H.-P. Deutsch and K. Binder, *J. Phys. II (France)* **3**, 1049 (1993).
- [3] M. E. Fisher, *Rev. Mod. Phys.* **46**, 597 (1974).
- [4] K. K. Mon and K. Binder, *Phys. Rev. E* **48**, 2498 (1993).
- [5] P. A. Rikvold, B. M. Gorman and M. A. Novotny, *Phys. Rev. E* **47**, 1474 (1993).
- [6] M. E. Fisher, *Scaling, Universality and Renormalization Group Theory*, in *Proceedings of the Summer School on Critical Phenomena, Stellenbosch, South Africa, 1982*, edited by F. J. W. Hahne (Springer, Berlin, 1983).
- [7] E. Brézin and J. Zinn-Justin, *Nucl. Phys. B* **257** [FS14], 867 (1985).
- [8] S.-k. Ma, *Modern Theory of Critical Phenomena* (Addison-Wesley, Redwood, California, 1976).
- [9] G. Kamieniarz and H. W. J. Blöte, *J. Phys. A* **26**, 201 (1993).
- [10] M. P. Nightingale and H. W. J. Blöte, *J. Phys. A* **15**, L33 (1982).
- [11] M. A. Anisimov, A. A. Povodyrev, V. D. Kulikov and J. V. Sengers, *Phys. Rev. Lett.* **75**, 3146 (1995).
- [12] C. Bagnuls and C. Bervillier, *Phys. Rev. Lett.* **76**, 4094 (1996).
- [13] M. A. Anisimov, A. A. Povodyrev, V. D. Kulikov and J. V. Sengers, *Phys. Rev. Lett.* **76**, 4095 (1996).
- [14] M. E. Fisher, *Phys. Rev. Lett.* **57**, 1911 (1986).
- [15] M. A. Anisimov, S. B. Kiselev, J. V. Sengers and S. Tang, *Physica A* **188**, 487 (1992).
- [16] M. E. Fisher and B. P. Lee, *Phys. Rev. Lett.* **77**, 3561 (1996).
- [17] K. Binder and H.-P. Deutsch, *Europhys. Lett.* **18**, 667 (1992).
- [18] E. Riedel and F. Wegner, *Z. Phys.* **225**, 195 (1969).
- [19] L. Onsager, *Nuovo Cimento (Suppl.)* **6**, 261 (1949).
- [20] B. M. McCoy and T. T. Wu, *The Two-Dimensional Ising Model* (Harvard University Press, Cambridge, Massachusetts, 1973).
- [21] W. L. Bragg and E. J. Williams, *Proc. R. Soc. London A* **145**, 699 (1934).
- [22] R. J. Baxter, *Exactly Solved Models in Statistical Mechanics* (Academic, London, 1982).
- [23] E. Barouch, B. M. McCoy and T. T. Wu, *Phys. Rev. Lett.* **31**, 1409 (1973).
- [24] T. T. Wu, B. M. McCoy, C. A. Tracy and E. Barouch, *Phys. Rev. B* **13**, 316 (1976).
- [25] J. S. Kouvel and M. E. Fisher, *Phys. Rev.* **136**, A1626 (1964).
- [26] D. R. Nelson and E. Domany, *Phys. Rev. B* **13**, 236 (1976).
- [27] D. J. Amit and Y. Y. Goldschmidt, *Ann. Phys. (N.Y.)* **114**, 356 (1978).
- [28] P. Seglar and M. E. Fisher, *J. Phys. C* **13**, 6613 (1980).
- [29] M. Corti and V. Degiorgio, *Phys. Rev. Lett.* **55**, 2005 (1985).

Appendix A

Some exact calculations for the mean-field model

On several occasions in this thesis, finite-size properties of the mean-field model are used as a simple illustration or as a check on various numerical results. Since the calculations of these properties are all based on the same approach we have collected them in this appendix.

The Hamiltonian describing the mean-field model is given by Eq. (2.22). The interaction between each pair of spins is identical and normalized by the number of spins (N) in the system. If the number of down spins is denoted by r , the partition function can be written as

$$Z = \sum_{r=0}^{r=N} c(r) , \quad (\text{A.1})$$

with

$$c(r) = \frac{N!}{r!(N-r)!} \exp \left[\frac{1}{2} K \frac{(N-2r)^2 - N}{N} \right] , \quad (\text{A.2})$$

where we have used Eq. (2.23). The average magnetization per spin is given by $m = (N - 2r)/N$. Replacing the sum in Eq. (A.1) by an integral (which introduces an error of order $1/N$) and changing the integration variable from r to m we find

$$Z = \frac{N}{2} \int_{-1}^{+1} dm \tilde{c}(m) [1 + \mathcal{O}(1/N)] , \quad (\text{A.3})$$

with

$$\tilde{c}(m) = \frac{N!}{\left[\frac{1}{2}N(1-m)\right]! \left[\frac{1}{2}N(1+m)\right]!} \exp \left[\frac{1}{2} K (Nm^2 - 1) \right] . \quad (\text{A.4})$$

The factor $N/2$ in Eq. (A.3) appears due to the change of variables. Likewise, we can write expressions for the average square magnetization density and the average of the fourth power of the magnetization density,

$$\langle m^2 \rangle = \frac{N}{2Z} \int_{-1}^{+1} dm m^2 \tilde{c}(m) [1 + \mathcal{O}(1/N)], \quad (\text{A.5})$$

$$\langle m^4 \rangle = \frac{N}{2Z} \int_{-1}^{+1} dm m^4 \tilde{c}(m) [1 + \mathcal{O}(1/N)]. \quad (\text{A.6})$$

To find the behaviour of these quantities for large N , we can expand $\ln[\tilde{c}(m)]$ using Stirling's formula, which yields

$$\begin{aligned} \ln[\tilde{c}(m)] &= -\frac{1}{2}[N(1-m)+1] \ln \left[\frac{1}{2}N(1-m) \right] \\ &\quad -\frac{1}{2}[N(1+m)+1] \ln \left[\frac{1}{2}N(1+m) \right] \\ &\quad + \frac{1}{2}Nm^2 + f + \mathcal{O}(1/N), \end{aligned} \quad (\text{A.7})$$

where f contains all terms not depending on m and we have set $K = 1$, because we want to evaluate all quantities at criticality. Upon expansion in m we find (\hat{f} is a new constant equal to f plus additional terms not depending on m)

$$\begin{aligned} \ln[\tilde{c}(m)] &= -\frac{1}{12}Nm^4 - \frac{1}{30}Nm^6 - \frac{1}{56}Nm^8 \\ &\quad + \frac{1}{2}m^2 + \frac{1}{4}m^4 + \frac{1}{6}m^6 + \hat{f} + \dots \end{aligned} \quad (\text{A.8})$$

Substituting this for $\tilde{c}(m)$ in Eq. (A.3) and expanding the exponentials yields

$$Z = \frac{N}{2} e^{\hat{f}} \int_{-\infty}^{+\infty} dm e^{-\frac{1}{12}Nm^4} \left(1 - \frac{1}{30}Nm^6 + \frac{1}{2}m^2 \right) [1 + \mathcal{O}(1/N)], \quad (\text{A.9})$$

where we have also extended the integration boundaries to $\pm\infty$, which introduces an error which decays exponentially with N . Indeed, the relative error can be expressed in terms of the incomplete Gamma function,

$$\begin{aligned} \int_1^{\infty} dm e^{-\frac{1}{12}Nm^4} &= \frac{1}{4} \left(\frac{12}{N} \right)^{1/4} \int_{N/12}^{\infty} dx x^{-3/4} e^{-x} \\ &= \frac{1}{4} \left(\frac{12}{N} \right)^{1/4} \Gamma \left(\frac{1}{4}, \frac{N}{12} \right) \\ &= \frac{3}{N} e^{-N/12} \sum_{n=0}^{\infty} \left[(-1)^n \frac{\Gamma(n + \frac{3}{4})}{\Gamma(\frac{3}{4})} \left(\frac{12}{N} \right)^n \right], \end{aligned} \quad (\text{A.10})$$

where in the last line we have used the asymptotic representation of $\Gamma(\alpha, N)$, see Ref. [1, (8.357)].

For the evaluation of Eq. (A.9) and similar expansions of Eqs. (A.5) and (A.6) we use

$$I_k = \int_{-\infty}^{+\infty} dm m^k \exp\left(-\frac{1}{12}Nm^4\right) = \left(\frac{12}{N}\right)^{\frac{k+1}{4}} \frac{1}{2} \Gamma\left(\frac{k+1}{4}\right). \quad (\text{A.11})$$

Thus, each factor m in the integrand yields an extra factor $N^{-1/4}$ in the result and terms of the form Nm^{k+4} are of the same order as terms of the form m^k . Therefore we retain only the terms up to order m^2 and Nm^6 in Eq. (A.8).

After some elementary calculations we find the following expression for the average square magnetization density

$$\langle m^2 \rangle = \sqrt{12} \frac{\Gamma(\frac{3}{4})}{\Gamma(\frac{1}{4})} \frac{1}{N^{1/2}} - \frac{12}{5} \left[\frac{\Gamma(\frac{3}{4})}{\Gamma(\frac{1}{4})} \right]^2 \frac{1}{N} + \mathcal{O}\left(\frac{1}{N^{3/2}}\right), \quad (\text{A.12})$$

i.e., the susceptibility diverges as \sqrt{N} , and for the fourth power of the magnetization density we find

$$\begin{aligned} \langle m^4 \rangle &= 12 \frac{\Gamma(\frac{5}{4})}{\Gamma(\frac{1}{4})} \frac{1}{N} - \frac{12^{3/2}}{5} \frac{\Gamma(\frac{3}{4})}{\Gamma(\frac{1}{4})} \frac{1}{N^{3/2}} + \mathcal{O}\left(\frac{1}{N^2}\right) \\ &= \frac{3}{N} - \frac{12^{3/2}}{5} \frac{\Gamma(\frac{3}{4})}{\Gamma(\frac{1}{4})} \frac{1}{N^{3/2}} + \mathcal{O}\left(\frac{1}{N^2}\right). \end{aligned} \quad (\text{A.13})$$

The dimensionless ratio $Q = \langle m^2 \rangle^2 / \langle m^4 \rangle$ is given by

$$\begin{aligned} Q &= 4 \left[\frac{\Gamma(\frac{3}{4})}{\Gamma(\frac{1}{4})} \right]^2 + \frac{16}{5} \sqrt{3} \left[\frac{\Gamma(\frac{3}{4})}{\Gamma(\frac{1}{4})} \right]^3 \frac{1}{\sqrt{N}} + \mathcal{O}\left(\frac{1}{N}\right) \\ &\approx 0.456947 + 0.214002 \frac{1}{\sqrt{N}} + \mathcal{O}\left(\frac{1}{N}\right). \end{aligned} \quad (\text{A.14})$$

For the absolute magnetization density (studied in Chapter 7), the calculation proceeds in precisely the same fashion, except that m^k in Eq. (A.11) is replaced by $|m|^k$. This yields

$$\begin{aligned} \langle |m| \rangle &= 12^{1/4} \frac{\Gamma(\frac{1}{2})}{\Gamma(\frac{1}{4})} \frac{1}{N^{1/4}} - \frac{12^{3/4}}{5\Gamma(\frac{1}{4})} \left[\frac{\Gamma(\frac{1}{2})\Gamma(\frac{3}{4})}{\Gamma(\frac{1}{4})} - \frac{1}{2} \right] \frac{1}{N^{3/4}} \\ &\quad + \mathcal{O}\left(\frac{1}{N^{5/4}}\right). \end{aligned} \quad (\text{A.15})$$

Finally, the specific heat per spin (see Chapter 6) can be easily calculated from

$$\frac{C}{k_B} = K^2 \left[\frac{1}{Z} \frac{\partial^2 Z}{\partial K^2} - \left(\frac{1}{Z} \frac{\partial Z}{\partial K} \right)^2 \right], \quad (\text{A.16})$$

which, to leading order, reduces to

$$\frac{C}{k_B} = \frac{1}{4} NK^2 (\langle m^4 \rangle - \langle m^2 \rangle^2) = \frac{1}{4} NK^2 \langle m^4 \rangle (1 - Q). \quad (\text{A.17})$$

Using Eqs. (A.13) and (A.14) we find at $K = 1$ in the thermodynamic limit $C/k_B = 0.407290\dots$

References

- [1] I. S. Gradshteyn and I. M. Ryzhik, *Table of Integrals, Series, and Products*, fifth edition (Academic, San Diego, 1994).

Appendix B

Fourier transform of a spherically shaped interaction profile

We define the following isotropic spin–spin interaction K_d (the subscript d denotes the dimensionality):

$$K_d(\mathbf{r}) \equiv \begin{cases} cR^{-d} & \text{if } |\mathbf{r}| \leq R \\ 0 & \text{if } |\mathbf{r}| > R \end{cases}, \quad (\text{B.1})$$

We have normalized the interaction strength, to make the integrated interaction (the energy) independent of the range. In a lattice model, one has to introduce a lower-distance cutoff as well, see below. In Chapter 7 we study the Landau–Ginzburg–Wilson Hamiltonian for this spin–spin interaction in the momentum-space representation. For this reason, we calculate in this appendix the Fourier transform of this interaction for a general number of dimensions. For $d = 1$ the calculation is trivial:

$$\tilde{K}_1(k) = \frac{c}{R} \int_{-R}^{+R} dx e^{ikx} = \frac{2c}{kR} \sin(kR). \quad (\text{B.2})$$

For $d = 2$ and $d = 3$ one obtains Bessel functions. Using the equality $J_{1/2}(x) = \sqrt{2/(\pi x)} \sin(x)$, the results for $d = 1, 2, 3$ can be summarized as

$$\tilde{K}_d(\mathbf{k}) = c \left(\frac{2\pi}{kR} \right)^{d/2} J_{d/2}(kR), \quad (\text{B.3})$$

where J_ν is a Bessel function of the first kind of order ν . This suggests that this equality is valid for general d , which can indeed be shown by induction. If we assign the

x coordinate to the $(d + 1)$ th spatial dimension and use the notation $k_d^2 = \sum_{j=1}^d k_j^2$, we may write

$$\begin{aligned}
 \tilde{K}_{d+1}(\mathbf{k}) &= \frac{c}{R^{d+1}} \\
 &\times \int_{-R}^{+R} dx \cos(k_x x) \left(\frac{2\pi}{k_d}\right)^{d/2} (R^2 - x^2)^{d/4} J_{d/2}\left(k_d \sqrt{R^2 - x^2}\right) \\
 &= \frac{2c}{R^{d+1}} \left(\frac{2\pi}{k_d}\right)^{d/2} \int_0^R dp \cos\left(k_x \sqrt{R^2 - p^2}\right) \frac{p^{(d+2)/2}}{\sqrt{R^2 - p^2}} J_{d/2}(k_d p) \\
 &= c \left(\frac{2\pi}{kR}\right)^{(d+1)/2} J_{(d+1)/2}(kR), \tag{B.4}
 \end{aligned}$$

where we have used a Hankel transform of general order; see, e.g., Ref. [1, p. 40, Eq. (48)].

If we add a spherically symmetric lower-distance cutoff a , Eq. (B.3) is generalized to

$$\tilde{K}_d(\mathbf{k}) = c \left(\frac{2\pi}{kR}\right)^{d/2} J_{d/2}(kR) - c \left(\frac{a}{R}\right)^d \left(\frac{2\pi}{ka}\right)^{d/2} J_{d/2}(ka). \tag{B.5}$$

The second term yields an additional range dependence in the shift of the critical temperature, see Chapter 7.

References

- [1] A. Erdélyi *et al.*, *Tables of Integral Transforms*, Vol. II (McGraw–Hill, New York, 1954).

Summary

Interaction Range, Universality and the Upper Critical Dimension

Close to their critical point, greatly different physical systems exhibit a strong similarity. Various macroscopic properties turn out to be independent of microscopic details, but are solely determined by a small number of global parameters, such as the dimensionality of the system and the symmetry and range of the interactions between the particles. This fascinating phenomenon, *universality*, is explained by the *renormalization-group theory*, which was developed in the early seventies by Kenneth G. Wilson (Nobel Prize in Physics 1982). In the last 25 years, the universal properties of a variety of critical systems have been calculated. Many of these predictions have been verified by computer simulations, especially for so-called *spin models*. However, the rôle of one parameter has until now largely evaded such a verification: the interaction range. This is caused by the fact that the required computational effort rapidly increases with increasing interaction range. Taking into account the small number of parameters that determines the universal properties, we view this as an important hiatus.

In this thesis, a simulation method for spin models is introduced, which has an efficiency that does not depend on the range of the interactions. Using this method, we treat several unsolved problems. Both the renormalization-group theory and computer simulations play an important rôle in our research. The relations between the various problems are outlined in the first chapter.

Chapter two is devoted to the new Monte Carlo method for spin models with long-range interactions. This method is a Wolff cluster algorithm and hence the autocorrelation time increases only very weakly as a function of the system size. We formulate the cluster formation process in such a way that only integrated spin–spin couplings have to be considered, which makes the total simulation time per spin independent of the range of the interactions. As an example, the algorithm is applied to a mean-field model. We also indicate how it can be generalized to $O(n)$ models.

In Chapter three, we first restrict ourselves to three models with short-range

interactions. These systems are supposed to belong to the universality class of the three-dimensional Ising model. By carrying out large-scale simulations for each of the models, we demonstrate that this is indeed the case. However, the corrections to scaling differ considerably for the three models. This property is used for a more accurate determination of the critical exponents and the fourth-order amplitude ratio.

Ising models with algebraically decaying ferromagnetic interactions are treated in Chapters four and five. These models are the generic example of systems for which the critical behaviour strongly depends on the range of the interactions (in this case on the decay parameter of the interactions). There are three different regimes: for very slowly decaying interactions the critical behaviour is essentially classical or mean-field-like. For somewhat faster decaying interactions, the critical behaviour belongs to an intermediate regime and for even faster decaying interactions the models exhibit short-range critical behaviour. No agreement exists on the boundaries of these regimes, nor on the nature of the critical behaviour in the intermediate regime. In Chapter four, we consider the classical regime for spin models in one, two and three dimensions. Various renormalization-group predictions are confirmed and we obtain accurate estimates for the critical temperatures. For two- and three-dimensional systems these are presumably the first results, whereas for one-dimensional systems various earlier approximation methods can be tested. The remaining two regimes are treated in Chapter five. We give a detailed treatment of the renormalization scenario for the crossover from the intermediate regime to the short-range regime. The numerical results yield accurate estimates for the critical exponents and temperatures and allow us to determine the location of the crossover. Furthermore, these results seem to have surprising implications for the ε -expansion for universal scaling functions.

The above-mentioned boundary between classical and nonclassical critical behaviour also exists in models with short-range interactions: the three-dimensional Ising model, which was examined in Chapter three, exhibits nonclassical critical behaviour, whereas the critical behaviour of models in more than four dimensions is classical. For this reason, the fourth dimension is called the *upper critical dimension*. The critical behaviour of the four-dimensional model itself is essentially classical, but according to the renormalization-group theory, at criticality logarithmic factors appear in the functions describing the thermodynamic properties. This is due to the appearance of a *marginal operator*. Because of these specific predictions, the four-dimensional model is very well suited to test the correctness of the theory. So, Chapter six is devoted to Ising models in four and five dimensions. The precise form of the logarithmic factors, which are difficult to observe, is determined with considerable precision and proves to be in good agreement with the theoretical predictions. Furthermore, we accurately confirm the classical nature of the critical behaviour of the five-dimensional Ising model.

Finally, we consider in Chapter seven the crossover from Ising-like to mean-field-like critical behaviour for interactions with an increasing range. This time, however, we choose the spin–spin coupling to be constant with a certain range and zero beyond this range. Thus, for any *finite* range the systems belong to the Ising universality class. We calculate the dependence of the thermodynamic properties on the interaction range, using renormalization-group theory, and check these predictions with numerical calculations for two-dimensional systems. In a system with a finite interaction range this crossover can also be induced by increasing the temperature distance to the critical point. This effect has been observed in various experimental systems, but since the temperature difference with the critical temperature may not become too large, it has not yet been possible to determine the precise nature of the crossover. Now, we have succeeded in doing so by varying not only the temperature, but also the interaction range in our model. This allowed us to answer a number of open questions. For example, there has been a lot of speculation whether so-called “effective critical exponents” can vary nonmonotonically in the crossover region. For the first time, we have shown in a theoretical model that this is indeed possible.

Samenvatting

Dracht van de Wisselwerkingen, Universaliteit en de Hogere Kritieke Dimensie

Fysische systemen van zeer uiteenlopende aard vertonen nabij hun kritieke punt sterke overeenkomsten. Verscheidene eigenschappen blijken namelijk niet afhankelijk te zijn van microscopische details, maar slechts te worden bepaald door een klein aantal globale parameters, waaronder de dimensionaliteit van het systeem en de symmetrie en dracht van de wisselwerking tussen de deeltjes. Dit fascinerende verschijnsel, *universaliteit* genaamd, wordt verklaard door de *renormalisatiegroeptheorie*, aan het begin van de jaren zeventig ontwikkeld door de Amerikaan Kenneth G. Wilson (Nobelprijs Natuurkunde 1982). In de laatste 25 jaar zijn met behulp van deze theorie de universele eigenschappen van een scala aan kritieke systemen berekend. Vele van deze voorspellingen zijn met computerberekeningen geverifieerd, met name voor zogeheten *spinmodellen*. De invloed van één parameter heeft zich echter goeddeels aan deze verificatie onttrokken: de dracht van de wisselwerking. De reden hiervoor is dat de hoeveelheid rekenwerk zeer sterk toeneemt wanneer de reikwijdte van de wisselwerkingen groter wordt. Gezien het kleine aantal factoren dat de universele eigenschappen bepaalt mag dit een belangrijke lacune worden genoemd.

In dit proefschrift wordt een numerieke berekeningsmethode voor spinmodellen geïntroduceerd, waarin langedrachtswisselwerkingen niet tot verlies aan efficiëntie leiden. Met deze methode worden vervolgens diverse tot nu toe onopgeloste problemen behandeld. Zowel de renormalisatiegroeptheorie als computerberekeningen spelen hierbij een belangrijke rol. In het eerste hoofdstuk wordt de onderlinge samenhang tussen deze problemen geschetst.

Hoofdstuk twee is gewijd aan de nieuwe Monte Carlo-methode voor systemen met langedrachtswisselwerkingen. Dit is een Wolff-clusteralgoritme, zodat de autocorrelatietijd niet of slechts zwak toeneemt als functie van de systeemgrootte. Wij formuleren de vorming van clusters zodanig, dat slechts geïntegreerde spin-spin koppelingen beschouwd hoeven te worden, waardoor de totale simulatietijd per spin

onafhankelijk wordt van de dracht van de interacties. De werking van dit algoritme wordt geïllustreerd aan de hand van een moleculair-veld model. Tevens wordt aangeduid hoe de methode kan worden gegeneraliseerd tot algemene $O(n)$ -modellen.

In hoofdstuk drie beperken we ons dan eerst tot een drietal modellen met kortedrachtswisselwerkingen. Deze systemen worden verondersteld te behoren tot de universaliteitsklasse van het driedimensionale Ising-model. Aan de hand van groot-schalige simulaties van de drie modellen wordt aangetoond dat dit inderdaad het geval is. De grootte van de correcties op het leidende schalingsgedrag blijkt echter per model te verschillen. We gebruiken dit gegeven voor een nauwkeuriger bepaling van de kritieke exponenten en de universele vierde-orde amplituderatio.

Ising-modellen met algebraïsch afvallende ferromagnetische interacties zijn het onderwerp van de hoofdstukken vier en vijf. Deze modellen zijn het generieke voorbeeld van systemen waarvan het kritieke gedrag een sterke afhankelijkheid van de dracht van de interactie (in dit geval de macht waarmee de interacties afvallen) vertoont. Er kunnen drie regimes worden onderscheiden: voor een zeer langzaam afvallende machtwet is het gedrag in essentie “klassiek”, dat wil zeggen zoals in een moleculair-veld model. Iets sneller afvallende interacties behoren tot een overgangsregime en nog sneller afvallende interacties komen overeen met kortedrachtswisselwerkingen. De precieze begrenzingen van deze regimes zijn een onderwerp van discussie, evenals de aard van het kritieke gedrag in het overgangsregime. In hoofdstuk vier beperken we ons tot het klassieke regime voor spinmodellen in één, twee en drie dimensies. Verscheidene voorspellingen van de renormalisatiegroeptheorie worden bevestigd en de kritieke temperaturen worden zeer nauwkeurig bepaald. Voor twee- en driedimensionale systemen zijn dit vermoedelijk de eerste resultaten, terwijl voor ééndimensionale systemen diverse eerdere benaderingsmethoden op hun merites kunnen worden beoordeeld. In hoofdstuk vijf komen de overige twee regimes aan bod. Het renormalisatiescenario voor de overgang van het tussenregime naar het kortedrachtsregime wordt in detail behandeld. De numerieke resultaten verschaffen nauwkeurige schattingen van de kritieke exponenten en temperaturen en maken het mogelijk om de locatie van de overgang te bepalen. Bovendien werpen deze resultaten een verrassend licht op de ε -expansie voor universele schalingsfuncties.

De bovengenoemde scheiding tussen klassiek en niet-klassiek kritiek gedrag bestaat ook in modellen met kortedrachtswisselwerkingen: het in hoofdstuk drie onderzochte driedimensionale Ising-model vertoont niet-klassiek gedrag, terwijl modellen in meer dan vier dimensies zich klassiek gedragen. Om deze reden wordt de vierde dimensie de *hogere kritieke dimensie* genoemd. Het kritieke gedrag van het vierdimensionale model zelf is in essentie klassiek, maar volgens de renormalisatiegroeptheorie verschijnen er op het kritieke punt, als gevolg van een *marginale operator*, logaritmische factoren in de functies die de thermodynamische eigenschappen beschrijven. Deze specifieke voorspellingen maken het vierdimensionale Ising-model bijzonder geschikt om de juistheid van de theorie te toetsen. Hoofdstuk zes

is daarom geheel gewijd aan het Ising-model in vier en vijf dimensies. De precieze vorm van de logaritmische factoren, die in het algemeen moeilijk waarneembaar zijn, wordt zeer nauwkeurig bepaald en blijkt in goede overeenstemming te zijn met de theoretische voorspellingen. Daarnaast bevestigen wij met grote precisie het klassieke karakter van het kritieke gedrag van het vijfdimensionale Ising-model.

Tot slot beschouwen we ook in hoofdstuk zeven de overgang van Ising-achtig naar moleculair-veld kritiek gedrag voor interacties met een toenemende reikwijdte. Nu hebben de spin-spin koppelingen echter een blokvorm, zodat voor elke *eindige* dracht de systemen tot de Ising-universaliteitsklasse behoren. Met behulp van renormalisatiegroeptheorie berekenen we hoe de thermodynamische eigenschappen afhangen van de dracht. We verifiëren dit vervolgens met numerieke berekeningen voor tweedimensionale systemen. Voor eindige dracht kan deze overgang echter eveneens worden geïnduceerd door het temperatuurverschil met de kritieke temperatuur te vergroten. Dit effect is in diverse experimentele systemen waargenomen, maar omdat het temperatuurverschil tegelijkertijd niet al te groot mag worden kon de precieze aard van het gedrag tot nu toe niet bepaald worden. Door in simulaties niet alleen de temperatuur, maar ook de dracht van de interacties te variëren, kunnen wij deze overgang wél volledig berekenen. Hierdoor konden diverse open vragen beantwoord worden. Zo wordt er sinds lange tijd gespeculeerd over de vraag of het mogelijk is dat zogenaamde “effectieve kritieke exponenten” niet-monotoon variëren bij deze overgang. Voor de eerste maal is nu in een theoretisch model aangetoond dat dit inderdaad het geval is.

Acknowledgements

Naturally, the work presented in this thesis could never have been done without the support, encouragement and patience of a number of people.

The first person I would like to thank is Henk Blöte. Few people can guess how many hours we spent together discussing physics, polishing articles and trying to interpret numerical results. His broad knowledge and great intuition have surprised me on quite a few occasions. Henk, I have profited enormously from your generosity and your willingness to teach me!

I am also grateful to the other people in the Theoretical Physics Group for the friendly atmosphere they provided. Furthermore, the interest of many people, either at seminars, workshops and Ph. D. courses or by letters and e-mail messages, has been very stimulating.

Next, I want to mention the warm support of Prof. Kurt Binder, who initiated the work described in Chapter 7 and invited me several times to visit his group in Mainz. I am looking forward to our collaboration in the forthcoming years!

Also from outside the physics community I received indispensable help. Friends and family often reminded me of the existence of the “real” world. The continued encouragement of my parents, Piet and Liesbeth, and my sister Mirjam has helped me on many occasions.

The most credits, however, should go to the dearest person in my life. Ellen, your incredible patience, your sense of humour and your company have contributed more to this thesis than I can express in words.

Erik Luijten, October 1997

Curriculum Vitae

The author of this thesis was born in Nijmegen (The Netherlands) on the 20th of January 1970. He received his secondary education between 1982 and 1988 at the Onze-Lieve-Vrouwe Lyceum in Breda.

Subsequently, he studied physics at the Department of Physics and Astronomy of the University of Utrecht, where he passed his first-year examination in June 1989 (Cum Laude). He wrote his Master's Thesis at the Institute for Theoretical Physics under the supervision of Prof. dr. Henk van Beijeren and received his Master's Degree ("Met genoegen") in December 1993.

In Januari 1994 he started to work in the Theoretical Physics Group at Delft University of Technology, under the guidance of Prof. dr. Henk Blöte. This resulted in the present Ph. D. Thesis.

Starting in January 1998, the author will receive a Fellowship from the Max-Planck Institute for Polymer Research in Mainz (Germany) and work in the Condensed Matter Theory Group of Prof. dr. Kurt Binder at the Johannes Gutenberg-University in Mainz.

List of publications

- E. Luijten, H. van Beijeren and H. W. J. Blöte
Physical Review Letters **73**, 456 (1994)
- E. Luijten and H. W. J. Blöte
International Journal of Modern Physics C **6**, 359 (1995)
- H. W. J. Blöte, E. Luijten and J. R. Heringa
Journal of Physics A: Mathematics and General **28**, 6289 (1995)
- E. Luijten and H. W. J. Blöte
Physical Review Letters **76**, 1557 (1996); **76**, 3662(E) (1996)
- E. Luijten, H. W. J. Blöte and K. Binder
Physical Review E **54**, 4626 (1996)
- E. Luijten
Europhysics Letters **37**, 489 (1997)
- H. W. J. Blöte and E. Luijten
Europhysics Letters **38**, 565 (1997)
- E. Luijten, H. W. J. Blöte and K. Binder
Physical Review Letters **79**, 561 (1997)
- E. Luijten and H. W. J. Blöte
Physical Review B **56**, 8945 (1997)
- E. Luijten, H. W. J. Blöte and K. Binder
Physical Review E, to appear in Vol. **56** (1997)